

Departament d'Estructura i Constituents de la Matèria

# Entanglement in many body quantum systems

**Arnau Riera Graells**

Memòria presentada per optar al títol de Doctor en Física.  
Tesi dirigida pel Dr. José Ignacio Latorre Sentís.

Febrer de 2010



UNIVERSITAT DE BARCELONA



Programa de doctorat “Física Avançada”  
Bienni 2005–2007



*I a vegades una carambola de sobte  
ens demostra que ens en sortim.*  
Manel.



---

# Agraïments

---

És difícil donar les gràcies a una llista tancada de persones. En aquesta llista no hi podria faltar sense cap mena de dubte el meu director de tesi, en José Ignacio, qui va tenir prou confiança en mi per agafar-me com a estudiant, de qui he après tantes coses (no únicament en l'àmbit acadèmic) i qui tants cops s'ha desesperat corregint la meva pèssima redacció en anglès. També hi serien sens falta els meus companys de grup i col·laboradors al llarg d'aquests 4 anys, el Sofyan, l'Escartin, el Román, la Nuri, el Dani, en Maciej, l'Ania, el Vicent, el Thiago, l'Octavi, l'Alessio, l'Adele, el Giuseppe i la Belén, amb qui tantes hores ens hem estat palplantats davant d'una pissarra discutint algun problema de física o estudiant un llibre o article. Tampoc no puc oblidar els meus companys de despatx: el Javier, el David, el Raül, el Giancarlo, en Jaume, l'Alessandro, l'Escartín i en Juan. Tantes vegades preguntant-nos els uns als altres per què no compilava un programa, amb quina nota havíem de puntuar un determinat examen, on estava l'error de LaTeX, i si algú sabia tal instrucció del mathematica. Finalment, he d'anomenar també a tots els companys del departament, la facultat i els cursos de doctorat amb qui hem compartit tants dinars, cafès, cues a la impresora i seminaris al llarg d'aquest temps. A tots i totes, moltíssimes gràcies per 4 anys en què he après tant de vosaltres.



---

# Resum

---

La intersecció entre els camps de la Informació Quàntica i la Física de la Matèria Condensada ha estat molt fructífera en els darrers anys. Per una banda, les eines desenvolupades en el marc de la Teoria de la Informació Quàntica, com les mesures d'entrellaçament, han estat utilitzades amb molt d'èxit per estudiar els sistemes de Matèria Condensada. En el context de la Informació Quàntica també s'han creat noves tècniques numèriques per tal de simular sistemes quàntics de moltes partícules i fenòmens de la Matèria Condensada. Per l'altra, la Física de la Matèria Condensada, juntament amb l'Òptica Quàntica i la Física Atòmica, està proporcionant els primers prototips de *computadors* i *simuladors quàntics*. A més, diversos sistemes de Matèria Condensada semblen esdevenir els candidats idonis per desenvolupar molts paradigmes de la Computació Quàntica.

En aquesta tesi, abordem tant la qüestió de l'estudi de sistemes de Matèria Condensada des de la perspectiva de la Informació Quàntica, com l'anàlisi de la manera com s'utilitzen els sistemes de Matèria Condensada, en particular els gasos ultrafreds, per tal de desenvolupar els primers *simuladors quàntics*. Així, en la primera part d'aquesta tesi ens centrem en l'estudi de l'entrellaçament en sistemes de molts cossos i estudiem les connexions entre les característiques d'un Hamiltonià, la quantitat d'entrellaçament del seu estat fonamental i la seva eficient simulació. En la segona part, discutim com podem tractar aquells sistemes que són massa entrellaçats per ser simulats amb un ordinador clàssic. En particular, estudiem les possibilitats dels àtoms

ultra-freds per simular-los.

## Entrellaçament

L'entrellaçament és la propietat que tenen alguns sistemes compostos de donar unes correlacions no-locales molt fortes que no poden ser generades per *operacions locals i comunicació clàssica* (LOCC). En el cas de sistemes bipartits (que tenen dues parts  $A$  i  $B$ ), considerem que aquestes transformacions LOCC són realitzades per dos observadors, l'Alice i en Bob, tenint cadascun d'ells accés a un dels sub-sistemes  $A$  i  $B$ . L'Alice i en Bob poden realitzar qualsevol tipus d'acció en la seva part del sistema: operacions unitàries, mesures, etc. També poden fer servir comunicació clàssica per tal de coordinar totes aquestes accions.

Així, si un estat  $\rho$  pot ser transformat mitjançant LOCC en un altre estat diferent  $\sigma$ , direm que  $\rho$  és tant o més entrellaçat que  $\sigma$ , ja que totes les correlacions que pot donar  $\sigma$  també les pot donar  $\rho$  amb unes quantes transformacions LOCC.

La noció d'entrellaçament que hem definit, per tant, depèn estrictament en la definició de transformacions LOCC. Si haguéssim considerat unes altres restriccions, les relacions entre 2 estats d'estar més o menys entrellaçats seria diferent.

Una *mesura d'entrellaçament* és una funció  $E$  que assigna a cada estat  $\rho$  un nombre real  $E(\rho)$  amb la següent condició

$$\rho \xrightarrow{\text{LOCC}} \sigma \Rightarrow E(\rho) \geq E(\sigma). \quad (1)$$

A continuació presentem les dues mesures d'entrellaçament que farem servir al llarg de tota la tesi:

- *Entropia d'entrellaçament.* És una bona mesura d'entrellaçament per a estats purs  $|\Psi\rangle$ . Es calcula mitjançant l'entropia de von Neumann de la matriu reduïda de cada part del sub-sistema. Més concretament,

$$S_A \equiv S(\rho_A) = -\text{tr} (\rho_A \log_2 \rho_A), \quad (2)$$

on  $\rho_A = \text{tr}_B(|\psi\rangle\langle\psi|)$ . És fàcil demostrar que  $S_A = S_B$ .

- *Entrellaçament d'una sola còpia.* Es defineix com,

$$E_1(\rho_A) = -\log \rho_A^{(1)}, \quad (3)$$

on  $\rho_A^{(1)}$  és l'autovalor màxim de la matriu densitat  $\rho_A$ .

## Entrellaçament en els sistemes quàntics de molts cossos

A continuació ens disposem a estudiar el comportament de l'entrellaçament en sistemes de moltes partícules. Ens volem centrar en cadenes d'espins i analitzar com escala l'entrellaçament d'un bloc d' $L$  spins amb la mida del bloc  $L$ .

Prenem com a exemple un model XX format per una cadena de  $N$  partícules spin- $\frac{1}{2}$  amb interaccions a primers veïns i un camp magnètic extern. L'Hamiltonià d'aquest sistema ve donat per

$$H_{XX} = -\frac{1}{2} \sum_{l=0}^{N-1} (\sigma_l^x \sigma_{l+1}^x + \sigma_l^y \sigma_{l+1}^y) + \frac{1}{2} \lambda \sum_{l=0}^{N-1} \sigma_l^z, \quad (4)$$

on  $l$  etiqueta  $N$  spins,  $\lambda$  és el camp magnètic extern i  $\sigma_l^\mu$  ( $\mu = x, y, z$ ) són les matrius de Pauli actuant en la posició  $l$ .

En la Ref. Vidal:2003-90, van determinar l'estat fonamental d'aquest sistema i en van calcular l'entrellaçament per a blocs de diferents mides. Van obtenir un gràfic com el de la Fig. 1. Observem uns comportaments de l'entropia d'entrellaçament diferents segons el valor del camp magnètic. Si el sistema està en una fase crítica,  $0 < \lambda < 2$ , l'entrellaçament escala de forma logarítmica amb la mida del bloc. Per contra, si el sistema es troba en la fase ferromagnètica, l'entrellaçament és nul. Aquesta qüestió ha estat també analitzada per altres models de cadenes d'espins (XY, XXZ, Ising, etc.) obtenint sempre el mateix comportament. Sembla ser que l'entrellaçament està estretament relacionat amb el tipus de fase del sistema, i en particular, és un perfecte testimoni de les transicions de fase.

Que l'estat fonamental d'un sistema sigui molt entrellaçat vol dir que és en el fons una superposició de molts estats producte diferents i, per tant, haurem d'utilitzar molts paràmetres per a descriure'l. En efecte, en la Ref. [1] es demostra que sistemes poc entrellaçats es poden simular de forma eficient amb un ordinador clàssic. L'entrellaçament és, per tant, el que definirà la frontera entre els sistemes quàntics que es poden simular de forma eficient amb mitjans clàssics i els que no.

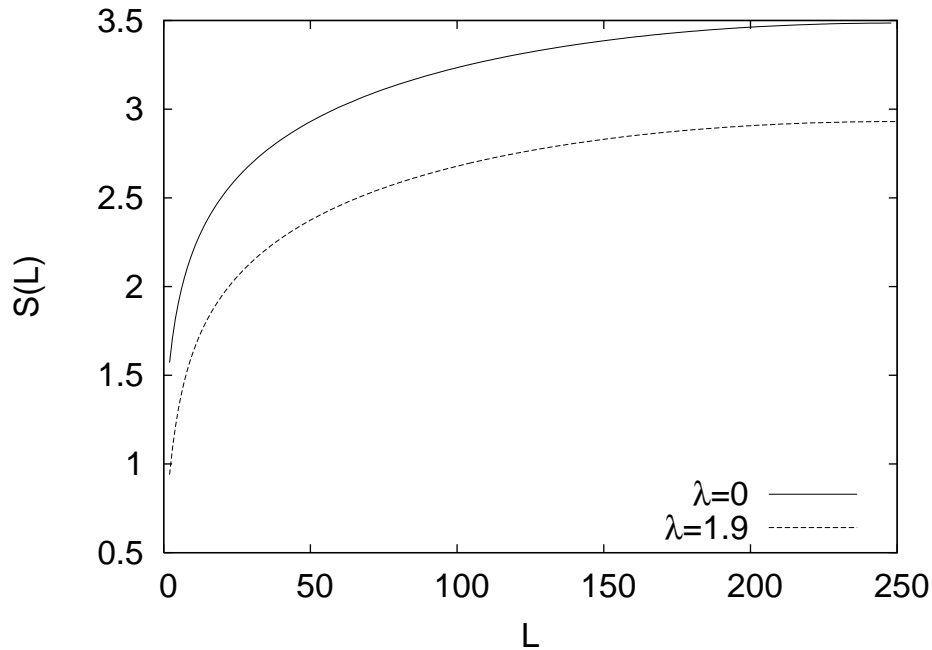


Figure 1: Entropia de la matriu reduïda de  $L$  spins pel model XX en el límit  $N \rightarrow \infty$  per diferents valors del camp magnètic  $\lambda$ . L'entropia és màxima quan el camp magnètic aplicat és zero. L'entropia decreix mentre augmentem el camp magnètic fins que arribem a  $\lambda = 2$ . En aquest instant el sistema arriba al límit ferromagnètic i l'estat fonamental pot ser descrit per un estat producte de tots els spins alineats en la direcció del camp.

## Llei d'àrea per a l'entropia d'entrellaçament en una xarxa d'oscil·ladors harmònics

La representació clàssica d'un estat quàntic arbitrari d' $N$  partícules

$$|\Psi\rangle = \sum_{i_1, \dots, i_N=1}^d c_{i_1, \dots, i_N} |i_1, \dots, i_N\rangle, \quad (5)$$

requereix un nombre exponencial ( $d^N$ ) de coeficients complexos  $c_{i_1, \dots, i_N}$ . Per tant, el tractament d'aquest estat, és a dir, determinar-ne l'evolució en el temps o calcular-ne els valors esperats d'alguns observables, també requerirà un nombre exponencial de passos. Aquesta és la raó per la qual no podem simular clàssicament qualsevol sistema quàntic de moltes partícules, i en particular, alguns interessants sistemes de la

Matèria Condensada (superconductors d'alta temperatura, efecte Hall quàntic fraccionari, etc.).

No obstant això, a la natura, els Hamiltonians típics (amb interaccions locals i invariants sota translacions) tenen estats fonamentals poc entrelaçats (la seva entropia d'entrelaçament escala com l'àrea de la regió considerada). Aquest tipus de comportament, on l'entropia és proporcional a l'àrea en lloc de ser extensiva, s'anomena *area-law*.

Les lleis d'àrea són freqüents en els estats fonamentals dels Hamiltonians amb interaccions locals. Això fa aquests estats molt peculiars. Si agafem a l'atzar un estat quàntic de l'espai de Hilbert d'un sistema de moltes partícules, mostrarà una gran quantitat d'entrelaçament en qualsevol partició que prenem. És a dir, l'entropia d'un subsistema és pràcticament màxima i creix amb el volum. Així doncs, un estat quàntic típic satisfà una llei de volum de l'entropia d'entrelaçament, i no una llei d'àrea. Podem dir, per tant, que els estats fonamentals dels Hamiltonians locals són una regió molt petita de tot l'espai de Hilbert.

En la Ref. [2] es demostra que qualsevol estat que verifiqui la llei d'àrea pot ser simulat per mitjans clàssics, així doncs, la llei d'àrea estableix la frontera entre els sistemes que poden ser simulats clàssicament i els que no.

Permeteu-nos considerar un sistema format per un camp de Klein-Gordon (*i. e.* una xarxa d'oscil·ladors harmònics) en  $D$  dimensions pel qual esperariem que verifiqués la llei d'àrea per l'entropia d'entrelaçament. El nostre càlcul serà la generalització del presentat en la Ref. [3] a  $D$  dimensions. L'Hamiltonià de Klein-Gordon ve donat per l'expressió

$$H = \frac{1}{2} \int d^D x \left( \pi^2(\vec{x}) + |\nabla \phi(\vec{x})|^2 + \mu^2 |\phi(\vec{x})|^2 \right), \quad (6)$$

on  $\pi(x)$  és el moment canònic associat al camp escalar  $\phi(x)$  de massa  $\mu$ .

Per aquest sistema calculem l'entropia d'entrelaçament i l'entrelaçament d'una còpia d'una regió de radi  $R$  per diferents dimensions del sistema. Dins del rang  $1 < D < 5$ , observem l'esperada llei d'àrea per l'entropia

$$S = k_S(\mu, D, a, N) \left( \frac{R}{a} \right)^{D-1}, \quad (7)$$

i el mateix comportament per l'entrelaçament d'una còpia

$$E_1 = k_E(\mu, D, a, N) \left( \frac{R}{a} \right)^{D-1}. \quad (8)$$

En la Fig.2 mostrem aquest comportament per les dues mesures d'entrelaçament.

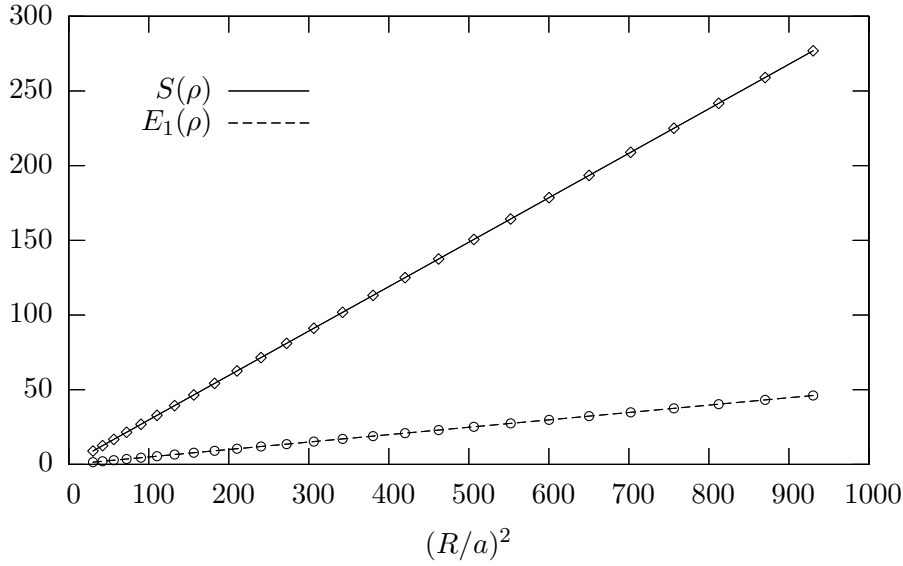


Figure 2: L'entropia  $S$  i l'entrellaçament d'una sola còpia  $E_1$ , resultat de traçar els graus de llibertat dins d'una esfera de radi  $R$  en l'estat fonamental d'un camp escalar sense massa en 3 dimensions.

A part de generalitzar el càlcul a  $D$  dimensions, per camps massius i completar-lo amb l'entrellaçament d'una còpia, també en fem un refinament que ens permet reproduir el resultat de la Ref. [3] amb una xifra significativa més

$$k_S(\mu = 0, D = 3, N \rightarrow \infty) = 0.295(1), \quad (9a)$$

$$k_E(\mu = 0, D = 3, N \rightarrow \infty) = 0.0488(1). \quad (9b)$$

## Violació de la llei d'àrea per l'entropia d'entrellaçament amb una cadena d'espins

La manera com escala l'entropia d'entrellaçament pels sistemes d'una dimensió invariants sota translacions està ben establerta. Per una banda, si el sistema té interaccions locals i gap, la llei d'àrea sempre emergeix. De l'altra, si el sistema és crític i per tant sense gap, apareix una divergència logarítmica. Aquesta dependència logarítmica de l'entropia d'entrellaçament està molt ben explicada per les teories de camps conformes [4, 5]. Naturalment, si considerem interaccions de llarg abast, aleshores la llei d'àrea pot ser perfectament violada.

Tot i que en els darrers anys hi ha hagut un immens progrés en establir les connexions entre les característiques d'un Hamiltonià i l'entrellaçament del seu estat fonamental (veieu Ref. [6]), les condicions necessàries i suficients per tenir una llei d'àrea encara no han estat definides. La qüestió que volem abordar aquí és quin és l'Hamiltonià més simple possible que té un estat fonamental altament entrellaçat.

En particular, prenem un model XX d'una cadena d'spins 1/2 amb interaccions a primers veïns definit per

$$H_{XX} = \frac{1}{2} \sum_{i=1}^L J_i (\sigma_i^x \sigma_{i+1}^x + \sigma_i^y \sigma_{i+1}^y), \quad (10)$$

el nostre objectiu és veure si per alguna configuració de les constants d'acoplament  $J_i$  l'estat fonamental verifica una llei de volum per l'entrellaçament.

Per fer-ho, utilitzem el grup de renormalització en espai real, introduït per Fisher [7] generalitzant els treballs de Dasgupta i Ma [8], i teoria de pertorbacions. De fet, el grup de renormalització en espai real ens motiva a estudiar una configuració de les constants d'acoplament on  $J_0$  és l'acoplament central de la cadena i el de valor més alt, mentre la resta decauen fortament a mesura que ens n'allunyem

$$J_i = \epsilon^{\alpha(i)}, \quad (11)$$

on  $\epsilon$  és un paràmetre molt menor que 1 i  $\alpha(i)$  una funció monòtona creixent. Per exemple,  $\alpha(i) \sim i^2$  correspondria a un decaïment gausià.

En la Fig. 3, mostrem com escala l'entropia per un decaïment exponencial i un altre de gausià. Observem que efectivament l'entropia creix linealment.

## Gasos ultra-freds i la simulació de la Física de la Matèria Condensada

Fins ara hem vist que no és possible simular sistemes altament entrellaçats amb un ordinador clàssic. Això ens obliga a buscar alternatives per estudiar aquests sistemes.

Feynman, el 1982, es va adonar que la manera més natural de simular la Mecànica Quàntica seria utilitzant ordinadors quàntics [9]. No obstant això, la tecnologia actual ens fa pensar que no tindrem el control experimental necessari per tenir aquests dispositius en un futur proper. En aquest context, els gasos ultra-freds apareixen com

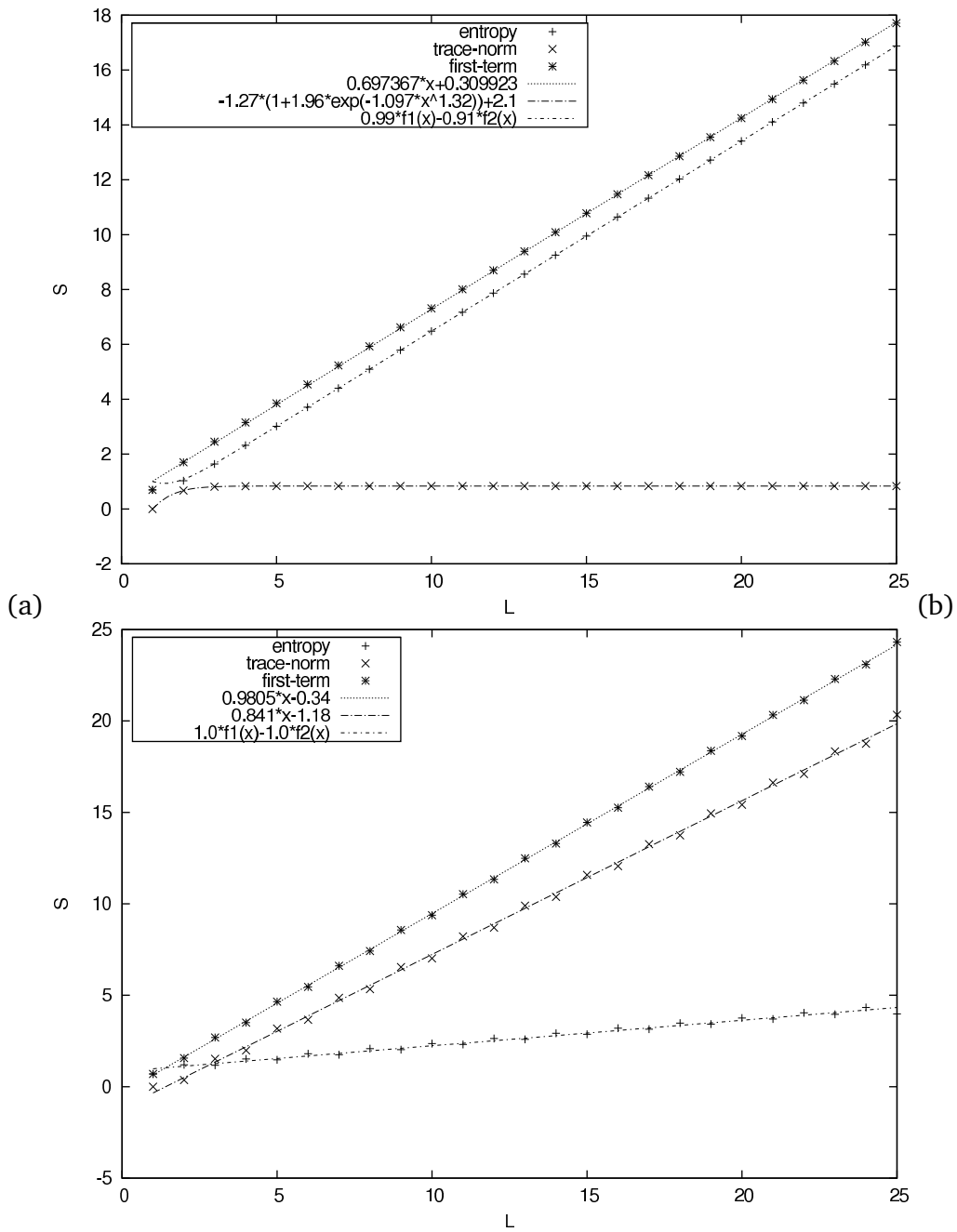


Figure 3: Entropia d'entrellaçament d'un bloc d'spins contigus respecte la mida del bloc  $L$  per l'estat fonamental d'un model XX amb acoblaments que decauen: (a) de forma gaussiana,  $J_n = e^{-n^2}$ , i (b) de forma exponencial  $J_n = e^{-n^2}$ . El camp magnètic és zero.

uns molt bons candidats per construir els primers *simuladors quàntics*, és a dir, sistemes quàntics que podem controlar experimentalment amb els que podem emular altres sistemes quàntics que són els que volem estudiar.

Els gasos ultra-freds permeten una observació controlada de molts dels fenòmens físics que han estat estudiats en Matèria condensada. Els àtoms poden ser atrapats, refredats i manipulats amb camps electro-magnètics externs, permetent modificar els paràmetres físics que controlen el seu comportament tant individual com col·lectiu.

Hi ha molts fenòmens i sistemes que són interessants d'estudiar amb simuladors quàntics: sistemes desordenats, el model de Bose-Hubbard, etc. Aquí ens volem centrar en l'efecte Hall quàntic fraccionari (FQHE) i l'estat de Laughlin, ja que aquest estat serà l'objectiu de les propostes de simulació que presentarem posteriorment.

L'FQHE consisteix en l'efecte de conductivitats transverses fraccionàries que mostra un gas d'electrons en dues dimensions per alguns valors particulars del camp magnètic transvers [10]. El 1983, Laughlin va proposar un Ansatz per la funció d'ona de l'estat fonamental del sistema [11]. Aquesta funció d'ona ve definida per

$$\Psi_m(z_1, \dots, z_N) \sim \prod_{i < j} (z_i - z_j)^m e^{-\sum_{i=1}^N |z_i|^2/2}, \quad (12)$$

on  $z_j = x_j + iy_j$ ,  $j = 1, \dots, N$  correspon a la posició de la partícula  $j$  i  $m$  és un nombre enter relacionat amb la fracció d'ocupació  $\nu = 1/m$ .

Una de les característiques més importants d'alguns estats de l'FQHE és que són estats de la matèria amb excitacions de quasipartícula que no són ni bosons ni fermions, sinó *anyons no abelians*. Aquests anyons no abelians es caracteritzen per obeir estadístiques d'intercanvi no abelianes. Aquestes fases de la matèria defineixen un nou tipus d'ordre a la natura anomenat *ordre topològic* [12] i desperten un gran interès ja que permetrien fer computació quàntica d'una manera molt robusta.

## Simulació de l'estat de Laughlin en una xarxa òptica

Tot i les grans possibilitats dels estats FQH, fins ara no s'han observat directament ni la funció d'ona de Laughlin ni les seves excitacions anyòniques. Des del punt de vista teòric, s'ha demostrat que l'FQHE pot ser realitzat simplement rotant un núvol de bosons en una trampa harmònica [13, 14]. La rotació fa la funció del camp magnètic pels àtoms neutres. En aquest sistema, l'estat de Laughlin és l'estat fonamental. El problema és que a la pràctica, a causa de les febles interaccions entre els àtoms, el gap és massa petit i no és possible baixar prou la temperatura per obtenir-lo i observar-lo.

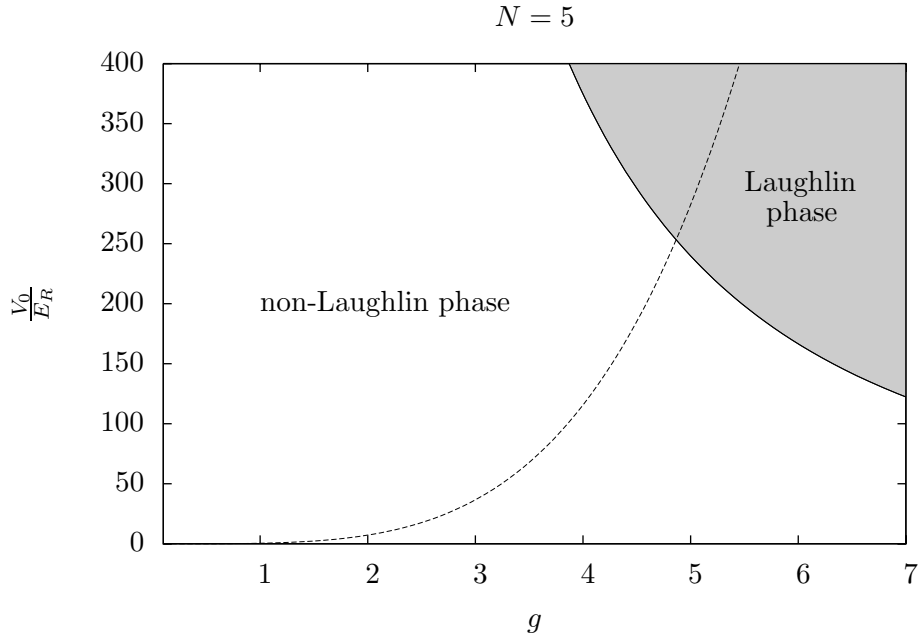


Figure 4: Diagrama de fases de l'estat fonamental respecte la intensitat del làser  $V_0$  i de la interacció de contacte  $g$  per un sistema amb  $N = 5$  partícules. Per tal de realitzar el diagrama, hem considerat la màxima freqüència de rotació possible  $\Omega_L$  per cada valor de  $V_0$ . La línia discontinua representa la dependència de  $g$  amb el confinament  $V_0$  pel cas d'àtoms de Rubidi.

Una possibilitat per evitar aquest problema és utilitzar xarxes òptiques [15, 16]. En aquests sistemes, les energies d'interacció són més grans ja que els àtoms estan confinats en un volum menor. Així, en la Ref. [17] trobem una proposta per generar un estat producte de funcions d'ona de Laughlin en una xarxa òptica. El seu principal inconvenient és que no tenen en compte la correcció anharmònica del potencial de cada lloc de la xarxa. Si estudiem amb detall la proposta, veiem que considerar aquesta correcció és imprescindible.

La correcció quàrtica introdueix una freqüència màxima de rotació menor que en el cas purament harmònic i, per tant, si no la consideréssim i volguéssim generar el Laughlin experimentalment, totes les partícules serien expulsades del seu pou de potencial. Aquest restrictiu límit centrífug fa més difícil conduir el sistema a l'estat de Laughlin. Tot i així, per sistemes amb un nombre petit de partícules en cada pou de la xarxa, és perfectament possible generar el Laughlin. En la Fig. 4 mostrem el diagrama de fases de l'estat fonamental respecte la intensitat del làser  $V_0$  i de la interacció de

contacte  $g$  per un sistema amb  $N = 5$  partícules. Observem que pel cas d'àtoms de Rubidi (línia discontinua) l'estat de Laughlin seria generat per una intensitat del làser realista.

## Trencament de simetria en petits núvols de bosons en rotació

Com ja hem dit, l'estat de Laughlin és l'estat fonamental d'un núvol de bosons que interactuen repulsivament en una trampa harmònica rotant a una freqüència  $\Omega$  quan la rotació és prou gran. A continuació ens agradaria estudiar quin tipus d'estructures té l'estat fonamental per freqüències de rotació menors. Ens preguntem si aquests estats corresponen a estats fortament correlacionats (com l'estat de Laughlin) o si, per contra, poden ser descrits mitjançant un paràmetre d'ordre de manera semblant a l'aproximació de camp mig [18].

Així, per aquells estats fonamentals  $|GS\rangle$  a una determinada rotació que formen estructures interessants (més d'un vòrtex), analitzem si podem descriure el sistema mitjançant una funció d'ona monoparticular que estigui macroocupada. La manera de veure-ho és determinar els valors i estats propis de la matriu densitat a un cos (OBDM) [18], és a dir, resoldre la següent equació d'autovalors

$$\int d\vec{r}' n^{(1)}(\vec{r}, \vec{r}') \psi_l^*(\vec{r}') = n_l \psi_l^*(\vec{r}), \quad (13)$$

on

$$n^{(1)}(\vec{r}, \vec{r}') = \langle GS | \hat{\Psi}^\dagger(\vec{r}) \hat{\Psi}(\vec{r}') | GS \rangle, \quad (14)$$

amb  $\hat{\Psi} = \sum_{m=0}^{\infty} \varphi_m(\vec{r}) a_m$  essent l'operador camp i  $\varphi_m(\vec{r})$  les funcions d'ona monoparticulars dels autoestats del moment angular. Si existeix un autovalor rellevant  $n_1 \gg n_k$  per  $k = 2, 3, \dots, m_0 + 1$ , aleshores

$$\sqrt{n_1} \psi_1(\vec{r}) e^{i\phi_1} \quad (15)$$

té el paper de paràmetre d'ordre on  $\phi_1$  és una fase arbitrària.

En la Fig. 5 podem comprovar com en valors d' $\Omega$  on l'estat fonamental té una estructura no trivial, el paràmetre d'ordre descriu molt bé les seves propietats tant de densitat com de vòrtex.

## Algoritme quàntic per l'estat de Laughlin

En aquest cas també volem generar l'estat de Laughlin, però d'una manera molt diferent d'una simulació amb àtoms freds. Ens proposem dissenyar un circuit quàntic que actui sobre un estat producte i generi l'estat de Laughlin. Creiem que aquest tipus de simulacions seran unes aplicacions interessants pels primers prototips d'ordinadors quàntics.

El nostre sistema consistirà en una cadena de  $n$  qudits (espais de Hilbert de  $d$  dimensions). Aquí ens centrarem en el cas de l'estat de Laughlin amb fracció d'ocupació 1, per tant necessitarem que la dimensió de cada qudit sigui  $d = n$ .

L'estat de Laughlin pot ser escrit en termes de les funcions d'ona monoparticulars del moment angular, també anomenades Fock-Darwin  $\varphi_l(z) = \langle z|l\rangle = z^l \exp(-|z|^2/2)/\sqrt{\pi l!}$ . Així doncs, per  $n$  qudits aquest tindrà la forma

$$|\Psi_L^{(n)}\rangle = \frac{1}{\sqrt{n!}} \sum_{\mathcal{P}} \text{sign}(\mathcal{P}) |a_1, \dots, a_n\rangle, \quad (16)$$

on sumem per totes les possibles permutacions del conjunt  $\{0, 1, \dots, n-1\}$ .

Pel cas de fracció d'ocupació 1 ( $m = 1$ ) som capaços de trobar un circuit que ens generi l'estat de Laughlin per un nombre arbitrari de partícules. En la Fig. 6 presentem el circuit pel cas de 5 partícules. Aquest està configurat per unes portes  $V_k^{[n+1]}$  definides per

$$V_k^{[n+1]} = \prod_{i=0}^{n-1} W_{in}, \quad (17)$$

on, alhora, els operadors  $W_{ij}(p)$  vénen donats per

$$\begin{aligned} W_{ij}(p)|ij\rangle &= \sqrt{p}|ij\rangle - \sqrt{1-p}|ji\rangle \\ W_{ij}(p)|ji\rangle &= \sqrt{p}|ji\rangle + \sqrt{1-p}|ij\rangle, \end{aligned} \quad (18)$$

per  $i < j$ ,  $0 \leq p \leq 1$ , i  $W_{ij}|kl\rangle = |kl\rangle$  if  $(k, l) \neq (i, j)$ .

És possible demostrar que la nostra proposta pot ser implementada experimentalment en forma de qubits. Així, cada qudit pot ser codificat en diversos qubits i els operadors  $W$  es poden realitzar com una sèrie d'operacions en forma de portes individuals (actuen a un sol qubit) i C-NOTs (actua a 2 qubits).

## Conclusions

Hem estudiat l'entrellaçament en sistemes quàntics de molts cossos i analitzat quines característiques han de tenir aquests sistemes per tal de poder ser simulats en un ordinador clàssic. Hem vist que qualsevol estat que verifiqui la llei d'àrea per l'entropia d'entrellaçament pot ser eficientment simulat mitjançant les representacions de xarxes de tensors. Així, la llei d'àrea estableix la frontera entre aquells sistemes que poden ser simulats per mitjans clàssics i aquells que no.

Una qüestió que no és gens clara encara és quines característiques ha de tenir un Hamiltonià per tal que el seu estat fonamental verifiqui la llei d'àrea. Com hem vist, hi ha sistemes amb interaccions locals amb un estat fonamental altament entrellaçat. Un línia de recerca futura seria establir les condicions necessàries i suficients per a donar llei d'àrea.

Una altra conclusió important és que la Informació Quàntica ha proporcionat noves eines per estudiar sistemes de Matèria Condensada. Ens referim concretament a les mesures d'entrellaçament, que hem comprovat que són uns bons testimonis de la criticalitat del sistema i, per tant, de la longitud de correlació d'aquest.

Respecte la simulació de sistemes quàntics amb altres sistemes quàntics, hem comprovat que, gràcies al gran control experimental que hi ha actualment, els gasos ultra-freds constitueixen els millors candidats per a realitzar aquest tipus de simulació. També hem plantejat un altre tipus de simulació de sistemes quàntics que consisteix a dissenyar algorismes quàntics. Per tots dos paradigmes de simulació, hem proposat la generació de l'estat de Laughlin com un exemple de simulació.

Creiem, doncs, que la intersecció dels camps d'Informació Quàntica i Física de la Matèria Condensada continuarà essent molt fructífera en el futur. Per una banda, els mètodes numèrics de xarxes de tensors ens permetran fer simulacions de sistemes de molts cossos que fins ara no eren possibles, esdevenint així unes eines idònies per fer propostes concretes de disseny de simuladors quàntics. Per altra banda, el control experimental en els sistemes de gasos ultra-freds ens permetrà realment dur a terme aquestes propostes teòriques i estudiar fenòmens de la Matèria Condensada que fins ara eren inaccessibles.

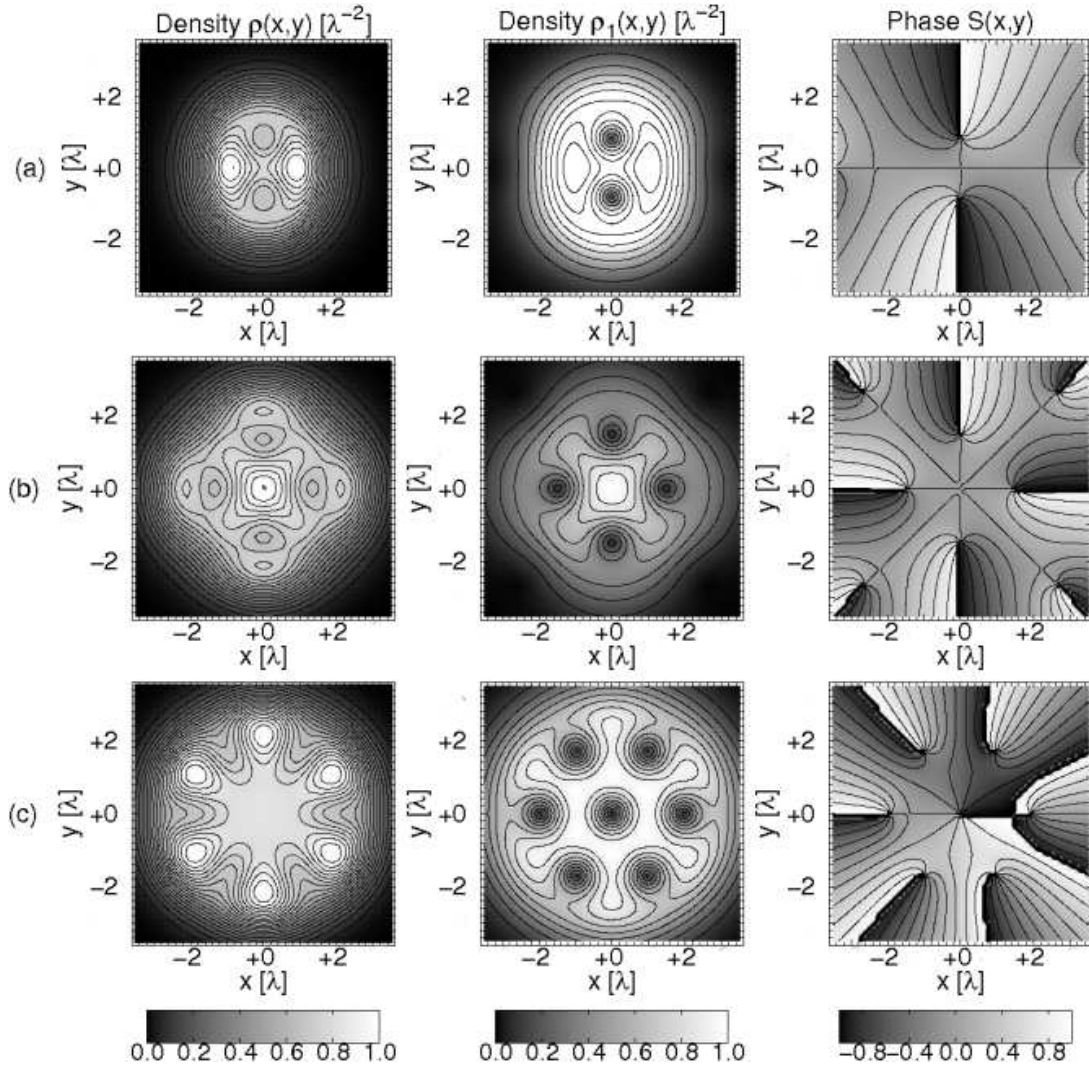


Figure 5: Per  $N = 6$  els primers dos gràfics en cada fila mostren la densitat de l'estat fonamental ( $\rho(x,y)$ ) i del paràmetre d'ordre ( $\rho_1(x,y)$ ) respectivament. El tercer gràfic mostra el la fase del paràmetre d'ordre. (a) Estructura de dos vòrtex a  $\Omega = 0.941$ . (b) Estructura de 4 vòrtex a  $\Omega = 0.979$ . (c) Estructura de 6 vòrtex a  $\Omega = 0.983$ .

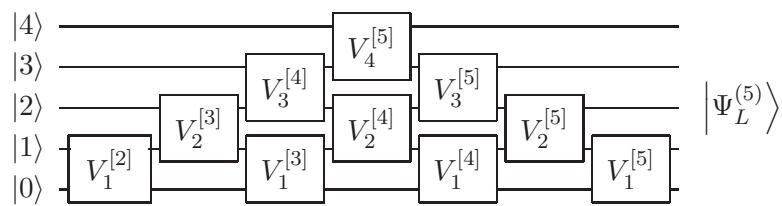


Figure 6: Circuit quàntic que produeix l'estat de Laughlin de 5 partícules actuant sobre un estat producte  $|01234\rangle$ .



# Contents

<b>Agraiments</b>	<b>v</b>
<b>Resum</b>	<b>vii</b>
<b>Introduction</b>	<b>1</b>
<b>I Entanglement in many body quantum systems</b>	<b>7</b>
<b>1 Entanglement</b>	<b>9</b>
1.1 Entanglement and LOCC transformations . . . . .	10
1.2 Separable and maximally entangled states . . . . .	10
1.2.1 Separable states . . . . .	10
1.2.2 Maximally entangled states . . . . .	11
1.2.3 Necessary and sufficient conditions to connect two pure states by LOCC operations . . . . .	12
1.3 Entanglement cost, entanglement distillation and entropy of entangle- ment . . . . .	13
1.3.1 Asymptotic limit . . . . .	13
1.3.2 Entanglement cost . . . . .	13
1.3.3 Entanglement distillation . . . . .	14
1.3.4 Entropy of entanglement . . . . .	14
1.3.5 Basic properties of entropy of entanglement . . . . .	15
1.4 Entanglement monotones and entanglement measures . . . . .	16
1.5 Entanglement in Condensed Matter physics . . . . .	17
1.5.1 Geometric entropy . . . . .	18
1.5.2 Single copy entanglement . . . . .	19
<b>2 Entanglement in many body quantum systems</b>	<b>21</b>

2.1	An explicit computation of entanglement entropy . . . . .	23
2.1.1	XX model . . . . .	23
2.1.2	Ground State . . . . .	24
2.1.3	Entanglement entropy of a block . . . . .	26
2.1.4	Scaling of the entropy . . . . .	29
2.1.5	Entanglement entropy and Toeplitz determinant . . . . .	31
2.2	Scaling of entanglement . . . . .	32
2.2.1	One-dimensional systems . . . . .	33
2.2.2	Conformal field theory and central charge . . . . .	34
2.2.3	Area law . . . . .	35
2.3	Other models . . . . .	37
2.3.1	The XY model . . . . .	37
2.3.2	The XXZ model . . . . .	39
2.3.3	Disordered models . . . . .	40
2.3.4	The Lipkin-Meshkov-Glick model . . . . .	42
2.3.5	Particle entanglement . . . . .	45
2.4	Renormalization of Entanglement . . . . .	46
2.4.1	Renormalization of quantum states . . . . .	46
2.4.2	Irreversibility of RG flows . . . . .	47
2.5	Dynamics of Entanglement . . . . .	49
2.5.1	Time evolution of the block entanglement entropy . . . . .	49
2.5.2	Bounds for time evolution of the block entropy . . . . .	51
2.5.3	Long range interactions . . . . .	52
2.6	Entanglement along quantum computation . . . . .	53
2.6.1	Quantum circuits . . . . .	53
2.6.2	Adiabatic quantum computation . . . . .	56
2.6.3	One way quantum computation . . . . .	59
2.7	Conclusion: entanglement as the barrier for classical simulations . . . . .	60
<b>3</b>	<b>Area-law in <math>D</math>-dimensional harmonic networks</b>	<b>61</b>
3.1	A brief review of the area law . . . . .	62
3.1.1	Volume vs. area law . . . . .	62
3.1.2	Locality and PEPS . . . . .	64
3.1.3	Renormalization group transformations on MPS and PEPS and the support for an area law . . . . .	66
3.1.4	Some explicit examples of area law . . . . .	67

3.1.5	Exceptions to the area law . . . . .	68
3.1.6	Physical and computational meaning of an area law . . . . .	69
3.2	Area law in $D$ dimensions . . . . .	70
3.2.1	The Hamiltonian of a scalar field in $D$ dimensions . . . . .	70
3.2.2	Geometric entropy and single-copy entanglement . . . . .	72
3.2.3	Perturbative computation for large angular momenta . . . . .	74
3.2.4	Area law scaling . . . . .	75
3.2.5	Vacuum reordering . . . . .	79
3.3	Entanglement loss along RG trajectories . . . . .	81
3.4	Conclusions . . . . .	83
<b>4</b>	<b>Violation of area-law for the entanglement entropy in spin 1/2 chains</b>	<b>85</b>
4.1	Real space Renormalization Group . . . . .	86
4.1.1	Introduction to real space RG approach . . . . .	86
4.1.2	Area-law violation for the entanglement entropy . . . . .	87
4.2	Solution of a spin model and its entanglement entropy . . . . .	91
4.2.1	Jordan-Wigner transformation . . . . .	91
4.2.2	Bogoliubov transformation . . . . .	92
4.2.3	Ground State . . . . .	92
4.2.4	Computation of the Von Neumann entropy corresponding to the reduced density matrix of the Ground State . . . . .	93
4.2.5	Summary of the calculation . . . . .	95
4.3	Expansion of the entanglement entropy . . . . .	95
4.4	Numerical Results . . . . .	97
4.5	Conclusions . . . . .	99
<b>II</b>	<b>Simulation of many body quantum systems</b>	<b>101</b>
<b>5</b>	<b>Ultra-cold atoms and the simulation of Condensed Matter physics</b>	<b>103</b>
5.1	Experimental control in cold atoms . . . . .	104
5.1.1	Temperature . . . . .	104
5.1.2	Trapping . . . . .	104
5.1.3	Interactions between atoms . . . . .	105
5.1.4	Optical lattices . . . . .	106
5.1.5	Several species . . . . .	106

5.2	Measurements . . . . .	107
5.2.1	Time of flight experiment . . . . .	107
5.2.2	Noise correlations . . . . .	108
5.3	Interesting Condensed Matter phenomena . . . . .	109
5.3.1	Bose-Hubbard model . . . . .	109
5.3.2	Disordered systems . . . . .	110
5.3.3	The Fractional Quantum Hall Effect and the Laughlin state . . .	110
<b>6</b>	<b>Simulation of the Laughlin state in an optical lattice</b>	<b>113</b>
6.1	One body Hamiltonian . . . . .	114
6.1.1	Harmonic case . . . . .	114
6.1.2	Quartic correction . . . . .	116
6.1.3	Maximum rotation frequency . . . . .	118
6.2	Many particle problem . . . . .	120
6.3	Results and discussion . . . . .	122
6.4	Conclusions . . . . .	127
<b>7</b>	<b>Symmetry breaking in small rotating cloud of trapped ultracold Bose atoms</b>	<b>129</b>
7.1	The model: macro-occupied wave function . . . . .	131
7.1.1	Description of the system . . . . .	131
7.1.2	Ordered structures in ground states . . . . .	132
7.1.3	Macro-occupied wave function . . . . .	134
7.2	Numerical results . . . . .	136
7.2.1	Order parameter . . . . .	136
7.2.2	Interference pattern . . . . .	139
7.2.3	Meaning of a time of flight measurement . . . . .	140
7.3	Conclusions . . . . .	141
<b>8</b>	<b>Quantum algorithm for the Laughlin state</b>	<b>145</b>
8.1	Algorithm design . . . . .	146
8.1.1	Two particles . . . . .	147
8.1.2	Three particles . . . . .	148
8.1.3	General case . . . . .	148
8.2	Circuit analysis . . . . .	150

---

8.2.1	Scaling of the number of gates and the depth of the circuit re- spect to $n$ . . . . .	150
8.2.2	Proof that the circuit is minimal . . . . .	151
8.2.3	Entanglement . . . . .	152
8.3	Experimental realization . . . . .	152
8.4	Conclusions . . . . .	155
<b>9</b>	<b>Conclusions and outlook</b>	<b>157</b>
<b>A</b>	<b>Contribution to the entanglement entropy and the single copy entan- glement of large angular momenta modes</b>	<b>161</b>
A.1	Perturbation theory . . . . .	161
A.1.1	Computation of the $\xi$ parameter . . . . .	162
A.1.2	Expansion of $\xi$ in terms of $l^{-1}$ powers . . . . .	165
A.1.3	The entropy . . . . .	167
A.1.4	The single-copy entanglement . . . . .	168
<b>B</b>	<b>Real space renormalization group in a XX model of 4 spins</b>	<b>171</b>



---

# Introduction

---

The interplay between Quantum Information and Condensed Matter Physics has been a fruitful line of research in recent years. Tools developed in the framework of Quantum Information theory, *e. g.* entanglement measures, have been used successfully to study quantum phase transitions in Condensed Matter systems. New numerical techniques as tensor networks have also been created in the context of Quantum Information in order to simulate many body quantum systems. Moreover, Condensed Matter Physics, together with Quantum Optics and Atomic Physics, are providing experimental grounds to develop prototypes of quantum computers and quantum simulators. In short, several Condensed Matter systems seem to provide suitable candidates to implement quantum computing paradigms.

In this thesis, we address both the issue of studying Condensed Matter systems from a Quantum Information perspective, and how some Condensed Matter systems can be used, in particular ultra-cold atoms, to provide the first quantum simulators. In the first part of the thesis, we address the issue of *entanglement in many body systems* and study the connections among the features of a Hamiltonian, the amount of entanglement of its ground state and its efficient numerical simulation. In the second part, we discuss how we can deal with those systems that are too entangled to be treated numerically with a classical computer. In particular, we study the possibilities of ultra-cold atoms in order to simulate many body quantum systems.

## Entanglement in many body quantum systems

The classical representation of an arbitrary quantum state of  $N$  particles

$$|\Psi\rangle = \sum_{i_1, \dots, i_N=1}^d c_{i_1, \dots, i_N} |i_1, \dots, i_N\rangle, \quad (19)$$

requires an exponential number ( $d^N$ ) of complex coefficients  $c_{i_1, \dots, i_N}$ . Therefore, the processing of the state, that is, the computation of its time evolution, or the calculation of observables also requires an exponential number of operations. This fact prevents us from simulating an arbitrary quantum system and makes it hard to study some interesting problems in Condensed Matter Physics that involve many particles (high temperature superconductivity, Fractional Quantum Hall Effect, etc.).

Nevertheless, in Nature, typical Hamiltonians (with local interactions and translationally invariant symmetry) have entangled ground states such that their *entanglement entropy* scales as the boundary of the region considered. This kind of scaling of the entanglement entropy, where entropy is proportional to the area instead of being extensive, is called *area-law*.

Area-laws is common to many ground states of local Hamiltonians. This makes these states very peculiar. In fact, if a quantum state of the Hilbert space is picked at random, it will exhibit a huge amount of entanglement. That is, the typical entropy of a subsystem is practically maximal and grows with its volume. Hence, a *typical* quantum state will asymptotically satisfy a volume law, and not an area law.

Ground states of local Hamiltonians are, therefore, a very small corner of the whole Hilbert space. Roughly speaking, if the ground state of a many-body system is slightly entangled, one might suspect that one can describe it with relatively few parameters and, therefore, it can be represented by classical means. This fact is, indeed, intelligently exploited in numerical approaches to study ground states of strongly correlated many body systems. It is not necessary to vary over all quantum states in variational approaches, but only over a much smaller set of states that are good candidates for approximating ground states of local Hamiltonians well, that is, states that satisfy an area law.

It would be very interesting by looking at a Hamiltonian, to know if it can be simulated by classical means or not. This leads to one of the most interesting issues in Quantum Information and Condensed Matter Physics: to rigorously understand the connections among the features of a Hamiltonian, the amount of entanglement of its ground state and its efficient numerical simulation.

## Simulation of many body quantum systems

From the previous section, another question emerges naturally: how can we deal with those systems that are highly entangled and cannot be treated with these efficient representations? Feynman, in 1982, realized that the most natural way to simulate Quantum Mechanics would be using a quantum computer [9]. Nevertheless, the present technology is still far from controlling more than tens of qubits (two level systems). In the most advanced prototypes, superposition states of 9 qubits are achieved in an ion trap [19]. In this context, ultra-cold atoms are seen as a very good candidates to construct the first *quantum simulators*, that is, experimentally controlled quantum systems that allow us to mimic the physics of some unknown quantum systems. Cold gases allow clean and controlled observation of many physical phenomena that have been studied in Condensed Matter systems. Atoms can be trapped, cooled, and manipulated with external electromagnetic fields, allowing many of the physical parameters that characterize their individual and collective behavior to be tuned.

A quantum simulator is a particular case of a quantum computer. In this context, another more ambitious approach to simulate quantum mechanics would consist in running an *exact quantum algorithm* that underlies the physics of a given quantum system in a quantum computer. Rather than searching for an analogical simulation, such an exact quantum circuit would fully reproduce the properties of the system under investigation without any approximation and for any experimental value of the parameters in the theory.

It is particularly interesting to devise new quantum algorithms for strongly correlated quantum systems of few particles. These could become the first non-trivial uses of a small size quantum computer.

## Outline

This thesis is made of two parts. In the first one, the issue of *entanglement in many body systems* is addressed. Chapter 1 is an introduction to the concept of entanglement. The entanglement measures that will be used in the rest of the thesis are also presented there.

In Chapter 2, some of the recent progress on the study of entropy of entanglement in many body quantum systems are reviewed. Emphasis is placed on the scaling properties of entropy for one-dimensional models at quantum phase transitions. We also

briefly describe the relation between entanglement and the presence of impurities, the idea of particle entanglement, the evolution of entanglement along renormalization group trajectories, the dynamical evolution of entanglement and the fate of entanglement along a quantum computation.

In Chapter 3, we focus on the area-law scaling of the entanglement entropy. With this aim, a number of ideas related to area law scaling of the geometric entropy from the point of view of Condensed Matter, Quantum Field Theory and Quantum Information are reviewed. An explicit computation in arbitrary dimensions of the entanglement entropy of the ground state of a discretized scalar free field theory that shows the expected area law result is also presented. For this system, it is shown that area law scaling is a manifestation of a deeper reordering of the vacuum produced by majorization relations. The same analysis for single-copy entanglement is presented. Finally, entropy loss along the renormalization group trajectory driven by the mass term is discussed.

In Chapter 4, we address the issue of how simple can a quantum system be such as to give a highly entangled ground state. In particular, we propose a Hamiltonian of a XX model with a ground state whose entropy scales linearly with the size of the block. It provides a simple example of a one dimensional system of spin-1/2 particles with nearest neighbor interactions that violates area-law for the entanglement entropy.

The second part of this thesis deals with the problem of simulating quantum mechanics for highly entangled systems. Two different approaches to this issue are considered. The one presented in Chapters 5, 6 and 7 consists of using ultra-cold atoms systems as quantum simulators.

In Chapter 5, we review some experimental techniques related to cold atoms that allow to simulate strongly correlated many body quantum systems. A few interesting Condensed Matter systems that could be simulated by ultra-cold atoms are listed.

In Chapter 6, an explicit example of simulation is presented. First, we show that the Laughlin state is the ground state of a cloud of repulsive interacting bosons in a rotating harmonic trap when the rotation frequency is large enough. Then, we analyze the proposal of achieving a Mott state of Laughlin wave functions in an optical lattice [17] and study the consequences of considering anharmonic corrections to each single site potential expansion that were not taken into account until now.

In Chapter 7, the character of the ground state of a cloud of repulsive interacting bosons in a rotating harmonic trap is studied. This time we focus on lower rotation frequencies than the typical ones in Chapter 6. In particular, we discuss whether

these states correspond to strongly correlated states (like the Laughlin case) or, on the contrary, they could be described by means of an order parameter, in a way similar to the mean-field approach. This order parameter description of small rotating clouds will allow us to address in a different point of view the issue of symmetry breaking in Bose-Einstein condensates and the problem of the interpretation of a time of flight measurement in the interference experiment of two Bose - Einstein condensates.

Finally, we consider a different approach to simulate strongly correlated systems: use small quantum computers to simulate them. In Chapter 8, an explicit quantum algorithm that creates the Laughlin state for an arbitrary number of particles  $n$  in the case of filling fraction equal to one is presented. We further prove the optimality of the circuit using permutation theory arguments and we compute exactly how entanglement develops along the action of each gate. We also discuss its experimental feasibility decomposing the qudits and the gates in terms of qubits and two qubit-gates as well as the generalization to arbitrary filling fraction.

In Chapter 9, we close this thesis with the conclusions, the most important open questions of the issues dealt with in this thesis, as well as, a brief discussion on the possible future directions of our work.



## **Part I**

# **Entanglement in many body quantum systems**



---

# Entanglement

---

One of the most celebrated discussions of Quantum Mechanics is the Einstein-Podolsky-Rosen paradox [20], in which strong correlations are observed between presently non-interacting particles that have interacted in the past. These non-local correlations occur only when the quantum state of the whole system is *entangled*, *i. e.*, not representable as a direct product of states of the parts. In particular, a pair of spin-1/2 particles prepared in the superposition state

$$|\Psi\rangle = \frac{1}{\sqrt{2}}(|00\rangle + |11\rangle), \quad (1.1)$$

and then separated, exhibit perfectly correlated spin components when locally measured along any axis. Bell showed that these statistics violate inequalities that must be satisfied by any classical local hidden variable model [21]. The repeated experimental confirmation of the non-local correlations predicted by quantum mechanics [22] forces to abandon, at least, one of the two assumptions (reality or locality) of the local hidden variable models.

In Quantum Information, entanglement is an indispensable resource to perform any quantum information process. For instance, quantum teleportation [23], quantum superdense coding [24] or quantum cryptography based on quantum key distribution protocol [25] require the sharing of entangled states to be performed. Thus, the utility of a quantum state to perform quantum information processes depends on

how much entangled it is. As more entangled a state is, it has more possibilities to be used in quantum information tasks.

In this chapter, we present an introduction to the issue of quantifying entanglement and, in particular, to the entropy of entanglement. Interested readers are encouraged to study several review articles that exist on the field [26, 27, 28, 29, 30, 31, 32, 33, 34].

## 1.1 Entanglement and LOCC transformations

Here, we will focus on bipartite entanglement, *i. e.*, entanglement of systems consisting of two parts  $A$  and  $B$  that are too far apart to interact, and whose state, pure or mixed, lies in a Hilbert space  $\mathcal{H} = \mathcal{H}^A \otimes \mathcal{H}^B$  that is the tensor product of Hilbert spaces of these parts. For simplicity, from now on, we will consider that  $\mathcal{H}^A$  and  $\mathcal{H}^B$  have the same dimension  $d$ .

*Entanglement* can be defined as the property that some compound states have of giving strong non-local correlations that cannot be generated by *local operations and classical communication* (LOCC). In the case of bipartite systems, we consider these transformations to be performed by two observers, Alice and Bob, each having access to one of the sub-systems. Alice and Bob are allowed to perform local actions, unitary transformations and measurements, on their respective subsystems along with whatever ancillary systems they might create in their own laboratories. Also classical communication between them is allowed in order to coordinate their actions.

Notice that the notion of entanglement that we have defined depends strictly on the definition of LOCC transformations. Had we consider other restrictions, the relations between two states to be more and less entangled would be different.

## 1.2 Separable and maximally entangled states

### 1.2.1 Separable states

Let us show first that there are two extreme cases: states with no entanglement and states that are maximally entangled. The states that contain no entanglement are called *separable* states [35], and they can always be expressed as

$$\rho_{AB} = \sum_{i=1}^m p_i \rho_A^i \otimes \rho_B^i, \quad (1.2)$$

where  $p_i$  is a classical probability distribution ( $p_i \geq 0 \forall i$  and  $\sum_i p_i = 1$ ) and  $m$  an arbitrary integer number. These states are not entangled because they can trivially be created by LOCC. Alice samples from the distribution  $p_i$ , informs Bob of the outcome  $i$ , and then Bob locally creates  $\rho_B^i$  and discards the information about the outcome  $i$ . In fact, it can be shown that a quantum state  $\rho$  may be generated perfectly using LOCC if and only if it is separable. Thus, we would have been able to define entangled states as those that cannot be written as Eq. (1.2).

For pure states, the states with no entanglement are called *product states*, and are all those states that can be written as

$$|\Psi_{AB}\rangle = |\Phi_A\rangle \otimes |\Phi_B\rangle. \quad (1.3)$$

### 1.2.2 Maximally entangled states

Suppose that a quantum state  $\rho$  can be transformed with certainty to another quantum state  $\sigma$  using LOCC operations. Then, anything that can be done with  $\sigma$  and LOCC operations, can also be achieved with  $\rho$  and LOCC operations. Hence the usefulness of quantum states cannot increase under LOCC operations, and one can rightfully state that  $\rho$  is at least as entangled as  $\sigma$ , i. e.,

$$\rho \xrightarrow{LOCC} \sigma \Rightarrow E(\rho) \geq E(\sigma) \quad (1.4)$$

where  $E()$  is a function that should quantify entanglement. Due to our definition of entanglement, the amount of entanglement of a given state cannot be increased by performing LOCC operations.

Thus, LOCC provides a notion of which states are entangled (the non-separable ones) and can also assert that one state is more entangled than another if it is possible to connect them by LOCC. A question that emerges naturally is, then, whether there exist states that are more entangled than all the others, that is, that can be transformed into any state by LOCC. In fact, in bipartite systems, these states exist and they correspond to any pure state that is local unitary equivalent to

$$|\psi_{AB}\rangle = \frac{1}{\sqrt{d}} (|0,0\rangle + |1,1\rangle + \dots + |d-1,d-1\rangle). \quad (1.5)$$

These states are called *maximally entangled states*. This means that any pure or mixed state of  $\mathcal{H}$  can be prepared from such states with certainty using only LOCC operations. Notice that the state presented above in Eq. (1.1) that violates Bell inequalities is maximally entangled for  $d = 2$ .

Let us point out that the notion of maximally entangled states is independent of any specific quantification of entanglement. In the bipartite case, LOCC operations tries to impose an order among more and less entangled states: if  $\rho$  can be converted into  $\sigma$  by means of LOCC operations,  $\rho$  is at least as entangled as  $\sigma$ . In fact, this has allowed us to define *maximally entangled states*. Nevertheless, in general, this notion of order is not complete, since there exist states that cannot be connected using LOCC.

### 1.2.3 Necessary and sufficient conditions to connect two pure states by LOCC operations

Only for pure states there is a criterion that establishes when two states can be connected by LOCC. If we have two pure states,  $|\Psi_1\rangle$  and  $|\Psi_2\rangle$ , by means of a Schmidt decomposition, they can always be written as

$$\begin{aligned} |\Psi_1\rangle &= \sum_{i=1}^d \lambda_i |\phi_i^A\rangle |\phi_i^B\rangle \\ |\Psi_2\rangle &= \sum_{i=1}^d \lambda'_i |\psi_i^A\rangle |\psi_i^B\rangle, \end{aligned} \quad (1.6)$$

where the Schmidt coefficients  $\lambda_i$  and  $\lambda'_i$  are given in decreasing order ( $\lambda_i^{(j)} > \lambda_j^{(i)}$  if  $i < j$ ) and  $\{|\phi_i^{A,B}\rangle\}$  and  $\{|\psi_j^{A,B}\rangle\}$  are two orthonormal basis.

In Ref. [36], it has been shown that a LOCC transformation converting  $|\psi_1\rangle$  into  $|\psi_2\rangle$  with unit probability exists if and only if the  $\{\lambda_i\}$  are *majorized* by  $\{\lambda'_i\}$ , i.e. if for all  $1 \leq k < d$  we have that

$$\sum_{i=1}^k \lambda_i^2 \leq \sum_{i=1}^k (\lambda'_i)^2, \quad (1.7)$$

where normalization ensures that  $\sum_{i=1}^d \lambda_i^2 = \sum_{i=1}^d (\lambda'_i)^2 = 1$ . This is a strong condition, and tells us that almost of pure states cannot be transformed between them using LOCC operations.

## 1.3 Entanglement cost, entanglement distillation and entropy of entanglement

### 1.3.1 Asymptotic limit

Thus, even for pure states there are *incomparable* states, that is, pairs of states that cannot be converted into the other by means of LOCC with certainty.

In order to make possible the conversion of any pair of states, and, in this way, establish a complete order between them, let us relax the conditions of LOCC and introduce the *asymptotic regime*. It consists of instead of asking whether for a single pair of particles the initial state  $\rho$  may be transformed to a final state  $\sigma$  by LOCC operations, ask whether for some large integers  $m, n$  it is possible implement the transformation  $\rho^{\otimes n} \rightarrow \sigma^{\otimes m}$ . Moreover, an imperfect transformation will be allowed, in such a way that  $\rho^{\otimes n}$  only must tend to  $\sigma^{\otimes m}$  in the asymptotic limit  $n, m \rightarrow \infty$  with its ratio  $r \equiv n/m$  constant.

Notice that the largest possible ratio  $r = m/n$  for which one may achieve this conversion indicates the relative entanglement content of these two states. If  $r > 1$ , it means that more  $\rho$ 's than  $\sigma$ 's are required to do the transformation, and hence,  $\sigma$  is more entangled than  $\rho$ .

As we are going to see next, this asymptotic setting yields a unique total order on pure states, and as a consequence leads to a very natural measure of entanglement that is essentially unique.

### 1.3.2 Entanglement cost

For a given state  $\rho$ , the *entanglement cost* quantifies the maximal possible rate  $r$  at which one can convert blocks of 2-qubit maximally entangled states into output states that approximate many copies of  $\rho$ , such that the approximations become vanishingly small in the limit of large block sizes. This can be mathematically written as

$$E_C(\rho) \equiv \inf \left\{ r : \lim_{n \rightarrow \infty} \left[ \inf_{\Psi} D \left( \rho^{\otimes n}, \Psi \left( |\Psi_{rn}^+\rangle \langle \Psi_{rn}^+| \right) \right) \right] = 0 \right\} \quad (1.8)$$

where  $\Psi$  represents a general trace preserving LOCC operations,  $|\Psi_{rn}^+\rangle \langle \Psi_{rn}^+|$  is the density matrix of a  $rn$  dimensional maximally entangled state, and  $D(\sigma, \sigma')$  is a suitable measure of distance between states [37, 38].

Notice that a block of  $m = rn$  2-qubit maximally entangled states is as entangled as a maximally entangled qudit with  $d = m$ .

### 1.3.3 Entanglement distillation

Roughly speaking, entanglement cost measures how many maximally entangled 2-qubits are required (on average) to create a copy of  $\rho$  by means of LOCC in the asymptotic limit. Naturally, another entanglement measure can be defined quantifying the reverse process, *i. e.* how many maximally entangled 2-qubits can we extract performing LOCC operations on a state  $\rho$  in the asymptotic limit. This entanglement measure is called *entanglement distillation* and is rigorously defined by

$$E_D(\rho) \equiv \sup \left\{ r : \lim_{n \rightarrow \infty} \left[ \inf_{\Psi} D \left( \Psi(\rho^{\otimes n}) - |\Psi_{rn}^+\rangle\langle\Psi_{rn}^+| \right) \right] = 0 \right\}. \quad (1.9)$$

These two entanglement measures have to fulfill the following constraint

$$E_C(\rho) \geq E_D(\rho) \quad \forall \rho, \quad (1.10)$$

since, if not, it would be possible to create entanglement using LOCC transformations. It is natural to wonder in which condition the previous inequality is saturated and  $E_C(\rho) = E_D(\rho)$ . In Ref. [39], it was shown that for pure states, entanglement distillation and entanglement cost coincide and are equal to the *entropy of entanglement*.

The fact that entanglement cost and entanglement distillation coincide for the pure states case is very relevant, since it allows us to connect always an arbitrary pair of pure states and, hence, order them from an entanglement criterion. In the asymptotic limit for pure states, then, LOCC transformations impose a unique order via the entropy of entanglement.

### 1.3.4 Entropy of entanglement

The entropy of entanglement for a pure state  $|\Psi\rangle \in \mathcal{H}^A \otimes \mathcal{H}^B$  is the von Neumann entropy of the reduced of each part of the system. That is,

$$S(A) \equiv S(\rho_A) = -\text{tr} (\rho_A \log_2 \rho_A), \quad (1.11)$$

where  $\rho_A = \text{tr}_B(|\psi\rangle_{AB}\langle\psi|_{AB})$ . According to the Schmidt decomposition, for any pure bipartite state we can always find two orthonormal basis  $\{|\varphi_i\rangle_A\}$  and  $\{|\phi_j\rangle_B\}$  such that the state  $|\psi\rangle$  can be written as

$$|\psi\rangle = \sum_{i=1}^d \lambda_i |\phi_i^A\rangle |\phi_i^B\rangle, \quad (1.12)$$

where  $\lambda_i$  are chosen real and positive. Then, the entanglement entropy can also be computed as the Shannon entropy of the square of the Schmidt coefficients,

$$S(A) = S(B) = - \sum_i \lambda_i^2 \log \lambda_i^2, \quad (1.13)$$

where it is trivial to see that  $S_A = S_B$ .

### 1.3.5 Basic properties of entropy of entanglement

From the definition of entropy of entanglement in Eq. (1.11) it is possible to deduce some of its properties.

- If the composite system  $AB$  is in a product state,  $S(A) = S(B)$ .
- Suppose  $p_i$  are probabilities and the states  $\rho_i$  have support on orthogonal subspaces. Then,

$$S \left( \sum_i p_i \rho_i \right) = H(p_i) + \sum_i p_i S(\rho_i), \quad (1.14)$$

where  $H(p_i) \equiv - \sum_i p_i \log p_i$  is the Shannon entropy of the set of probabilities  $p_i$ .

- **Joint entropy theorem:** In the previous equation, let us assume that  $|i\rangle$  are orthogonal states for  $A$ , and  $\rho_i$  is any set of density operators for  $B$ . Then,

$$S \left( \sum_i p_i |i\rangle\langle i| \otimes \rho_i \right) = H(p_i) + \sum_i p_i S(\rho_i). \quad (1.15)$$

- **Klein's inequality:** The quantum relative entropy, defined as  $S(\rho||\sigma) \equiv \text{tr} (\rho \log \rho) - \text{tr} (\rho \log \sigma)$ , is non-negative, i. e.,

$$S(\rho||\sigma) \geq 0, \quad (1.16)$$

with equality if and only if  $\rho = \sigma$ .

These results allow us to prove the following properties and inequalities which are more frequently used:

- **Entropy of a tensor product:**

$$S(\rho \otimes \sigma) = S(\rho) + S(\sigma). \quad (1.17)$$

- **Sub-additivity inequality:**

$$S(A, B) \leq S(A) + S(B). \quad (1.18)$$

- **Triangle inequality:**

$$S(A, B) \geq |S(A) - S(B)|. \quad (1.19)$$

- **Concavity inequality:**

$$S\left(\sum_i p_i \rho_i\right) \geq \sum_i p_i S(\rho_i). \quad (1.20)$$

- **Strong sub-additivity inequality:** The sub-additivity and triangle inequalities for two quantum systems can be extended to three systems  $A$ ,  $B$ , and  $C$ . The result is the *Strong sub-additivity* inequality and it states that,

$$S(A, B, C) + S(B) \leq S(A, B) + S(B, C). \quad (1.21)$$

Some of these properties that entropy of entanglement has in a natural way will be required to other measures of entanglement.

## 1.4 Entanglement monotones and entanglement measures

It has been shown that the entropy of entanglement is a good measure of entanglement for pure states. Nevertheless, the situation is not so clear for mixed states, since the notion of reversibility disappears and it is not possible to connect two arbitrary mixed states with LOCC transformations.

This forces us to change the ordering approach followed so far, by an axiomatic one. An *entanglement monotone*,  $E(\rho)$ , is defined as any mapping from density matrices into positive real numbers:

$$E : \mathcal{H} \rightarrow \mathbb{R}^+, \quad (1.22)$$

with the following properties [28, 40, 41]:

- (i)  $E(\rho) = 0$  if and only if  $\rho$  is separable.
- (ii) If  $\rho$  and  $\sigma$  are two states Local Unitary equivalents, i. e., can be converted one into each other by means of local unitary operations, then  $E(\rho) = E(\sigma)$ .

- (iii)  $E$  does not increase on average under LOCC, i.e.,

$$E(\rho) \geq \sum_i p_i E \left( \frac{A_i \rho A_i^\dagger}{\text{tr} A_i \rho A_i^\dagger} \right) \quad (1.23)$$

where the  $A_i$  are the Kraus operators describing some LOCC protocol and the probability of obtaining outcome  $i$  is given by  $p_i = \text{tr} (A_i \rho A_i^\dagger)$ .

The term *entanglement measure* will be used for any quantity that also satisfies the condition:

- (iv) For pure state  $|\psi\rangle\langle\psi|$  the measure reduces to the entropy of entanglement  $E(|\psi\rangle\langle\psi|) = S(\text{tr}_B(|\psi\rangle\langle\psi|))$ .

Moreover, for the entanglement measures, sometimes it is convenient to demand two more properties:

- (v) Convexity:  $E(\sum_i p_i \rho_i) \leq \sum_i p_i E(\rho_i)$ .
- (vi) Additivity:  $E(\rho^{\otimes n}) = nE(\rho)$ .

Another important feature of an entanglement measure is if it can be efficiently computed. For instance, the *entanglement of formation*, defined as

$$E_F(\rho) = \inf \sum_i p_i S(|\psi_i\rangle\langle\psi_i|), \quad (1.24)$$

where the infimum is taken over all the possible decompositions  $\rho = \sum_i |\psi_i\rangle\langle\psi_i|$ , is, in general, very difficult to determine.

A lot of bipartite *entanglement monotones* and *entanglement measures* have been proposed in the literature. A detailed explanation of them can be found in several reviews [26, 27, 28, 29, 30, 31, 32, 33, 34]. Nevertheless, except for the pure states case, there is not an entanglement measure that satisfies all the required conditions and it is easy to compute.

## 1.5 Entanglement in Condensed Matter physics

So far, we have seen entanglement as a required resource to perform quantum information processes. Along the next two chapters, we will see that entanglement is, furthermore, a useful tool to study Condensed Matter systems. For instance, we will

realize that the scaling of the entanglement entropy is a good witness for quantum phase transitions, or that entanglement gives us a notion of the amount of correlations of the ground state.

A lot of studies of different measures of entanglement have been presented recently for several Condensed Matter systems. We cannot discuss all of them here, so we will focus on the *geometric entropy* and the *single copy entanglement*.

Let us just mention that in Refs. [42, 43, 44, 45] quantum phase transitions are characterized in terms of the overlap (fidelity) function between two ground states obtained for two close values of external parameters. When crossing the critical point a peak of the fidelity is observed. Also the *concurrence*, that is a good measure of entanglement for the two q-bits case, has been extensively used to study correlations, dynamics of entanglement, and quantum phase transitions in several spin models (see Ref. [30]).

### 1.5.1 Geometric entropy

In general a set of particles will be distributed randomly over space. Entanglement entropy can be computed for all sorts of partitions of the system, yielding information about the quantum correlations among the chosen subparts. A particular class of physical systems are those made of local quantum degrees of freedom which are arranged in chains or, more generally, in lattices. For such systems it is natural to analyze their entanglement by studying geometrical partitions, that is, computing the entanglement entropy between a set of contiguous qubits versus the rest of the system. We shall refer to this particular case of entanglement entropy [3] as *geometric entropy* [46] (also called *fine grained entropy* in [47]).

The appearance of scaling of the geometric entropy with the size of the sub-system under consideration has been shown to be related to quantum phase transitions in one-dimensional systems, further reflecting the universality class corresponding to the specific phase transition under consideration [46, 4]. Broadly speaking, a large entropy is related to the presence of long distance correlations, whereas a small entropy is expected in the presence of a finite correlation length. The precise scaling of geometric entropy does eventually determine the limits for today's efficient simulation of a physical quantum system on a classical computer.

### 1.5.2 Single copy entanglement

Another measure of entanglement for pure states is *single copy entanglement*. We have seen that the entropy of entanglement has an asymptotic operational meaning. Given infinitely many copies of a bipartite quantum state, it quantifies how many EPR pairs can be obtained using local operations and classical communication. The single-copy entanglement, defined by

$$E_1(\rho_A) = -\log \rho_A^{(1)}, \quad (1.25)$$

where  $\rho_A^{(1)}$  is the maximum eigenvalue of  $\rho_A$ , provides the amount of maximal entanglement that can be extracted from a single copy of a state by means of LOCC [48, 49, 50, 51]. As we shall see later on, the von Neumann entropy and the single-copy entanglement appear to be deeply related in some Condensed Matter systems in any number of dimensions.



---

# Entanglement in many body quantum systems

---

Quantum systems are ultimately characterized by the observable correlations they exhibit. For instance, an observable such as the correlation function between two spins in a typical spin chain may decay exponentially as a function of the distance separating them or, in the case the system undergoes a phase transition, algebraically. The correct assessment of these quantum correlations is tantamount to understanding how entanglement is distributed in the state of the system. This is easily understood as follows. Let us consider a connected correlation

$$\langle \Psi | O_i O_j | \Psi \rangle_c \equiv \langle \Psi | O_i O_j | \Psi \rangle - \langle \Psi | O_i | \Psi \rangle \langle \Psi | O_j | \Psi \rangle, \quad (2.1)$$

where  $O_i$  and  $O_j$  are operators at sites  $i$  and  $j$  respectively. This connected correlator would vanish identically for any product state  $|\Psi\rangle = \otimes_i |\psi_i\rangle$ . That is,  $O_i \otimes O_j$  is a product operator and, consequently, its correlations can only come from the amount of entanglement in the state  $|\Psi\rangle$ . It follows that the ground state of any interesting system will be highly correlated and, as a particular case, even the vacuum displays a non-trivial entanglement structure in quantum field theories.

Notice that, at this point, our emphasis has moved from Hamiltonians to states. It is perfectly sensible to analyse entanglement properties of specific states per se, which may be artificially created using a post-selection mechanism or may effectively

be obtained in different ways using various interactions. We are, thus, concerned with the entanglement properties that characterize a quantum state. Yet, we shall focus on states that are physically relevant. In particular, we shall study the entanglement properties of ground states of Hamiltonians that describe the interaction present in spin chains.

It is clear that the property of entanglement can be made apparent by studying correlations functions on a given state. We could consider two-, three- or n-point connected correlation functions. Any of them would manifest how the original interactions in the Hamiltonian have operated in the system to achieve the observed degree of entanglement. For instance, free particles (Gaussian Hamiltonians) produce n-point correlators that reduce to products of two-point correlators *via* Wick's theorem. Nonetheless, the study of specific correlation functions is model dependent. How can we compare the correlations of a Heisenberg Model with those of Quantum Chromodynamics? Each theory brings its own set of local and non-local operators that close an Operator Product Expansion. Different theories will carry different sets of operators, so that a naive comparison is hopeless. A wonderful possibility to quantify degrees of entanglement for unrelated theories emerges from the use of Renormalization Group ideas and the study of universal properties. For instance, a system may display exponential decays in its correlations functions which is globally controlled by a common correlation length. A model with a larger correlation length is expected to present stronger long-distance quantum correlations.

We may as well try to find a universal unique figure of merit that would allow for a fair comparison of the entanglement present in *e. g.* the ground state of all possible theories. Such a figure of merit cannot be attached to the correlations properties of model-dependent operators since it would not allow for comparison among different theories. The way to overcome this problem is to look for an operator which is defined in every theory. It turns out that there is only one such operator: the stress tensor. To be more precise, we can use the language of conformal field theory which establishes that there always is a highest weight operator that we call the Identity. The Identity will bring a tower of descendants, the stress tensor being its first representative. Indeed, the stress tensor is always defined in any theory since it corresponds to the operator that measures the energy content of the system and it is the operator that couples the system to gravity. Correlators of stress tensor operators are naturally related to entanglement. In particular, the coefficient of the two-point stress tensor correlator in a conformal field theory in two dimensions corresponds to the central

charge of the theory.

There is a second option to measure entanglement in a given state with a single measure of entanglement which is closer in spirit to the ideas of Quantum Information. The basic idea consists of using the von Neumann (entanglement) entropy of the reduced density matrix of a sub-part of the system which is analysed. Indeed, the entanglement entropy quantifies the amount of surprise that a sub-part of a system finds when discovering it is correlated to the rest of the system. Therefore, entanglement entropy is a *bona fide* measure of the correlations in the system. The advantage of the von Neumann entropy of entanglement is that it can be defined for any system. We expect its general properties, as the way it scales with the size of the sub-part of the system we are considering, should characterize the quantum state in a quite refined way.

It is tantalizing to exhaustively explore the behaviour of the entropy of entanglement in relevant physical systems. For instance, will the entropy of entanglement scale differently at a critical point as compared to a non-critical one? Will scaling properties depend on the dimensionality of the system. Is disorder relevant for long-distance correlations? Are there non-local systems where entropy obeys some singular behaviour? How does entanglement renormalize? How does entanglement evolve dynamically? We can even go further away from standard dynamical models and question whether entanglement is somehow related to computational complexity problems, both NP-complete and QMA-complete. We shall now briefly review some of these questions.

## 2.1 An explicit computation of entanglement entropy

Let us start our discussion with the study of the behaviour of entanglement at different regimes (critical and non-critical) of the XX model. As we shall see, entanglement entropy will be a good tool to describe the properties of the quantum phase transition which characterizes this model [4, 5].

### 2.1.1 XX model

We shall now present a computation of entanglement entropy for the reduced density matrix of the ground state of the widely studied XX model [4, 5]. This theory captures the non-trivial structure of a quantum phase transition, while remaining simple

enough to carry explicit computations throughout. The XX model consists of a chain of  $N$  spin  $\frac{1}{2}$  particles with nearest neighbour interactions and an external magnetic field. Its Hamiltonian is given by

$$H_{XX} = -\frac{1}{2} \sum_{l=0}^{N-1} (\sigma_l^x \sigma_{l+1}^x + \sigma_l^y \sigma_{l+1}^y) + \frac{1}{2} \lambda \sum_{l=0}^{N-1} \sigma_l^z, \quad (2.2)$$

where  $l$  labels the  $N$  spins,  $\lambda$  is the magnetic field and  $\sigma_l^\mu$  ( $\mu = x, y, z$ ) are the Pauli matrices at site  $l$ .

Without loss of generality, we are going to consider that the magnetic field is oriented in the positive Z direction ( $\lambda > 0$ ), since, if this was not the case, we could always map the system onto an equivalent one with  $\lambda > 0$  by simply interchanging the spin states up and down.

### 2.1.2 Ground State

Next, we need to compute the ground state  $|GS\rangle$  of the XX Hamiltonian (2.2). In order to do this, we will follow two steps: (i) first, we will perform a Jordan-Wigner transformation to rewrite  $H_{XX}$  as a quadratic form of fermionic operators, and then (ii) we will take profit of the translational invariance of the system realizing a Fourier transform which will diagonalize the Hamiltonian. A third step which is needed in the more general XY model, the Bogoliubov transformation, is not necessary in this particular case. Let us remark that this computation is standard and appears in many text books [52, 53, 54].

The Jordan-Wigner transformation maps a spin chain of interacting qubits onto an equivalent system of interacting fermions. This powerful transform is defined by the following relation between the Pauli matrices and the creation and annihilation of the fermionic modes

$$a_l = \left( \prod_{m=0}^{l-1} \sigma_m^z \right) \frac{\sigma_l^x - i\sigma_l^y}{2}. \quad (2.3)$$

We, indeed, can check that the fermionic operators  $a_l$  fulfil the canonical commutation relations

$$\{a_l^\dagger, a_m\} = \delta_{lm}, \quad \{a_l, a_m\} = 0. \quad (2.4)$$

The idea behind the transformation is to identify the state of the spin  $l$  (0 or 1 in the computational basis) with the occupation number of the corresponding fermionic mode. Thus, in Eq. 2.3, the factor  $(\sigma_l^x - i\sigma_l^y)/2$  corresponds to the operator  $|0\rangle\langle 1|$  in

the computational basis, and the product  $\prod_{m=0}^{l-1} \sigma_m^z$  generates the appropriate sign in order to satisfy the commutation relations.

The Jordan-Wigner transformation casts the XX Hamiltonian onto

$$H_{XX} = - \sum_{l=0}^{N-1} (a_l^\dagger a_{l+1} + a_{l+1}^\dagger a_l) + \lambda \sum_{l=0}^{N-1} a_l^\dagger a_l, \quad (2.5)$$

which corresponds to a model of free fermions with chemical potential  $\lambda$ .

Now, let us exploit the translational symmetry of the system by introducing the Fourier transformed fermionic operators

$$b_k = \frac{1}{\sqrt{N}} \sum_{l=0}^{N-1} a_l e^{-i \frac{2\pi}{N} k l}, \quad (2.6)$$

where  $0 \leq k \leq N-1$ . As the Fourier transform is a unitary transformation, these new  $b_k$  operators also satisfy the canonical commutation relations and, therefore, they are fermionic operators.

The Hamiltonian, written in terms of these  $b_k$  operators, displays a diagonal structure

$$H_{XX} = \sum_{k=0}^{N-1} \Lambda_k b_k^\dagger b_k, \quad (2.7)$$

where the energy that penalizes (or favours, depending on the sign) the occupation of mode  $k$  is

$$\Lambda_k = \lambda - 2 \cos \frac{2\pi k}{N}. \quad (2.8)$$

We have assumed that the system satisfied periodic boundary conditions. If this was not the case, the Hamiltonian would not be diagonal due to an extra term proportional to  $\frac{1}{N}$ . In the thermodynamic limit, therefore, this extra term disappears.

We realize that, on one hand, if  $\lambda > 2$ , then  $\Lambda_k \geq 0 \forall k$ . This implies that the ground state of the system is the state annihilated by all  $b_k$  operators

$$b_k |GS\rangle = 0 \quad \forall k, \quad (2.9)$$

and, therefore, it has 0 energy.

On the other hand, if  $2 > \lambda \geq 0$ , the ground state is the state annihilated by the operators  $b_k$  with  $\Lambda_k > 0$  and  $b_m^\dagger$  with  $\Lambda_m < 0$ ,

$$\begin{aligned} b_k |GS\rangle &= 0 \quad \text{if } \Lambda_k > 0 \\ b_m^\dagger |GS\rangle &= 0 \quad \text{if } \Lambda_m < 0, \end{aligned} \quad (2.10)$$

and its energy is simply  $\sum_m \Lambda_m \forall \Lambda_m < 0$ . In Fig. 2.1 and Eq. (2.8), we can see that if  $k_c \geq k \geq 0$  or  $N - 1 \geq k \geq N - k_c$ , where  $k_c$  is defined by

$$k_c = \left\lfloor \frac{N}{2\pi} \arccos\left(\frac{\lambda}{2}\right) \right\rfloor, \quad (2.11)$$

then  $\Lambda_k < 0$ , whereas for the rest of cases  $\Lambda_k \geq 0$ . In Eq. (2.11), the brackets  $\lfloor \cdot \rfloor$  represent the *floor* function.

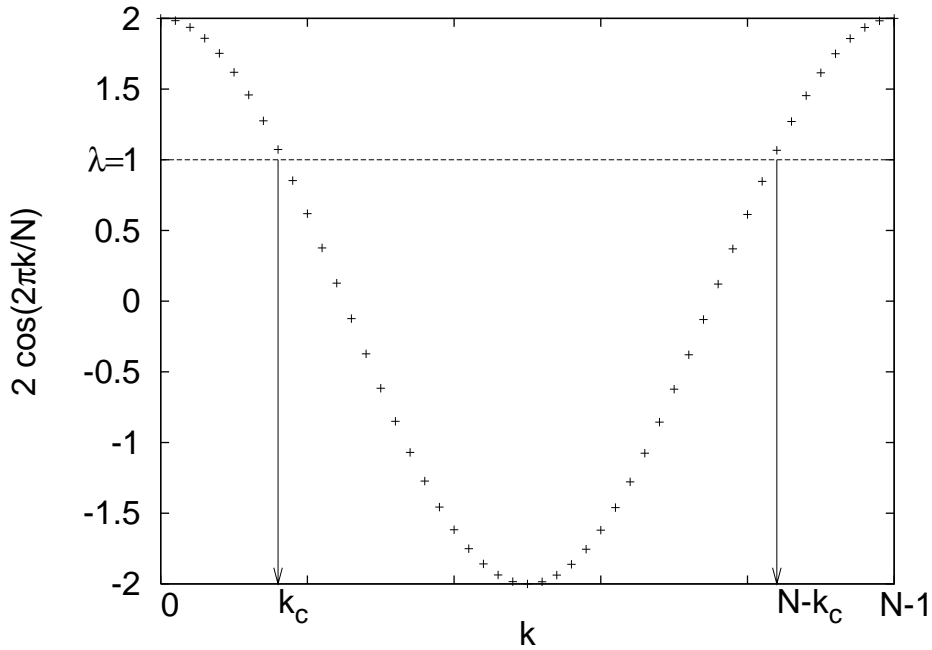


Figure 2.1: The two terms of  $\Lambda_k$ , Eq. (2.8), are plotted for the particular case  $\lambda = 1$ . We realize that if  $2 \cos\left(\frac{2\pi k}{N}\right) > \lambda$ ,  $\Lambda_k < 0$  while if  $2 \cos\left(\frac{2\pi k}{N}\right) < \lambda$ ,  $\Lambda_k > 0$ .

### 2.1.3 Entanglement entropy of a block

The strategy to get the Von Neumann entropy of a block of  $L$  spins first consists in computing the correlation matrix  $\langle a_m^\dagger a_n \rangle$  of the GS in this block. Then, the eigenvalues of this correlation matrix are related with the eigenvalues of the reduced density matrix of the block which are required to determine the entanglement entropy.

The simple structure of the GS, shown in Eqs. (2.9) and (2.10), makes easy to

compute its correlation matrix

$$\langle b_p^\dagger b_q \rangle = \begin{cases} \delta_{pq} & \text{if } \Lambda_p < 0 \\ 0 & \text{if } \Lambda_p > 0 \end{cases}. \quad (2.12)$$

From now on, we will consider the case in which  $2 > \lambda \geq 0$ . Notice that if  $\lambda > 2$ , then  $\langle b_p^\dagger b_q \rangle = 0$  for all  $p$  and  $q$ . This case is trivial to analyse, since the correlators  $\langle a_m^\dagger a_n \rangle$  are also null, and the GS is in a product state.

The next step is to go back in the Fourier transform to get the correlation matrix of the  $a_n$  operators

$$\langle a_m^\dagger a_n \rangle = \frac{2}{N} \sum_{k=0}^{k_c} \cos \left[ \frac{2\pi}{N} k(m-n) \right]. \quad (2.13)$$

In the thermodynamic limit, the previous sum becomes an integral and it can be determined analytically. In this case, the correlation matrix of the block of  $L$  fermions in position space is,

$$A_{mn} = \langle a_m^\dagger a_n \rangle = \frac{1}{\pi} \frac{\sin k_c(m-n)}{m-n}, \quad (2.14)$$

where  $L \geq m, n \geq 0$ . Notice that, by means of Wick's theorem, any operator that acts on the block can be written in terms of the correlation matrix  $A_{mn}$ . For instance,

$$\langle a_k^\dagger a_l^\dagger a_m a_n \rangle = \langle a_k^\dagger a_n \rangle \langle a_l^\dagger a_m \rangle - \langle a_k^\dagger a_m \rangle \langle a_l^\dagger a_n \rangle. \quad (2.15)$$

This is due to the fact that the system is Gaussian, and its eigenstates are determined by the first and second moments of some fermionic operators.

The correlation matrix  $A_{mn}$  could also be computed using the density matrix of the block  $\rho_L$ ,

$$A_{mn} = \text{Tr}(a_m a_n \rho_L). \quad (2.16)$$

We, thus, need to invert the previous equation, that is, to compute the density matrix  $\rho_L$  from the correlation matrix  $A_{mn}$ .

The matrix  $A_{mn}$  is Hermitian, so it can be diagonalized by a unitary transformation,

$$G_{pq} = \sum_{m,n=0} u_{pm} A_{mn} u_{nq}^* = \langle g_p^\dagger g_p \rangle \delta_{pq}, \quad (2.17)$$

where  $g_p = \sum_m u_{pm} a_m$ . In this case, the density matrix of the block must also verify

$$G_{mn} = \text{Tr}(g_m^\dagger g_n \rho_L) = v_m \delta_{mn}, \quad (2.18)$$

which implies that  $\rho_L$  is uncorrelated and it can be written as

$$\rho_L = \varrho_1 \otimes \cdots \otimes \varrho_L, \quad (2.19)$$

where  $\varrho_m$  is the density matrix corresponding to the  $m$ -th fermionic mode excited by  $g_m^\dagger$ .

In order to determine the eigenvalues of the density matrix of one mode, let us express the  $g_m$ ,  $g_m^\dagger$  and  $\varrho_m$  operators in its matrix representation. That is,

$$g_m = \begin{pmatrix} 0 & 0 \\ 1 & 0 \end{pmatrix} \quad g_m^\dagger = \begin{pmatrix} 0 & 1 \\ 0 & 0 \end{pmatrix}, \quad (2.20)$$

and

$$\varrho_m = \begin{pmatrix} \alpha_m & \beta_m \\ \beta_m^* & 1 - \alpha_m \end{pmatrix}, \quad (2.21)$$

where  $\alpha_m$  and  $\beta_m$  are the matrix elements of  $\varrho_m$  that we want to determine. It is easy to see that  $\beta_m = 0$ , since

$$\langle g_m \rangle = \text{Tr}(g_m \rho_L) = \beta_m = 0. \quad (2.22)$$

Moreover, rewriting Eq. 2.18 in terms of these matrices

$$\text{Tr}(g_m^\dagger g_m \rho_L) = \text{Tr} \left[ \begin{pmatrix} 1 & 0 \\ 0 & 0 \end{pmatrix} \begin{pmatrix} \alpha_m & 0 \\ 0 & 1 - \alpha_m \end{pmatrix} \right] = \nu_m \quad (2.23)$$

we realize that  $\alpha_m = \nu_m$ .

The entanglement entropy between the block and the rest of the system is therefore,

$$S_L = \sum_{l=1}^L H_2(\nu_l). \quad (2.24)$$

where  $H_2(x) = -x \log x - (1-x) \log(1-x)$  denotes the binary entropy.

Summing up, the three steps that we have to follow in order to compute the entanglement entropy of the GS of a block of  $L$  spins for the XX model are: (i) to determine the correlation matrix  $A_{mn}$  by evaluating Eq. (2.14) for  $L \geq m, n \geq 0$ , (ii) to diagonalize this correlation matrix and, with its eigenvalues, (iii) to compute the entanglement entropy according to Eq. (2.24).

Let us emphasize that this method is computationally efficient, since its computational cost scales polynomially with the number of spins of the block  $O(L^3)$ , whereas the Hilbert space of the problem has dimension  $2^N$ .

It is also necessary to recall a quite subtle point that we have skipped along our previous discussion. It turns out that there is no need to perform a final transformation back to spins, that is, there is no need to invert the Jordan-Wigner transformation.

This is due to the fact that the coefficients of a given state are identical when written in terms of the spin basis or in terms of the fermionic  $a_l$  operators. More precisely,

$$\begin{aligned} |\psi\rangle &= \sum_{i_1, i_2, \dots, i_n} C^{i_1, i_2, \dots, i_n} |i_1, i_2, \dots, i_n\rangle \\ &= \sum_{i_1, i_2, \dots, i_n} C^{i_1, i_2, \dots, i_n} (a_1^\dagger)^{i_1} (a_2^\dagger)^{i_2} \dots (a_n^\dagger)^{i_n} |\text{vac}\rangle. \end{aligned} \quad (2.25)$$

Thus, the same coefficients appear in the ket, either when written in the initial spin basis, or when expressed as creation operators in the fermionic vacuum,  $|\text{vac}\rangle$ . Consequently, the reduced density matrix entropy of entanglement is identical for both expressions.

Finally, let us mention that the computation of the geometric entropy of Gaussian systems have been systematized in Refs. [55, 56, 57]. In particular, it is shown that for solvable fermionic and bosonic lattice systems, the reduced density matrices can be determined from the properties of the correlation functions. This subject is also reviewed in Ref. [58].

#### 2.1.4 Scaling of the entropy

It is now easy to compute the entanglement entropy of the ground state of the XX model for arbitrary values of the block size  $L$  and magnetic field  $\lambda$ .

In Fig. 2.2, we show how the entropy of the reduced density matrix of a block of  $L$  spins varies with  $L$  for different values of the magnetic field. The maximum entropy is reached for  $\lambda = 0$ . In particular, we recover the result in Ref. [5] and see that for  $\lambda = 0$  the leading scaling of the entropy is perfectly fitted by a logarithm,

$$S_L = \frac{1}{3} \log_2 L + a, \quad (2.26)$$

where  $a$  is a constant that was determined analytically in Ref. [59].

As we increase the magnetic field, but it is still less than 2, the entropy decreases although it keeps its logarithmic behaviour with  $L$ . When  $\lambda > 2$ , the entropy saturates to zero, since the ground state is already in a product state in the spin basis corresponding to the ferromagnetic phase,  $\prod_i |\uparrow\rangle_i$ .

The relation between logarithmic scaling and entropy is confirmed by similar computations in different models. The general result is that entanglement entropy obeys a logarithmic scaling relation at critical points, that is when the system is at a phase transition, whereas a saturation of entanglement is found away from criticality. This

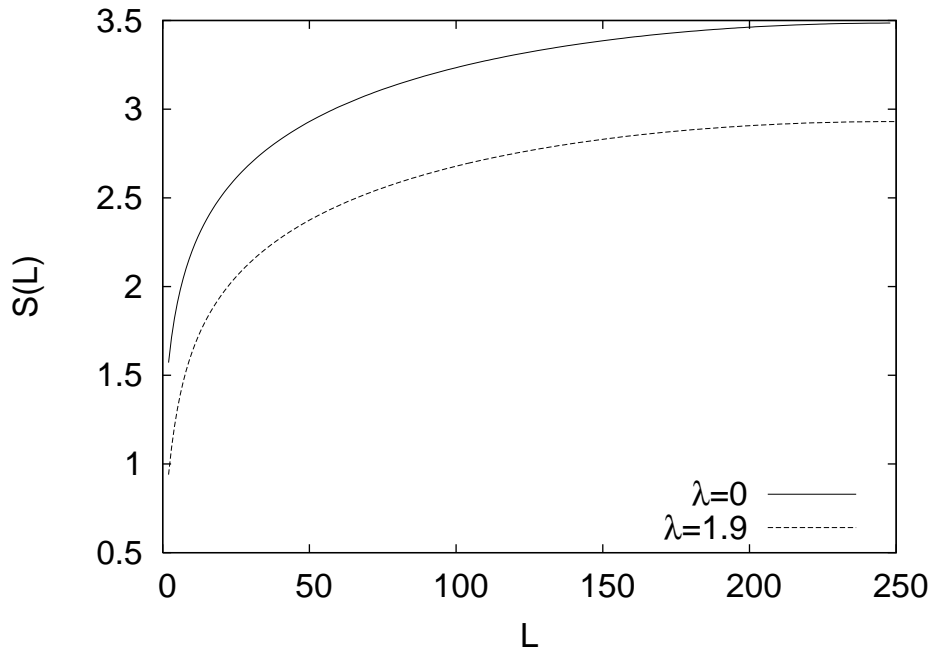


Figure 2.2: Entropy of the reduced density matrix of  $L$  spins for the XX model in the limit  $N \rightarrow \infty$ , for two different values of the external magnetic field  $\lambda$ . The maximum entropy is reached when there is no applied external field ( $\lambda = 0$ ). The entropy decreases while the magnetic field increases until  $\lambda = 2$  when the system reaches the ferromagnetic limit and the ground state is a product state in the spin basis.

universal logarithmic at critical points must emerge from the basic symmetry that characterizes phase transitions, namely conformal invariance. We shall come to this developments in the next section.

Let us mention that the scaling of entanglement entropy was formerly studied in the context of quantum field theory and black-hole physics. There, the system sits in higher dimensions. The entanglement entropy scales following an area law that we shall discuss later on. Yet, it is important to note that one-dimensional systems are an exception to the area law. Entanglement pervades the system at any distance, not staying just at the point-like borders of a block.

Summing up, we have seen that the scaling entropy is a good witness for quantum phase transitions. Many other studies of different measures of entanglement at quantum phase transitions have been presented recently. Let us here mention that in Refs. [42, 43, 44, 45], quantum phase transitions are characterized in terms of

the overlap (fidelity) function between two ground states obtained for two close values of external parameters. When crossing the critical point a peak of the fidelity is observed.

### 2.1.5 Entanglement entropy and Toeplitz determinant

Before finishing this section, we would like to sketch how the particular structure of the correlation matrix in Eq. (2.14) allows us to derive an analytical expression for the scaling law of the entanglement entropy. This result is presented in Ref. [59].

In order to obtain an analytical expression for the entanglement entropy, let us introduce the function

$$D_L(\mu) = \det(\tilde{A}(\mu)), \quad (2.27)$$

where  $\tilde{A}(\mu) \equiv \mu I_L - A$ ,  $I_L$  is the identity matrix of dimension  $L$ , and  $A$  is the correlation matrix defined in Eq. (2.14). If we express the matrix  $A$  in its diagonal form, we trivially have

$$D_L(\mu) = \prod_{m=1}^L (\mu - \nu_m), \quad (2.28)$$

where  $\nu_m$ , with  $m = 1, \dots, L$ , are the eigenvalues of  $A$ . Then, according to Cauchy residue theorem, the entanglement entropy  $S_L$  can be expressed in terms of an integral in the  $\mu$ -complex plane as follows

$$S_L = \lim_{\epsilon \rightarrow 0^+} \lim_{\delta \rightarrow 0^+} \frac{1}{2\pi i} \oint_{c(\epsilon, \delta)} e(1 + \epsilon, \mu) d \ln D_L(\mu) = \sum_{m=1}^L H_2(\nu_m), \quad (2.29)$$

where  $c(\epsilon, \delta)$  is a closed path that encircles all zeros of  $D_L(\mu)$  and  $e(1 + \epsilon, \mu)$  is an arbitrary function that is analytic in the contour  $c(\epsilon, \delta)$  and verifies  $e(1, \nu_m) = H_2(\nu_m) \forall m$ .

Thus, if we could obtain an analytical expression for the  $D_L(\mu)$  function, we would be able to get a closed analytical result for the entanglement entropy.

Notice that both the correlation matrix  $A_{mn}$ , defined in Eq. (2.14), and  $\tilde{A}$  are Toeplitz matrices, that is to say, matrices in which each descending diagonal from left to right is constant,

$$A = \begin{pmatrix} f_0 & f_{-1} & \cdots & f_{1-L} \\ f_1 & f_0 & & \vdots \\ \vdots & & \ddots & \vdots \\ f_{L-1} & \cdots & \cdots & f_0 \end{pmatrix}, \quad (2.30)$$

where, in this case,  $f_m = \frac{1}{\pi} \frac{\sin k_c m}{m}$ .

The asymptotic behaviour (when  $L \rightarrow \infty$ ) of the determinant of Toeplitz matrices has been widely studied in many cases, giving the famous Fisher-Hartwig conjecture (see Refs. [60, 61, 62, 63, 64]). In our particular case, the expression for the determinant of  $\tilde{A}$  was proven in Ref. [62] and, therefore, it is a theorem instead of a conjecture. In this way, we may insert this result in Eq. (2.29), perform the corresponding complex integral and obtain the asymptotic analytical expression for the entanglement entropy of the XX model. This computation is presented explicitly in Ref. [59] with the final result,

$$S_L = \frac{1}{3} \ln L + \frac{1}{6} \ln \left( 1 - \left( \frac{\lambda}{2} \right)^2 \right) + \frac{\ln 2}{3} + \Upsilon_1, \quad (2.31)$$

where

$$\Upsilon_1 = - \int_0^\infty dt \left\{ \frac{e^{-t}}{3t} + \frac{1}{t \sinh^2(t/2)} - \frac{\cosh(t/2)}{2 \sinh^3(t/2)} \right\}. \quad (2.32)$$

Indeed, we realize that this analytical expression for the scaling of the entanglement entropy is compatible with the numerical fit of Eq. (2.26) and, moreover, it fixes the value of the independent term.

This procedure is also used to obtain an analytical expression for the entanglement entropy of the XY model in Refs. [65, 66, 67]. In Ref. [68], the scaling of the Renyi entropy is determined for the XY model in terms of Klein's elliptic  $\lambda$  - function showing a perfect agreement with the previous results in the particular case in which the Renyi entropy becomes the von Neumann entropy.

## 2.2 Scaling of entanglement

The logarithmic scaling law that entanglement entropy obeys in the critical regime is a sign of the conformal symmetry of the system. For second order phase transitions, the correlation length diverges and the system becomes scale invariant. This scaling symmetry gets enlarged to the conformal group [69] which, in the case of on-dimensional systems, allows for a very precise characterization of the operator structure of the underlying theory. The development of conformal field theory is a remarkable achievement that we cannot present in this short review [70, 71].

### 2.2.1 One-dimensional systems

For a conformal theory in 1+1 dimensions, the scaling behaviour of the entropy was proven to be logarithmic in Ref. [72]. The general result reads

$$S_L \sim \frac{c + \bar{c}}{6} \log_2 L, \quad (2.33)$$

where  $c$  and  $\bar{c}$  are the so called central charges for the holomorphic and anti-holomorphic sectors of the conformal field theory. These central charges classify conformal field theories and are *universal* quantities which depend only on basic properties of the system, like effective degrees of freedom of the theory, symmetries or spatial dimensions, and they are independent of the microscopic details of the model. For free bosons  $c = 1$ , whereas for free fermions  $c = 1/2$ .

This result matches perfectly our geometric entropy computation of the critical XX model. In this case, the central charge  $c = \bar{c} = 1$  and the model is seen to belong to the free boson universality class.

The previous result of Eq. (2.33) was further elaborated and extended to finite systems, finite temperature and disjoint regions in Refs. [72, 73, 74]. For instance, the scaling of the entropy for a system with periodic boundary conditions reads

$$S_A \sim \frac{c}{3} \log \left( \frac{L}{\pi a} \sin \frac{\pi \ell}{L} \right) + c'_1, \quad (2.34)$$

whereas for the open boundary conditions case is

$$S_A = \frac{c}{6} \log \left( \frac{2L}{\pi a} \sin \frac{\pi \ell}{L} \right) + \tilde{c}'_1. \quad (2.35)$$

In Ref. [75], the scaling of the entropy of a conformal semi-infinite chain is presented. In Ref. [76], conformal symmetry is further exploited and an analytical computation of the distribution of eigenvalues of the reduced density matrix of a block in a one-dimensional systems is presented.

Let us finally mention that the scaling of entanglement have been also studied for other entanglement measures by means of conformal field theory. In particular, in Ref. [48, 50], it is shown that the single copy entanglement scales as

$$E_1(\rho_L) = \frac{c}{6} \log L - \frac{c}{6} \frac{\pi^2}{\log L} + O(1/L). \quad (2.36)$$

Note that entropy sub-leading corrections to scaling are suppressed as  $1/L$  whereas single copy entanglement suffers from  $1/\log L$  modifications. This makes the numerical approach to the latter more difficult.

## 2.2.2 Conformal field theory and central charge

We stated above that the central charge is a quantity that characterizes the universality class of a quantum phase transition. We also mentioned in the introduction that a possible figure of merit for entanglement could be constructed from correlation functions made out some operator which is always present in any theory. Let us now see that both ideas merge naturally.

In 1+1 dimensions, conformal field theories are classified by the representations of the conformal group [70]. The operators of the theory fall into a structure of highest weight operators and its descendants. Each highest weight operator carries some specific scaling dimensions which dictates those of its descendants. The operators close an algebra implemented into the operator product expansion. One operator is particularly important: the energy-momentum tensor  $T_{\mu\nu}$ , which is a descendant of the identity. It is convenient to introduce holomorphic and anti-holomorphic indices defined by the combinations  $T = T_{zz}$  and  $\bar{T} = T_{\bar{z}\bar{z}}$  where  $z = x^0 + ix^1$  and  $\bar{z} = x^0 - ix^1$ . Denoting by  $|0\rangle$  the vacuum state, the central charge of a conformal field theory is associated to the coefficient of the correlator

$$\langle 0|T(z)T(0)|0\rangle = \frac{c}{2z^4}, \quad (2.37)$$

and the analogous result for  $\bar{c}$  in terms of the correlator  $\langle 0|\bar{T}(z)\bar{T}(0)|0\rangle$ . A conformal field theory is characterized by its central charge, the scaling dimensions and the coefficients of the operator product expansion. Furthermore, unitary theories with  $c < 1$  only exist for discrete values of  $c$  and are called minimal models. The lowest lying theory corresponds to  $c = \frac{1}{2}$  and represents the universality class of a free fermion.

The central charge plays many roles in a conformal field theory. It was introduced above as the coefficient of a correlator of energy-momentum tensors, which means that it is an observable. The central charge also characterizes the response of a theory to a modification of the background metric where it is defined. Specifically, the scale anomaly associated to the lack of scale invariance produced by a non-trivial background metric is

$$\langle 0|T_\mu^\mu|0\rangle = -\frac{c}{12}R, \quad (2.38)$$

where  $R$  is the curvature of the background metric. This anomaly can also be seen as the emergence of a non-local effective action when the field theory modes are integrated out in a curved background.

Therefore, the central charge which appears as the coefficient of the entanglement entropy is naturally related to the stress tensor, which is the operator that is guaran-

teed to exist in any theory. It is also possible to derive a direct relation between entropy and the trace of the stress tensor as shown in the original Ref. [72].

### 2.2.3 Area law

The conformal group does not constrain the structure of the Hilbert space in spatial dimensions higher than one as much as it does in one dimension. Actually, the conformal group no longer brings an infinite number of conserved charges (as it does in one dimension) but becomes a finite group.

Nevertheless, a geometric argument establishes the scaling behaviour of entropy. The basic idea goes as follows. Let us consider a volume of spins (or any local degrees of freedom) contained in a larger space. For theories with local interactions, it is expected that entanglement will be created between the degrees of freedom that lie outside and inside the surface that encloses the volume we are considering. It follows that the entropy should naturally scale as an area law even if the model displays a finite correlation length.

These arguments were put forward in the study of entanglement entropy in quantum field theory as a possible source for black-hole entropy [3, 77, 78]. Furthermore, the relation between the entropy and the effective action in a curved background was developed in Ref. [79]. Let us mention these results. For general quantum field theories the entropy is a divergent extensive quantity in more than one spatial dimension obeying an area law

$$S_L \sim c_1 \left( \frac{L}{\epsilon} \right)^{d-1} \quad d > 1, \quad (2.39)$$

where  $L^d$  is the size of the volume,  $\epsilon$  stands for an ultraviolet regulator and the coefficient  $c_1$  counts components of the field which is considered. This coefficient is again found in the effective action on a gravitational field and, thus, in the trace anomaly as a divergent term. A form for the former can be found as

$$\Gamma_{eff} = \int_{s_0}^{\infty} ds \frac{e^{-sm^2}}{s^{d/2}} \left( \frac{c_0}{s} + c_1 R + c_{2F} s F + c_{2G} s G + \dots \right), \quad (2.40)$$

where  $s_0$  acts as a ultraviolet regulator,  $R$  is the curvature,  $F$  the Weyl tensor and  $G$  the Euler density. The main conceptual result to be retained is that entropy measures a very basic counting of degrees of freedom. Note that previous efforts to make a general c-theorem are all base on  $c_{2F}$  and  $c_{2G}$ , not on  $c_1$ . In one spatial dimension, the effective action has a unique structure proportional to the central charge. That is, the

central charge takes over all manifestations of the trace anomaly, at variance with the separate roles that appear in higher dimensions.

It is worth mentioning that computations done in massive theories in any number of dimensions show that  $S_L(m \neq 0) - S_L(m = 0)$  comes out to be ultraviolet finite [80]. Actually, the ultraviolet cut-off cancels in the computation. This is precisely what is needed to make the RG flow meaningful in such a case. This comment hints at the non-trivial issue about observability of the entropy. The standard prejudice is that the leading area law coefficient is not observable since it comes divided by a necessary ultraviolet cut-off. Yet, if such a coefficient is also responsible for finite corrections, the situation may not be as trivial.

A review on methods to calculate the entanglement entropy for free fields and some particular examples in two, three and more dimensions are presented in Ref. [81]. Further explicit computations of area law scaling of entropy in spin and harmonic systems in higher dimensions can be found in Refs. [82, 83, 84, 6]. A quite remarkable result found in Ref. [85] is the fact that certain fermionic systems may develop logarithmic violations of the area law, while keeping local interactions. This is somehow analogous of the logarithmic scaling in one-dimension. The system is more correlated than what is expected from pure geometrical arguments. In this respect, the leading term in the scaling of the entropy for fermionic systems was computed analytically assuming the Widom conjecture in Ref. [86]. This result was checked numerically for two critical fermionic models in Ref. [84] finding a good agreement.

For other steps into a description of systems with two spatial dimensions in the framework of conformal field theory see Refs. [87, 88]. For a class of critical models in two spatial dimensions (including the quantum dimer model), it is found that  $S(\rho_I) = 2f_s(L/a) + cg \log(L/a) + O(1)$ , where  $L$  is the length of the boundary area,  $f_s$  is an area law coefficient that is interpreted as a *boundary free energy*, and  $g$  is a coefficient that depends on the geometric properties of the partition. That is, in addition to a non-universal area law, one finds a universal logarithmically divergent correction. For a further discussion of steps towards a full theory of entanglement entropies in  $d + 1$ -dimensional conformal field theories, see Refs. [87, 88].

A particularly interesting issue is the holographic entanglement entropy that emerges from the AdS (anti-de-Sitter)/CFT correspondence. The AdS/CFT correspondence is the conjectured equivalence between a quantum gravity theory defined on one space, and a quantum field theory without gravity defined on the conformal boundary of this space. The entanglement entropy of a region of the boundary in the conformal field

theory is then related with the degrees of freedom of part of the AdS space in the dual gravity side. In Refs. [88, 89], this relation is established explicitly and, in Ref. [90] the recent progress on this topic is presented.

Let us also mention the line of research that deals with topological entropy. Some Hamiltonians produce states such that a combination of geometric entropies exactly cancels the dominant area law. Then, a topological entropy term characterizes the system [91]. This subject is nowadays a large field of research that we cannot include in the present review. In this respect, a review on the scaling of the entanglement entropy of 2D quantum systems in a state with topological order is presented in Ref. [92].

## 2.3 Other models

We can find in the literature the computation of the scaling of the entanglement entropy for other spin models. In XY and XXZ models, this logarithmic scaling will confirm the role of the underlying conformal symmetry. We shall also discuss that in disordered systems, although the conformal symmetry is lost for one particular realization of the disorder, we recover the logarithmic scaling of the entropy with a different central charge of the corresponding homogeneous model, if we do the average over all the possible realizations of the disorder. We shall also study the scaling of entropy in systems where the notion of geometric distance is lost. This is the case of the Lipkin-Meshkov-Glick model, in which the logarithmic behaviour of the entropy will be due to the equilibrium of a competition between the long range interactions, that try to increase the entanglement, and the symmetries of the problem, that force the ground state to belong to a reduced subspace of the Hilbert space. A different case are those systems composed of itinerant particles. In particular, we will present the scaling of entropy of the Laughlin wave function.

### 2.3.1 The XY model

The XY model is defined as the XX model in Eq. (2.2), adding an extra parameter  $\gamma$  that determines the degree of anisotropy of spin-spin interaction in the XY plane. Its Hamiltonian reads

$$H_{XY} = -\frac{1}{2} \sum_l \left( \frac{1+\gamma}{2} \sigma_l^x \sigma_{l+1}^x + \frac{1-\gamma}{2} \sigma_l^y \sigma_{l+1}^y + \lambda \sigma_l^z \right), \quad (2.41)$$

where, as in the previous section,  $l$  labels the  $N$  spins,  $\sigma_l^\mu$  ( $\mu = x, y, z$ ) are the Pauli matrices and  $\lambda$  is the transverse magnetic field in the  $z$  direction. This notation will be also followed for the rest of models that are going to be presented.

Notice that if  $\gamma = 0$  we recover the XX model, whereas if  $\gamma = 1$ , it becomes the quantum Ising model with a transverse magnetic field, with Hamiltonian

$$H_{\text{Ising}} = -\frac{1}{2} \sum_l (\sigma_l^x \sigma_{l+1}^x + \lambda \sigma_l^z). \quad (2.42)$$

The XY model was solved in detail in Ref. [5]. In order to do this, the previous works on spin chains required to solve the XY Hamiltonian were reviewed. In concrete, the XY model without magnetic field was solved exactly in Ref. [93], the spectrum of the XY model with magnetic field was computed in Ref. [94], the correlation function for this model was obtained in Ref. [95], and the entropy  $S_L$  was computed in Ref. [4].

Later, an extent analytical analysis of the entropy of XY spin chain was presented in Refs. [65, 66, 67]. In this work, in a similar way as we have seen previously for the XX model, an analytical expression for the scaling of the entanglement entropy is determined for the XY model by means of Toeplitz determinants.

The XY model with  $\gamma \neq 0$  is critical for  $\lambda = 1$ . In this case, the entropy of a block scales as

$$S_{XY}(L) = \frac{1}{6} \log_2 L + a(\gamma), \quad (2.43)$$

where  $a(\gamma)$  is a function that only depends on  $\gamma$ . This entanglement behaviour corresponds to the scaling dictated by a conformal theory, Eq. (2.33), with central charge  $c = 1/2$ . The XY model, therefore, falls into the free fermion universality class.

In the non-critical case, that is for  $\lambda \neq 1$ , the entanglement entropy saturates to a constant.

Let us mention that an exact relationship between the entropies of the XY model and the XX model has been found recently [96]. Using this relation it is possible to translate known results between the two models and obtain, among others, the additive constant of the entropy of the critical homogeneous quantum Ising chain and the effective central charge of the random XY chain.

Finally, with respect to the particular case of the Ising model, in Ref. [97], the computation of the leading correction to the bipartite entanglement entropy at large sub-system size, in integrable quantum field theories with diagonal scattering matrices is presented. This result is used to compute the exact value of the saturation in

the Ising model and showed it to be in good agreement with numerical results. This work is reviewed in detail in Ref. [98].

### 2.3.2 The XXZ model

The XXZ model consists of a chain of  $N$  spins with nearest neighbour interactions and an external magnetic field. Its Hamiltonian is given by,

$$H_{XXZ} = \sum_l \left( \frac{1}{2} [\sigma_l^x \sigma_{l+1}^x + \sigma_l^y \sigma_{l+1}^y + \Delta \sigma_l^z \sigma_{l+1}^z] + \lambda \sigma_l^z \right), \quad (2.44)$$

where  $\Delta$  is a parameter that controls the anisotropy in the  $z$  direction.

As it happened for the  $\gamma$  parameter of the XY model, the  $\Delta$  parameter of the XXZ model has two particular interesting values. If  $\Delta = 0$ , we trivially recover the XX model, and if  $\Delta = 1$ , the system becomes the XXX model that has a fully isotropic interaction

$$H_{XXX} = \sum_l \left( \frac{1}{2} [\sigma_l^x \sigma_{l+1}^x + \sigma_l^y \sigma_{l+1}^y + \sigma_l^z \sigma_{l+1}^z] + \lambda \sigma_l^z \right). \quad (2.45)$$

The XXZ model can be solved analytically by means of the Bethe Ansatz technique [99]. Bethe Ansatz takes profit of the two symmetries of the system to find its eigenstates. The first symmetry is the rotational symmetry respect to the  $z$  axis. It implies that the  $z$ -component of the total spin,  $S_z = 1/2 \sum_l \sigma_l^z$ , must be conserved and, therefore, the Hamiltonian must be diagonal in boxes of constant  $S_z$ . The other symmetry is the translational invariance, that allow us to diagonalize these boxes using a kind of generalized Fourier transform. Once the ground state is obtained, the correlation functions can be computed in terms of certain determinants (see Ref. [100]). This model is qualitatively different from the XY, since it presents a point of non-analyticity of the ground state energy for finite systems. In the XY model, the level crossing between the ground state and the first excited state only occurs in the thermodynamic limit. In this case, instead, the terms of the Hamiltonian  $\sigma_l^x \sigma_{l+1}^x + \sigma_l^y \sigma_{l+1}^y$ ,  $\sigma_l^z \sigma_{l+1}^z$  and  $\sigma_l^z$  commute and are independent of  $\Delta$  and  $\lambda$ , which implies that there will be an actual level crossing.

Both the isotropic case and the anisotropic one for  $\lambda = 0$  are solved in Refs. [101, 5]. The phases of the system are found to be:

- In the XXX model, Eq. (2.45), there are two limit behaviours. On one hand, when  $|\lambda| > 2$  the system is gapped and it is in a product state in which all spins point at the direction of the magnetic field (ferromagnetic phase). On the other

hand, for  $\lambda = 0$  the magnetization is zero and the system is in an entangled state (anti-ferromagnetic case). In the interval between these two cases  $2 > \lambda \geq 0$  the system is gap-less and, therefore, critical.

- With respect to the anisotropic case with magnetic field equal to zero, the system shows a gap-less phase in the  $1 \geq \Delta \geq -1$  interval. Outside this interval, there is a gap between the ground and the first excited states. These two phases are separated by two phase transitions in  $\Delta = 1$  and  $\Delta = -1$ . The first one is a Kosterlitz-Thouless phase transition, while the second one is of first order.

The scaling of the entanglement entropy is presented in Refs. [5, 102]. These numerical results show that the entanglement entropy behaviour converges to a logarithmic scaling as the size of the system increases, if the system is critical. On the contrary, if the system is not in a critical phase, the entropy saturates to a constant value. In particular, in the isotropic model without magnetic field, the entropy scales as

$$S_L \sim \frac{1}{3} \log_2 L, \quad (2.46)$$

which means that the XXX model with  $\lambda = 0$  has central charge  $c = 1$  and falls into the universality class of a free boson.

Finally, let us mention that, recently, analytic expressions for reduced density matrices, several correlation functions and the entanglement entropy of small blocks (up to 6 spins) have been found for the XXZ model with  $\Delta = 1/2$  (see Refs. [103] and [104]).

### 2.3.3 Disordered models

So far, we have only considered translational invariant systems. This symmetry plus the scaling invariance at a critical point produces the conformal symmetry that implies universal properties of the scaling of entanglement. Nevertheless, natural systems exhibit a certain amount of *disorder* due to impurities and imperfections of the system. This disorder breaks the translational symmetry and we wonder what happens with the scaling of the entropy taking into account that the conformal invariance is lost.

This question was addressed in Ref. [105]. They computed analytically the block entropy for the Heisenberg, XX and quantum Ising models with random nearest-neighbour couplings under the hypothesis of strong disorder by means of the real space renormalization group technique. This approach was introduced in Ref. [8] and was generalized in Ref. [7].

This strong disorder hypothesis assumes that if one takes the strongest coupling of the chain, its neighbours are much weaker than it. Thus, it is possible to diagonalize this strongest bond independently of the rest of the system, project the system onto the ground state of this subspace (a singlet for the previous models) and then perform perturbation theory respect to the neighbour couplings. The final result is that two sites have been eliminated and the Hamiltonian energy scale has been reduced. This process can be iterated until we arrive at the ground state of the system which is a random singlet phase, that is to say, a set of singlets connected randomly and for arbitrarily long distances.

Notice that although this method is not correct when applied to a system with weak disorder, it becomes asymptotically correct at large distances [7].

For a particular realization of the disorder, the translational symmetry of the system is broken and, therefore, the conformal symmetry too. Hence, the scaling of the entanglement entropy of this realization of the disorder will not be logarithmic, but fluctuating.

In Ref. [105], it was shown that although the conformal symmetry is broken, if we take the average over all the realizations of the disorder the entropy keeps scaling logarithmically with an effective central charge  $\tilde{c} = c \ln 2$ , where  $c$  is the central charge for the same model but without disorder. This result has been further checked numerically both for the XX model in Ref. [106] and for the Heisenberg model in Ref. [107].

In Ref. [106], the disordered XX spin- $\frac{1}{2}$  chain with periodic boundary conditions and positive random spin couplings chosen in a flat uniform distribution within the interval  $[0, 1]$  was studied. The magnetic field was set to zero. It was shown that for a block large enough (larger than 20 spins), the entropy scales logarithmically according to [105], using around  $10^4$  samples for  $N = 500, 1000, 2000$  and  $2 \times 10^4$  samples for  $100 \leq N \leq 400$ , in order to do the average over all the possible realizations of the disorder.

The same result was shown for the Heisenberg model in Ref. [107]. In this work, a uniform distribution in the interval  $[0, 1]$  for the couplings between the spins was also chosen. For a system of  $N = 50$  and after averaging the entanglement entropy over  $10^4$  different configurations of disorder, the logarithmic scaling of the entropy with an effective central charge  $\tilde{c} = c \ln 2$  is recovered. Let us point out that these one dimensional systems are particular cases of chains of quantum group (or q-deformed) spins studied in Ref. [108]. It is also interesting to mention that this robustness of

the entanglement scaling respect to the disorder is not kept for other models like the Bose-Hubbard model (see Ref. [109]).

In the case of higher dimensions, the scaling of the entanglement entropy in the 2D random Ising model was studied in Refs. [110, 111]. In particular, in Ref. [111], the entanglement entropy of a  $L \times L$  region located in the centre of a square lattice which is governed by the Hamiltonian

$$H = - \sum_{\langle i,j \rangle} J_{ij} \sigma_i^z \sigma_j^z - \sum_i \lambda_i \sigma_i^x, \quad (2.47)$$

was computed. The Ising couplings  $J_{ij}$  and the transverse magnetic fields  $\lambda_i$  take random values given by the uniform probability distributions in the intervals  $[0, 1]$  and  $[0, \lambda_0]$  respectively. By means of a generalized version for 2 dimensions of the real space renormalization group, it was found that the critical field is at  $\lambda_0^c = 5.37 \pm 0.03$ , and for both critical and non-critical  $\lambda_0$  the entropy scaling fulfils the area law:  $S(L) \sim L$  in the leading term.

Let us mention some disordered spin systems have also been studied from the fidelity susceptibility point of view in Refs. [112, 113]. Finally, it is interesting to point out that, in other systems, the translational invariance is not broken by means of random couplings but due to a quantum impurity or a physical boundary. The behaviour of the entanglement entropy in this kind of systems is reviewed in Ref. [114].

### 2.3.4 The Lipkin-Meshkov-Glick model

The Lipkin-Meshkov-Glick model was proposed in Ref. [115, 116, 117]. Unlike the previous models we have considered, where the spins had short range interactions, in the LMG model, each spin interacts with all the spins of the system with the same coupling strength. This system is described by the Hamiltonian

$$H_{LMG} = -\frac{1}{N} \sum_{i < j} \left( \sigma_i^x \sigma_j^x + \gamma \sigma_i^y \sigma_j^y \right) - \lambda \sum_i \sigma_i^z. \quad (2.48)$$

Notice the apparent similarity between this model and the XY model in Eq. (2.41). The essential difference between them is that while in the XY Hamiltonian the interaction only takes place between nearest neighbours, in the LMG model, all spins interact among themselves. This highly symmetric interaction pattern forces the loss of the notion of geometry, since there is no distance between the spins. This implies

that it no longer makes sense to define a block of  $L$  spins as a set of  $L$  contiguous spins or to study decays of the correlations between two spins.

As in previous cases, our aim is to study the scaling properties of the entanglement entropy for the ground state reduced density matrix of a block of  $L$  spins respect to the rest of  $N_L$  spins. We face a somewhat contradictory situation. On one hand, we expect that the non-local connectivity of the interactions would produced a ground state more entangled than those that emerge from nearest neighbour interaction models. On the other hand, the symmetry of the Hamiltonian implies that all the spins must be indistinguishable in the ground state, therefore, it must belong to a symmetric subspace, which restricts its entanglement. The explicit computation will clarify this issue.

The Hamiltonian (2.48) can be written in terms of the total spin operators  $S_\alpha = \sum_i \sigma_\alpha^i / 2$  as

$$H = -\frac{1}{N}(1 + \gamma) (\mathbf{S}^2 - S_z^2 - N/2) - 2\lambda S_z - \frac{1}{2N}(1 - \gamma) (S_+^2 + S_-^2), \quad (2.49)$$

where  $S_\pm$  are the ladder angular momentum operators. In Eq. (2.49), we realize that  $[\mathbf{S}^2, H] = 0$  and, therefore, we can diagonalize the Hamiltonian in boxes of constant  $S$ . From Eq. (2.49), it is easy to see that the ground state must belong to the subspace of  $S = N/2$ . Then, we have to span this subspace in terms of a basis  $|N/2, M\rangle$  fully symmetric under the permutation group and eigenstates of  $\mathbf{S}^2$  and  $S_z$ . These states  $|N/2, M\rangle$  are called Dicke states.

Notice that the restricted subspace where the ground state must live due to the symmetries of the Hamiltonian will limit the scaling of the entanglement entropy of a block of  $L$  spins with respect to the remaining  $N_L$ . As the ground state reduced density matrix is spanned by the set of  $(L + 1)$  Dicke states, the entropy of entanglement obeys the constrain  $S_{L,N} \leq \log_2(L + 1)$  for all  $L$  and  $N$ , where the upper bound corresponds to the entropy of the maximally mixed state  $\rho_{L,N} = \mathbb{1}/(L + 1)$  in the Dicke basis. This argument implies that entanglement, as measured by the Von Neumann entropy, cannot grow faster than the typical logarithmic scaling observed in the previous cases.

Both the ground state and the entanglement entropy were computed for the LMG model in Ref. [118]. For the isotropic case ( $\gamma = 1$ ) and in the thermodynamic limit ( $N, L \gg 1$ ),  $H_{LMG}$  is diagonal in the Dicke basis. Then, for  $\lambda \geq 1$ , the entanglement entropy is strictly zero since the ground state is in a fully polarized product state. Instead, if  $1 > \lambda \geq 0$ , we recover the logarithmic scaling of the entropy,

$$S_{L,N}(\lambda, \gamma = 1) \sim \frac{1}{2} \log [L(N - L)/N]. \quad (2.50)$$

Although the kind of scaling does not depend on the strength of the magnetic field, its absolute value is smaller for weaker magnetic fields, according to the equation

$$S_{L,N}(\lambda, \gamma = 1) - S_{L,N}(\lambda = 0, \gamma = 1) \sim \frac{1}{2} \log(1 - \lambda^2), \quad (2.51)$$

and thus diverges, at fixed  $L$  and  $N$ , in the limit  $h \rightarrow 1^-$ .

In the anisotropic case, we can study the limits of very strong and very weak magnetic fields. On one hand, when  $\lambda \rightarrow \infty$ , the GS is in the product state  $\prod_i |\uparrow\rangle_i$  and therefore is not entangled. In the thermodynamic limit, this state is also the ground state just for  $\lambda > 1$ . On the other hand, for  $\lambda \rightarrow 0$  the entanglement entropy saturates and goes to a constant that depends on  $\gamma$ . In the particular case of  $\gamma = 0$ , the ground state is degenerate and lives in the subspace generated by the states  $\prod_i |\rightarrow\rangle_i$  and  $\prod_i |\leftarrow\rangle_i$ , where  $|\rightarrow\rangle$  and  $|\leftarrow\rangle$  are the eigenstates of the  $\sigma^x$  operator. In practice, this degeneration would be broken by any perturbation of the environment.

These two different phases suggests the existence of a quantum phase transition between  $\lambda \gg 1$  and  $\lambda \ll 1$ . In particular, it has, numerically, been checked in Ref. [118] that, in the thermodynamic limit, the entanglement entropy displays a logarithmic divergence around  $\lambda_c = 1$  according to the law

$$S_{L,N}(\lambda, \gamma) \sim -\log|1 - \lambda|. \quad (2.52)$$

Indeed, it is shown that at  $\lambda = 1$  the entropy scales logarithmically with a coefficient that depends on  $\gamma$ . However, in the thermodynamic limit, this coefficient is independent of  $\gamma$  and takes a value closed to  $1/3$ . In Ref. [119], the previous relation, Eq. 2.52, is computed analytically obtaining the same result and fixing the coefficient to  $1/3$ . In this same work, the finite size corrections to the scaling of entropy are also studied.

Although the behaviour of entanglement is very similar to the XY model, that is to say, it scales logarithmically in the critical point and saturates to a constant in the non-critical phase, the reasons of these scaling laws are different. In the XY model, entanglement is limited by the facts that interactions are local and the system is translationally invariant. At the critical point, the correlation length becomes infinite, the system is conformal symmetric, and the logarithmic scaling of the entanglement entropy appears as a manifestation of this symmetry. Instead, in the LMG model, the long range interactions should allow for larger correlations, that is, larger entanglement. Nevertheless, the symmetries of the system restrict the subspace where the GS must belong and, therefore, the scaling law of entanglement. The final result is

the same logarithmic scaling law but which has nothing to do with any underlying conformal symmetry.

Finally, let us mention that other analytical calculations of the spectrum of the LMG model both in the thermodynamic limit and finite size case have appeared recently [120]. Moreover, the entanglement entropy for general free bosonic two-mode models is presented in Ref. [121]. In particular, a complete classification of the possible scaling behaviours for the entanglement entropy in the related collective models as the LMG, the Dicke model, or the Lieb-Mattis model is obtained.

### 2.3.5 Particle entanglement

In a similar way than LMG model, where the notion of distance was lost, one can try to compute the entanglement entropy in systems of moving fermions and bosons. In such itinerant systems, as the particles are indistinguishable, moving and partially de-localized, it is not obvious to define the geometric entropy.

What we, indeed, can compute is the von Neumann entropy for any subset of particles for a system of  $N$  indistinguishable particles in the state  $\Psi(r_1, \dots, r_n)$ . Notice that, in this case, this von Neumann entropy cannot be interpreted as the number of distillable EPR pairs. Due to the symmetrization, it is impossible to associate a label with the particles and perform the appropriate distillation operations. This is a subtle difference respect to the LMG model.

A particular interesting physical system is the Fractional Quantum Hall Effect (FQHE) [10]. Although a complete understanding of it is still missing, it is commonly believed that the interactions between the particles are essentially responsible for the strange states of matter that the 2D electron gas shows at some particular values of the transverse magnetic field. These states would present a new kind of order called topological order and their quasi-particle excitations are neither bosons nor fermions, but anyons, that is to say, quasi-particles with any-statistics [12]. In this respect, in 1983, Laughlin proposed an Ansatz for the wave function of the ground state of the system [11]. This wave function is defined by

$$\Psi_L^{(m)}(z_1, \dots, z_n) \sim \prod_{i < j} (z_i - z_j)^m e^{-\sum_{i=1}^n |z_i|^2/2}, \quad (2.53)$$

where  $z_j = x_j + iy_j$ ,  $j = 1, \dots, n$  stands for the position of the  $j$ -th particle. It describes fractional quantum Hall state at a filling fraction  $\nu = 1/m$ , where  $m$  is an integer number.

In particular, in Ref. [122], the entanglement entropy of  $k$  particles respect the rest of the system is computed for the Laughlin wave function with filling fraction one

$$S_{n,k} = \log_2 \binom{n}{k}. \quad (2.54)$$

Notice that, in this case, although the state also belongs to a completely anti-symmetric subspace, the entanglement entropy of half a system grows linearly with the number of particles.

In Refs. [123, 124], these ideas are extended, and the *particle entanglement*, defined as the entanglement between two subsets of particles making up the system, is studied. The general structure of particle entanglement in many-fermion ground states, analogous to the *area law* for the more usually studied entanglement between spatial regions, are also formulated, and the basic properties of particle entanglement are uncovered by considering relatively simple itinerant models. All these ideas are widely reviewed in Ref. [125].

## 2.4 Renormalization of Entanglement

A natural question arising within the study of entanglement in quantum system is how entanglement evolves along Renormalization Group (RG) trajectories. We shall now address this issue discussing first the RG of quantum states and, then, the study of particular systems.

### 2.4.1 Renormalization of quantum states

It is customary to present RG transformations on Hamiltonians or observables. In general, a Hamiltonian is described by a set of coupling constants times operators  $H = \sum_i g^i \mathcal{O}_i$ . This set of operators may be infinite, including relevant, marginal and irrelevant operators or, as in the case of renormalizable quantum field theories in the continuum, it may reduce to a finite set of relevant and marginal operators. Then, upon coarse graining of short-distances and an adequate rescaling, the system is described by a new set of coupling constants. So to speak, the operator algebra acts as a basis. The concept of RG trajectory corresponds to analysing observables along the flow  $\frac{d}{dt} = -\beta_i \frac{d}{dg^i}$ , where the beta functions correspond to  $\beta_i \equiv \frac{dg^i}{dt}$  are related to the change of the coupling constants as the coarse graining proceeds.

Yet, RG transformations can be understood as an action on any quantum state, regardless of its relation to any Hamiltonian [126]. Coarse graining is independent of any dynamics. This RG procedure on quantum states is not presented as common lore since explicit knowledge of *e. g.* the ground state of a system is not available in general. Let us address this issue.

The basic idea to perform RG on states is to produce a coarse graining of short-distance degrees of freedom, followed by a clever choice of local basis to retain the long-distance information which is retained in an optimal way. Let us take a quantum state  $\psi_0$  and determine its RG transformed,  $\psi'_0$ , as follows. We pairwise group the sites in the system and define a coarse-graining transformation for every pair of local  $d$ -dimensional basis states, *e.g.* for the sites  $2j$  and  $2j + 1$ , as  $|p\rangle_{2j}|q\rangle_{2j+1} = |pq\rangle_j$ . This transformation yields  $\psi_0 \rightarrow \psi$ . Then we have  $\psi'_0 = U \otimes \dots \otimes U|\psi\rangle$ , where the  $d^2 \times d^2$  unitary matrix  $U$  performs the change of representative in the coarse-grained space. Note that the matrix  $U$  is non-local as seen from the  $2j$  and  $2j + 1$  sites. Some local information is now washed out, while preserving all the quantum correlations relating the coarse-grained block to other ones.

Operators also get coarse-grained along the above transformation. Take for instance an operator acting on one local Hilbert space, *e.g.*  $O_{2j}$ . Expectation values must remain unchanged,

$$\langle \psi_0 | O_{2j} | \psi_0 \rangle = \langle \psi'_0 | O'_j | \psi'_0 \rangle, \quad (2.55)$$

which leads to

$$O'_j = U(O_{2j} \otimes I_{2j+1})U^\dagger, \quad (2.56)$$

where  $I$  is the identity matrix. To complete a RG transformation we simply need to rescale distances, *i.e.*, to double the lattice spacing.

This analysis can be made completely explicit in the case of states which are described as a matrix product state [126]. There, the above transformation amount to a flow on the matrices that represent the state. In turn, a flow related to the transfer matrix can be computed. Explicit irreversibility of RG flows and the characterization of critical points followed from the flow on this transfer matrix.

## 2.4.2 Irreversibility of RG flows

We may as well return to the standard construction of RG transformations on Hamiltonians and perform a detailed study in some particular case. For instance, we may

consider the quantum Ising model in a transverse field  $\lambda$ . It is known that the parameter  $\lambda$  provides a relevant deformation of the model, departing from its critical value  $\lambda^* = 1$ . For instance, the departure that makes  $\lambda > 1$  get larger and larger corresponds to the increase of the mass of the underlying fermionic description.

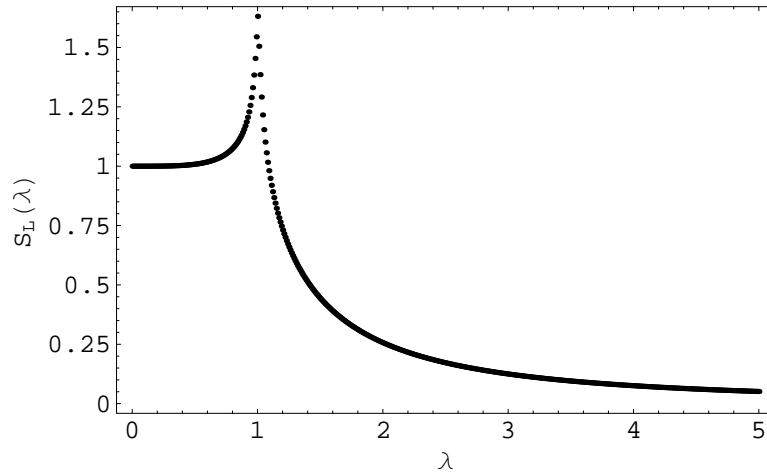


Figure 2.3: Entropy of entanglement is shown to decrease monotonically along the RG trajectory that takes the external magnetic field  $\lambda$  away from its critical value  $\lambda^* = 1$ . Towards the left the flow takes the system to a GHZ-line state whereas, towards the right, the system is a product state.

An analysis of this RG trajectory can be illustrated using Fig. 2.3 ( see Refs. [118, 73, 74]). This result shows that RG trajectories are monotonically irreversible as dictated by the c-theorem in 1+1 dimensions. Furthermore, it can be seen that the ground state obeys majorization relations. That is, irreversibility is orchestrated at a very refined level, since the reshuffling of the ground state obeys an exponential set of ordering relations [82].

Irreversibility for the entanglement entropy should then be obtained as a fundamental theorem, equivalent to the c-theorem which is usually formulated in terms of the stress tensor. This was indeed done in Ref. [127]. Once, the relation between entropy and the properties of the stress tensor are made apparent.

## 2.5 Dynamics of Entanglement

So far, we have studied the properties of entanglement entropy of the ground state of the system. Next, we would like to analyse how entanglement evolves in time when the system is prepared in a state that is *not* an eigenstate of the Hamiltonian.

### 2.5.1 Time evolution of the block entanglement entropy

In Ref. [128], the time evolution of the entropy of entanglement of a block of  $L$  spins in a one-dimensional system is studied. It is considered a system prepared in a pure state  $|\psi_0\rangle$ , which corresponds to an eigenstate of  $H(\lambda_0)$  with  $\lambda_0 \neq \lambda$ . Then, for example, at time  $t = 0$ , the parameter is suddenly quenched from  $\lambda_0$  to  $\lambda$ . In general,  $|\psi_0\rangle$  will not be an eigenstate of  $H(\lambda)$ , and thus the system will evolve according to the equations of motion given by  $H(\lambda)$ . In this work, two computations are performed: one based on conformal field theory and the other on a particular solvable spin model, the Ising model. In the first case, the path integral formulation and the CFT are used in order to calculate the time evolution of the entanglement entropy of a high energy state of the system which is not an eigenstate. Then, one has to assume that the Hamiltonian is critical in order to make the theory conformally invariant. Instead, in the Ising model case, it is possible to perform calculations starting from a variety of initial states, considering both critical and non-critical regimes.

In both calculations, the entanglement entropy increases linearly with time  $t$  (after transients die away in the lattice case), up to  $t^* = L/2$ , in units where the maximum propagation speed of excitations is taken to be unity. For  $t \gg t^*$ ,  $S_L(t) \sim L$  saturates at an asymptotic value. This behaviour can be summarized in the following equation:

$$S_L(t) \sim \begin{cases} t & t \leq t^* \\ L & t \geq t^* \end{cases} . \quad (2.57)$$

This behaviour of the entanglement entropy has been checked in several lattice models both analytically and numerically [107, 129, 130, 131, 132]. In particular, in Ref. [129], the previous results are provided analytically using Toeplitz matrix representation and multidimensional phase methods for the XY model and considering large blocks.

In Ref. [128], a simple interpretation of this behaviour is proposed in terms of quasi-particles excitations emitted from the initial state at  $t = 0$  and freely propagating with velocity  $v \leq 1$ . The idea is that at,  $t = 0$  and at many points of the chain,

a pair of entangled quasi-particles begin to propagate in opposite directions at some constant velocity  $v$  that we will consider 1 for simplicity (see Fig.2.4). The entanglement between the block of  $L$  spins and the rest of the system at an arbitrary time is given by the number of pairs that have one quasi-particle in the block while the other is outside. Thus, the entanglement entropy increases linearly with time until it saturates when the excitations that started in the middle of the block arrive at its boundary.

All the previous results are explained in detail in the Ref. [133], where, apart from quantum quenches, a general conformal field theory approach to entanglement entropy is reviewed.

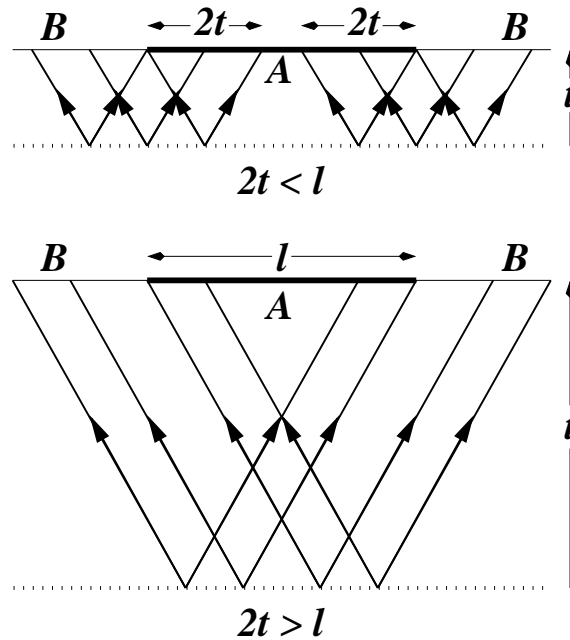


Figure 2.4: Schematic representation of the dynamics of block entropy. Entangled particles are emitted from the region  $A$ , they will contribute to the block entropy as long as one of the two particles ends in the region  $B$  [from [128]].

Let us point out that this increase of the entanglement entropy is unrelated to the second law of thermodynamics. Entanglement entropy can decrease or even oscillate in standard time evolution.

Let us also mention that in Ref. [107] the dynamics of entanglement was analysed for disordered systems, *i. e.* when the couplings between the spins take random values. In particular, the XXZ model with the couplings between the spins follow-

ing a uniform distribution in the interval  $[0, 1]$  was studied. It turns out that, in the presence of disorder, the entanglement entropy does not increase linearly but logarithmically. This logarithmic behaviour does not follow from an extension of the argument for the clean case assuming a diffusive propagation of the excitations, but it requires some kind of entanglement localization. This behaviour is also observed in Ref. [134] where the propagation of information through the disordered XY model is studied. In particular, both classical and quantum correlations are exponentially suppressed outside of an effective light-cone whose radius grows at most logarithmically with time.

### 2.5.2 Bounds for time evolution of the block entropy

All these results are compatible with the rigorous bounds found in Refs. [135, 136] by means of the Lieb-Robinson bound [137] and its generalizations presented in Refs. [138, 139, 140].

The Lieb-Robinson bound states that the operator norm of the commutator of two operators  $O_A$  and  $O_B$  that act on different regions  $A, B$  of a spin network with local interactions,  $h_{ij}(t)$ , and in different times verifies

$$\| [O_A(t), O_B(0)] \| \leq c N_{min} \|O_A\| \|O_B\| e^{-\frac{L-\nu|t|}{\xi}}, \quad (2.58)$$

where  $L$  is the distance between  $A$  and  $B$  (the number of edges in the shortest path connecting  $A$  and  $B$ ),  $N_{min} = \min\{|A|, |B|\}$  is the number of spins in the smallest of  $A$  and  $B$ , while  $c, \nu, \xi > 0$  are constants depending only on  $g = \max_{(i,j) \in E} \max_t \|h_{ij}(t)\|$  and the architecture of the spin lattice.

Thus, the Lieb Robinson bound, Eq. (2.58), tells us that the norm of the commutator of two operators at different times is exponentially small outside the light-cone given by the velocity  $\nu$  that we can understand like the speed of sound. Notice that, by dimensional analysis, this velocity must be proportional to the energy scale  $g$ . It is interesting to point out that this result is also valid for the case of fermions or local Hamiltonians with exponentially decaying interactions.

In Ref. [135], it is shown, using the Lieb-Robinson bound and its generalizations [138, 139, 140], that correlations and information are propagated at a finite velocity in a spin network with nearest-neighbour interactions. This is a non-trivial result since in non-relativistic quantum mechanics there doesn't exist the notion of a light-cone, i. e. local operations could be used, in principle, to send information at long distances in arbitrary short times.

Moreover, it is quantified the entanglement entropy that can be generated per unit of time between a block of spins and the rest of the system. In particular, it is found that

$$S_L(t) - S_L(0) \leq c^* g P t \quad (2.59)$$

where  $c^* \simeq 1.9$  is a constant and  $P$  is the perimeter of the block. Finally, let us mention that all these results are complemented in Ref. [136].

### 2.5.3 Long range interactions

The Lieb-Robinson bound is only valid for short range interactions. Then, it is interesting to study how does entanglement evolve in systems with long range interactions. This question is addressed in Ref. [141].

In general, systems with long range interactions are numerically intractable since, in them, the entanglement entropy scales with the volume  $S_L \sim L$ . Nevertheless, in Ref. [141], the interactions are restricted to Ising-type which allows to study both the static and the dynamical entanglement properties of the system.

It is considered a lattice composed by  $N$  spins that interact according to the Hamiltonian,

$$H = \sum_{k < l} f(k, l) \frac{1}{4} (\mathbb{1} - \sigma_z^{(k)}) \otimes (\mathbb{1} - \sigma_z^{(l)}), \quad (2.60)$$

where the coefficients  $f(k, l)$ , that describe the strength of the interaction between the spins  $l$  and  $k$ , obey a distance law, that is to say,  $f(k, l) = f(\|k - l\|)$ .

It is assumed that the initial state is a product state of all spins pointing to the x-direction  $|\Psi_0\rangle = |\rightarrow\rangle^{\otimes N}$ . In order to perform the time evolution of this state, a description in terms of Valence Bond Solids (VBS) is used (see Ref. [142]). With this method, it is possible to calculate the reduced density operator of few particles for large systems (the computational time grows linearly with the whole size of the system but exponentially with the size of the block).

In concrete, it is studied for some fixed time  $t$  the scaling properties of entanglement of a system with algebraically decaying interactions  $f(k, l) = \|k - l\|^{-\alpha}$ . It turns out that for  $\alpha \leq 1/2$  (strong long-range interactions) the entanglement grows unbounded and the correlations do not practically decay, while for  $\alpha > 1$  the system contains a bounded amount of entanglement and the correlations decay algebraically.

The dynamics of entanglement are also studied. In the limit of an infinite chain, the entanglement entropy of any block saturates for large times ( $t \rightarrow \infty$ ) to its maximal value  $S_L = L$  in a similar way as in Eq. (2.57).

## 2.6 Entanglement along quantum computation

It is known that slightly entangled quantum systems can be simulated efficiently in a classical computer [1, 143, 144]. This implies that any quantum algorithm that would exponentially accelerate a classical computation must create, at some point, a highly entangled state. Otherwise, the quantum algorithm could be simulated efficiently in a classical computer.

Next, we want to briefly study how the entanglement evolves along a computation. In order to do this, we will consider the three most common paradigms of quantum computation: quantum circuits, adiabatic quantum computation, and one way quantum computing.

### 2.6.1 Quantum circuits

A quantum circuit is a sequence of unitary transformations (quantum gates) on a register of qubits (see Ref. [145] for a pedagogical introduction). An efficient quantum circuit is characterized by the fact that the number of elementary gates that form it only scales polynomially in the number of qubits of the register.

The study of entanglement along a quantum circuit was addressed in Refs. [146] and [147] by means of majorization theory. In these works the introduction of entanglement in Shor's algorithm and the Grover's algorithm were analysed respectively.

Let us remind the concept of Majorization relations, which is a more refined measure of ordering of probability distributions than the usual entropy one. We say that a probability distribution  $\{p_i\}$  majorizes another probability distribution  $\{q_i\}$  (written as  $\vec{p} \prec \vec{q}$ ) if, and only if,

$$\sum_{i=1}^k p_i \leq \sum_{i=1}^k q_i \quad k = 1 \dots d - 1, \quad (2.61)$$

where  $d = 2^N$  is the number of possible outcomes and it will correspond to the dimension of the Hilbert space.

These Majorization relations can be related to quantum circuits in the following way: let  $|\psi_m\rangle$  be the pure state representing the register in a quantum computer in the computational basis at an operating stage labeled by  $m = 0, 1 \dots M - 1$ , where  $M$  is the total number of steps of the algorithm. We can naturally associate a set of sorted probabilities  $p_x^{(m)}$  corresponding to the square modulus of the coefficients of the state in the computational basis ( $x \in \{|0 \dots 0\rangle, |0 \dots 01\rangle, \dots, |1 \dots 1\rangle\}$ ). A quantum

algorithm will be said to majorize step by step this probability distribution if

$$\vec{p}^{(m)} \prec \vec{p}^{(m+1)} \quad \forall m = 1, \dots, M . \quad (2.62)$$

In such a case, there will be a neat flow of probability directed to the values of highest weight, in a way that the probability distribution will be steeper and steeper as the algorithm goes ahead. This implies that the state is becoming less entangled along the computation. Notice that the majorization relations are stricter than an inequality in the entanglement entropy, in such a way that the reverse statement is not true.

In Ref. [148], the step-by-step majorization was found in the known instances of fast and efficient algorithms, namely in the quantum Fourier transform, in Grover's algorithm, in the hidden affine function problem, in searching by quantum adiabatic evolution and in deterministic quantum walks in continuous time solving a classically hard problem. On the other hand, the optimal quantum algorithm for parity determination, which does not provide any computational speed-up, does not show step-by-step majorization.

Recently, a new class of quantum algorithms have been presented. Those are exact circuit that faithfully reproduce the dynamics of strongly correlated many-body system. In Ref. [149], the underlying quantum circuit that reproduces the physics of the XY Hamiltonian for  $N$  spins was obtained. The philosophy inspiring that circuit was to follow the steps of the analytical solution of that integrable model. Looking at the architecture of the circuit in Fig. 2.5, it is easy to realize that the entanglement between the two sets of contiguous  $N/2$  spins is transmitted through the  $N/2$  SWAP gates. Therefore, the maximum entanglement entropy between these two half's of the system that this proposal may allow is  $N/2$ . This is because the maximum entanglement that can generate a quantum gate that acts on two qubits is 1, that is, from a product state to a maximally entangled state (Bell basis). Thus, the scaling law of the entanglement entropy that this proposal will allow will be

$$S(N/2) \leq N/2. \quad (2.63)$$

Notice that, as we have seen in the previous sections, the entanglement entropy of the ground state in the XY model scales only logarithmically. The above circuit, then, can create much more entropy than what is present in the ground state. Yet, we have also discussed the fact that time evolution does create maximum entanglement. This, indeed, is what the above circuit achieves. This shows that the previous proposal is

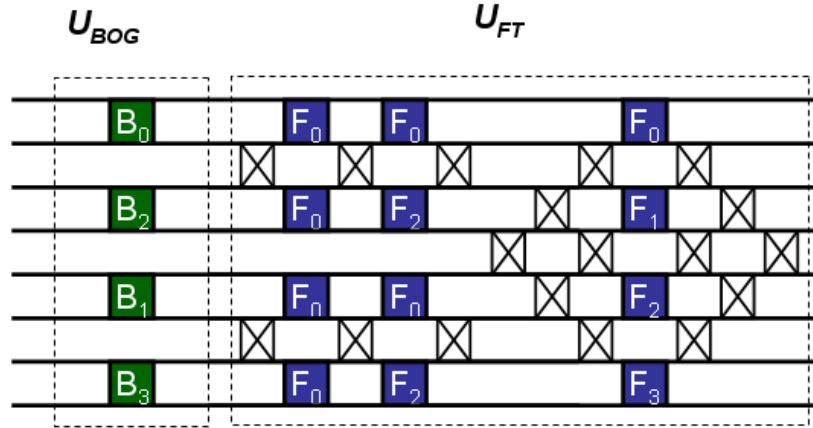


Figure 2.5: Structure of the quantum circuit performing the exact diagonalization of the XY Hamiltonian for 8 sites. The circuit follows the structure of a Bogoliubov transformation followed by a fast Fourier transform. Three types of gates are involved: type-B (responsible for the Bogoliubov transformation and depending on the external magnetic field  $\lambda$  and the anisotropy parameter  $\gamma$ ), type-fSWAP (depicted as crosses and necessary to implement the anti-commuting properties of fermions) and type-F (gates associated to the fast Fourier transform). Some initial gates have been eliminated since they only amount to some reordering of initial qubits [from [149]].

optimal since it carries the minimum possible number of gates such that maximum entanglement can be created.

Let us also add a final example on exact quantum circuits. In Ref. [150], a quantum circuit that creates the Laughlin state (Eq. 2.53) for an arbitrary number of particles (qudits)  $n$  in the case of filling fraction one is presented. The way in which entanglement grows along the circuit is also related to the amount of entanglement that each gate of the circuit can generate. In the case of this Laughlin wave function, the depth of the circuit grows linearly with the number of qudits, so linear entanglement  $S \sim n$  can be supported by the circuit. This is precisely the entanglement that the Laughlin wave function with filling fraction one requires as shown in Ref. [122].

The exact circuits we have discussed (XY and Laughlin states) are both able to create linear entanglement entropy. It is then impossible they can be simulated classically in an efficient way.

## 2.6.2 Adiabatic quantum computation

The framework of adiabatic quantum computation (AQC) was introduced in Ref. [151]. The idea of AQC is the following:

1. A quantum register is initially prepared on the ground state of a known initial Hamiltonian  $H_0$ .
2. The system is then made to evolve adiabatically from this Hamiltonian to a new one  $H_p$  whose ground state codifies the solution to an e.g. NP-complete problem

$$H(s(t)) = (1 - s(t))H_0 + s(t)H_p . \quad (2.64)$$

3. Slow evolution from  $s(t = 0) = 0$  to  $s(t = T) = 1$  guarantees that the system will not jump from the instantaneous ground state of the system to the first excited state.

Quantum adiabatic computation is proven efficient provided that the minimum gap along the adiabatic evolution is only polynomially small in the number of qubits. If this was not the case, the adiabatic computation would require an exponentially large time as measure in terms of the number of qubits in the register.

Thus, according to the previous arguments, at some point of the adiabatic evolution of a hard quantum computation the system must be highly entangled, in a similar way as it happened in the previous sections at the quantum phase transitions. This makes us expect some sort of quantum phase transition for a concrete value  $s_c$  of the Hamiltonian, point that would be characterized by a minimum energy gap.

In Ref. [152], adiabatic quantum computation is used to solve the NP-Complete Exact Cover problem that is a particular case of the 3-SAT problem. It is defined as follows: given the  $n$  Boolean variables  $\{x_i\}_{i=1,\dots,n}$ ,  $x_i = 0, 1 \forall i$ , where  $i$  is the bit index, we define a *clause*  $C$  involving the three bits  $i$ ,  $j$  and  $k$  by the constraint  $x_i + x_j + x_k = 1$ . There are only three assignments of the set of variables  $\{x_i, x_j, x_k\}$  that satisfy this equation, namely,  $\{1, 0, 0\}$ ,  $\{0, 1, 0\}$  and  $\{0, 0, 1\}$ . An *instance* of the Exact Cover problem is a collection of clauses which involves different groups of three qubits. The problem is to find a string of bits  $\{x_1, x_2, \dots, x_n\}$  which satisfies all the clauses.

This problem can be mapped to finding the ground state of a Hamiltonian  $H_p$  in the following way [152]: given a clause  $C$  define the Hamiltonian associated to this

clause as

$$\begin{aligned}
 H_C = \frac{1}{8} & \left( (1 + \sigma_i^z)(1 + \sigma_j^z)(1 + \sigma_k^z) \right. \\
 & + (1 - \sigma_i^z)(1 - \sigma_j^z)(1 - \sigma_k^z) + (1 - \sigma_i^z)(1 - \sigma_j^z)(1 + \sigma_k^z) \\
 & \left. + (1 - \sigma_i^z)(1 + \sigma_j^z)(1 - \sigma_k^z) + (1 + \sigma_i^z)(1 - \sigma_j^z)(1 - \sigma_k^z) \right), \tag{2.65}
 \end{aligned}$$

where  $\sigma^z|0\rangle = |0\rangle$ ,  $\sigma^z|1\rangle = -|1\rangle$ . The quantum states of the computational basis that are eigenstates of  $H_C$  with zero eigenvalue (ground states) are the ones that correspond to the bit string which satisfies  $C$ , whereas the rest of the computational states are penalized with an energy equal to one. The problem Hamiltonian is constructed as the sum of all the Hamiltonians corresponding to all the clauses in the instance,

$$H_p = \sum_{C \in \text{instance}} H_C. \tag{2.66}$$

The ground state of this Hamiltonian corresponds to the quantum state whose bit string satisfies *all* the clauses.

It is known that Exact Cover is a NP-complete problem, so it cannot be solved in a polynomial number of steps in a classical computer [153, 154]. This makes the Exact Cover problem, particularly interesting, since if we had an algorithm to efficiently solve Exact Cover, we could also solve all problems in the much larger NP family <sup>1</sup>.

In Ref. [155], the evolution of the entanglement properties of the system are studied in order to see the expected sign of a quantum phase transition. 300 random instances for the Exact Cover are generated with only one possible satisfying assignment for a small number of qubits. This instances are produced by adding clauses at random until there is exactly only one satisfying assignment. In order to apply adiabatic quantum computation the initial Hamiltonian  $H_0$  taken is a magnetic field in the  $x$  direction

$$H_0 = \sum_{i=1}^n \frac{d_i}{2} (1 - \sigma_i^x), \tag{2.67}$$

where  $d_i$  is the number of clauses in which qubit  $i$  appears. Then, for each instance, the ground state is computed for several values of  $s$  of the Hamiltonian,  $H(s) = (1 - s)H_0 + sH_p$  and its corresponding entanglement entropy of half a chain. The mean of the entanglement entropy over these 300 instances is performed and plotted respect to the  $s$  parameter for different sizes of the system in Fig. 2.6. We can observe a peak of the entropy around the critical value  $s_c \sim 0.7$ .

<sup>1</sup>The NP problems are those whose solutions can be verified in a polynomial time.

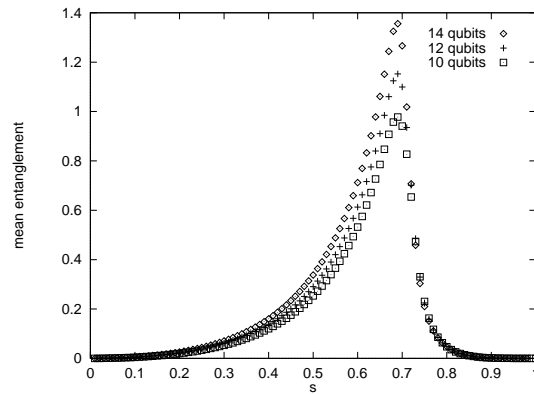


Figure 2.6: Average over 300 instances of the entanglement entropy between two blocks of size  $n/2$  as a function of the parameter  $s$  controlling the adiabatic evolution. A peak appears for  $s_c \sim 0.7$ . The plot also shows the increase of the peak as the number of qubits grows  $n = 10, 12, 14$  [from [155]].

We interpret this behaviour of the entanglement entropy as follows: initially the system is in a product state and its entanglement is zero. Then, the evolution makes the system explore different solutions by means of superposition states of them, that is, it becomes more and more entangled. Finally, the system throws away the bad solutions, the entanglement decreases, until the best solution is found and it rests in a product state again. Roughly speaking, the power of the quantum computer respect to the classical one underlies in the parallelism during the computation that the superposition principle allows.

Let us make some warning remarks. The numerical simulations performed for the Exact Cover problem cannot determine the complexity class for the quantum algorithm. It is generally believed that quantum computers will not be able to handle NP-complete problems. Yet, the simulation shows that the best this quantum algorithm can achieve still requires a huge amount of entanglement in the register.

The divergence of the entanglement entropy that occurs at the critical point  $s_c$  have also been observed in Shor's factoring algorithm in Ref. [155], where entropy grows exponentially fast respect the number of qudits. This, again, makes this algorithm hard to simulate classically.

Notice that in the solution of other problems, the explosion of the entropy could occur at  $s_c = 1$  in such a way that the entanglement entropy was monotonically increasing. This similar behaviour of the entropy to the quantum phase transition is, therefore, problem dependent.

Recently, there has been appeared a new quantum algorithm for SAT problems that improve the previous results. It consists of a hybrid procedure that alternates non-adiabatic evolution with adiabatic steps [156].

### 2.6.3 One way quantum computation

The one-way quantum computation (or measurement based QC) is a method to perform quantum computation that consists of: (i) first, an entangled resource state is prepared, and (ii) then single qubit measurements are performed on it. It is called "one-way" because the entanglement of the state, which is the resource of the quantum computation, is destroyed by the measurements as the computation is being performed. Although the output of each individual measurement is random, they are related in such a way that the computation always succeeds. The idea is that depending on the previous outcome, one chooses the basis for the next measurements. This implies that the measurements cannot be performed at the same time.

This kind of computation was introduced in Refs. [157, 158, 159] where there was shown that with an initial particular state, called cluster state, any quantum computation could be simulated. Later on, other useful states to perform one-way quantum computation were found [160, 161, 162, 163, 164]

The fact that the measurement based quantum computation is universal is non-obvious, since a quantum computation is a unitary process, while a measurement is a random process. The key point is that there are two kinds of qubits in the spin system: the cluster qubits which will be measured in the process of computation and the logical qubits which constitute the quantum information that is going to be processed.

Although, globally, entanglement is expected to decrease along the quantum computation due to the single qubit measurements, in the set of logical qubits (the register that will be read out at the end of the computation), the entanglement may increase. Notice that if the initial state fulfils an area law, the entanglement is enough that the register of the logical qubits is as entangled as possible. That is, area law on a 2D state is just what is needed to have linear maximal entanglement on a register defined on a line in that state. Cluster states are just enough to handle the expected entanglement in the register. In this respect, it has been recently shown that most quantum states are too entangled to be useful in order to perform measured based quantum computation [165].

## 2.7 Conclusion: entanglement as the barrier for classical simulations

Entanglement is the genuine quantum property that escapes classical physics. The Hilbert space structure of a multi-partite quantum system allows for superpositions of exponentially many elements of the basis. Entropy of entanglement is a way to quantify the amount of quantum correlation between parts of such a multi-partite system. Entanglement entropy is, then, a genuine measure of the global quantumness of the state.

It serves as a conclusion to recall the deep implications of entanglement entropy in the possibility of producing faithful classical simulations of quantum mechanics. In Ref. [1], it was proven that efficient simulations are possible for any system where all its Schmidt decompositions in two arbitrary parts would carry little entropy. Therefore, entanglement is at the heart of the separation between efficient and non-efficient simulations of quantum mechanics.

What is not fully understood is what is the best strategy to classically account for quantum correlations. Two general and clever ideas are available in the literature. The first idea consists in exploiting the fact that typical interactions are local. This suggests that entanglement should be created sequentially in space from each local degree of freedom to its nearest neighbours. Then, a one-dimensional state can be represented as a matrix product state which captures such a principle [166, 167]. In higher dimensions, states can be represented as Projected Entangled Pairs (see Refs. [142, 168]). The second idea to classically represent quantum states as efficiently as possible consists in reconstructing the correlations in the system as a renormalization group tree. This goes under the name of Multiscale Entanglement Renormalization Ansatz (MERA) is a more sophisticated representation which is specially suited for critical systems. The accuracy of the approximations can be quantify using the amount of entropy of entanglement that the approximation can accommodate [169, 170].

Multi-partite entanglement branches in many others subjects that escape this short review. Very likely, much more work is still needed to get a profound understanding of the role of entanglement in highly structured quantum systems.

---

# Area-law in $D$ -dimensional harmonic networks

---

As we have seen in the previous chapter, the amount of entanglement present in a quantum state is of fundamental relevance to determine how hard it is to simulate it by classical means. It is generally argued that a highly entangled quantum state carries a huge superposition of product states that cannot be handled on a classical computer. Yet, this statement must be made precise, since a small amount of entanglement can indeed be simulated efficiently. The relevant precise question is, thus, how much entanglement can be efficiently simulated classically.

This abstract question should at least be clarified when considering relevant physical systems. Can the amount of entanglement present in a two-dimensional lattice of harmonic oscillators be efficiently represented in a classical computer? Although the answer to this question is not yet settled, qualitative progress has been recently achieved. One of the ingredients essential to this discussion is the area law for the geometric entropy and the representation of quantum states by projected entangled pairs.

A important related problem is to understand how entanglement varies along renormalization group (RG) trajectories. We shall bring growing evidence for the idea that RG flows entail a loss of entanglement. This entanglement loss will be

shown compatible with area law scaling of the entropy.

We organize the contents of this chapter by first reviewing a number of previous results on area law scaling of ground state entropy in different systems using the language of condensed matter, quantum field theory and quantum information theory. For a deeper comprehension of the field, interested readers are encouraged to study the recent review [6]. Next, we will present a computation of entanglement entropy on a discretized bosonic free field theory in arbitrary dimensions. This gives us control on the eigenvalues of the reduced density matrix on a subsystem which, in turn, allows for a discussion of majorization relations obeyed by the reduced density matrix of the system. We extend this discussion to the single-copy entanglement measure. RG loss of entanglement is also verified in detail for arbitrary dimension networks of harmonic oscillators.

## 3.1 A brief review of the area law

### 3.1.1 Volume vs. area law

Random states are known to carry large entanglement. To be precise, let us consider a random infinite system of qubits. On average, the density matrix for a random subset of  $N$  qubits carries maximum von Neumann entropy,

$$S(\rho_N) \simeq N . \quad (3.1)$$

This result [171] shows that the entropy of random states grows as the number of particles included in the subset. This is referred to as a *volume law* scaling. An arbitrary state uses the maximum possible superposition of the basis elements with no symmetry whatsoever among their coefficients. Its efficient representation by classical means appears certainly difficult.

Physical theories create entanglement through interactions, which are typically local. Thus, e.g. the ground state of a sensible physical Hamiltonian is not a random state. It is natural to expect a low amount of entropy since local interactions will entangle the non-contiguous degrees of freedom in a somewhat sequential way. We may encounter local intense entanglement that dilutes at long distance. This is precisely the structure of standard quantum theories, with correlations that decay with a power law at phase transitions and with an exponential law away from them. It is then reasonable to ask what is the limit of efficient simulability in terms of the entanglement present in a given state.

In many physical theories, local degrees of freedom are arranged in a specific geometrical way as mentioned previously. We may have quantum systems defined on spin chains, networks or, in general,  $D$ -dimensional lattices. Those systems may have a continuum limit described by a quantum field theory or, alternatively, may be devised as quantum simulators, a preview of quantum computers. We may then discuss the amount of geometrical entanglement present on the system from three complementary points of view: condensed matter, quantum field theory and quantum information.

As we shall see, the basic ingredient of locality of interactions suggests that entropy for a geometrical region should be dominated by the entanglement present on the surface separating it from the rest of the system. To be precise, consider an infinite  $D$ -dimensional lattice where we assign part  $A$  to an inner hypercube of size  $L$ ,  $N = L^D$ , and part  $B$  to the outside. Locality seems to suggest

$$S(\rho_L) \sim L^{D-1} \sim N^{\frac{D-1}{D}}. \quad (3.2)$$

This behavior is commonly referred to as *area law* scaling for the geometric entropy. Let us note that one-dimensional quantum systems correspond to a well understood limiting case for the above formula, where the power law turns out to be substituted with a logarithmic scaling at phase transitions, that is

$$S(\rho_L) \sim \log L, \quad (3.3)$$

and saturates away from them

$$S(\rho_L) < \text{constant}, \quad \forall L, \quad (3.4)$$

as shown in Ref. [4, 59, 73] These results are deeply connected to conformal symmetry and control the classical simulability of the system.

Recent evidence hints at a log violation of the area law in some two-dimensional systems made with anticommuting variables [85, 86, 172, 84]. To be precise, some of these models display an entropy scaling law of the type

$$S(\rho_L) \sim L^{D-1} \log L. \quad (3.5)$$

It is unclear whether such systems support a limiting quantum field theory description in the continuum limit.

It is important to make a general remark concerning the different approaches to the computation of entanglement in quantum systems. Let us note that discretized

quantum systems allow for uncontroversial computations of the entropy. This is not the case of quantum field theories, where regularization and renormalization are needed since the number of degrees of freedom is formally unbounded. In such a framework, the adimensional entropy requires the appearance of some short-distance regulator  $\epsilon$

$$S(\rho_L) \sim \left(\frac{L}{\epsilon}\right)^{D-1} \quad (3.6)$$

which entails the necessary discussion of its renormalization and its observability. Let us just mention here that the coefficient of the area law is universal for  $D = 1$  systems whereas remains scheme-dependent in higher dimensions.

The problem turns extremely subtle in the case of gravity, where the geometry of space-time is dynamical and the way to compute for a black hole the Bekenstein area law pre-factor from first principles is far from clear [173, 89, 174]. Recent progress on the side of AdS/CFT correspondence seems to link entanglement entropy in a quantum field theory living on the boundary to the black-hole entropy of the bulk [89, 174].

### 3.1.2 Locality and PEPS

The basic heuristic argument for an area law scaling of entropy for the ground state of physical systems is rooted in the locality of the interactions. Steps to make this argument quantitative have been made in Refs. [142, 175, 176, 177, 178, 2].

A local Hamiltonian tends to entangle nearest neighbors. Long-distance entanglement emerges as a coherent combination of local interactions. The correctness of this argument would imply that the reduced entropy of a geometric bipartition of a system will get its main contribution from the entanglement between degrees of freedom at opposite sites of the boundary that separates the regions. This, in turn, implies an area-law scaling. Let us note that such a naive argument works in any dimension and does not depend on the correlation length present in the system. Area law would emerge from locality, whatever the mass-gap is. We shall discuss the limitations of this argument shortly.

This argument needs a clear formulation and verification. Although we lack definite answers about the necessary and sufficient conditions a Hamiltonian must obey to produce a ground state with area law entropy, some progress has been achieved using one-dimensional Matrix Product States (MPS) and their generalization to higher dimensions, Projected Entangled Pair States (PEPS). We first consider a one-dimensional

system with open boundary conditions described by a MPS

$$|\psi\rangle = \sum \left( A_{\alpha_1}^{i_1} A_{\alpha_1 \alpha_2}^{i_2} \dots A_{\alpha_{n-1}}^{i_n} \right) |i_1 \dots i_n\rangle, \quad (3.7)$$

where the sum extends to  $i_1, \dots, i_n = 1, \dots, d$ , which are physical indices attached to local Hilbert spaces, and  $\alpha_1, \dots, \alpha_{n-1} = 1, \dots, \chi$ , which are ancillae indices. The tensors  $A_{\alpha\beta}^i$  can be viewed as projectors from the ancillae indices to a physical one. This representation provides the basis for the density matrix renormalization group technique.

The generalization of the MPS construction to higher dimensional networks carries the name of PEPS. In a  $D$ -dimensional network, where ancillae degrees of freedom are linked to their nearest neighbors, the role of the MPS projector is taken by a tensor of the form

$$A_{\alpha\beta}^a, \quad (3.8)$$

where the physical indices span a  $D$ -dimensional lattice and ancillae run from 1 to  $\chi$ . Again, the role of each tensor  $A$  is to project maximally entangled pairs connecting local neighbors onto a physical local space. Entanglement is thus carried by the links connecting ancillae. Each entangled pair, that is, each sum over one ancilla index hides a connecting bond of the type  $\sum_{\alpha=1}^{\chi} \frac{1}{\sqrt{\chi}} |\alpha\alpha\rangle$ . If one of the two ancillae in the bond is traced out, the entropy for the remaining ancilla is  $S = \log \chi$ .

We are now in a position to present the argument in Ref. [142] showing that finite  $\chi$  PEPS entail area law scaling for the entropy. Let us assume that the ground state of a quantum system is described by a PEPS with finite  $\chi$ . It follows that the entropy of a subpart of the system is bounded by the number of bonds which are cut by the separating surface times the entropy per broken bond. This amounts to an area law

$$S(\rho_A) \leq (\# \text{cut bonds}) \log \chi \sim \text{Area} \log \chi. \quad (3.9)$$

A violation of the area law within the PEPS representation requires infinite-dimensional ancillae.

We should again distinguish the one-dimensional case, where the ground state of infinite critical systems are known to carry logarithmic entropy [4],

$$S(\rho_L) \sim \frac{c}{3} \log \frac{L}{a}, \quad (3.10)$$

where  $a$  is the lattice spacing and  $c$  the central charge that characterizes the universality class of the phase transition. Yet, the boundary of a one-dimensional block is

made by two single points. Such a state with logarithmic entropy cannot be represented using finite dimensional MPS and we must resort to arbitrarily large  $\chi$ . This limitation is at the heart of the problems that the DMRG technique encounters when applied to quantum phase transitions. On the other hand, the entropy is bounded away from critical points and MPS provide an efficient way to represent the system. MPS states with finite  $\chi$  are often referred to as finitely correlated states.

Coming back to higher dimensions, it is then a major issue to establish whether finite  $\chi$  PEPS can describe faithfully the ground state of physical systems. The fact that PEPS with finite  $\chi$  can incorporate an area law is appealing. Recently, a particular class of finite PEPS has been constructed that display polynomial decay laws, that is long range correlation [2]. These PEPS are also shown to describe ground states of frustration-free Hamiltonians and such states can approximate exponentially well any finitely correlated state. It is still unclear whether the ground states of standard quantum systems fall into this description or, alternatively, they need infinite  $\chi$ . This may set apart what is efficiently simulable from what is not.

### 3.1.3 Renormalization group transformations on MPS and PEPS and the support for an area law

We have argued that one-dimensional finite  $\chi$  MPS can support a maximum amount of entropy independent of the size of the system and that, in contradistinction, finite  $D$ -dimensional PEPS can accommodate an area law. Let us give an independent quantitative argument for this statement.

Consider a renormalization group transformation of a MPS state with constant  $A$  defined by the coarse graining of two sites [179]

$$A_{\alpha\beta}^i A_{\beta\gamma}^j \equiv \tilde{A}_{\alpha\gamma}^{ij} = \sum_{l=1}^{\min(d2, \chi^2)} \lambda_l U_l^{(ij)} V_{\alpha\gamma}^l \quad (3.11)$$

where we have decomposed the product of two adjacent matrices using a singular value decomposition. We can understand the unitary matrix  $U$  as a change of basis on the new coarsed degree of freedom and construct a new MPS with  $A_{\alpha\gamma}^l = \lambda_l V_{\alpha\gamma}^l$ . Therefore, the ancillae indices close under such operation whereas the physical index grows. Upon iteration of this operation, the range of the physical index will reach a maximum value  $\chi^2$  and will get locked to that value. This is the magic of one dimension. The long-distance properties of the system are completely described by a single square effective matrix! Entropy is then bounded.

The analogous argument in two-dimensional systems follows a slightly different path. The coarse graining step reads

$$\begin{array}{c} A^a \\ \alpha^\gamma \mu \\ A^c \\ \alpha' \delta \mu' \end{array}
 \begin{array}{c} A^b \\ \mu \gamma' \beta \\ A^d \\ \mu' \delta' \beta' \end{array}
 = \tilde{A}^{ab}{}_{\alpha\alpha' \delta\delta' \beta\beta'}
 = \sum_{l=1}^{\min(d^4, (\chi^4)^2)} \lambda_l U_l^{cd} V_l^{ab}{}_{\alpha\alpha' \delta\delta' \beta\beta'} \quad (3.12)$$

As before, we can absorb the global  $U$  as a change of the local coarse-grained basis and assign a new PEPS to  $\lambda V$ . Note the different growth of indices. On the one hand, physical indices merge in groups of four and would naively need a volume law increase,  $d^4$ . On the other hand, the ancillae rank increase from  $\chi^4$  to  $(\chi^4)^2$ , that is, it follows an area law. Given that the singular value decomposition will be locked by the smallest dimension of the two above, the area law will define the rank of the tensor that contains the effective long distance description of the model. The argument generalizes to  $D$  dimensions where the PEPS  $A_{\alpha_1, \dots, \alpha_{2D}}^i$  with a physical index  $i = 1, \dots, d$  and ancillae indices  $\alpha_1, \dots, \alpha_{2D} = 1, \dots, \chi$ . A renormalization group transformation of this PEPS makes the new collective physical index to run  $i' = 1, \dots, d^{2D}$ , that is, with a volume law, and the new collective ancillae  $\alpha'_1, \dots, \alpha'_{2D} = 1, \dots, \chi^{2^{D-1}}$ , that is, as an area law. The singular value decomposition makes all the long-distance properties of the state to be contained in an effective PEPS with a number of degrees of freedom that grows with just an area law. The rank of the effective PEPS is  $\log \chi_{eff} = 2^{D-1} \log \chi$ . From this simple argument, it follows that PEPS can support an area law scaling for the geometrical entropy.

### 3.1.4 Some explicit examples of area law

There is an extensive literature on computations of the entropy for particular cases that cannot be faithfully summarized here.

One-dimensional spin systems (e.g. quantum Ising model, XX model and Heisenberg model) obey a logarithmic scaling at the critical point [59, 73, 38, 4, 65, 180]. Away from the quantum phase transition point, the entropy gets saturated. This explicit computation falls into the universal scaling predicted by conformal invariance. This result has been further verified and extended to many other quantum systems in one dimension.

The literature on computations of entanglement entropy in higher dimensional systems is far less extensive due to the difficulty to produce explicit results. The first analysis of the entanglement entropy in two- and three-dimensional systems were done in discretized approaches to quantum field theory [3, 78, 77]. Further analysis

---

Spin chains away from criticality	$S \sim \text{constant}$
Critical spin chains	$S \sim \log N$
$D$ -dimensional harmonic networks	$S \sim N^{\frac{D-1}{D}}$
NP-complete problems	$S \sim N$

---

showed that the entanglement entropy is related to the trace anomaly in curved space times giving an explicit relation between the actual results for free fermions and free bosons [79].

Rigorous computations in discretized harmonic networks proved no departure from the area law [176, 177, 181]. Further analysis of entanglement entropy on higher dimensional networks has been done in Refs. [182, 183, 141].

### 3.1.5 Exceptions to the area law

We have argued that the area law is deeply connected to locality of interactions. It is, therefore, reasonable to expect violations of such scaling in models with non-local interactions. This is the generic case of a quantum computation of an NP-complete problem. It has been numerically verified that this is the case when an adiabatic quantum computation is applied to the NP-complete Exact Cover problem, a variant of the 3-SAT problem. Along the computation, the ground state becomes maximally entangled, that is its entropy scales as the volume of the system [155, 184, 185]. A physical quantum computer will definitely need to face the challenge of maintaining those huge fine-tuned superpositions of states.

Locality of interactions is not the only ingredient that controls entropy. Entropy is related to the eigenvalues of the Schmidt decomposition of a system in two parts. If the subsystems retain a lot of symmetry, the sub Hilbert spaces organize themselves in representations of the symmetry group. This entails a reduction of the Schmidt number of the above decomposition, that is, a lower entropy. Such a counter mechanism to reduce the entropy in highly connected systems has been explicitly checked in the case of the Lipkin-Meshkov model which is defined by a spin system fully and symmetrically connected. Although it is tempting to argue that the system is infinite-dimensional (the geometry of the Hamiltonian corresponds to a simplex of  $N \rightarrow \infty$  vertices), the entropy scales only logarithmically, which is the actual bound for symmetric spaces [118]. This logarithmic scaling of the entropy follows the one-dimensional log law, which might just be an accident.

It should not come as a surprise that slightly entangled states that do not correspond to an eigenstate of a given Hamiltonian dynamically evolve to highly entangled states under its action. This has been analyzed in Refs. [128, 107] even for simple Hamiltonians like the quantum Ising chain. No area law is expected for slightly entangled random states when they are evolved with local Hamiltonians.

As mentioned previously, a case of non-trivial violation of the area law was first considered in [85] and then analyzed in [86, 172]. Some two-dimensional systems with anticommuting variables were found to display a log correction to the area law, that is,  $S \sim L \log L$ . On the other hand, some previous computations for free Dirac fermions seem to produce no area-law violation [186, 80, 187] in any number of dimensions. This issue deserves further investigation. Moreover, in the computation of quantum corrections to the entropy of a black hole, logarithmic corrections have also been obtained [188].

Finally, let us mention an recent work in which a one dimensional non-translational invariant system composed of a line of 12 level quantum particles with nearest neighbor interactions that violates area-law is presented [189]. In particular, it is shown that the problem of approximating the ground state energy of such system is QMA-complete. In computational complexity theory, QMA is the quantum analogue to NP complexity class. This precise example shows that a quantum computer could not simulate any one dimensional system, and, moreover, that there exist one-dimensional systems which take an exponential time to relax to their ground states at any temperature, making them candidates for being one-dimensional spin glasses. Then, it seems that if we want to obtain a volume law for a system with local interactions, we must break the translational symmetry.

### 3.1.6 Physical and computational meaning of an area law

We can attach physical meaning to an area law scaling of entropy in different but related ways. We may argue that entropy is a measure of surprise due to quantum correlations and that a state that obeys an area law carries less correlations than a random state. As the size of the inner block increases, we only get a reduced amount of surprise, compare to the maximum possible, when discovering that our block was correlated to the exterior. It is then arguable that the theory that has produced such a state may accept a simpler description. In some sense, this argument is implicit in the holographic description of some quantum systems.

From a computational point of view, low entropy means small quantum corre-

lations, that is, small entanglement. It is known that states that are only slightly entangled can be efficiently simulated by classical means [1]. A fundamental question is thus formulated: what entropy growth law can be efficiently simulated by a classical computer?

So far, this question can only be answered partially. In one dimension,  $D = 1$ , quantum critical phenomena show a logarithmic scaling which cannot be reproduced using finite MPS techniques. Formally, the simulation remain efficient in the sense that to reproduce critical behavior we need  $\chi$  to be polynomial in  $L$ . This, though, produces an obvious practical computational slowing down and limitation. A new promising idea to represent a quantum state with a different and non-local tensor structure has been proposed in Ref. [190] with the name of multi-scale entanglement renormalization ansatz (MERA). The basic idea is to substitute a linear MPS representation with a RG-inspired construction that also identifies the key use of disentangling operations for blocks before proceeding to a coarsened description.

The question in two dimensions has been addressed in [142] in a sequential way. A PEPS is taken as lines of spins that are collected into effective degrees of freedom which are further treated in a MPS manner.

## 3.2 Area law in $D$ dimensions

### 3.2.1 The Hamiltonian of a scalar field in $D$ dimensions

Let us consider the theory of a set of harmonic oscillators in  $D$  dimensions which is expected to verify area law scaling of the entropy. A number of non-trivial issues can be discussed in this explicit example. First, we shall analyze the regularized version of a scalar free field theory in order to get its reduced density matrix when an inner geometrical ball is integrated out. Its eigenvalues can, then, be used to compute the geometrical entropy that will scale as dictated by the area law. Second, we can compare the behavior of the entropy to the one of the single-copy entanglement. Third, we can analyze whether area law scaling is backed by a deeper sense of order, namely majorization theory.

Our computation will generalize the one presented in Ref. [3] to  $D$  dimensions. Let us consider the Klein-Gordon Hamiltonian

$$H = \frac{1}{2} \int d^D x \left( \pi^2(\vec{x}) + |\nabla \phi(\vec{x})|^2 + \mu^2 |\phi(\vec{x})|^2 \right), \quad (3.13)$$

where  $\pi(x)$  is the canonical momentum associated to the scalar field  $\phi(x)$  of mass  $\mu$ . The  $D$ -dimensional Laplacian reads

$$\Delta\phi = \frac{1}{r^{D-1}} \frac{\partial}{\partial r} \left( r^{D-1} \frac{\partial\phi}{\partial r} \right) + \frac{1}{r^2} \hat{L}^2 \phi, \quad (3.14)$$

where  $r = |\vec{x}|$  and  $\hat{L}^2$  is the total angular momentum operator in  $D$  dimensions. It is convenient to introduce the real spherical harmonic functions  $Z_{l\{m\}}$ , which are eigenfunctions of  $\hat{L}^2$  with eigenvalues  $l(l+D-2)$ . The set of numbers  $\{m\}$  stand for other Casimir and component labels in the group  $SO(D)$ . We now project the angular part of the scalar fields  $\pi$  and  $\phi$ ,

$$\pi_{l\{m\}}(r) = r^{\frac{D-1}{2}} \int d^D x Z_{l\{m\}}(\theta_1, \dots, \theta_{D-2}, \varphi) \pi(\vec{x}) \quad (3.15a)$$

$$\phi_{l\{m\}}(r) = r^{\frac{D-1}{2}} \int d^D x Z_{l\{m\}}(\theta_1, \dots, \theta_{D-2}, \varphi) \phi(\vec{x}), \quad (3.15b)$$

where  $r, \theta_1, \dots, \theta_{D-2}$  and  $\varphi$  define the spherical coordinates in  $D$  dimensions. The Hamiltonian now reads

$$H = \sum_{l\{m\}} H_{l\{m\}} \quad (3.16)$$

where,

$$H_{l\{m\}} = \frac{1}{2} \int dr \left( \pi_{l\{m\}}^2(r) + r^{D-1} \left( \frac{\partial}{\partial r} \left( \frac{\phi_{l\{m\}}(r)}{r^{\frac{D-1}{2}}} \right) \right)^2 + \left( \frac{l(l+D-2)}{r^2} + \mu^2 \right) \phi_{l\{m\}}^2(r) \right). \quad (3.17)$$

An ultraviolet regularization of the radial coordinate in the above Hamiltonian will transform the scalar field theory into a chain of coupled harmonic oscillators. This is achieved by discretizing the continuous radial coordinate  $r$  into a lattice of  $N$  discrete points spaced by a distance  $a$ ,

$$H_{l\{m\}} = \frac{1}{2a} \sum_{j=1}^N \left( \pi_{l\{m\},j}^2 + \left( j + \frac{1}{2} \right)^{D-1} \left( \frac{\phi_{l\{m\},j+1}}{(j+1)^{\frac{D-1}{2}}} - \frac{\phi_{l\{m\},j}}{j^{\frac{D-1}{2}}} \right)^2 + \left( \frac{l(l+D-2)}{j^2} + \mu^2 \right) \phi_{l\{m\},j}^2(x) \right). \quad (3.18)$$

The size of the system is  $L = (N+1)a$ , where  $a$  and  $L$  act as an ultraviolet and infrared cutoff respectively. We can compare this expression with the Hamiltonian of an open chain of  $N$  coupled harmonic oscillators,

$$H = \frac{1}{2} \sum_{i=1}^N p_i^2 + \frac{1}{2} \sum_{i,j=1}^N x_i K_{ij} x_j \quad (3.19)$$

and identify  $K_{ij}$  as

$$\begin{aligned}
K_{ij} = & \left( \frac{l(l+D-2)}{j^2} + \mu^2 \right) \delta_{ij} \\
& + \left( 1 - \frac{1}{2j} \right)^{D-1} \theta \left( j - \frac{3}{2} \right) \delta_{ij} \\
& + \left( 1 + \frac{1}{2j} \right)^{D-1} \theta \left( N - \frac{1}{2} - j \right) \delta_{ij} \\
& + \left( \frac{j + \frac{1}{2}}{\sqrt{j(j+1)}} \right)^{D-1} \delta_{i,j+1} + \left( \frac{i + \frac{1}{2}}{\sqrt{i(i+1)}} \right)^{D-1} \delta_{i+1,j}, \quad (3.20)
\end{aligned}$$

where  $\theta$  is the step function.

### 3.2.2 Geometric entropy and single-copy entanglement

We now proceed to trace out an inner geometric ball around the origin to obtain the reduced density matrix of the ground state of the system on the exterior of that ball. Following similar steps as in [3] we define  $\Omega$  as the square root of  $K$ , that is  $K = \Omega^2$ . The gaussian ground state of the system can be expressed as,

$$\psi_0(x_1, \dots, x_N) = \pi^{-N/4} (\det \Omega)^{1/4} e^{-\frac{x^T \Omega x}{2}}, \quad (3.21)$$

where  $x \equiv (x_1, \dots, x_N)$ . We construct the density matrix  $\rho_{out}$  by tracing over the inner  $n$  oscillators,

$$\rho_{out}(x, x') \sim e^{-\frac{1}{2}(x^T \cdot \gamma \cdot x + x'^T \cdot \gamma \cdot x') + x^T \cdot \beta \cdot x'}, \quad (3.22)$$

where  $\beta$  and  $\gamma$  are defined by

$$\beta \equiv \frac{1}{2} B^T A^{-1} B \quad (3.23a)$$

$$\gamma \equiv C - \beta \quad (3.23b)$$

and  $A = \Omega(1 \div n, 1 \div n)$ ,  $B = \Omega(1 \div n, n + 1 \div N)$  and  $C = \Omega(n + 1 \div N, n + 1 \div N)$  are sub-matrices of  $\Omega$ .

We proceed with the diagonalization of this structure rotating and rescaling the variables  $x = V^T \gamma_D^{-1/2} y$  where  $\gamma = V^T \gamma_D V$  and  $\gamma_D$  is diagonal. Using this transformation,  $\gamma$  becomes identity,  $\beta \rightarrow \beta' = \gamma_D^{-1/2} V \beta V^T \gamma_D^{-1/2}$  and the density matrix reads

$$\rho_{out}(y, y') \sim e^{-\frac{1}{2}(y^2 + y'^2) + y^T \cdot \beta' \cdot y'}. \quad (3.24)$$

If we do the appropriate change of coordinates  $y = W \cdot z$  (where  $W$  is an orthogonal matrix) such that  $W^T \cdot \beta' \cdot W$  becomes diagonal with eigenvalues  $\beta'_i$ , we get  $\rho_{out}$  as a tensor product of the two coupled harmonic oscillators density matrices,

$$\rho_{out}(z, z') \sim \prod_{i=1}^{N-n} e^{-\frac{1}{2}(z_i^2 + z_i'^2) + \beta'_i z_i z_i'} . \quad (3.25)$$

We can now compute the entropy associated to the reduced density matrix  $\rho_{out}$ . This entropy can be expressed as a sum over contributions coming from each term in the reduced density matrix tensor product structure,

$$S_{l\{m\}} = \sum_{i=1}^{N-n} S_{l\{m\},i}(\xi_i) , \quad (3.26)$$

where

$$S_{l\{m\},i}(\xi_i) = -\log(1 - \xi_{l\{m\},i}) - \frac{\xi_{l\{m\},i}}{1 - \xi_{l\{m\},i}} \log \xi_{l\{m\},i} \quad (3.27)$$

is the entropy associated to each sub-density matrix in the product shown in Eq.(3.25) and  $\xi_{l\{m\},i}$  is the parameter that generates the eigenvalues of these densities matrices. Note that each eigenvalue  $\xi = \xi_{l\{m\},i}$  entails a set of probabilities of the form

$$p_n = (1 - \xi)\xi^n \quad n = 0, 1, 2, 3, \dots \quad (3.28)$$

defined by  $\xi_i = \beta'_i / (1 + (1 - \beta_i'^2)^{1/2})$  for each  $l\{m\}$  set.

To compute the total entropy, we have to sum over all possible values of  $\{m\}$  and  $l$ .

$$S = \sum_{l\{m\}} S_{l\{m\}} . \quad (3.29)$$

We realize from Eq.(3.17) that  $H_{l\{m\}}$  only depends on  $l$ , so the entropy associated to its ground state will also be  $\{m\}$  independent, and therefore

$$S = \sum_{l=0}^{\infty} \nu(l, D) S_l , \quad (3.30)$$

being  $\nu(l, D)$  the degeneracy of the total angular momentum operator  $\hat{L}^2$  for a fixed  $l$ . In three dimensions, for example,  $\{m\} = m$  can go from  $-l$  to  $l$  so that  $\nu(l, 3)$  is  $2l+1$ . The same computation in  $D$  dimensions requires the computation of the degeneracy of  $SO(D)$  representations

$$\nu(l, D) = \binom{l+D-1}{l} - \binom{l+D-3}{l-2} . \quad (3.31)$$

Given the explicit knowledge of all the eigenvalues of the reduced density matrix, we can also obtain a formula for the single copy entanglement Eq.(1.25). The largest eigenvalue of density matrix for two coupled harmonic oscillators is  $(1 - \xi)$ . This largest eigenvalue of the density matrix  $\rho_{out}$  will be the product of the largest eigenvalues of the density matrices which compound  $\rho_{out}$ ,

$$\rho_{out}^{(1)} = \prod_{l\{m\}} \prod_{i=1}^{N-n} (1 - \xi_{l\{m\},i}) \prod_{l=0}^{\infty} \left( \prod_{i=1}^{N-n} (1 - \xi_{l\{m\},i}) \right)^{v(l,D)}. \quad (3.32)$$

The single copy entanglement finally reads

$$E_1(\rho_L) = - \sum_{l=0}^{\infty} v(l,D) \left( \sum_{i=1}^{N-n} \log(1 - \xi_i) \right). \quad (3.33)$$

### 3.2.3 Perturbative computation for large angular momenta

Note that our expressions for the entropy and the single copy entanglement depend on a final sum that ranges over all the values of angular momentum  $l$ . This sum may not be convergent as the radial discretization we have implemented is not a complete regularization of the field theory. To be precise, the asymptotic dependence on  $l$  should be under control in order to correctly assess the convergence of the series.

Let us note that, for  $l \gg N$ , the non diagonal elements of  $K$  Eq.(3.20) are much smaller than the diagonal ones. These suggests the possibility of setting up a perturbative computation.

We split up the  $K$  matrix in a diagonal  $K_0$  and non diagonal  $\lambda\eta$  matrices, where parameter  $\lambda$  is just introduced to account for the order in a perturbative expansion of the non-diagonal piece,

$$K = K_0 + \lambda\eta. \quad (3.34)$$

This expansion is somewhat tedious and non illuminating. Technical details are presented in Appendix A. The main observation is that the first contribution  $i = 1$  out of every set of  $\xi_{l,\{m\},i}$  elements is relevant and it can further be expanded as a series in  $l^{-1}$ ,

$$\xi \equiv \xi_{l,\{m\},1} = \frac{1}{l^4} \sum_{k=0}^5 \frac{\xi_k}{l^k} + O(l^{-10}) \quad (3.35)$$

We can then get the entropy  $S_{l\{m\}}$ .

$$S_{l\{m\}} \simeq S_{l\{m\},1} = \sum_{k=1}^{\infty} \left( \frac{1}{k} - \log(\xi) \right) \xi^k = \frac{1}{l^4} \sum_{k=0}^5 \frac{s_k + t_k \log l}{l^k} + O(l^{-10}), \quad (3.36)$$

where the coefficients  $s_k$  and  $t_k$  are defined in Appendix A. A similar result for the single copy entanglement reads,

$$\begin{aligned} E_1 &\simeq \sum_{l=0}^{\infty} -\nu(l, D) \log(1 - \xi) + O(l^{-10}) \\ &= \sum_{l=0}^{\infty} \nu(l, D) \sum_{k=1}^{\infty} \frac{\xi^k}{k} \simeq \sum_{l=0}^{\infty} \nu \sum_{j=1}^5 \frac{\kappa_j}{l^{4+j}} + O(l^{-10}), \end{aligned} \quad (3.37)$$

where  $\kappa_j$  are the coefficients of the expansion given also in Appendix A. Finally, using Eq.(3.31) and defining  $\tau_k \equiv \sum_{j=0}^k \nu_j t_{k-j}$  and  $\sigma_k \equiv \sum_{j=0}^k \nu_j s_{k-j}$  where  $\nu_j$  are the coefficients of the degeneracy expansion, we determine the contribution to the total entropy, for  $l = l_0 \dots \infty$ , where  $l_0$  is big enough such that the approximations are valid

$$\Delta S \simeq \sum_j^5 \sigma_j \left( \zeta(6 - D + j) - \sum_{l=1}^{l_0} \frac{1}{l^{6-D+j}} \right) - \sum_j^5 \tau_j \left( \zeta'(6 - D + j) + \sum_{l=1}^{l_0} \frac{\log l}{l^{6-D+j}} \right) \quad (3.38)$$

where  $\zeta(n)$  is the Riemann Zeta function and  $\zeta'(n)$  its derivative. Defining  $\Lambda_k \equiv \sum_{j=0}^k \nu_j \kappa_{k-j}$ , the single copy entanglement becomes,

$$\Delta E_1 \simeq \sum_{j=0}^5 \Lambda_j \left( \zeta(6 - D + j) - \sum_{l=1}^{l_0} \frac{1}{l^{6-D+j}} \right) \quad (3.39)$$

The above results show that the sum over angular momenta  $l$  converges for  $D < 5$ . A radial discretization of a scalar field theory produces finite results for  $D < 5$  and needs further regularization in orthogonal (angular) directions to the radius in higher dimensions. We will come back to this question later.

### 3.2.4 Area law scaling

The analysis of the scaling law obeyed by the geometric entropy proceeds as follows. The analytical treatment of the chain of oscillators lead to the final sum over angular momenta in Eq.(3.30). The computation of this sum requires polynomial, rather than exponential, effort as the size of the system increases. This justifies why large systems are accessible within this approach. The eigenmodes  $\xi_{l\{m\},i}$  are obtained by diagonalization of matrices of order less than  $N$ . Finally the tail of the sum over angular momenta is computed using the asymptotic expressions given in Eq.(3.38).

We have computed the geometrical entropy and the single-copy entanglement for different dimensionalities of the system. Within the range  $1 < D < 5$  we do observe the expected area law scaling

$$S = k_S(\mu, D, a, N) \left( \frac{R}{a} \right)^{D-1}, \quad (3.40)$$

as well as a similar scaling for the single copy entanglement

$$E_1 = k_E(\mu, D, a, N) \left( \frac{R}{a} \right)^{D-1}, \quad (3.41)$$

where in all our considerations the lattice spacing can be taken  $a = 1$ . Fig.3.1 shows this perfect scaling for both measures of entanglement.

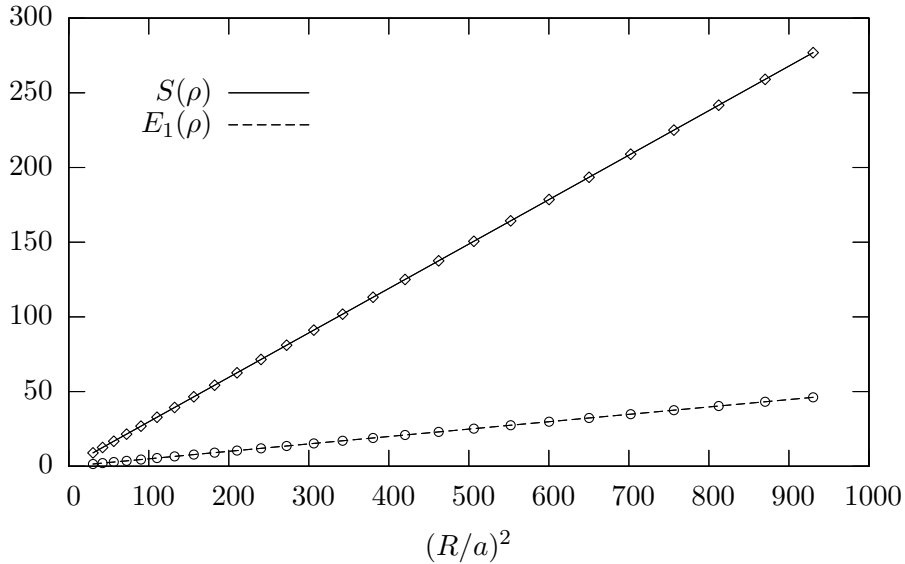


Figure 3.1: The entropy  $S$  and the single copy entanglement  $E_1$  resulting from tracing the ground state of a massless scalar field in three dimensions, over the degrees of freedom inside a sphere of radius  $R$ .

The explicit pre-factor in the area law is regularization dependent but can be computed and compared with previous analysis. Fig.3.2 shows the result obtained for this pre-factor in the area law for the case of  $D = 3$  and  $\mu = 0$  as the size of the system increases.

Good stability is already reached for  $N = 600$ , where we recover the result of [3]

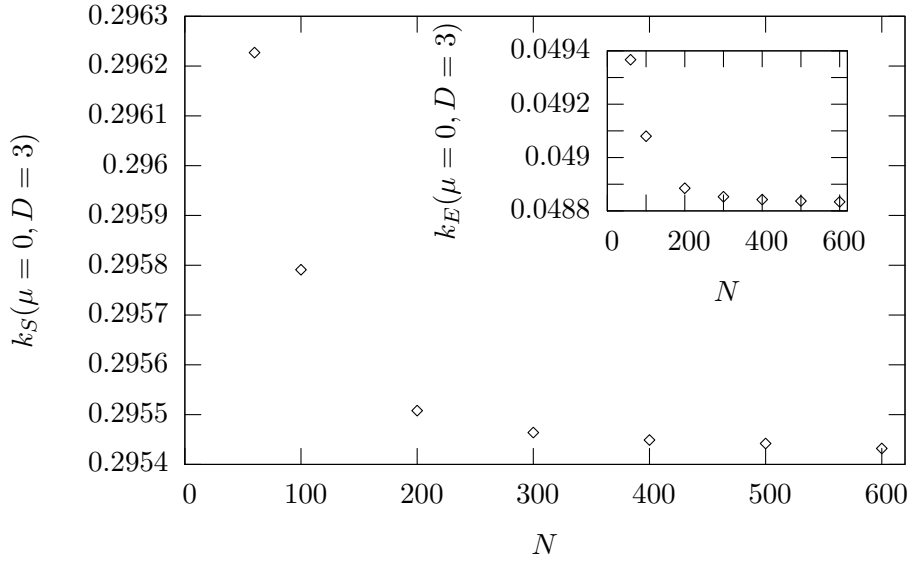


Figure 3.2: Coefficient for entropy the area law in  $D = 3$  as a function of size of the system. Good stability is reached for  $N = 600$ . In the inset, the corresponding coefficient for the single copy area law is plotted.

and complete it with the single copy entanglement

$$k_S(\mu = 0, D = 3, N \rightarrow \infty) = 0.295(1), \quad (3.42a)$$

$$k_E(\mu = 0, D = 3, N \rightarrow \infty) = 0.0488(1). \quad (3.42b)$$

Let us note that the ratio of the area law pre-factors for the entropy and the single copy entanglement is close to 6. This value is much larger than the factor of 2 computed to be the exact ratio in one-dimensional critical systems [50]. We thus conclude that the amount of entanglement that can be extracted from a single copy of a system as compared to the asymptotic value for infinite copies does decrease with the dimensionality.

We can analyze in more detail the dependence of our two measures of entanglement as a function of the dimensionality of the system. This is shown in Fig.3.3. for an  $N = 60$  and  $5 \leq n \leq 30$  as a function of  $R^{D-1}$  and we verify that the area law is observed for any value of the dimension  $D$ .

The robustness of area scaling law for arbitrary mass  $\mu$  is also readily checked (see Fig.3.5). The appearance of a mass term in the Hamiltonian produces exponential decays of correlators but does not affect the short-distance entanglement which is ultimately responsible for the area law. This supports the idea that geometric en-

entropy comes from the local neighborhood of the surface separating the region which is integrated out. The exponential decay of massive modes is immaterial and their contribution to the entanglement entropy is as important as the one coming from massless modes.

Let us concentrate briefly in the dependence of  $k_S$  and  $k_E$  on the dimension  $D$ . Those coefficients present divergences at  $D = 1$  and  $D = 5$  (see Fig. 3.3 ). The first one is due to the fact that in one dimension the strict power area law breaks down, since the limiting case carries a logarithmic dependence. For  $D \geq 5$ , as we have shown before, the sum over partial waves does not converge. This is due to the fact that we have regularized the Hamiltonian using a radial lattice. This regularization is insufficient to handle higher dimensional modes due to the increase of degrees of freedom per radial shell. To avoid this problem, a more elaborated regularization of the initial  $D$ -dimensional Hamiltonian is required. Such a regularization will likely have to break the rotational symmetry and will make the computations rather involved.

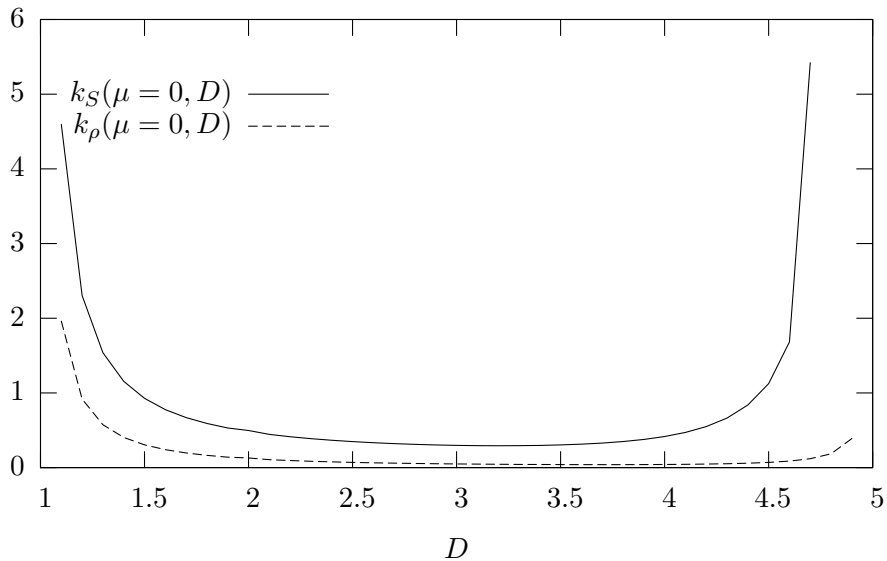


Figure 3.3: Dependence of the geometric entropy and single copy entanglement slopes,  $k_S$  and  $k_E$ , on the dimension  $D$  for a massless scalar field. Note the divergence at  $D = 5$  due to the insufficient radial regularization of the original field theory.

We observe in Fig.3.4 that the entropy to single-copy entanglement ratio verifies the expected limit 2, for  $D$  tending to 1.

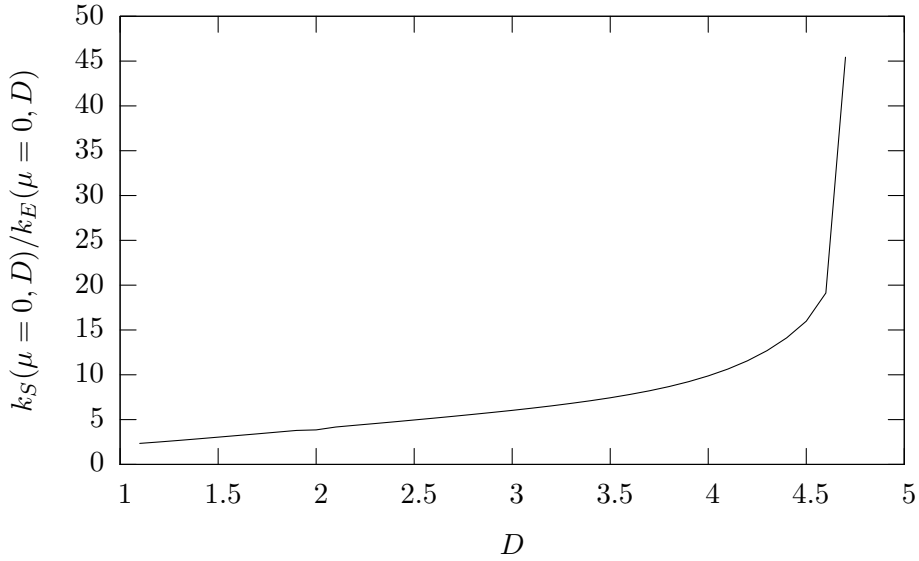


Figure 3.4: Evolution of entropy to single-copy entanglement ratio  $S/E_1$  as a function of the dimension  $D$ . The line starts at a value of 2, as demonstrated analytically in [50] and grows monotonically. The higher the dimension is, the less entanglement is carried by a single copy of the system as compared to many copies.

### 3.2.5 Vacuum reordering

Area law implies that entropy grows with the size of the system, that is, the eigenvalues of the density matrix, properly sorted from the largest to the smallest, decay in a slower way for larger systems. It has been numerically shown in Ref.[191] that this order relation between systems of different length verifies the strong condition of majorization, a fact proven analytically for conformal field theories in Ref.[192]. As the size of the system increases from  $L$  to  $L' > L$ , it is verified that  $\rho_{L'} \prec \rho_L$ , where  $\rho_L$  and  $\rho_{L'}$  are the set of eigenvalues for the corresponding reduced density matrices.

Majorization relations characterize strong ordering. Every eigenvalue changes in a way that is consistent with a set of majorization constraints. We shall refer to this fact as *vacuum reordering*.

We show that the same underlying reordering of the vacuum is present in any number of dimensions. Unfortunately, a similar analytical treatment to the  $D = 1$  case is out of reach because the conformal group in  $D > 1$  is spanned by a finite number of generators. As a consequence, there is no full control on the partition function of conformal field theory in  $D > 1$  dimensions, which could be used to generalize the

one-dimensional theorem.

Vacuum reordering can be treated within our semi numerical approach. From Eq.(3.25) we see that the reduced density matrix of the exterior of a ball of radius  $R$ , can be expressed as a tensor product of simpler density matrices,

$$\rho_{out}(R) = \prod_{l\{m\}} \rho_{l\{m\}}(R) = \prod_{l\{m\}} \left( \prod_{i=1}^{N-n} \rho_{l\{m\},i}(R) \right), \quad (3.43)$$

where  $\rho_{l\{m\}}$  is what we call  $\rho_{out}$  in Sec.(3.2.2) and  $\rho_{l\{m\},i}$  are defined in the same section. A similar composition applies for another size  $R'$ ,

$$\rho_{out}(R') = \prod_{l\{m\}} \rho_{l\{m\}}(R') = \prod_{l\{m\}} \left( \prod_{i=1}^{N-n'} \rho_{l\{m\},i}(R') \right). \quad (3.44)$$

It is shown as a lemma in Ref.[191] that, if majorization relations are satisfied by each  $\rho_{l\{m\}}(R)$  and  $\rho_{l\{m\}}(R')$ , they will be also satisfied by  $\rho(R)$  and  $\rho(R')$ . Note, though, that it is not possible to follow the same argument for  $\rho_{l\{m\},i}(R)$  and  $\rho_{l\{m\},i}(R')$  since  $n \neq n'$ . To make dimensions agree, we need to complete with identity operators the smallest set. We then find that some majorization relations for the subparts are obeyed in one sense, and the rest in the opposite one. Thus, we construct the density matrices  $\rho_{l\{m\}}(R)$  and  $\rho_{l\{m\}}(R')$  doing the tensorial product of their components which are generated using Eq.(3.28). Once we have their eigenvalues we are ready to check that if  $R < R'$ , then

$$\rho_{out}(R') \prec \rho_{out}(R), \quad (3.45)$$

which means by definition

$$\sum_{i=1}^k p'_i \leq \sum_{i=1}^k p_i \quad \forall k = 1, \dots, \infty \quad (3.46)$$

where  $p_i$  and  $p'_i$  are the eigenvalues of  $\rho_{out}(R)$  and  $\rho_{out}(R')$  respectively. For the  $l \sim N$  case, we have done a numerical computation with  $N = 60$  and truncating the vector of eigenvalues at the 50th element. Several dimensions  $D$  and traced sizes  $n$  have been studied, and all majorization relations are satisfied in all of them, as expected. When  $l \gg N$ , we can use the analytical results of the Appendix A to check the same result.

### 3.3 Entanglement loss along RG trajectories

We shall now exploit the control achieved on the eigenvalues of the reduced density matrix in  $D$  dimensions to study how entanglement evolves along renormalization group transformations. This was studied for the quantum Ising model in Ref. [191]. We shall now add equivalent results for the set of harmonic oscillators in  $D$  dimensions. Results will turn out to be qualitatively similar, reinforcing the concept of entanglement loss along RG flows.

The renormalization of a bosonic field is particularly simple since the Hamiltonian only carries one coupling, namely the mass term. After a block transformation, the rescaling of fields is used to make the kinetic term to be normalized to  $\frac{1}{2}$ . The RG flow of the massive scalar field reduces to an effective change of the mass. That is, the study of the long distance behavior of a correlator is viewed as taking a larger mass for the field, modulo a scaling factor. This implies the existence of two fixed points which are  $\mu = 0$  (ultraviolet, UV) and  $\mu = \infty$  (infrared, IR). Since no other fixed point is possible, the RG flow must be monotonic in  $\mu$ .

Entanglement loss comes along this flow. First, we study this change from a global perspective. We observe the obvious global loss of entanglement. For  $\mu = 0$ , geometric entropy grows with a slope  $k_S(D, \mu = 0)$  for the massless field and it is zero for the  $\mu = \infty$  case. Thus,

$$S_{UV} \geq S_{IR} \quad \forall R \quad (3.47)$$

This result is related to the c-theorem as discussed in Refs. [193, 194, 195, 127, 75], which states global irreversibility in the RG trajectory which interpolates between UV and IR fixed points.

On top of this global loss of entanglement, the geometric entropy obeys a monotonic decrease along the RG flow. This behavior is illustrated for  $D = 3$  in Fig.3.5 the entropy for different masses where it is seen that

$$\mu' > \mu \implies k_S(\mu') < k_S(\mu). \quad (3.48)$$

Thus, the system is more ordered as the mass increases.

It is natural to pose the question if this order relation verifies also stricter majorization relations, that is, vacuum reordering. Specifically, we analyze whether  $\rho(\mu')$  and  $\rho(\mu)$ , the density matrices corresponding to the free bosonic model with masses  $\mu' > \mu$  respectively, obey  $\vec{p}(\mu')$  and  $\vec{p}(\mu)$ .

$$\vec{p}(\mu) \prec \vec{p}(\mu'). \quad (3.49)$$

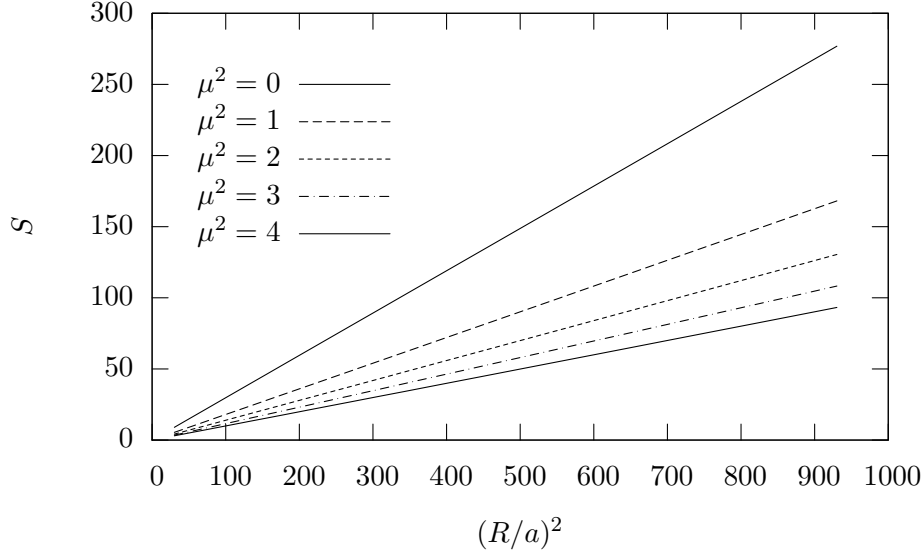


Figure 3.5: Geometric entropy  $S$  for a sphere of radius  $R$  in  $D = 3$  as a function of the mass  $\mu$ . Note that larger masses produce a smaller coefficient in the scaling are law.

Using similar arguments as in the previous section, we only need to check that each

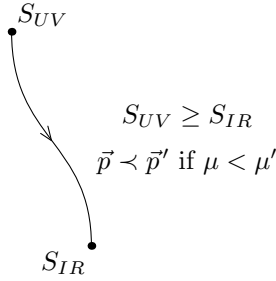


Figure 3.6: Entanglement loss along the RG trajectories seen in the space spanned by the eigenvalues of the reduced density matrix.

$\rho_{l\{m\},i}(\mu)$  majorizes  $\rho_{l\{m\},i}(\mu')$ . Considering Eq.(3.28), that means,

$$\sum_{i=1}^k (1 - \xi) \xi^i \leq \sum_{i=1}^k (1 - \xi') \xi'^i \quad \forall k = 1, \dots, \infty, \quad (3.50)$$

and therefore,

$$(1 - \xi^{k+1}) \leq (1 - \xi'^{k+1}) \quad \forall k = 1, \dots, \infty. \quad (3.51)$$

This happens if and only if  $\xi' \leq \xi$ . As in the previous section, we have verified this fact numerically in the  $l \sim N$  regime, and analytically using the perturbation calculus done in Appendix A.

It should be noted that monotonic loss of entanglement is mandatory in such a simple model with a single parameter ( $\mu$ ) controlling the flow. It is far from obvious that such entropy loss is rooted in a such a subtle reordering of the vacuum as the one dictated by majorization.

### 3.4 Conclusions

Area law scaling for the geometric entropy is present in harmonic networks of arbitrary dimensions. This follows from a computation that makes use of an analytical approach capable of making an analytical extension of the computation to arbitrary  $D$ , followed by a final numerical resummation of angular momenta, whose tail is controlled analytically.

A similar scaling law is observed for the single-copy entanglement. This result suggests that entanglement, whatever measure we use, scales with an area law due to the fact that entanglement is concentrated on the surface of the region which is traced out. The ratio of single-copy entanglement to geometric entropy tends to zero as the dimension of the network increases.

It is natural to interpret a change in the size of the subsystem which is traced out as well as any modification of the parameters in the Hamiltonian as a probe on the vacuum. Our explicit computations unveil ubiquitous vacuum reordering governed by majorization relations of the vacuum state reduced density matrix eigenvalues. Geometric entropy scaling is just one manifestation of this set of order relations.

The fact that finite PEPS support an area law scaling makes them a natural tool to investigate regularized quantum field theories.



---

# Violation of area-law for the entanglement entropy in spin 1/2 chains

---

In the previous chapter, it has been shown that any state that verifies the area-law for the entanglement entropy can be efficiently represented by a PEPS. It seems, then, that area-law establishes the frontier between those systems that can be simulated by classical means and those that can not. Let us mention that this frontier is not well defined yet. On one hand, tensor networks can even represent logarithmic violations of area-law. On the other hand, it has been proven that the complexity of simulating and contracting PEPS is  $\#\text{P}$ -complete [196].

A question that emerges naturally in this context is which features a Hamiltonian must have in order that its ground state fulfills area-law. This leads to one of the most interesting issues in Quantum Information and Condensed Matter Physics: to rigorously understand the connections among the features of a Hamiltonian, the amount of entanglement of its ground state and its efficient numerical simulation.

As we have seen along the first part of this thesis, the situation of the scaling of entanglement entropy for one dimensional translationally invariant systems is well established. On one hand, if the system has local interactions and it is gapped, area-

law always emerges [197]. On the other hand, if the system is at the critical point, and therefore gapless, a logarithmic divergence is encountered. This logarithmic scaling of the entanglement entropy is very well explained by conformal field theory [4, 5]. Naturally, if we consider systems with long range interactions then area-laws can be perfectly violated.

Although, in recent years, there has been a huge progress on this topic and most of all the connections between the features of a Hamiltonian and the entanglement of its ground state have been established (see Ref. [6]), the necessary and sufficient conditions for an area-law have not been defined yet. For instance, in Ref. [189], it is shown a one dimensional non-translational invariant system composed of a line of 12 level quantum particles with nearest neighbor interactions whose ground state presents a volume law.

The issue that we want to address in this chapter is how simple can be a quantum system to give a highly entangled ground state. In particular, we want to show that a simple spin 1/2 model with nearest neighbors interactions with a suitable fine tuning of the coupling constants may have a ground state with a volume law for the entanglement entropy. Our proposal is based on the translational symmetry breaking, and this makes, at the same time, that the area-law violation can not be maintained for any bipartition of the system.

## 4.1 Real space Renormalization Group

### 4.1.1 Introduction to real space RG approach

The real-space RG approach was introduced by Fisher in Ref. [7] generalizing the works by Dasgupta and Ma in Ref. [8]. It is a method for finding the effective low energy Hamiltonian and the ground state of random spin chains. The couplings have to satisfy the hypothesis of strong disorder, *i. e.* the logarithm of its probability distribution is wide. When this happens, the ground state of the system can be very well approximated by a product state of singlets whose spins are arbitrarily distant.

Let us review the real-space RG method for the inhomogeneous XX model case

$$H_{XX} = \frac{1}{2} \sum_{i=1}^N J_i (\sigma_i^x \sigma_{i+1}^x - \sigma_i^y \sigma_{i+1}^y). \quad (4.1)$$

First, we find the strongest bond  $J_i \gg J_{i+1}, J_{i-1}$  and diagonalize it independently of the rest of the chain. According to the previous Hamiltonian, this leads to a singlet

between spins  $i$  and  $i + 1$  (see appendix B). Therefore, the ground state at zeroth order in perturbation theory respect the couplings  $J_{i-1}$  and  $J_{i+1}$  is

$$|\psi^{(0)}\rangle = |\psi_{x<i}\rangle |\psi_{-}\rangle |\psi_{x>i+1}\rangle \quad (4.2)$$

where  $|\psi_{-}\rangle = \frac{1}{\sqrt{2}} (|01\rangle_{i,i+1} - |10\rangle_{i,i+1})$  is a singlet state between the spins  $i$  and  $i + 1$ , and  $|\psi_{x<i}\rangle$  and  $|\psi_{x>i}\rangle$  correspond to the states of the rest of the system.

In order to know the corrections of the ground state at higher orders, we use perturbation theory as it is shown in appendix B. This leads to an effective interaction between the distant spins  $i - 1$  and  $i + 2$  with an effective coupling

$$\tilde{J}_{i-1,i+2} = \frac{J_{i-1}J_{i+1}}{2J_i}. \quad (4.3)$$

In summary, we have eliminated two spins, and reduced the Hamiltonian's energy scale. Notice that this new effective low energy Hamiltonian couples the spins  $i - 1$  and  $i + 2$ , therefore, it has non-local interactions. Iterating this procedure for a XX model with random couplings, we would see that the ground state would be described by a random singlet phase, *i. e.* each spin would form a singlet pair with another one (see Fig. 4.1a). Most pair with nearby spins, but some of them with arbitrarily long distances.

In Ref. [105], Refael and Moore use real-space RG to show that, for random spin chains where the ground state is a random singlet phase, the entanglement entropy also scales logarithmically at the critical point as in the homogeneous case. That is,

$$S_L \sim \frac{\tilde{c}}{3} \log_2 L, \quad (4.4)$$

where  $\tilde{c} = c \ln 2$  is an effective central charge proportional the central charge for the same model but without disorder  $c$ .

### 4.1.2 Area-law violation for the entanglement entropy

Let us now tune the couplings  $J_i$  of our XX model in such a way that the entanglement entropy of the ground state of the system scales with the volume of the block of spins. An easy way of achieving this is to generate a ground state with a concentric singlet phase as it is shown in Fig. 4.1b. We see that the system is in a product state of distant singlets between the positions  $N/2 - (i - 1)$  and  $N/2 + i$  for  $1 \leq i \leq N/2$ . It is trivial to see that the entanglement entropy of this configuration would scale with the size

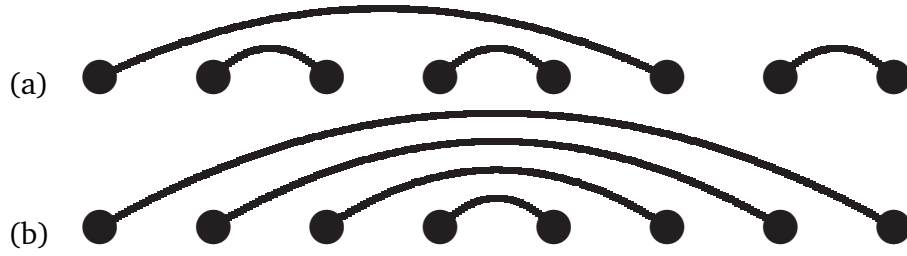


Figure 4.1: Diagram of a random singlet phase (a) and the concentric singlet phase (b). Each spin forms a singlet pair with another spin indicated by the bond lines.

of the block, since it merely corresponds to the number of bonds cut by the bipartition (see Fig. 4.2a).

Nevertheless, this linear behavior wouldn't be robust in front of the position of the block. If we took concentric blocks, the entanglement entropy would be 0 as it is shown in Fig. 4.2b. As the translational invariance of the system is broken, the entanglement entropy of a block not only depends on the size of it but also in its position.

In order to measure how entangled is a state for non-translationally invariant systems, it is useful to introduce the average entanglement entropy over all the possible positions of the block, that is

$$\bar{S}_L = \frac{1}{N-L} \sum_{i=1}^{N-L} S_L(i) \quad (4.5)$$

where  $S_L(i)$  is the entanglement entropy of the block of size  $L$  from the  $i$ -th spin to the  $(i+L)$ -th one.

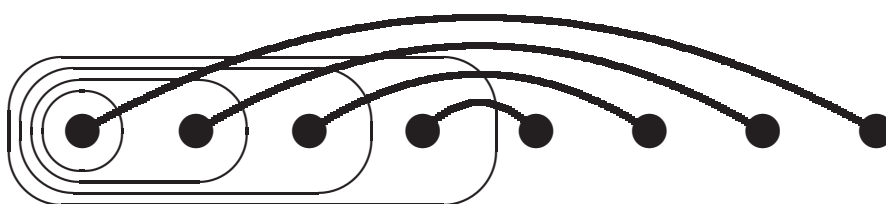
According to the previous definition, the average entanglement entropy of the concentric singlet phase reads

$$\bar{S}_L = \left(1 - \frac{L}{2(N-L)}\right) L. \quad (4.6)$$

Although for the concentric singlet phase the average entropy losses its linear behavior for large blocks,  $L \sim \left(1 - \frac{1}{\sqrt{3}}\right) N$ , it always fulfills the condition  $\bar{S}_L \geq \frac{1}{2}L$ . Thus, the concentric singlet phase represents a simple and explicit example of area-law violation of scaling of the entanglement.

The aim of our work is to tune the coupling constants  $J_i$  of the XX model, such that, the concentric singlet phase becomes the ground state of the system, and, in this way,

(a)



(b)

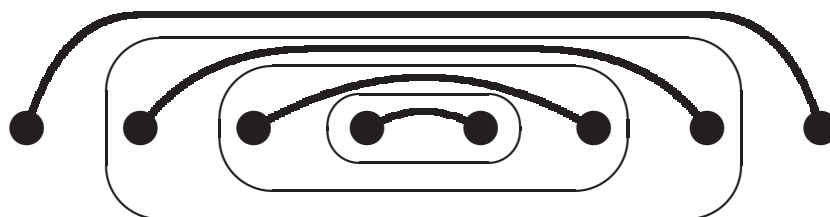


Figure 4.2: Diagram of the entanglement entropy scaling for the concentric singlet phase. The entanglement entropy grows maximally if we take blocks at one extreme (a) and is zero if the blocks are centered at the middle of the chain. This is an explicit example that in the non-translationally invariant systems the entanglement entropy depends on the position of the block.

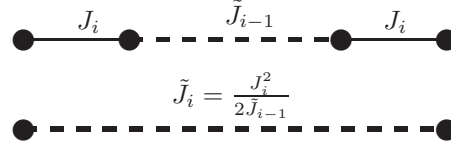


Figure 4.3: Diagram of the formation of an effective coupling  $\tilde{J}_i$  if the condition  $\tilde{J}_{i-1} \gg J_i$  is fulfilled.

to obtain an explicit example of a Hamiltonian with nearest neighbor interactions of spins that violate the area-law scaling of entanglement.

Due to the symmetry of the state that we pretend to generate, let us consider a XX chain of  $N$  spins where the central coupling between spins  $N/2$  and  $N/2 + 1$  is  $J_0$  and the rest of them are chosen as follows

$$J_{N/2+i, N/2+i+1} = J_{N/2-i, N/2-i+1} \equiv J_i \quad \forall 1 \leq i \leq \frac{N}{2} - 1 \quad (4.7)$$

where the coupling  $J_{N/2 \pm i}$  connects the spins  $N/2 \pm i$  and  $N/2 \pm i + 1$ .

We are going to use real space renormalization group ideas in order to see at which values we have to tune the coupling constants, such that, the concentric singlet phase becomes the ground state of the system. If  $J_0 \gg J_1$ , in the low-energy limit, an effective interaction between the spins  $N/2 - 1$  and  $N/2 + 2$  appears. We label this effective coupling as  $\tilde{J}_1$  and, according to Eq. (4.3), it reads

$$\tilde{J}_1 = \frac{J_1^2}{2J_0}. \quad (4.8)$$

Then, if  $\tilde{J}_1 \gg J_2$ , the effective low-energy Hamiltonian will have an effective bond between the spins  $N/2 - 2$  and  $N/2 + 3$ . We would like to proceed in this way in order to generate iteratively the concentric singlet phase.

Thus, if the condition  $\tilde{J}_i \gg J_{i+1}$  is fulfilled in general, where  $\tilde{J}_i$  is defined by

$$\tilde{J}_i = \frac{J_i^2}{2\tilde{J}_{i-1}}, \quad (4.9)$$

we expect that the ground state of the system is the concentric singlet phase.

Specifically, if we impose that  $J_i = \epsilon \tilde{J}_{i-1}$  for any  $i$ , such that it is always possible to apply Eq. 4.9, we see that the couplings  $J_i$  must decay very rapidly

$$J_i = \epsilon \left( \frac{\epsilon^2}{2} \right)^{i-1} J_0. \quad (4.10)$$

In general, we are going to study chains with couplings that decay

$$J_i = \epsilon^{\alpha(i)}, \quad (4.11)$$

where  $\alpha(i)$  is a function that is monotonically increasing. If  $\alpha(i) \sim i^2$ , we would have a Gaussian decaying.

Next, we want to solve the XX model with the coupling constants defined in Eq. (4.11), and study how the entanglement entropy scales depending on the kind of decaying.

## 4.2 Solution of a spin model and its entanglement entropy

Let us consider a general spin chain with nearest neighbor couplings  $J_i^x, J_i^y$  and an arbitrary transverse magnetic field  $\lambda_i$  in each spin. This system is described by the Hamiltonian:

$$H = -\frac{1}{2} \sum_{i=1}^N \left( J_i^x \sigma_i^x \sigma_{i+1}^x + J_i^y \sigma_i^y \sigma_{i+1}^y \right) - \sum_{i=1}^N \lambda_i \sigma_i^z \quad (4.12)$$

in terms of the Pauli-matrices  $\sigma_i^{x,y,z}$  at site  $i$ . The XX model presented before is a particular case of this Hamiltonian (4.12) for  $J_i^x = J_i^y$  and  $\lambda_i = 0 \forall i$ .

### 4.2.1 Jordan-Wigner transformation

The essential technique in the solution of  $H$  is the mapping to spinless fermions by means of the Jordan-Wigner transformation. First, we express the spin operators  $\sigma_i^{x,y,z}$  in terms of fermion creation (annihilation) operators  $c_i^\dagger$  ( $c_i$ ):  $c_i^\dagger = a_i^+ \exp \left[ \pi i \sum_j^{i-1} a_j^+ a_j^- \right]$  and  $c_i = \exp \left[ \pi i \sum_j^{i-1} a_j^+ a_j^- \right] a_i^-$ , where  $a_j^\pm = (\sigma_j^x \pm i \sigma_j^y)/2$ . Doing this,  $H$  can be rewritten in a quadratic form in fermion operators:

$$H = \sum_{i,j=1}^N A_{ij} c_i^\dagger c_j + \frac{1}{2} \sum_{i,j=1}^N B_{ij} (c_i^\dagger c_j^\dagger - h.c.), \quad (4.13)$$

where the matrices  $A$  and  $B$  are defined by

$$\begin{aligned} A_{ij} &= 2\lambda_i \delta_{i,j} + (J_i^x + J_i^y) \delta_{i+1,j} + (J_j^x + J_j^y) \delta_{i,j+1} \\ B_{ij} &= (J_i^x - J_i^y) \delta_{i+1,j} - (J_j^x - J_j^y) \delta_{i,j+1}, \end{aligned} \quad (4.14)$$

with  $1 \leq i, j \leq N$ .

### 4.2.2 Bogoliubov transformation

In the second step, the Hamiltonian is diagonalized by a Bogoliubov transformation

$$\eta_k = \sum_{i=1}^N \left( \frac{1}{2} (\Phi_k(i) + \Psi_k(i)) c_i + \frac{1}{2} (\Phi_k(i) - \Psi_k(i)) c_i^\dagger \right) \quad (4.15)$$

where the  $\Phi_k$  and  $\Psi_k$  are real and normalized vectors:  $\sum_i \Phi_k^2(i) = \sum_i \Psi_k^2(i) = 1$ , so that we have

$$H = \sum_{k=1}^N \Lambda_k (\eta_k^\dagger \eta_k - 1/2). \quad (4.16)$$

The fermionic excitation energies,  $\Lambda_k$ , and the components of the vectors,  $\Phi_k$  and  $\Psi_k$ , are obtained from the solution of the following equations:

$$(A - B)\Phi_k = \Lambda_k \Psi_k \quad (4.17)$$

$$(A + B)\Psi_k = \Lambda_k \Phi_k. \quad (4.18)$$

It is easy to transform them into an eigenvalue problem,

$$(A + B)(A - B)\Phi_k = \Lambda_k^2 \Phi_k \quad (4.19)$$

$$(A - B)(A + B)\Psi_k = \Lambda_k^2 \Psi_k, \quad (4.20)$$

from where  $\Lambda_k$ ,  $\Phi_k$  and  $\Psi_k$  can be determined.

### 4.2.3 Ground State

In Eqs. (4.18) and (4.17), we realize that transforming  $\Phi_k$  into  $-\Phi_k$  (or  $\Psi_k$  into  $-\Psi_k$ ),  $\Lambda_k$  is changed to  $-\Lambda_k$ . This allows us to restrict ourselves to the sector corresponding to  $\Lambda_k \geq 0$ ,  $k = 1, 2, \dots, N$ . Thus, considering Eq. (4.16) and the fact that all  $\Lambda_k$  are positive, the ground state is a state  $|GS\rangle$  which verifies,

$$\eta_k |GS\rangle = 0 \quad \forall k. \quad (4.21)$$

In practice, what we do to restrict ourselves to the sector of positive  $\Lambda_k$  is to determine  $\Phi_k$  and  $\Lambda_k$  by solving Eq. (4.19), and calculate  $\Psi_k = \frac{1}{\Lambda_k}(A - B)\Phi_k$ .

#### 4.2.4 Computation of the Von Neumann entropy corresponding to the reduced density matrix of the Ground State

Following Refs. [56, 57], the reduced density matrix  $\rho_L = \text{tr}_{N-L}|GS\rangle\langle GS|$  of the ground state of a block of  $L$  sites in a system of free fermions can be written as

$$\rho_L = \kappa e^{-\mathcal{H}}, \quad (4.22)$$

where  $\kappa$  is a normalization constant and  $\mathcal{H}$  a free fermion Hamiltonian.

Let us very briefly justify why the density matrix must have this structure. First, notice that the Hamiltonian defined by Eq. (4.13) has Slater determinants as eigenstates. Thus, according to Wick theorem, any correlation function of the ground state (or any other eigenstate) can be expressed in terms of correlators of couples of creation and annihilation operators. For instance,

$$\langle c_n^\dagger c_m^\dagger c_k c_l \rangle = \langle c_n^\dagger c_l \rangle \langle c_m^\dagger c_k \rangle - \langle c_n^\dagger c_k \rangle \langle c_m^\dagger c_l \rangle + \langle c_n^\dagger c_m^\dagger \rangle \langle c_k c_l \rangle. \quad (4.23)$$

If all these indices belong to a subsystem of  $L$  sites, the reduced density matrix  $\rho_L$  must reproduce the expectation values of the correlation functions, *i. e.*

$$\begin{aligned} \text{tr} \left( \rho_L c_n^\dagger c_m^\dagger c_k c_l \right) &= \text{tr} \left( \rho_L c_n^\dagger c_l \right) \text{tr} \left( \rho_L c_m^\dagger c_k \right) \\ &\quad - \text{tr} \left( \rho_L c_n^\dagger c_k \right) \text{tr} \left( \rho_L c_m^\dagger c_l \right) \\ &\quad + \text{tr} \left( \rho_L c_n^\dagger c_m^\dagger \right) \text{tr} \left( \rho_L c_k c_l \right). \end{aligned} \quad (4.24)$$

This is only possible if  $\rho_L$  is the exponential of an operator  $\mathcal{H}$  which also contains creation and annihilation processes, *i. e.*

$$\mathcal{H} = \sum_{i,j=1}^L \tilde{A}_{ij} c_i^\dagger c_j + \frac{1}{2} \sum_{i,j=1}^L \tilde{B}_{ij} \left( c_i^\dagger c_j^\dagger - h.c. \right). \quad (4.25)$$

We can diagonalize this Hamiltonian  $\mathcal{H}$  by means of another Bogoliubov transformation

$$\xi_k = \sum_{i=1}^L \left( \frac{1}{2} (v_k(i) + u_k(i)) c_i + \frac{1}{2} (v_k(i) - u_k(i)) c_i^\dagger \right), \quad (4.26)$$

where  $v_k(i)$  and  $u_k(i)$  are real and normalized. Then, the Hamiltonian reads

$$\mathcal{H} = \sum_{k=1}^L \epsilon_k \xi_k^\dagger \xi_k, \quad (4.27)$$

where  $\xi_k^\dagger$  and  $\xi_k$  are the creation and annihilation operators of some fermionic modes. In terms of these modes, the density matrix  $\rho_L$  is uncorrelated and can simply be expressed as

$$\rho_L = \otimes_{k=1}^L \tilde{\rho}_k \quad (4.28)$$

where

$$\tilde{\rho}_k = \frac{1}{1 + e^{-\epsilon_k}} \begin{pmatrix} e^{-\epsilon_k} & 0 \\ 0 & 1 \end{pmatrix} = \begin{pmatrix} \frac{1+v_k}{2} & 0 \\ 0 & \frac{1-v_k}{2} \end{pmatrix}. \quad (4.29)$$

In the previous equation, the new parameters  $v_k$  have been introduced in order to ensure the normalization of  $\tilde{\rho}_k$ ,  $\text{tr}(\tilde{\rho}_k) = 1$ . This way of expressing  $\tilde{\rho}_k$  will be useful next.

Thus, the entanglement entropy of the density matrix  $\rho_L$  is merely the sum of binary entropies

$$S(L) = \sum_{k=1}^L S(\tilde{\rho}_k) = \sum_{k=1}^L H\left(\frac{1+v_k}{2}\right). \quad (4.30)$$

where  $H(p) \equiv -p \log_2 p - (1-p) \log_2 (1-p)$  is the binary Shannon entropy.

In order to determine the spectrum of  $\tilde{\rho}_k$ , let us consider the correlation matrix,

$$G_{m,n} \equiv \langle GS | (c_n^\dagger - c_n)(c_m^\dagger + c_m) | GS \rangle. \quad (4.31)$$

Notice that the matrix  $G$  can be computed using the  $\Phi_k$  and  $\Psi_k$  vectors,

$$G_{m,n} = - \sum_{k=1}^N \Psi_k(m) \Phi_k(n), \quad (4.32)$$

where the correlations  $\langle \eta_k^\dagger \eta_q \rangle = \delta_{kq}$  and  $\langle \eta_k \eta_q \rangle = 0$  have been considered.

In the subspace of  $L$  spins,  $G$  is completely determined by the reduced density matrix. To avoid any confusion, let us define  $T \equiv G(1:L, 1:L)$  as the  $L \times L$  upper-left sub-matrix of the correlation matrix  $G$ . Then,  $T$  can be expressed in terms of the expected values  $\langle \xi_k^\dagger \xi_q \rangle$ ,

$$\begin{aligned} T_{i,j} &= \sum_{k,q=1}^L u_k(i) v_q(j) \left( \langle \xi_k^\dagger \xi_q \rangle - \langle \xi_k \xi_q^\dagger \rangle \right) \\ &= \sum_{k=1}^L u_k(i) v_k(j) v_k, \end{aligned} \quad (4.33)$$

where the  $i$  and  $j$  indices run from 1 to  $L$ . This equation leads to the relations,

$$T u_q = v_q v_q \quad (4.34)$$

$$T^T v_q = v_q u_q, \quad (4.35)$$

that can be translated to the eigenvalue problem

$$T^T T u_q = v_q^2 u_q \quad (4.36)$$

$$T T^T v_q = v_q^2 v_q. \quad (4.37)$$

Once the  $v_q$  variables are computed, we can determine the entanglement entropy by means of Eq. (8.12).

### 4.2.5 Summary of the calculation

To sum up, let us enumerate the steps that we have to follow in order to calculate the entanglement entropy of a block  $L$ .

1. Write down the matrices  $A$  and  $B$  in terms of the couplings of the Hamiltonian (4.12) according to Eqs. (4.14).
2. Determine  $\Lambda_k$ ,  $\Phi_k$  and  $\Psi_k$  by solving the eigenvalue problem from Eq. (4.19).
3. Calculate the correlation matrix  $G$  defined in Eq. (4.31).
4. Take the sub-matrix  $T$  and to determine the eigenvalues  $v_k$  from Eq. (4.37).
5. Compute the entanglement entropy by means of Eq. (8.12).

## 4.3 Expansion of the entanglement entropy

We would like to tune the coupling constants of the Hamiltonian (4.12), such that the scaling of the entanglement entropy of its ground state violates the area-law. The entanglement entropy only depends on the variables  $v_k$ . Then, we can separate the Shannon entropy of the probabilities  $\frac{1 \pm v_k}{2}$  into

$$H\left(\frac{1 + v_k}{2}\right) = 1 - h(v_k), \quad (4.38)$$

where  $h(x) = -\frac{1}{2} \log(1 - x^2) - \frac{x}{2} \left(\frac{1-x}{1+x}\right)$ , is a positive function. Thus, the entanglement entropy reads

$$S(L) = L - \sum_{k=1}^L h(v_k). \quad (4.39)$$

Notice that the scaling of the entropy only depends on the sum  $\sum_{k=1}^L h(v_k)$ . More concretely, we can define the parameter,

$$\beta \equiv \lim_{L \rightarrow \infty} \frac{1}{L} \sum_{k=1}^L h(v_k), \quad (4.40)$$

that describes the asymptotic behavior of the scaling of the entropy for large blocks:

- $\beta = 0$ : maximal entanglement,
- $\beta < 1$ : volume-law,
- $\beta = 1$ : sub-volume-law.

Let us focus on the case  $\beta \sim 0$ . Let us analyze if it is possible to design a spin chain with nearest neighbor interactions whose ground state is maximally entangled. First, we realize that  $\beta$  is strictly zero if and only if all the variables  $v_k = 0$ . Thus, if we want to consider small deviations of the maximally entangled case, we can assume that  $v_k \sim 0$  and expand  $\beta$  in series of  $v_k$ ,

$$\beta = \lim_{L \rightarrow \infty} \frac{1}{2L} \sum_{k=1}^L (v_k^2 + O(v_k^4)). \quad (4.41)$$

Considering Eq. (4.37), we can express  $\beta$  in terms of the matrix-elements of  $T$ ,

$$\beta = \lim_{L \rightarrow \infty} \text{tr} (T T^T) = \lim_{L \rightarrow \infty} \sum_{i,j=1}^L T_{ij}^2 = 0. \quad (4.42)$$

Let us notice that to fulfill this condition requires that the average of the matrix-elements of  $T$  tend to zero for large  $L$ ,

$$\lim_{L \rightarrow \infty} \frac{1}{L^2} \sum_{i,j=1}^L |T_{i,j}| = 0. \quad (4.43)$$

If we assume a smooth behavior for the matrix-elements of  $T$ , according to Eq. (4.42), they must decay faster than the inverse square root function,

$$T_{ij} \sim \frac{1}{(ij)^{\frac{1}{2}+\epsilon}}, \quad (4.44)$$

such that  $\beta = 0$ .

In conclusion, in order that the entanglement entropy scales close to the maximal way, the matrix-elements of  $T$  matrix have to be very close (or decay rapidly) to zero. If this is the case, the entanglement entropy can be simplified to

$$S(L) = L - \|T\|_F^2, \quad (4.45)$$

where  $\|T\|_F$  is the Frobenius norm of  $T$ , defined by  $\|T\|_F = \sqrt{\text{tr}(T^T T)}$ .

Let us now study if it is possible to tune the coupling constants of a spin chain in order that  $\|T\|_F$  is strictly (or close to) zero. The possibility of having a null  $T$  is discarded because it cannot be achieved with nearest neighbor interactions models. Despite this, there is a wide freedom to tune the coupling constants such that the matrix-elements of  $T$  fulfill condition (4.42). This arbitrariness makes very difficult to specify the shape of the distribution of coupling constants in order that area-law is violated. With this aim, we can exploit the idea of real space Renormalization Group presented before.

## 4.4 Numerical Results

We can follow the steps described in Sec. 4.2.5 in order to calculate the entanglement entropy of the XX chain presented in Sec. 4.1.2 and check if the entanglement entropy grows linearly with the size of the block.

This XX model is characterized by having the strongest bond in the middle of the chain,  $J_0$ , while the value of the rest of bonds  $J_n$  decrease rapidly with the distance  $n$  to the central one. In particular, we have studied two different kinds of decay for the coupling constants  $J_n$ : (i) *Gaussian* decay,  $J_n = e^{-n^2}$ , and (ii) *exponential* decay  $J_n = e^{-n}$ . Let us notice that due to the rapidly decaying of the coupling constants and the finite precision of the computer, we can only consider small systems.

In Fig. 4.4(a), the entanglement entropy is plotted for the Gaussian case. As we expected scales linearly with the size of the block  $L$  with a slope practically equal to one. Notice that although the slope is 1 for large blocks, the entanglement is not the maximal due to the non-linear behavior of the entropy for the smaller ones. This can be better understood analyzing if the approximation of the previous section given by Eq. (4.45) is fulfilled. With this aim, the square Frobenius norm  $\|T\|_F^2$  and the sum  $S(L) + \|T\|_F^2$  are also plotted. In fact, we observe that the sum  $S(L) + \|T\|_F^2$  coincides with the maximal entropy, as Eq. (4.45) suggests.

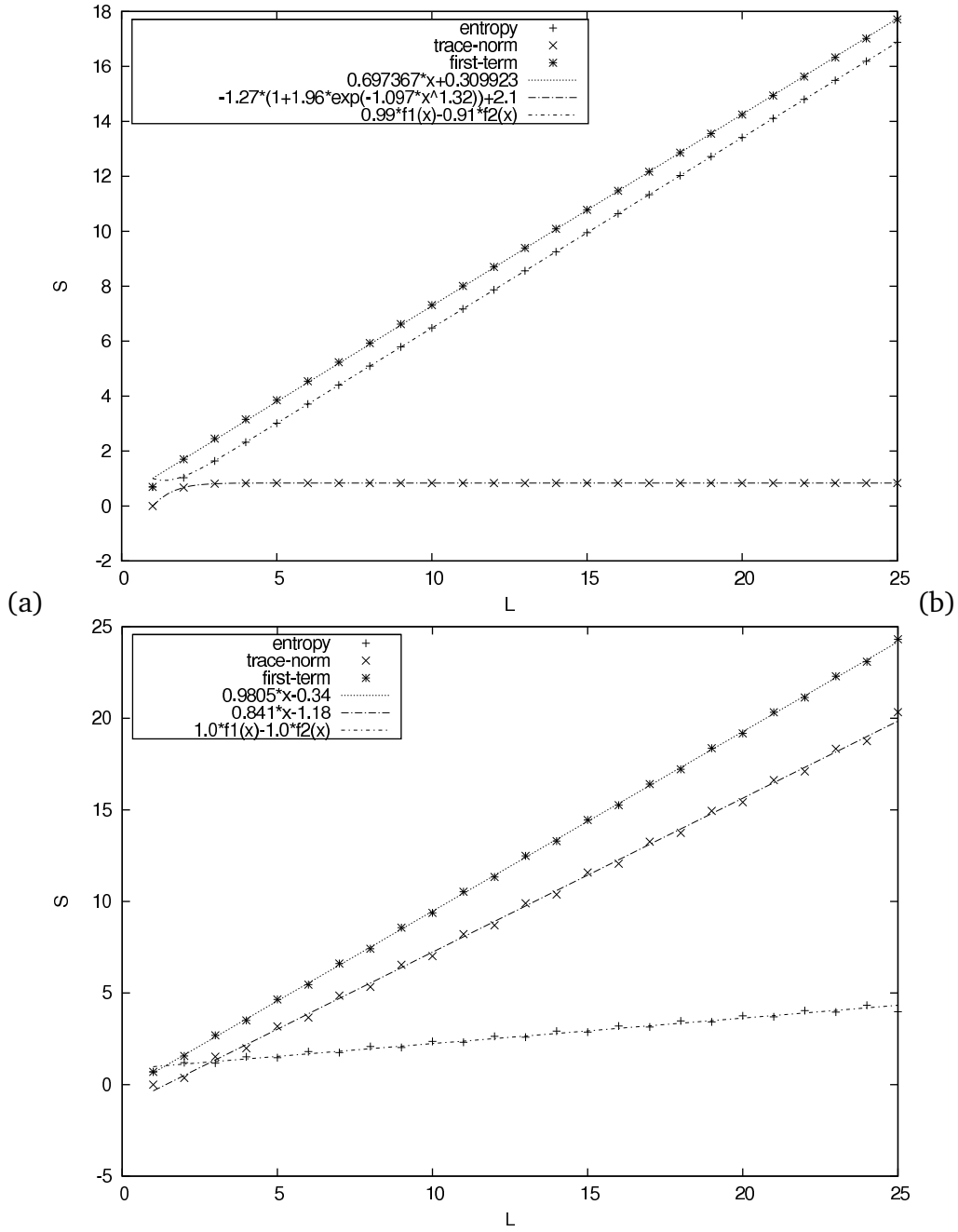


Figure 4.4: Scaling of the entanglement entropy of a block of contiguous spins with respect to the size of the block  $L$  for the ground state of a XX model with couplings that decay: (a) in a Gaussian,  $J_n = e^{-n^2}$ , and (b) in an exponential,  $J_n = e^{-n}$ , way. The magnetic field is set to zero. The Frobenius norm of the  $T$  matrix related to this system and the sum  $S(L) + \|T\|_F$  are also plotted. This allows us to check how accurate is the approximation (4.45) both in the case of Gaussian decay (a) and in the exponential one (b).

The same plot can be realized for an exponential decay of the coupling constants, see Fig. 4.4(b). In this case, although the entanglement entropy also scales linearly, its slope is less than one. Thus, we observe a volume law, but the entropy is not maximal. Therefore, Eq. (4.45) is not fulfilled in this case. We can, actually, see that the Frobenius norm  $\|T\|_F$  increases linearly with  $L$  instead of saturating to a small value.

We have repeated the same computations for the same kind of decays but other basis. The same behaviors for the Gaussian and the exponential cases have been obtained. For the Gaussian case, a faster decay implies a saturation to a smaller value for  $\|T\|_F$ , that is, a closer situation to the maximal entropy. For the exponential case,  $\|T\|_F$  continues increasing linearly but with a smaller slope.

## 4.5 Conclusions

We have presented a one dimensional system composed by spin- $\frac{1}{2}$  particles with nearest neighbor interactions with a geometric entropy of the ground state that scales with the volume of the size of the block.

Our proposal is interesting from an academical point of view, since it could never be realized experimentally due to the fine tuning of the coupling constants of the Hamiltonian and its gapless spectrum in the thermodynamic limit. Nevertheless, it shows that a Hamiltonian with nearest neighbor interactions can have a very entangled ground state and, therefore, that the reason of area-law is not only nearest neighbor interactions.

The price we have paid for violating area-law is to break the translational symmetry of the system. This is a feature that any other proposal that violates area-law will have .



## **Part II**

# **Simulation of many body quantum systems**



---

# Ultra-cold atoms and the simulation of Condensed Matter physics

---

In this chapter we want to motivate the use of ultra cold atoms in order to simulate many body quantum systems and, in particular, interesting Condensed Matter phenomena. As it has been shown in the first part of this thesis, it is not possible to simulate a highly entangled or strongly correlated system with a classical computer. This forces us to address the issue of how to study those quantum systems that cannot be dealt with classical means.

The current experimental control on ultra-cold atoms allows the observation of many quantum phenomena and makes them suitable candidates to develop *quantum simulators*. Let us mention here the superfluid-Mott insulator quantum phase transition in cold atoms in an optical lattice as example. It corresponds to a transition between a product and a strongly correlated state [198]. Its experimental observation by the Bloch–Hänsch group [199] represented the beginning of age of the experimental studies of strongly correlated systems with ultra-cold atoms[200].

The physics of ultra-cold atoms, in the interplay among Condensed Matter Physics, Quantum Information, Atomic Physics and Quantum Optics, has made an enormous progress in the studies of strongly correlated systems in recent years. In this chapter, we would like to briefly review what are their possibilities and what kind of systems

they will allow us to study. Interested readers are again encouraged to study recent reviews on the field [15, 16].

## 5.1 Experimental control in cold atoms

Let us briefly mention the main techniques and possibilities that allow us to manipulate and control cold gases in order to simulate other quantum systems.

### 5.1.1 Temperature

To generate an Bose-Einstein condensate (BEC) the temperature must be of order of nano-Kelvins. Similarly, the temperature of superfluid Fermi gases are in the range of tens of nK. Using evaporative cooling it is even possible to achieve lower temperatures. Therefore, temperatures in the range of tens of nK are nowadays becoming a standard.

There are many proposals for reaching lower temperatures employing additional cooling and filtering procedures [201]. Superfluid-Mott insulator transition occurs in the regime of temperatures accessible nowadays. Many of the strongly correlated phases occur in the regime when the tunneling  $t$  is much smaller than  $U$  and require temperatures of order  $k_B T \simeq t^2/U$ , *i. e.* 10-20 nK, or even less (see Bose-Hubbard model in Sec. 5.3.1 for a more complete description of  $t$  and  $U$  parameters). This is at the border of the current possibilities, but the progress in cooling and quantum engineering techniques allow us to believe that these limitations will be overcome very soon.

### 5.1.2 Trapping

To perform any experiment it is required to confine the gas using an external potential, otherwise the gas would expand through the room. Various types of external potentials can be applied to the atoms, depending on the situations.

One can use *magnetic potentials* whose shape can be at least controlled on the scale of few microns. Magnetic traps are based on the state-dependent force on the magnetic dipole moment in an inhomogeneous field. They represent ideal conservative traps with typical depths in the order of 100 mK, and are excellent tools for evaporative cooling and Bose-Einstein condensation. For further applications, a fundamental restriction is imposed by the fact that the trapping mechanism relies on

the internal atomic state. This means that experiments concerning the internal dynamics are limited to a few special cases. Furthermore, possible trapping geometries are restricted by the necessity to use arrangements of coils or permanent magnets. Magnetic potentials with larger gradients can be created on atom chips [202].

The most flexible external potentials are *optical potentials* [203]. Optical dipole traps rely on the electric dipole interaction with far-detuned light. Under appropriate conditions, the trapping mechanism is independent of the particular sub-level of the electronic ground state. The internal ground-state dynamics can thus be fully exploited for experiments, which is possible on a time scale of many seconds. Moreover, a great variety of different trapping geometries can be realized as, e.g., highly anisotropic or multi-well potentials. Apart from limitations set by the diffraction limit, they can have practically any desired shape and can form any kind of optical lattice: regular, disordered, modulated, etc.

Let us finally mention the great possibilities offered by the radio frequency potentials that have been demonstrated in Ref. [204].

### 5.1.3 Interactions between atoms

Due to the low energies of the atoms in a cold gas, the s-wave scattering approximation can be considered. Then, the interactions between atoms are controlled by scattering lengths, which can be modified using Feshbach resonances in magnetic fields [205, 206] or optical Feshbach resonances (for theory see Ref. [207], for experiments Refs. [208, 209]). Thus, there is a complete control on the interactions. They can be set to zero, repulsive or even attractive.

The concept of Feshbach resonances was first introduced in nuclear physics in the context of reactions forming a compound nucleus [210]. Quite generally, a Feshbach resonance in a two-particle collision appears whenever a bound state in a closed channel is coupled resonantly with the scattering continuum of an open channel. The two channels may correspond, for example, to different spin configurations for the atoms.

Let us also point out that in dipolar gases, the interaction is anisotropic, then, by changing the shape of the trap, the strength and the character of the interaction can be modified.

### 5.1.4 Optical lattices

A particularly interesting case of optical potentials are *optical lattices*, that is, a periodic optical potential. In this setup, atoms are cooled and congregated in the potential minima. As mentioned above, practically any lattice geometry may be achieved with optical potentials.

The *tunneling* of atoms between nearest neighbor sites can be very well controlled using a combination of pure tunneling (controlled by the laser intensity), laser assisted coherent transitions (adding a phase to the wave function of the atom), and lattice tilting (acceleration) techniques. The prominent example of such control describe the proposals for creating artificial magnetic fields [211, 212, 213, 214].

We have already mentioned the control on the on-site interactions that Feshbach resonance provides. Furthermore, in optical lattices, effective models obtained by calculating effect of tunneling in the Mott insulator phases, contain typically short range (next neighbor) interactions of energies  $\propto t^2/U$ . Also stronger interactions can be achieved using dipolar interactions, such as those proposed in Refs. [215, 216, 217]. Dipolar interactions are of long range type, are anisotropic, and exhibit a very rich variety of phenomena (for a review, see [218]). This allow us to implement models with *long range* interactions.

Let us also mention that more complex lattices can be created with the the superposition of two standing-wave lattices with comparable amplitudes and with different wavelengths. These kind of lattices are called *superlattices* and they may be used to simulate, for instance, spin 1/2 models.

### 5.1.5 Several species

Nowadays it is also possible to have several species in the same experimental setup. It may consist of atoms with two internal degrees of freedom, or really having two different elements. In the first case, the state of the atoms can be controlled by Rabi transitions, even achieving superposition states. In the second case, a particular kind of mixtures are the so called Bose-Fermi mixtures [219] formed by bosonic and fermionic atoms. The degree of control of such systems is really high. For instance, the mobility of both species can be tunned independently in an optical lattice allowing to simulate disorder and impurity effects.

Before finishing this section, let us mention that the time scales of coherent unitary dynamics of these systems are typically in the millisecond range. It implies that, in

contrast to Condensed Matter systems, all of the controls discussed above can be made time dependent, adiabatic, or diabatic, on demand. Some of the fascinating possibilities include change of lattice geometry, or turn-on of the disorder in real time.

## 5.2 Measurements

Apart from having an excellent experimental control of cold atom systems, a fundamental feature of any quantum simulator is the experimental access to the result of the simulation. This requires a series of techniques that allow us to characterize the quantum state of the system.

### 5.2.1 Time of flight experiment

The standard time of flight technique consists of (i) switching the trap off, (ii) leaving the gas to expand freely, and (iii) taking a picture of the final cloud. The resulting absorption image provides information about which was the state of the atoms in the trap.

Suppose that the system is initially in some pure state  $|\Phi\rangle$ . In a typical experimental setup, the trapping potential is turned off suddenly, and the atoms evolve *independently* under the influence of the free propagator  $U_0(t)$ . This is valid provided that the free-atom collision cross-section is not too large. Such conditions can be achieved by switching the magnetic field to values far from the Feshbach resonance when turning off the trap. We also consider a long time of flight times, in such a way that the initial size of the atom cloud in the trap can be neglected.

In such time of flight experiments, the column integrated density of the expanding cloud is measured by light absorption imaging [220]. The images are commonly analyzed by comparing to theoretical predictions for the density expectation value:

$$\langle \hat{n}(\vec{r}) \rangle_t = \langle \Phi | U_0^\dagger(t) \psi^\dagger(\vec{r}) \psi(\vec{r}) U_0(t) | \Phi \rangle \quad (5.1)$$

where  $\psi$  is the field operator for bosons or fermions. After a long time of flight the density distribution becomes proportional to the momentum distribution in the initial trapped state  $\langle n(\vec{r}) \rangle_t \approx \langle \hat{n}_{\vec{k}} \rangle$ . The wave-vector  $\vec{k} = m\vec{r}/(\hbar t)$  defines a correspondence between position in the cloud and momentum in the trap.

Thus, by means of a time of flight experiment, we can know the momentum distribution of the atoms in the trap. Nevertheless, in order to probe interacting many-body

quantum states with strong correlations, it is essential to use detection methods that are sensitive to higher order correlations. Recent proposals for using analogues of quantum optical detection techniques have proven to be novel tools for analyzing strongly interacting quantum matter [221, 222, 223, 224]. Most of these techniques make use of the fact that the quantum fluctuations in many observables, *e. g.* the visibility of the interference pattern between two released quantum gases or the fluctuations in the momentum distribution after release from the trap, contain information of the initial correlated quantum state. Whereas in the usual time of flight momentum distributions one essentially probes first order coherence properties of the system, the noise-correlation techniques introduced below will yield information on the second (or higher) order correlation properties and therefore possible long range order in real space.

### 5.2.2 Noise correlations

In the standard time of flight experiment, it is important to realize, that in each experimental image, a single realization of the density is observed, not the expectation value. Equation (5.1) is still meaningful, because the density is a self averaging quantity. Moreover, each pixel in the image records on average a substantial number  $N_\sigma$  of atoms. For each of those pixels the number of atoms recorded in a *single realization* of an experiment will exhibit shot noise fluctuations of relative order  $1/\sqrt{N_\sigma}$  which will be discussed below.

Note that since  $N_\sigma$  is not macroscopic, the density fluctuations are visible. They are characterized by the correlation function:

$$g(\vec{r}, \vec{r}') = \langle \hat{n}(\vec{r})\hat{n}(\vec{r}') \rangle_t - \langle \hat{n}(\vec{r}) \rangle_t \langle \hat{n}(\vec{r}') \rangle_t. \quad (5.2)$$

In analogy with Eq. (5.1) this can be related to ground state momentum correlations:

$$g(\vec{r}, \vec{r}') \propto \langle \hat{n}(\vec{k})\hat{n}(\vec{k}') \rangle - \langle \hat{n}(\vec{k}) \rangle \langle \hat{n}(\vec{k}') \rangle, \quad (5.3)$$

The proportionality constant is  $(m/\hbar t)^6$  and we shall omit it henceforth. In practice it may be more convenient to consider the quantity  $\Delta n(\vec{r}, \vec{r}') \equiv n(\vec{r}) - n(\vec{r}')$  whose fluctuations are closely related to  $g(\vec{r}, \vec{r}')$ . If  $\langle n(\vec{r}) \rangle_t = \langle n(\vec{r}') \rangle_t$ , then

$$\langle \Delta n(\vec{r}, \vec{r}')^2 \rangle_t = g(\vec{r}, \vec{r}) + g(\vec{r}', \vec{r}') - 2g(\vec{r}, \vec{r}'). \quad (5.4)$$

Then, performing a statistical analysis of several single shots, it is possible to determine the correlation function  $\langle \hat{n}(\vec{k})\hat{n}(\vec{k}') \rangle$  of the original state.

Let us finally mention that all the correlation techniques for strongly correlated quantum gases can also greatly benefit from efficient single atom detectors that have recently begun to be used in the context of cold quantum gases [225, 226].

## 5.3 Interesting Condensed Matter phenomena

So far, we have seen the possibilities both for the design and the measures that cold atoms systems have. In this section, we would like to mention some interesting Condensed Matter problems in which quantum simulators can give non-trivial results.

### 5.3.1 Bose-Hubbard model

The Hamiltonian of an homogeneous Bose-Hubbard model is defined as

$$H = -t \sum_{\langle i,j \rangle} (b_i^\dagger b_j + h.c.) + \frac{U}{2} \sum_{i=1}^M b_i^\dagger b_i^\dagger b_i b_i - \mu \sum_{i=1}^M b_i^\dagger b_i, \quad (5.5)$$

where  $\langle i, j \rangle$  denotes sum over nearest neighbors,  $t$  is the tunneling energy,  $U$  is the on-site interaction energy between two atoms and  $\mu$  denotes the chemical potential. The operators  $b_i^\dagger$  and  $b_i$  are the standard creation and annihilation operators that fulfill the canonical commutation relations  $[b_i, b_j^\dagger] = \delta_{i,j}$ . We assume  $b_i$  ( $b_i^\dagger$ ) annihilates (creates) a particle in the site  $i$  of a regular  $d$ -dimensional lattice consisting on  $M$  sites.

The problem of finding the ground state of the Bose-Hubbard model is very easy in the limit of  $t/U \rightarrow \infty$ . The interactions between atoms are negligible and all the particles are in a product state of zero quasi-momentum. In a similar way the opposite limit,  $t/U \rightarrow 0$ , can be solved. In this case, the ground state is a Mott insulator state. Nevertheless, for arbitrary values of  $U$ ,  $t$  and  $\mu$  the system cannot be solved using a mean-field approach and an exact diagonalization must be performed. In this approach, only small systems can be solved since the size of the Hilbert space increases enormously with the number of particles and sites of the system.

Cold atoms in optical lattices are, then, the natural candidates to simulate the Bose-Hubbard model or any of its variants (Fermi-Hubbard or Fermi-Bose-Hubbard) and to characterize the properties of its ground state.

### 5.3.2 Disordered systems

Let us define disordered systems as those systems for which certain parameters of the Hamiltonian (e.g., interaction couplings, potential strengths) are random (classical) variables. Therefore, in such systems, the exact simulation of their dynamics requires to perform many evolutions, one for each realization of the set of random variables, and this makes them numerically intractable.

The interest for these systems comes from the fact that the presence of randomness can dramatically change the behavior of quantum many-body physics, leading to fascinating phenomena. In fact, there are many interesting Condensed Matter phenomena that require disorder: Anderson localization, spin glasses, etc. Moreover, the answer to puzzles as the unusual transport properties of high temperature superconductor materials is inextricably tied to the understanding of phase transitions and transport in the presence of disorder [227].

In this context, the creation of randomness in a controlled way by means of atomic systems in optical lattices [228, 200], highly versatile and controllable, are one of the most promising candidates.

### 5.3.3 The Fractional Quantum Hall Effect and the Laughlin state

Before concluding this chapter, we would like to focus on the Fractional Quantum Hall Effect and its ground state, the Laughlin wave function, since this state will be the target of the proposals of simulations of the second half of this thesis.

The fractional quantum Hall effect (FQHE) is one of the most studied phenomena in Condensed Matter Physics [10]. Despite the fact that a complete understanding of it is still missing, it is commonly believed that the interactions between the particles are essentially responsible for the strange states of matter that the 2D electron gas shows at some particular values of the transverse magnetic field. In this respect, in 1983, Laughlin proposed an Ansatz for the wave function of the ground state of the system [11]. This wave function, defined by

$$\Psi_m(z_1, \dots, z_N) \sim \prod_{i < j} (z_i - z_j)^m e^{-\sum_{i=1}^N |z_i|^2/2}, \quad (5.6)$$

where  $z_j = x_j + iy_j$ ,  $j = 1, \dots, N$  stands for the position of the  $j$ -th particle, and  $m$  is an integer number, describes the fractional quantum Hall state at a filling fraction  $\nu = 1/m$ . However, this state has only been proven to be an exact eigenstate of

very specific Hamiltonians [229] and for some specific values of the filling fraction; it contains the relevant properties that the ground state of the real system must have.

One of the most important features of some of the fractional quantum Hall states is that they are states of matter whose quasiparticle excitations are neither bosons nor fermions, but particles known as *non-Abelian anyons*, meaning that they obey *non-Abelian braiding statistics*. These new phases of matter define a new kind of order in nature, a *topological order* [12]. Such systems have become very interesting from the quantum computation perspective. Quantum information could be stored in states with multiple quasiparticles, which would have a topological degeneracy. The unitary gate operations would be simply carried out by braiding quasiparticles, and then measuring the multi-quasiparticle states. In this respect, let us also mention that several spin systems with topological order has been proposed recently as candidates for robust quantum computing [230, 231]. It has also been shown that these proposals could be implemented by means of cold atoms [232, 216].

Since the work of Laughlin [11], there has been enormous progress in our understanding of the fractional quantum Hall effect (FQHE) [233]. Nevertheless, many challenges remain open: direct observation of the anyonic character of excitations, observation of other kinds of strongly correlated states, etc. FQHE states might be studied with trapped ultra-cold rotating gases [234, 235]. Rotation induces there effects equivalent to an "artificial" constant magnetic field directed along the rotation axis. There are proposals how to detect directly fractional excitations in such systems [13]. Optical lattices might help in this task in two aspects: first, as we will see in the next chapter, FQHE states of small systems of atoms could be observed in a lattice with rotating site potentials, or an array of rotating microtraps [17, 236]. Second, "artificial" magnetic field might be directly created in an lattices via appropriate control of tunneling (hopping) matrix element in the corresponding Hubbard model [211]. Such systems will also allow to create FQHE type states [212, 237, 214].



---

# Simulation of the Laughlin state in an optical lattice

---

In the previous chapter, the potential that cold atoms have in order to simulate highly entangled and strongly correlated many body quantum systems have been exposed, as well as a list of interesting Condensed Matter phenomena that one would like to study. In the present chapter, the problem of generating the Laughlin state is addressed as a particular case of a quantum simulation.

Despite the great possibilities of the FQH states explained in the previous chapter, neither the Laughlin wave function nor its anyonic excitations have been observed directly in an experiment so far. Nevertheless, recent experimental advances in the field of ultra-cold atomic gases suggest that they could be good systems to simulate many Condensed Matter phenomena, and, in particular, the FQHE. From the theoretical point of view, it has been shown that the FQH can be realized by merely rotating a bosonic cloud in a harmonic trap (see Ref. [13, 14]). The rotation plays the role of the magnetic field for the neutral atoms. Thus, in the fast rotation regime, the atoms live in the lowest Landau level (LLL) and, if a repulsive interaction is introduced, they form the Laughlin wave function. In this system, the Laughlin state is a stable ground state, however, in practice, due to the weak interaction between the particles, the gap is too small, and it is not possible to achieve it experimentally.

An idea to avoid this problem is to use optical lattices [15, 16]. In such systems, the interaction energies are larger, since the atoms are confined in a smaller volume. This yields a larger energy gap and, therefore, opens the possibility of achieving FQH states experimentally.

In the present chapter, we want to improve the existing proposal of achieving the Laughlin state in an optical lattice presented in Ref. [17] by studying the consequences of considering not only the harmonic approximation to the single site potential expansion, but also the anharmonic corrections. Our work is organized as follows: first, we analyze the one body Hamiltonian of our system. We review the solution of the 2D harmonic oscillator and we discuss a more realistic model for the single site potential of a triangular optical lattice. Then, we study the many particle problem by introducing a repulsive contact interaction between the particles. We compute, by means of exact diagonalization, the fidelity of the ground state of the system with the Laughlin wave function for a wide range of the experimental parameters. Finally, we discuss which are the required experimental conditions and the procedure to obtain the Laughlin state.

## 6.1 One body Hamiltonian

### 6.1.1 Harmonic case

Let us consider one atom confined in a harmonic potential which rotates in the  $x$ - $y$  plane at a frequency  $\Omega$ . We will assume that the confinement in the  $z$  direction is sufficiently strong so that we can ignore the excitations in that direction. The Hamiltonian associated with this system is

$$\hat{H}'_0 = \frac{1}{2M} (\hat{p}_x^2 + \hat{p}_y^2) + \frac{1}{2} M \omega^2 (\hat{x}^2 + \hat{y}^2) - \Omega \hat{L}, \quad (6.1)$$

where  $M$  is the mass of the particle,  $\hat{p}_x$  and  $\hat{p}_y$  are the canonical momenta associated with the position coordinates  $x$  and  $y$ ,  $\omega$  is the frequency of the trap and  $\hat{L}$  is the angular momentum of the particle.

We can easily diagonalize this Hamiltonian by defining the creation and annihilation operators of some circular rotation modes  $\hat{a}_\pm = \frac{1}{\sqrt{2}} (\hat{a}_x \pm i\hat{a}_y)$ , where  $\hat{a}_{x,y}$  are the standard annihilation operators of the 1D harmonic oscillator in the directions  $x, y$ . In terms of the number operators  $\hat{n}_\pm \equiv \hat{a}_\pm^\dagger \hat{a}_\pm$  corresponding to these circular creation and annihilation operators, the angular momentum can be written as  $\hat{L} = \hbar (\hat{n}_+ - \hat{n}_-)$

and the Hamiltonian reads

$$\hat{H}'_0 = \hbar\omega(\omega - \Omega)\hat{n}_+ + \hbar(\omega + \Omega)\hat{n}_- + \hbar\omega. \quad (6.2)$$

Its spectrum is, therefore,

$$E_{n_+, n_-}^0 = \hbar(\omega - \Omega)n_+ + \hbar(\omega + \Omega)n_- + \hbar\omega, \quad (6.3)$$

where  $n_{\pm}$  are the integer eigenvalues of the number operators  $\hat{n}_{\pm}$ .

In the fast rotation regime ( $\Omega \rightarrow \omega$ ), the family of states

$$|m\rangle \equiv |n_+ = m, n_- = 0\rangle = \frac{1}{\sqrt{m!}} (a_+^\dagger)^m |0\rangle, \quad (6.4)$$

where  $|0\rangle$  is the state annihilated by both  $\hat{a}_+$  and  $\hat{a}_-$ , form the subspace of lowest energy. It corresponds to the LLL. We can write the wave function of these states

$$\varphi_m(z) \equiv \langle z|m\rangle = \frac{1}{\sqrt{\pi m!}} z^m e^{-\frac{|z|^2}{2}}, \quad (6.5)$$

where  $|z\rangle = |x, y\rangle$  are the eigenstates of  $\hat{x}$  and  $\hat{y}$ ,  $z = \frac{x+iy}{\ell}$  is a complex variable and  $\ell = \sqrt{\frac{\hbar}{M\omega}}$  is a characteristic length of the system.

Notice that if the rotation frequency is high but smaller than the trap frequency, the lowest energy subspace is only formed by states with  $m < \frac{\omega+\Omega}{\omega-\Omega}$ . In this limit, we can find an effective Hamiltonian of our system by projecting the original Hamiltonian onto the LLL,

$$\hat{H}_0 = \hbar(\omega - \Omega)\hat{L}. \quad (6.6)$$

Indeed, we can see that although Hamiltonians of Eqs. (6.2) and (6.6) are different, their projections onto the LLL coincide,  $PH'_0P^\dagger = PH_0P^\dagger$ , where  $P = \sum_m |m\rangle\langle m|$  is the projector onto the LLL.

In Ref. [17], the formation of fractional quantum Hall states in rotating optical lattices is studied under the approximation of a single particle Hamiltonian as the presented in Eq. (6.6). Nevertheless, the potential of a site of an optical lattice is not infinite as the parabolic one. Next, we would like to see how we can model in a more realistic way this single site potential and which consequences this will have in order to generate the fractional quantum Hall states.

### 6.1.2 Quartic correction

#### From the lattice potential to our model

We will consider a system of bosonic atoms loaded in a 2D triangular optical lattice [238]. The lattice is 2D due to the confinement in the  $x - y$  plane created by two counter propagating lasers in the  $z$  direction. In each of this planes a triangular lattice is realized by means of 3 lasers pointing at the directions  $\hat{k}_1 = (\sin \theta, 0, \cos \theta)$ ,  $\hat{k}_2 = (-\sin \theta/2, \sqrt{3} \sin \theta/2, \cos \theta)$  and  $\hat{k}_3 = (-\sin \theta/2, -\sqrt{3} \sin \theta/2, \cos \theta)$ , where  $\theta$  is the angle between these directions and the  $z$  axis.

In the region where the atoms are, the electric field created by each of these lasers can be modeled as a plane wave,  $\vec{E}_j(\vec{x}, t) = A\vec{\epsilon}e^{i(\vec{k}_j \cdot \vec{x} - \omega_L t)}$ , where  $\vec{k}_j = \frac{2\pi}{\lambda}\hat{k}_j$  for  $j = 1, 2, 3$  are the wave vectors of the lasers and  $\lambda$  is the wavelength of the light used. Notice that all the lasers share the same frequency  $\omega_L$  and polarization  $\epsilon$ . The atoms are subject to the superposition of the electric field  $\vec{E}_i(\vec{x}, t)$  created by each of the lasers,

$$\vec{E}(\vec{x}, t) = \sum_{i=1}^3 \vec{E}_i(\vec{x}, t) = E(\vec{x})\vec{\epsilon}e^{i\omega_L t}. \quad (6.7)$$

After averaging over time, the effective potential that atoms feel is, therefore, the correction to the energy of its internal state due to the AC-Stark effect. This energy shift is proportional to the square of the amplitude of the electric field  $|E(\vec{x})|^2$  and, in our particular case, it can be written as

$$V(\vec{x}) = -\frac{2}{9}V_0 \sum_{(i,j)} \cos [(\vec{k}_i - \vec{k}_j) \cdot \vec{x}], \quad (6.8)$$

where the sum runs over the 3 different couples of  $ij = 12, 23, 31$ , and  $V_0$  is the intensity of the laser. The minima of this potential form a Bravais triangular lattice with basis vectors  $\vec{a}_1 = \frac{2}{3} \frac{\lambda}{\sin \theta} \left(-\frac{1}{2}, \frac{\sqrt{3}}{2}\right)$  and  $\vec{a}_2 = \frac{2}{3} \frac{\lambda}{\sin \theta} (1, 0)$ .

Let us assume that the intensity of the laser is  $V_0 \gg E_R$ , where  $E_R = \hbar^2 k^2 / 2M$  is the recoil energy, with  $k = 2\pi/\lambda$ . In this limit, tunneling of atoms between different sites is forbidden, and the lattice can be treated as a system of independent wells. Thus, the ground state of the system is a product state of the state of each site (Mott phase) and we can study the whole system by studying each site of the lattice independently of the others.

In order to describe the potential of a single site, we expand the previous lattice

potential in Eq. (6.8) around the equilibrium position  $\vec{x} = \vec{0}$ ,

$$V(\vec{x}) \sim \frac{1}{2}M\omega^2(x^2 + y^2) - \frac{3}{32}k^4V_0(x^2 + y^2)^2 + O(x^6). \quad (6.9)$$

We get a harmonic oscillator term with frequency  $\omega = 2\sqrt{V_0E_R}/\hbar$  plus a quartic perturbation and higher order corrections. Notice that both terms of the expansion respect the circular symmetry. This is actually the reason why we have considered a triangular lattice instead of the simpler square one. In the square lattice, the circular symmetry is broken in fourth order of the expansion, while in the triangular one, this does not happen until the sixth order. From now on, we will consider that our single site potential is adequately described by only these harmonic and quartic terms of the expansion of the potential. This approximation is reasonable since we have already assumed  $V_0 \gg E_R$ .

Furthermore, by introducing some phase modulators into the lasers that form the lattice, it is possible to create time averaged potentials that generate an effective rotation of the single lattice sites. If this rotation  $\Omega$  is close to  $\omega$ , the system is in the fast rotation regime and we can obtain the low energy Hamiltonian proceeding as before. Written in units of  $\hbar\omega$ , it becomes

$$\hat{H} = \hbar \left( 1 - \frac{\Omega}{\omega} \right) \hat{L} - \gamma \left( \frac{\hat{x}^2 + \hat{y}^2}{\ell^2} \right)^2, \quad (6.10)$$

where  $\gamma \equiv \frac{3}{32} \frac{V_0 k^4 \ell^4}{\hbar \omega} = \frac{3}{64} \sqrt{\frac{E_R}{V_0}}$  is a perturbation parameter. Notice that the perturbation parameter,  $\gamma$ , only depends on the intensity of the laser in units of the energy recoil.

In summary, we have described the whole sophisticated optical lattice by a set of independent wells modeled by the simple Hamiltonian presented in Eq. (6.10). This effective Hamiltonian is the same from Eq. (6.6) plus a quartic correction term which will be responsible for all the new physics that we are going to study next.

### Exact solution

Now, we want to find the lowest energy eigenstates of the Hamiltonian presented in Eq. (6.10). First of all, we realize that both  $H$  and  $H_0$  are rotationally invariant, therefore,  $[H, H_0] = [H, L] = 0$ . Thus,  $H, H_0$  and  $L$  must have a common eigenbasis, and this can only be  $\{|m\rangle\}$ . We determine the eigenvalues of  $H$  by merely computing the expected values

$$E_m = \langle m|H|m\rangle = \left( 1 - \frac{\Omega}{\omega} \right) m - \gamma(m+1)(m+2), \quad (6.11)$$

in units of  $\hbar\omega$ .

It is interesting to point out that the commutator between the Hamiltonians of the harmonic and anharmonic systems before being projected onto LLL,  $[H', H'_0]$ , is not zero. Therefore, their lowest energy eigenstates only coincide in the fast rotation regime.

It is important to know which is the fast rotation regime for the Hamiltonian (6.10) or, in other words, under which conditions our low energy description of the system is correct. To see this, we can compute, using perturbation theory, the first correction to the energy of the second Landau level (NL) states

$$E_m^{NL} = (m + 2) - \gamma(m + 7)(m + 2). \quad (6.12)$$

We realize that the LLL is a good description of the lowest energy states, *i. e.*  $E_m \ll E_m^{NL}$ , if  $3\gamma(m + 1) \ll 1$ . In this regime, the projection of the Hamiltonian onto the LLL is a good effective description of our system. From now on, this condition will be always assumed.

### 6.1.3 Maximum rotation frequency

In the harmonic case, we realize that if the rotating frequency  $\Omega$  exceeds the frequency of the trap  $\omega$  (see Eq. (6.6)), the lower energy states have an infinite angular momentum, *i. e.* all the particles of the system are expelled from the trap. This maximum frequency is usually known as the centrifugal limit. What we are going to study now is, therefore, how the introduction of the quartic perturbation will affect the centrifugal limit of the system. In order to answer this question we realize two different analysis that give quite similar results.

The first argument consists of a semi-classical interpretation of the dynamics of the particle. In the anharmonic system, we have a competition between the attractive force of the harmonic trap and the repulsive forces corresponding to the quartic correction and the fictitious centrifugal force. In the central region, the harmonic trap dominates and the particles are confined, while if a particle was in the exterior region, it would be expelled. The limit radius between these two regions corresponds to the maximum of the effective potential that includes both the trap and centrifugal terms. Furthermore, from the semi-classical point of view, each stationary state  $|m\rangle$  follows a circular trajectory of radius  $r \sim \sqrt{m}$  around the origin. We expect then that those states whose associated radius is less than the limit radius are bound states. Thus, we find that the maximum rotation frequency, or the centrifugal limit, depends on the

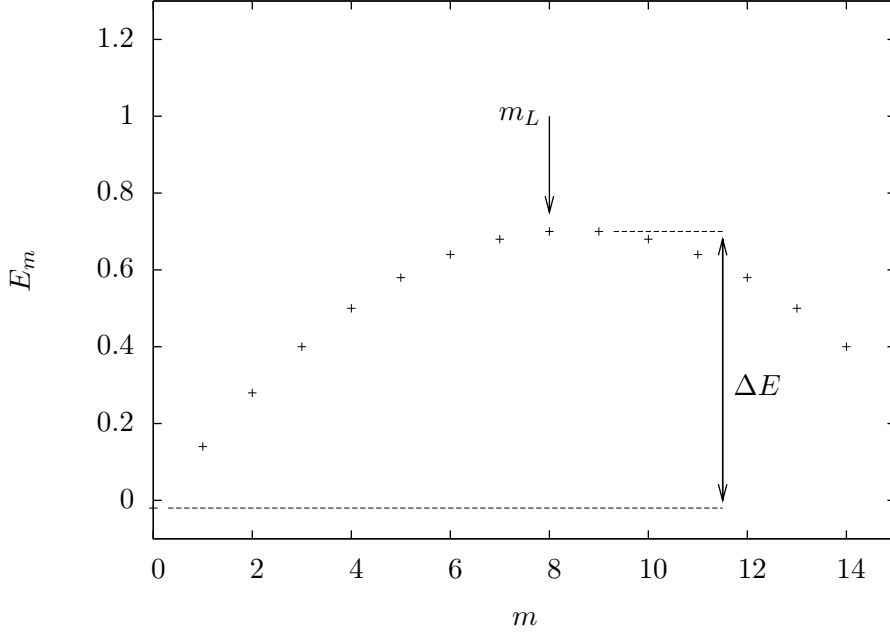


Figure 6.1: Spectra of the single-particle Hamiltonian shown in Eq. (6.10) that models the dynamics of a particle in a rotating single site of a triangular optical lattice. This plot has been realized for  $\gamma = 0.01$  and  $\Omega = 0.8\omega$ . Notice that for these particular values of the frequency rotation and the laser intensity, particles with an angular momentum larger than  $m_L = 8$  would be expelled.

maximum angular momentum that we want to keep in the trap. This is a remarkable difference with respect to the harmonic case, where the centrifugal limit was the same for any angular momentum state. In particular and according to this semi-classical criterion, the centrifugal limit for a particle with an angular momentum equal or less than  $m_L$  is

$$\Omega_L = \omega \sqrt{1 - 4\gamma m_L} \simeq \omega(1 - 2\gamma m_L). \quad (6.13)$$

Another approach is to think in terms of the slope of the spectra  $E_m$  presented in Eq. (6.11) and plotted in Fig. 6.1. We realize that the single particle energy  $E_m$  begins growing with  $m$  from  $m = 0$ , reaches a maximum at  $\left[ \frac{1-\Omega-3\gamma}{2\gamma} + \frac{1}{2} \right]$ , (where the brackets  $[ ]$  represent the integer part function), and becomes monotonically decreasing from this point. We interpret this in the same way as the harmonic case, that is to say, those states  $|m\rangle$  that are in an energy interval with a negative slope are unstable. According to this interpretation, the angular momentum of a particle must be less than  $\left[ \frac{1-\Omega-3\gamma}{2\gamma} + \frac{1}{2} \right]$  in order to be trapped. This implies that the centrifugal

limit for a trapped particle with angular momentum  $m_L$  is

$$\Omega_L = \omega(1 - 2\gamma m_L - 4\gamma). \quad (6.14)$$

Although the previous approaches are different, notice that they predict practically the same centrifugal limit. In our simulations presented in Sec. 6.3, we have taken the condition given by Eq. (6.14), since it is the most restrictive one.

At this point, we have completely solved the one particle problem. Let us note that whereas in the harmonic case the maximum rotation frequency coincides always with the trap frequency, in the system with the quartic perturbation, this centrifugal limit depends on which is the maximum angular momentum of a particle that we want to keep trapped. This difference will be crucial to understand why it will be more difficult to obtain the Laughlin state in the anharmonic case than in the harmonic one.

## 6.2 Many particle problem

The Laughlin state is a strongly correlated state, therefore, interaction between atoms will play an essential role in its experimental realization.

Let us consider, then, a set of  $N$  bosons trapped in a well as the one described previously, and interacting by means of a repulsive contact potential,

$$V(\vec{r} - \vec{r}') = g\delta(\vec{r} - \vec{r}'), \quad (6.15)$$

where the parameter  $g$  accounts for the strength of the interaction, and is related to the s-wave scattering length,  $a_s$ , and to the localization length in the  $z$  direction,  $\ell_z$ , by  $g = \sqrt{\frac{2}{\pi}} \frac{a_s}{\ell_z}$ .

We are interested in knowing the ground state of the system for a wide range of  $g$  and  $V_0/E_R$  in order to see under which conditions the Laughlin state could be realized experimentally. The solution of this problem is trivial in the extreme cases  $g \rightarrow 0$  and  $g \rightarrow \infty$ .

When  $g = 0$ , the atoms do not interact and the ground state of the system is merely a product state with all the atoms with angular momentum zero.

If  $g \rightarrow \infty$ , the atoms will find a configuration in which they are always in a different position with the minimum total angular momentum possible. This configuration that minimizes the interaction energy at the expense of the angular momentum of the particles is precisely the Laughlin state. As we can see in Eq. (8.1), the interaction

energy in the Laughlin wave function is strictly zero since the probability that two atoms are in the same position is null.

For a finite  $g$ , the problem of finding the ground state of the system has to be addressed numerically. In particular, we will solve it by means of exact diagonalization. With this aim, we can write the Hamiltonian of this system in 2nd quantization form,

$$\hat{H} = \sum_{j=1}^L \left( (1 - 3\gamma - \Omega)\hat{n}_j - \gamma\hat{n}_j^2 + 1 - 2\gamma \right) + \frac{1}{2} \sum_{i < j} V_{ijkl} b_i b_j b_k^\dagger b_l^\dagger, \quad (6.16)$$

where  $b_j$  and  $b_j^\dagger$  are the creation and annihilation operators of the mode  $j$  which corresponds to the LLL state with angular momentum  $j$  presented in Eq. (6.5),  $\hat{n}_j \equiv b_j^\dagger b_j$  counts the number of particles with angular momentum  $j$ , and  $V_{ijkl}$  are the coefficients of the interaction in this basis defined by

$$V_{m_1 m_2 m_3 m_4} = \langle m_1 m_2 | \hat{V} | m_3 m_4 \rangle = \frac{g}{2\pi} \frac{\delta_{m_1+m_2, m_3+m_4}}{\sqrt{m_1! m_2! m_3! m_4!}} \frac{(m_1 + m_2)!}{2^{m_1+m_2}}. \quad (6.17)$$

The cylindrical symmetry of the Hamiltonian allows the diagonalization to be performed in different subspaces of well defined total z-component of  $L = \sum_{i=1}^N m_i$ .

Thus, given the parameters  $\Omega, V_0/E_R$  and  $g$  and a subspace of total angular momentum  $L$ , we construct the multi-particle basis of  $N$  particles compatible with  $L$ , calculate the matrix-elements of the Hamiltonian in this subspace by means of Eq. (6.16), and perform its diagonalization. Once the ground state for each subspace  $L$  is determined, we find the ground state of the system by merely selecting the state with lowest energy.

An important issue that we have to take into account when we perform the simulation is to be careful with the centrifugal limit. As we have already seen in Sec. 6.1.3, if we want that the particle with the maximum angular momentum does not escape from the trap, we have to keep the rotation below the centrifugal limit given by Eq. (6.14). In our case, in which we want to drive the system into the Laughlin state, this centrifugal limit is determined by the maximum angular momentum of a single particle in the Laughlin state, that is  $N(N-1)/2$ . Thus, the maximum rotation frequency is given by Eq. (6.14) taking

$$m_L = N(N-1)/2. \quad (6.18)$$

### 6.3 Results and discussion

In what follows, we display the results obtained from exact diagonalization described in the previous section.

We want to study under which conditions the Laughlin wave function is the ground state of the system and discuss if these conditions can be realized experimentally. With this aim, in Fig. 6.2, we present a phase diagram where the fidelity between the Laughlin state and the ground state of the system is plotted versus the laser intensity  $V_0/E_R$  and the strength of the contact interaction  $g$ . For each value of  $V_0/E_R$ , we have taken the maximum possible rotation frequency, defined by Eq. (6.14), since it corresponds to the best condition to achieve the Laughlin wave function. The plot shows two separated phases. In one of them, the Laughlin state is perfectly obtained ( $\langle GS|\Psi_L\rangle = 1$ ). It corresponds to high values of the laser intensity and strength of the interaction. On the contrary, for low values of  $V_0/E_R$  and  $g$  the fidelity between the ground state and the Laughlin state is zero. This phase corresponds to other states with less angular momenta and not so correlated.

Notice that the transition between the Laughlin and non-Laughlin phases is very abrupt. This is because the ground state in the non-Laughlin phase has an angular momentum smaller than the angular momentum that Laughlin state requires. States with different angular momentum are orthogonal and therefore the fidelity between them is zero. Nevertheless, when interaction is high enough and it is sufficiently favorable for the system to have total angular momentum  $L = N(N - 1)$ , the Laughlin wave function is instantly achieved. This argument is illustrated in Fig. 6.3 for the case of  $N = 4$  particles. We can see how the system increases its angular momentum depending on the confinement  $V_0$  and the interaction  $g$ .

In Fig. 6.2, the shape of the boundary between the Laughlin and non-Laughlin phases can be easily explained. According to the argument presented in the previous section, the configuration of the ground state of the system depends on the ratio between the strength of the interaction  $g$  and the energy difference of the single particle spectrum  $\Delta E \equiv E_{m_L} - E_0 = \gamma m_L(m_L + 1)$  (see Fig. 6.1). In particular, we expect two regimes:

- If  $g \gg \Delta E$ , the ground state is the Laughlin state,
- while if  $g \ll \Delta E$ , then ground state is a product state with all the particles with angular momentum 0.

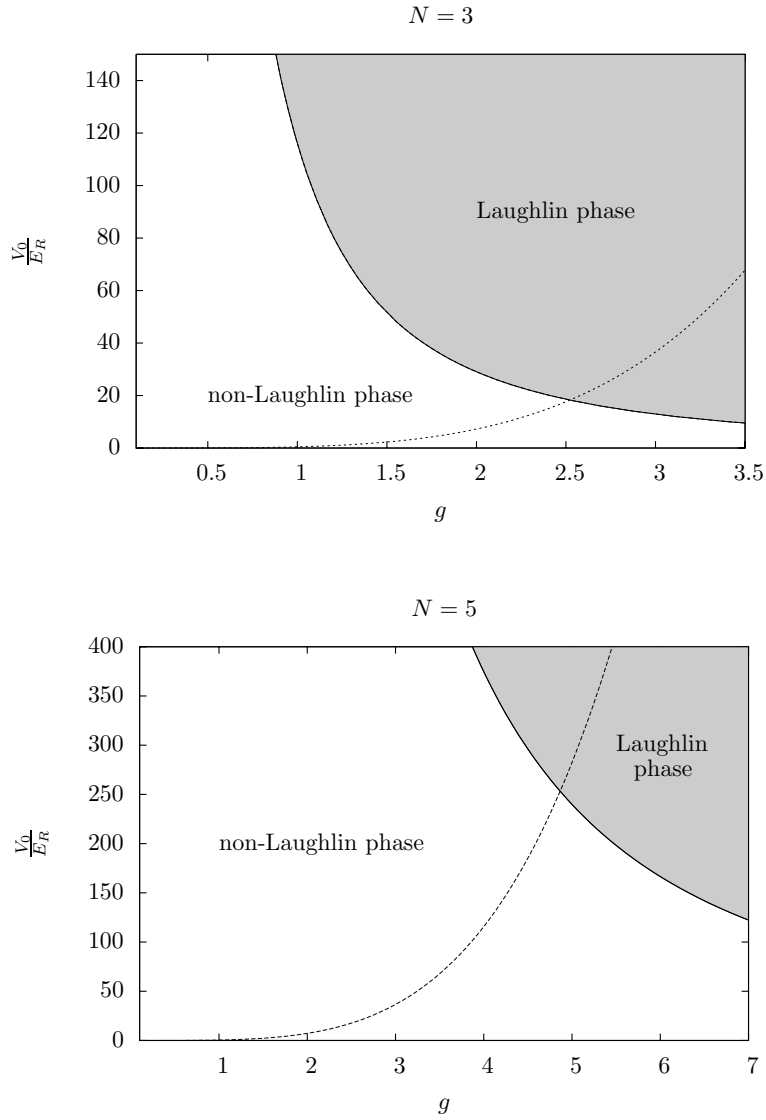


Figure 6.2: Density plot of the fidelity between the ground state of the system and the Laughlin wave function versus the laser intensity  $V_0$  and the strength of the contact interaction  $g$  for different number of particles ( $N=3$  and 5). In order to realize the diagram, the maximum possible rotation frequency  $\Omega_L$  has been considered for each value of  $V_0$ . The dashed line represents the dependence of  $g$  on the confinement  $V_0$  for the Rubidium atoms case. Although the  $V_0$  needed to get the Laughlin as the ground state increases enormously with the number of particles, we realize that for small values of  $N$ , the laser intensity required is achievable.

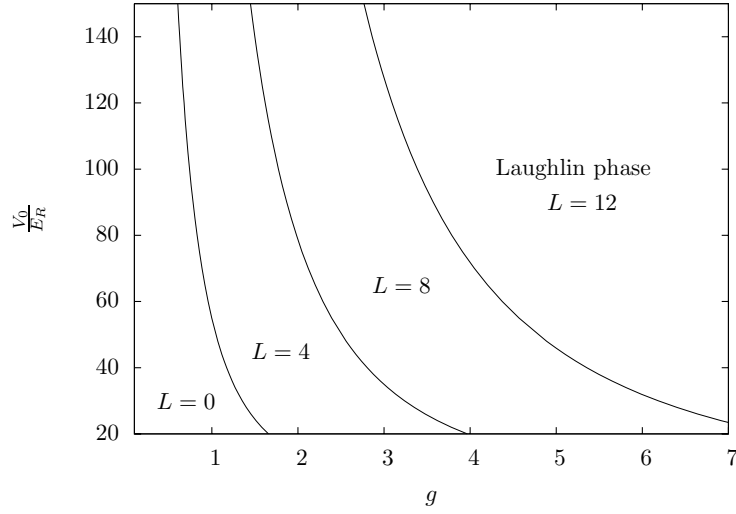


Figure 6.3: Density plot of the angular momentum of the ground state of the system respect to the laser intensity  $V_0$  and the strength of the contact interaction  $g$  for  $N=4$ . In order to realize the diagram, the maximum possible rotation frequency  $\Omega_L$  has been considered for each value of  $V_0$ .

The transition, then, takes place between these two regimes, that is, when  $g \sim \Delta E$ . This condition implies that

$$g = f(N) \sqrt{\frac{E_R}{V_0}} \quad (6.19)$$

where  $f(N) \sim m_L(m_L + 1)$  is a function that depends on  $N$ .

In Fig. 6.4, we plot the numerical data  $(\sqrt{\frac{E_R}{V_0}}, g)$  corresponding to the points of the border between the Laughlin and non-Laughlin phases of Fig. 6.2 for  $N = 4$  in order to see if Eq. (6.19) is fulfilled. We observe a perfect fit between numerical data and Eq. (6.19) and, performing a linear regression, we determine the slope  $f(4) = 33.876(1)$ . The same perfect agreement has been found for  $N = 3$  and  $N = 5$  cases, with slopes  $f(3) = 10.779(1)$  and  $f(5) = 77.427(3)$  respectively.

According to Eq. (6.19), we would expect that function  $f(N)$  scales as  $\sim N(N - 1)(N(N - 1) + 2)$ . Nevertheless, although  $f(3)$ ,  $f(4)$  and  $f(5)$  seem to scale in this way, three points are not enough to confirm this behavior.

The dashed line in Fig. 6.2 expresses the dependence of  $g$  on the confinement  $V_0$  for the Rubidium atoms case (see Eq. (6.20)). It shows the natural path that the system would follow increasing the intensity of the laser without improving the strength of the interaction by means of Feshbach resonance techniques. This illustrates the

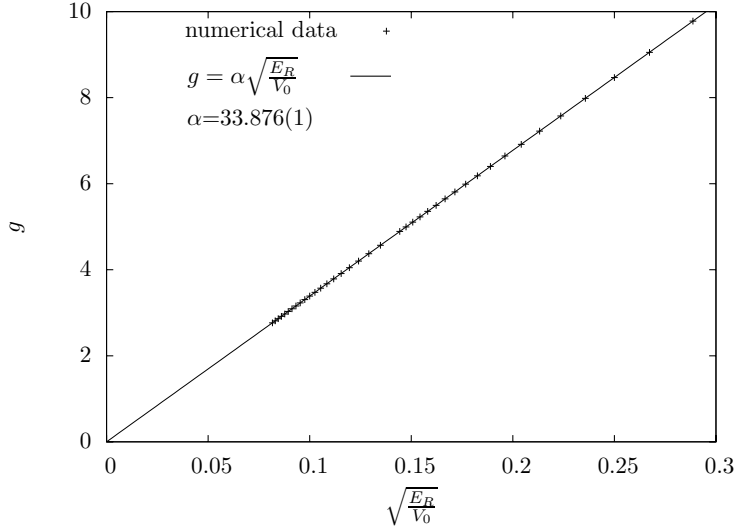


Figure 6.4: Plot of the points  $(\sqrt{\frac{E_R}{V_0}}, g)$  of the border between the two phases (Laughlin and non-Laughlin) of Fig. 6.2 for  $N = 4$ . We realize that Eq. 6.19 describes perfectly its behavior.

advantages of confining ultra-cold gases in an optical lattice. The high confinement increases the scattering length of the interaction between the atoms,

$$g = \sqrt{2}a_s|k| \left( \frac{V_0}{E_R} \right)^{1/4}, \quad (6.20)$$

which, at the end of the day, is responsible for the high correlation of the ground state.

Moreover, this enhanced interaction produces a larger energy gap which makes the optical lattice proposal more robust compared to the harmonic trap setup. This enhancement in the energy gap of the excitation spectrum can alleviate some of the challenges for experimental realization of the quantum Hall state for ultra-cold atoms.

In Fig. 6.2, we also realize that the larger the number of atoms of the system is, higher the laser intensity needed to achieve the Laughlin state. The reason for this is that for larger  $N$ , the maximum angular momenta allowed before the atoms escape from the trap is larger,  $m_L = N(N - 1)/2$ . This implies a smaller maximum rotation frequency  $\Omega_L$  (see Eq. (6.14)), and the requirement of increasing the laser intensity  $V_0$  to compensate this effect. Let us note that increasing  $V_0$  we achieve both larger maximum rotation frequency and a stronger interaction  $g$ .

It is interesting to point out that driving the system into the Laughlin wave function

is not possible by simply increasing the rotation frequency, since the symmetric shape of the potential conserves the angular momenta and the system would rest in a trivial non-entangled state with angular momentum zero. To avoid this, we should introduce some deformation to the wells of the lattice in order to break the spherical symmetry. For our optical lattice setup this can be achieved by introducing a couple of electro-optical fast phase modulators whose effect in the rotating frame would be a new trapping potential with the form  $V_p \propto (\omega + \Delta\omega)^2 x^2 + \omega^2 y^2$ . This modification would change our original Hamiltonian in a new one  $H + H_\epsilon$ , where

$$H_\epsilon = \frac{\epsilon}{4} \sum_m \beta_m b_{m+2}^\dagger b_m + (m+1) b_m^\dagger b_m + \text{h.c.}, \quad (6.21)$$

where  $\beta_m = \sqrt{(m+2)(m+1)}$  and  $\epsilon = \Delta\omega/\omega$  is a small parameter.

The previous perturbation (6.21) leads to quadrupole excitations, so that states whose total angular momentum differ by two units are coupled, and the system can increase its angular momentum. In order to drive the system into the Laughlin state, we could follow some adiabatic paths in the parameter space  $(\Omega, \epsilon)$  such that the gap along this paths is as large as possible, and in this way, keep the system in its ground state according to the adiabatic theorem [239]. Another possibility would be to study the optimal control technique which consists of finding a particular variation of the experimental parameters such that the system finishes at the Laughlin state after exploring other excited states.

Finally, let us briefly discuss how to check that we have driven the system to the Laughlin state. First, notice that as the system is in a Mott phase, any measurement signal will be enhanced by a factor equal to the number of occupied lattice sites.

According to Ref. [240], for any lowest-Landau-level state of a trapped, rotating, interacting Bose gas, the particle distribution in coordinate space in a time of flight experiment is related to that in the trap at the time it is turned off by a simple rescaling and rotation. Thus, it is possible to measure the density profile of our state by merely accomplishing a time of flight experiment. Notice that by means the density profile it is possible to estimate the total angular momentum of the system.

Although we can measure the angular momentum of the system, there are many states with the same angular momentum that are not the Laughlin state. In order to really distinguish if we got the Laughlin state, or not, we require the measurement of other properties. One possibility is the measurement of correlations. In Ref. [17], an interesting technique is proposed to measure the correlation functions  $g_1 = \langle \psi^\dagger(\mathbf{r})\psi(\mathbf{r}') \rangle$  and  $g_2 = \langle \psi^\dagger(\mathbf{r})\psi^\dagger(\mathbf{r}')\psi(\mathbf{r})\psi(\mathbf{r}') \rangle$ . These functions are very partic-

ular for the Laughlin state. In particular,  $g_2 \propto |r - r'|^4$ , since, in the Laughlin state, all the particles have a relative angular momentum  $m_r = 2$  between them. Let us just present the scheme of this technique. The technique is based on the use of gases of two species that can be coupled via Raman transitions (hyperfine levels). First, all the atoms are in the same state and the system is driven to the Laughlin state. Then, we can create an equal superposition of the two species by means of a  $\pi/2$ -pulse with the laser. Next, we can shift the atoms a small distance compared to the lattice spacing by moving the lattice of one of the species (as was proposed in Ref. [241] and experimentally realized in Ref. [242]). Finally, another  $\pi/2$ -pulse is performed in order to put all the atoms in the same state and the time of flight measurement is accomplished.

## 6.4 Conclusions

The method for achieving the Laughlin state in an optical lattice presented in Ref. [17] has been studied. It has been shown that it is essential to take into account the anharmonic corrections. A quartic anharmonic term introduces a maximum rotation frequency that is smaller than in the harmonic case and, therefore, if this was not considered all the particles would be expelled from their single lattice sites.

Although this more restrictive centrifugal limit makes more difficult to drive the system into the Laughlin state, since it requires higher values of  $V_0$ , for systems with a small number of particles, the Laughlin state is achievable experimentally.

The shape of the boundary between the Laughlin and non-Laughlin phases in the phase diagram of the system respect to the confinement  $V_0$  and the strength of the interaction  $g$  plotted in Fig. 6.2 has been physically explained and analytically described.



---

## Symmetry breaking in small rotating cloud of trapped ultracold Bose atoms

---

In the previous chapter, it has been shown that the Laughlin state is the ground state of a cloud of repulsive interacting bosons in a rotating harmonic trap when the rotation frequency is large enough. In this chapter, we want to study which kind of structures the ground state of the same system has at lower rotation frequencies. In particular, we wonder if these states would correspond to strongly correlated states (like the Laughlin case) or, on the contrary, they could be described by means of an order parameter, in a similar way to the mean-field approach [18]. This order parameter description of small rotating clouds will allow us to address in a different point of view the issue of symmetry breaking in Bose-Einstein condensates and the problem of the interpretation of a time of flight (TOF) measurement in the interference experiment of two Bose-Einstein condensates.

Symmetry breaking in finite systems has been a subject of intensive debate in physics, in general (cf. the Ref.[243]), and in physics of ultracold gases in particular over the years. For Bose-Einstein condensates (BEC) two symmetries play a particular role:  $U(1)$  phase symmetry and  $SU(2)$  (or  $SO(3)$ ) rotational symmetry. In the large  $N$  limit, one breaks these symmetries by hand, as proposed originally by Bogoliubov [244]. Thus, the accurate way to deal with macroscopic Bose Einstein condensates

(BEC's) is by the use of a classical field, also called an order parameter, or the wave function of the condensate. This function is a single particle wave function, which is the solution of the Gross Pitaevskii equation within the mean field approximation, that characterizes the system in a proper way [245]. It has an arbitrary, but fixed phase, and for rotating systems with more than one vortex it exhibits arbitrarily places, but fixed vortex array. For dilute ultracold Bose gases (i.e. when  $n|a|^3 \ll 1$  [18] where  $n$  is the density and  $a$  is the s-wave scattering length) mean field (or Bogoliubov approach) is capable to reproduce very well the main properties, despite the fact for finite, fixed  $N$  and total angular momentum  $L$ , which are both constants of the motions, mean field theory cannot be exact.

This observation has stimulated a lot of discussion about the nature of the phase of BEC [246, 247, 248, 249, 250], and particle-conserving Bogoliubov approach [251, 252, 253]. The modern point of view (for a recent discussion see [254]) implies that two BEC's with fixed  $N$  each one, will produce a well defined interference pattern of fringes as a result of the measurement in only one shot (comparable with the calculated n-correlation function) in contrast with the density, which would be obtained as a mean image of random interference patterns from several shots. The position of fringes in the given measurement are determined by subsequent localization of atoms arriving at detectors; the first atom is completely random, second is correlated, third even more correlated etc. [248, 249]. Thus the information about the pattern is obtained from the many-body wave function by looking at pair, triple, ... correlations. The breaking of rotational symmetry should occur in large rotating clouds in the similar way, and a pure L-state would show, in a time-of-flight experiment, a definite interference pattern accurately represented by n-correlation functions, different from a circular symmetric profile of the single particle density. It would be a test of the meaning assigned to the measurement. Unfortunately, for large N-systems, the total angular momentum of the stationary states is not well defined and there is no qualitative difference between density and n-correlation function, usually showing in both cases vortex arrays. For small rotating clouds the situation is, however, different, as we have shown in Ref. [236]. Typically, the ground states are pure-L states for most of the values of  $\Omega$ . Only, in the very narrow window of frequencies, where the ground states is degenerated with respect to  $L$ , vortex arrays can be obtained, arbitrary small symmetry breaking deformation of the trap potential leads to the appearance of symmetry breaking vortex arrays both in density and pair-correlations. Namely, in the regime of pure L ground states, small systems would provide a suit-

able test for the meaning of the measurement distinguishing between the density or the pair-correlation output.

In this chapter we study the effects of symmetry breaking in small rotating clouds of trapped ultracold Bose atoms in more depth, by introducing the rigorous definition of the condensate wave function, defined as an eigenvector of the one body density matrix operator (OBDM), corresponding to the largest eigenvalue. Such definition of the order parameter has been introduced in classical papers on *off-diagonal long range order* [255, 256, 257, 258]. It has, however, rarely been used since its application requires the knowledge of the full many-body wave function, or at least of the exact OBDM. Since for quantum gases exact analytic solutions are either not known (2D and 3D), or very difficult to handle (1D), so far this definition has been only applied to the case of model system with harmonic forces.

Here we apply for the first time to the rotating gas, using exact numerically calculated OBDM for few atom systems. We identify in this way possible states with vortices, and obtain phase characteristics of the wave function (reflecting quantized circulation of vortices), and provide unambiguous definition of the degree of condensation. With such calculated order parameter we then reproduce the density and interference patterns for two condensed clouds, and shed new light on the discussion of the origins of symmetry breaking in finite mesoscopic systems.

## 7.1 The model: macro-occupied wave function

### 7.1.1 Description of the system

We consider a two-dimensional system of few Bose atoms trapped in a parabolic rotating trap around the  $z$ -axis. The rotating frequency  $\Omega$  is strong enough to consider the Lowest Landau Level regime with atoms interacting via contact forces. As we have seen in the previous chapter, in the second quantized form, the Hamiltonian of the system projected onto the LLL in the rotating reference frame is described by [236],

$$\hat{H} = \alpha \hat{L} + \beta \hat{N} + \hat{V} + \hat{V}_p \equiv \hat{H}_0 + \hat{V} + \hat{V}_p, \quad (7.1)$$

where  $\alpha = \hbar(\omega_{\perp} - \Omega)$ ,  $\beta = \hbar\omega_{\perp}$ ,  $\hat{L}$  and  $\hat{N}$  are the total  $z$ -component angular momentum and particle number operators, respectively, and

$$\hat{V} = \frac{1}{2} \sum_{m_1 m_2 m_3 m_4} V_{1234} a_1^{\dagger} a_2^{\dagger} a_4 a_3, \quad (7.2)$$

where the matrix elements of the interaction term are given by

$$V_{1234} = \langle m_1 m_2 | V | m_3 m_4 \rangle = \frac{g}{\ell^2 \pi} \frac{\delta_{m_1+m_2, m_3+m_4}}{\sqrt{m_1! m_2! m_3! m_4!}} \frac{(m_1 + m_2)!}{2^{m_1+m_2+1}}, \quad (7.3)$$

where  $g$  is the interaction coefficient that approximates the potential of the Van der Waals forces in the very dilute limit,  $\ell = \sqrt{\hbar/2M\omega_\perp}$ , and  $M$  is the atomic mass. The last term in Eq. 7.1 is the anisotropic term that mimics the stirring laser and is given by  $\hat{V}_p = A \sum_{i=1}^N (x^2 - y^2)_i$  or in second quantized form as

$$\hat{V}_p = \frac{A}{2} \ell^2 \sum_m \left[ \sqrt{m(m-1)} a_m^+ a_{m-2} + \sqrt{(m+1)(m+2)} a_m^\dagger a_{m+2} \right]. \quad (7.4)$$

We assume this term to be a small perturbation of the system, thus,  $\frac{A\ell^2/2}{\hbar(\omega_\perp - \Omega)} \ll 1$ .

In the previous equations, the operators  $a_m^\dagger$  and  $a_m$  create and annihilate a boson with single-particle angular momentum  $m$ , respectively. These single-particle wave functions are called Fock-Darwin, and are given by

$$\varphi_l(\vec{r}) = e^{im\theta} r^l e^{-r^2/2} / \sqrt{\pi m!} \quad (7.5)$$

in units of  $\ell$ , where  $m$  is the single particle angular momentum. Notice that the many-body wave functions formed by the product of Fock-Darwin's are the solutions of  $\hat{H}_0$  in Eq. (7.1).

The conditions for validity of LLL regime are given by  $(N-1)g/(4\pi) \ll (1+\Omega/\omega_\perp)$  and  $(1-\Omega/\omega_\perp) \ll (1+\Omega/\omega_\perp)$  where  $\ell$  and  $\hbar\omega_\perp$  are taken as units of length and energy, respectively, meaning that the interaction and the kinetic contributions to the energy per particle are smaller than the energy gap between Landau levels which is given by  $(1+\Omega/\omega_\perp)$ . This means that for  $g=1$  and  $N$  less than about 10 particles the LLL assumption is valid down to frequencies significantly lower than the critical frequency  $\Omega_c$ , where the nucleation of the first vortex takes place.

### 7.1.2 Ordered structures in ground states

In Fig. 7.1, it is shown the total angular momentum of the ground state of a system of  $N=5$  particles without the anisotropic perturbation  $\hat{V}_p$  while  $\Omega$  grows from zero to  $\omega_\perp$ , the maximum possible value before the system becomes centrifugally unstable. We observe that the ground state angular momentum remains constant for a finite range of  $\Omega$  until transitions to new angular momenta take place at critical values

labeled as  $\Omega_{cn}$ . Not all  $L$ -values can be associated with the ground states. However, on the steps, different  $L$ -states may be degenerate in energy as in the case of the states with  $L = 8, 10$  and  $12$  on the third step (indicated by stars in Fig. 7.1). In Ref. [236], it is shown that structures of more than one vortex can only be obtained at very specific plateau steps  $\Omega_{cn}$ . Only in this steps is possible the unique situation where vortices are generated in the density corresponds to the steps in the  $L_{gs}$  dependence on  $\Omega$ , where a degeneracy of states with different  $L$  takes place at  $\Omega_{cn}$ . At first sight, this result does not agree with the experimental results reported by Chevy *et al.* [259]. However, it can be attributed to an essentially different behavior of systems with a large and a small number of atoms, respectively. As  $N$  grows, the size of some of the plateaus shown in Fig. 7.1 drastically shrinks in such a way that finite ranges of  $\Omega$ -values with energetically degenerate states become possible; not only at critical values  $\Omega_{cn}$ .

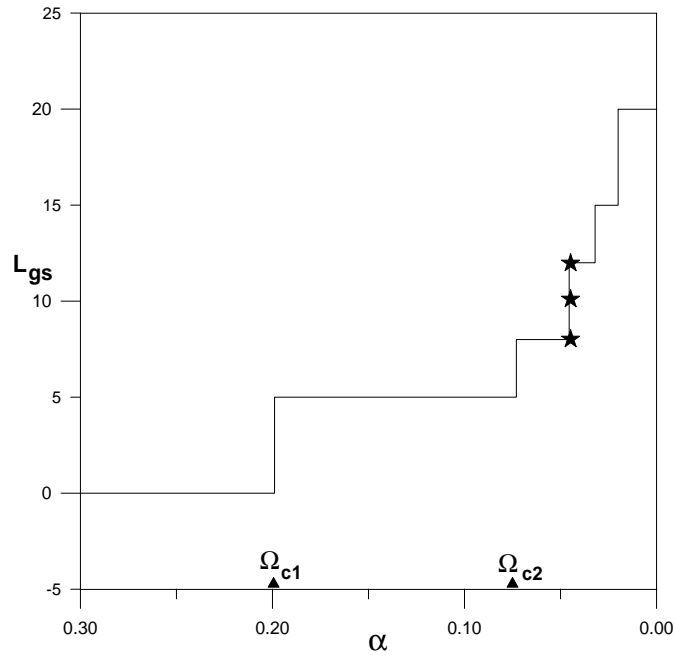


Figure 7.1: Change of the ground state angular momentum  $L_{gs}$  for  $N = 5$  as the rotation frequency increases; transitions take place at critical values of the rotational frequency labeled by  $\Omega_{cn}$ . ( $\alpha = \hbar(\omega_{\perp} - \Omega)$ ).

Let us mention, in connection with the previous chapter, that the last possible ground state at  $L = N(N - 1)$  is the Laughlin state, for which the interaction energy is zero due to the fact that the wave function of each atom has zeros of order two at

the positions of the other  $N - 1$  atoms; this can be easily deduced from the analytical expression of the many-body wave function given by,

$$\Psi_{Laughlin} = \mathcal{N} \prod_{i < j} (z_i - z_j)^2 e^{-\sum |z_i|^2 / 2\ell^2} . \quad (7.6)$$

Our main goal is the description of the stationary states for different values of  $\Omega$ , analyzed from the rotating frame of reference, unless otherwise stated. Our analysis is performed using the exact diagonalization formalism, valid for arbitrary interactions and densities. However, in contrast to the mean field approach, this method deals with multi-particle wave functions and loses the intuitive picture provided by the mean field order parameter. Our goal is to obtain in a precise way a complex scalar field that models efficiently the system, and allows to reproduce the important features, such as the vortex states.

In the regime of relatively low rotation frequency, where the degree of condensation is high and some vortices appear distributed in an ordered arrays, this scalar field plays the role of a genuine order parameter. On the other hand, it loses its capability to represent the system as  $\Omega$  approaches the melting point, where the prediction [235] is that the vortex lattice disappears and the systems turns, for large systems, into a Laughlin liquid.

### 7.1.3 Macro-occupied wave function

To obtain the single particle macro-occupied wave function we proceed as follows. In the first step we generate a vortex state tuning  $\Omega$  around the critical frequency within a narrow window where energy degeneracy takes place among eigenfunctions of  $\hat{H}_0 + \hat{V}$ , and adjust the anisotropy (the parameter  $A$  in Eq. (7.4) to obtain the appropriate linear combination. A necessary condition to generate vortices is given by the presence, in the linear combination, of  $L$  states with  $L$  and  $L \pm 2n$  where  $n$  is an integer, as can be inferred from Eq. (7.4). The anisotropic term must be extremely small in such a way that the ground state is extremely similar to the appropriate combination of the degenerated eigenstates of the symmetric Hamiltonian. To be concrete,  $AL/2$  must be larger than the energy differences of the  $L$  states involved in the linear combination, and lower than the gaps to their excited states. The output is quite robust against variations inside these limits. Once the exact vortex ground state is obtained, information about the mostly occupied Fock-Darwin function is also available.

The way to know if there is a "macro-occupied" single particle wave function in the ground state  $|GS\rangle$  is to look at the eigenvalues and eigenvectors of the OBDM [18]. That is to say, one must solve the eigenvalue equation

$$\int d\vec{r}' n^{(1)}(\vec{r}, \vec{r}') \psi_l^*(\vec{r}') = n_l \psi_l^*(\vec{r}), \quad (7.7)$$

where

$$n^{(1)}(\vec{r}, \vec{r}') = \langle GS | \hat{\Psi}^\dagger(\vec{r}) \hat{\Psi}(\vec{r}') | GS \rangle, \quad (7.8)$$

with  $\hat{\Psi} = \sum_{m=0}^{\infty} \varphi_m(\vec{r}) a_m$  being the field operator. If there exist a relevant eigenvalue  $n_1 \gg n_k$  for  $k = 2, 3, \dots, m_0 + 1$ , then

$$\sqrt{n_1} \psi_1(\vec{r}) e^{i\phi_1} \quad (7.9)$$

plays the role of the order parameter of the system, where  $\phi_1$  is an arbitrary constant phase. Here,  $m_0$  is an integer equal to the largest total angular momentum  $L$  involved in the expansion of the ground state on  $L$  eigenfunctions. The order parameter may be expanded in the form  $\psi_1(\vec{r}) = \sum_{m=0}^{m_0} \beta_{1m} \varphi_m(\vec{r})$ , where  $\varphi_m$  are the Fock-Darwin functions. Notice that  $m$  labels the single particle angular momentum from  $m = 0, 1, \dots, m_0$ , whereas  $k = 1, \dots, m_0 + 1$  is a label that distinguishes between the eigenfunctions of the OBDM.

An alternative, and perhaps even more appropriate single particle basis is determined by the functions  $\psi_k(\vec{r})$ . One can define a set of canonical creation and annihilation operators for them:

$$\hat{b}_k^\dagger = \int d\vec{r}' \psi_k^*(\vec{r}') \hat{\Psi}(\vec{r}'), \quad (7.10)$$

and  $\hat{b}_k$  being the hermitian conjugate of  $\hat{b}_k^\dagger$ . The Hilbert space attain then a tensor structure with respect to the modes  $\hat{b}_k$ , and the new Fock (occupation number) many body basis  $|n_1\rangle \otimes |n_2\rangle \otimes \dots$ . The macro-occupied mode contains on average  $n_1$  atoms, but this number fluctuates. This implies that atom number fluctuations between the macro-occupied mode (condensate) and the rest of the modes (that could be regarded as phonon modes, quasi-particles) will tend to reduce the fluctuations of the phase. A natural consequence of this observation is to expect that a very fine approximation of the ground state is given by the coherent state  $|\alpha_1\rangle$ , such that  $\hat{b}_1 |\alpha_1\rangle = \sqrt{n_1} \psi_1 e^{i\phi_1} |\alpha_1\rangle$ . If  $n_k$  for  $k = 2, 3, \dots$  are smaller than  $n_1$  we may neglect them, and approximate the many body wave function by  $|\alpha_1\rangle \otimes |0_2\rangle \otimes |0_3\rangle \otimes \dots$

This representation implies that the next simplifying step would be the representation of ground state by a classical field containing all the involved coherent states  $|\alpha_k\rangle$ ,  $k = 1, \dots, m_0 + 1$  as  $\Psi(\vec{r}) = \sum_{k=1}^{m_0+1} \sqrt{n_k} \psi_k e^{i\phi_k}$  with random phases. Calculation of quantum mechanical averages would then in principle require averaging over random phases, which makes this approach technically difficult.

As long as the exact ground state is a state with well defined angular momentum, (a pure  $L$ -state solution of the Hamiltonian for  $\Omega$  far from the narrow windows where the slight anisotropy has no effect), it is easy to demonstrate that the FD functions are the eigenstates of Eq. 7.7 and the eigenvalues  $n_l$  are the occupations usually used in literature. However, at certain values of  $\Omega$  where degeneracy takes place and vortex states without circular symmetry (except the case of only one centered vortex) are possible [236], the eigenfunctions of Eq. 7.7 are linear combinations of the FD functions and the macro-occupied function  $\psi_1$  that represents the vortex state has expected single particle angular momentum given by  $\hbar\tilde{m} = \int \psi_1^*(\vec{r}) \hat{L} \psi_1(\vec{r}) d\vec{r} = \sum_{m=0}^{m_0} |\beta_{1j}|^2 \hbar m$ .

A convenient definition of the degree of condensation which is sensitive to the loss of macro-occupation reads

$$c = \frac{n_1 - \tilde{n}}{N}, \quad (7.11)$$

where  $N$  is the total number of atoms and  $\tilde{n}$  is the mean occupation calculated without the first value  $n_1$ , that is,  $\frac{1}{m_0} \sum_{k=2}^{m_0+1} n_k$ . Notice that the usual definition given by  $n_1/N$  for  $N \gg 1$  is not appropriate for small systems as the total number of implied states ( $m_0 + 1$ ) is now a small number, and so even in the absence of condensation with all levels equally occupied, such definition implies a condensate fraction of a few percent. Equation 7.7, on the other hand, approaches zero for equal occupations, as one would expect.

## 7.2 Numerical results

### 7.2.1 Order parameter

In what follows, we show some results that confirm the convenience to represent the whole system by  $\psi_1$  at certain values of  $\Omega$ . First of all, we plot in Fig. 7.2 the degree of condensation as a function of  $N$ , for  $L = N$ . Clearly  $c$  approaches 1 rapidly as  $N$  grows and is larger than 80% for 8–9 atoms.

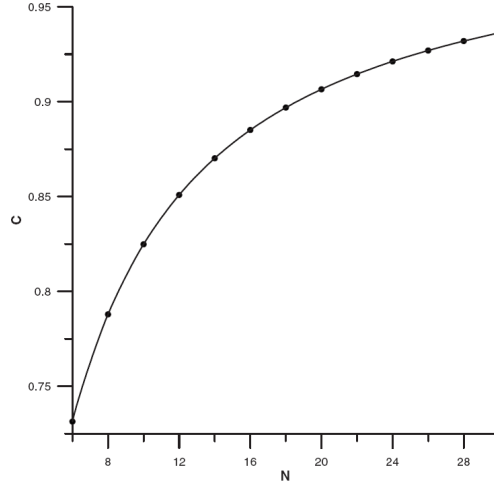


Figure 7.2: Degree of condensation (see Eq. 7.11) as a function of the number of atoms  $Nm$  for the state with  $L = N$ .

As a general result, for vortex states,  $n_1$  is always larger than the occupation of the most important FD state within the exact ground state. In addition,  $\psi_1$  provides a non-ambiguous way to characterize vortices, not only showing dimples in the density profile, but also indicating the position of each one by the change on multiples of  $2\pi$  of the phase  $S(\vec{r})$  in  $\psi_1(\vec{r}) = |\psi_1(\vec{r})| e^{iS(\vec{r})}$  when moving around each vortex.

In Figs. 7.3 and 7.4, for  $N = 6$  atoms, we show for three different values of  $\Omega$ , where degeneracy takes place, the comparison between the contour plots of the density of the exact ground state and the density of  $\psi_1$ , as well as the map of the phase  $S(\vec{r})$  of  $\psi_1$ . In the first case, Fig. 7.4(a), the ground state contains two vortices that appear in a clearer way in the order parameter, as it excludes the non condensed part that smears the structure of the ground state. The same picture is shown in Fig. 7.4(b) where four vortices become visible. In the second case, the map of the phase not only localizes vortices with one unit of quantized circulation, but also indicates that incipient vortices are growing at the edge of the system. In the last case, Fig. 7.4(c), a six-fold symmetry is obtained not attached in this case to vortices, but to a mixed structure of dimples and bumps, a precursor of the Wigner type structure observed for few atoms in the Laughlin state at an angular momentum of  $L = 30$  [236].

The degree of condensation decreases as 0.343, 0.192 and 0.015 from Fig. 7.4(a) to Fig. 7.4(c). The order in vortices and disorder in atoms evolves to order in atoms.

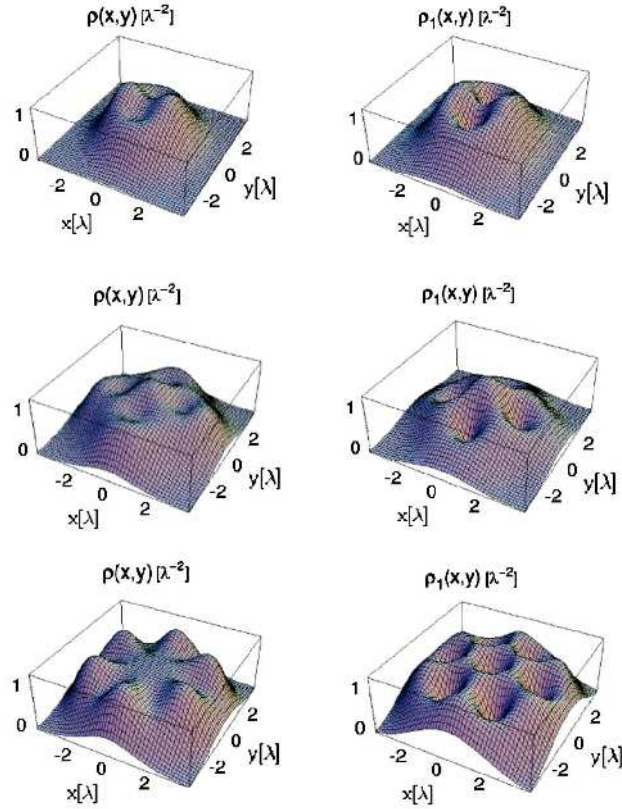


Figure 7.3: For  $N = 6$ , each row shows three dimensional plots of the density of the ground state and the  $\psi_1$  function, respectively. The first row shows a two-vortex structure at  $\Omega/\omega_\perp = 0.941$  (degeneracy between  $L = 10, 12$  and  $14$ ). The second row shows a four-vortex structure,  $\Omega/\omega_\perp = 0.979$  (degeneracy between  $L = 20, 22$  and  $24$ ). The third row shows a sixfold structure,  $\Omega/\omega_\perp = 0.983$  (degeneracy between  $L = 24, 26, 28$  and  $30$ ). In all cases  $\omega_\perp = g = 1$  in units of  $\ell$  and  $\hbar\omega_\perp$ .

To test the validity of the identification of the order parameter with that of a coherent state, we calculated the fluctuations of  $n$  for the cases considered in Fig. 7.3. We obtained  $\Delta n = 2.01, 1.32$  and  $1.25$  in qualitative agreement with the values of  $\sqrt{n}$  (the fluctuations of real coherent states with the same expected occupation) given by  $1.52, 1.15$  and  $0.97$ , respectively. This results suggests even better localization of the phase than for coherent states, and thus justifies the interference calculation of the following section. As  $\Omega$  approaches the frequency of the trap, the occupations tend to equalize and in the Laughlin state, where  $n_l$  are the FD occupations (since it is a pure L-state), and the degree of condensation tends to zero.

### 7.2.2 Interference pattern

Let us now address the issue of the interference pattern produced by the overlap of two initially independent condensates represented by  $\psi_1$  functions. This study is motivated by an increasing amount of recent work revealing the possibility of obtaining very detailed experimental information on the interference pattern produced not only during the overlap of two, or more independent condensates [260, 261, 223, 222], but also within a unique condensate [262].

The idea underlying our assumption is the following: we represent the two independent condensates which we call  $a$  and  $b$  by their macroscopic occupied function  $\psi_a$  and  $\psi_b$  respectively. By this we mean that the condensates are in two unknown coherent states  $|\alpha_a\rangle$  and  $|\alpha_b\rangle$  from which we know their order parameter except for their constant phases  $\phi_a$  and  $\phi_b$  (see Eq.(3)). At time  $t = 0$  s the condensates are separated by a distance  $d$  and the traps are switched off. The time evolution of the system is obtained (once the transformation to the laboratory frame of reference is performed, multiplying the functions by  $\exp(-i\Omega t \hat{L}_z)$ ) in three steps: First, the Fourier transform of the total order parameter (the sum of the two contributions) is performed. Then, the time evolution of the Fourier components by multiplying them by exponentials of the type  $\exp(i\hbar k^2 t/2m)$  is realized; this step is done under the assumption that during the time-of-flight the interactions are irrelevant. Finally, in the third step, inverse Fourier transformation is performed. The results are shown in Fig. 7.5 where three different times are considered. Fortunately, the uncertain about the phase relation  $\phi = \phi_a - \phi_b$  is not important in the case considered, as only two terms are involved and a change on the relative phase would only produce a global shift of the interference pattern.

### 7.2.3 Meaning of a time of flight measurement

We would like to emphasize that systems of small number of particles provide new possibilities not attachable for large systems with thousands of particles, usually used in experiments with rotating BEC. This is the case of a possible test on the meaning of a TOF experiment (see Sec. 5.2). We suggest several possibilities for such experiments. Two types of states could be the appropriate candidates: a pure  $L$  state with a high degree of condensation at relatively low  $\Omega$ , and the Laughlin state at  $\Omega$  close to  $\omega_{\perp}$ . In both cases, the density and the pair-correlation function have different profiles in such a way that the outcome of a TOF experiment would distinguish between the two meanings of measuring.

As an example, we show in Fig. 7.6 the outputs of the Laughlin state for  $N = 5$ . One can consider two different possible ways to realize multiple copies of identical small systems. Arrays of rotating microtraps, or lattices with rotating on-site potential wells could be used in one, two, or three dimensions. Alternatively, a one dimensional lattice rotating around its axis could be employed. Therefore, it is possible to prepare isolated identical states of few atoms such it has already been shown in the previous chapter. However, the multiple copies of the systems coming from each site of the lattice, needed to enhance the signal, could, in principle, destroy the patterns. To preserve the pattern structures present in each site, it is necessary to ensure the same orientation (breaking rotational symmetry) and the same global phase (breaking gauge symmetry) of all copies in the same way. For our first candidate both symmetries must be broken, whereas for our second candidate only the second one is needed. The Laughlin state is a unique number state, linear combination of phase states not phase degenerated. To achieve the observability of the pattern, we suggest the following procedure. On one hand, the presence of a small anisotropy of the trap potential would break rotational symmetry in the same way in each site and, on the other hand, phase correlation could be restored, by embedding the microtraps in a “large” BEC consisting of the same atoms in a different internal state. Such “large” BEC (a reservoir with a fixed global phase) would provide the phase symmetry-breaking mechanism for all “small” BEC if a weak Raman coupling between the “large” and “small” system were used [263, 264]. Namely, the measurement, e.g., of unique Laughlin-like states should reveal the Wigner-like structures (according to the  $n$ -PCF sampling) if measurement means correlation function and not density. We expect this possibility to happen. Other ways of detecting small rotating clouds of atoms have also been discussed in the previous chapter (see Ref. [17]).

As a last comment let us note that even for 5 atoms the density of the Laughlin state (see Fig. 7.6) at the center, given by  $\rho(0) = 0.155$ , is quite close to its analytical value in the thermodynamic limit, given by  $\rho(0) = 1/(2\pi) = 0.159$ , that is to say, apart from non-essential edge effects, the small systems provide a quite good qualitative picture typical of larger systems with the same filling factor (or density). It gives us confidence in our interpretations of stationary states as vortex states, using the same parameters and definitions used for macro systems.

### 7.3 Conclusions

We conclude that, we have demonstrated that the use of the eigenfunctions of the OBDM operator provides a useful and precise tool to analyze the exact ground state obtained from exact diagonalization and specially the vortex states. These eigenfunctions localize and quantize the vortices and reproduce the time evolution of the interference pattern of two overlapping condensates. This offers an alternative interpretation about a subject that has attracted much attention recently related with the interference pattern formation. One possibility suggested by Mullin and collaborators [254] is that the experimental measurement projects the initial condensates in Fock states into phase states, the atom distribution between the two components become uncertain and the pattern formation is possible. The other possibility discussed by Cederbaum *et al.* [265], is that the interference pattern appears if one includes interaction during the time-of-flight even for states that initially are Fock states. In our case, the real initial states are Fock states and no interaction is included during the time-of-flight. However, we assume that the degree of condensation of the initial states is large enough to be properly represented by an order parameter (condensate wave function). Fluctuations of the number of condensed atoms reduce the phase fluctuations and determine the order parameter phase. In effect, exact ground state manifest themselves as phase states even for small number of particles, and in this way the interference pattern is produced. Note, however, that in our picture the process of determination of phase is itself random, and various phases  $\phi_k$  are expected to show up from shot to shot.

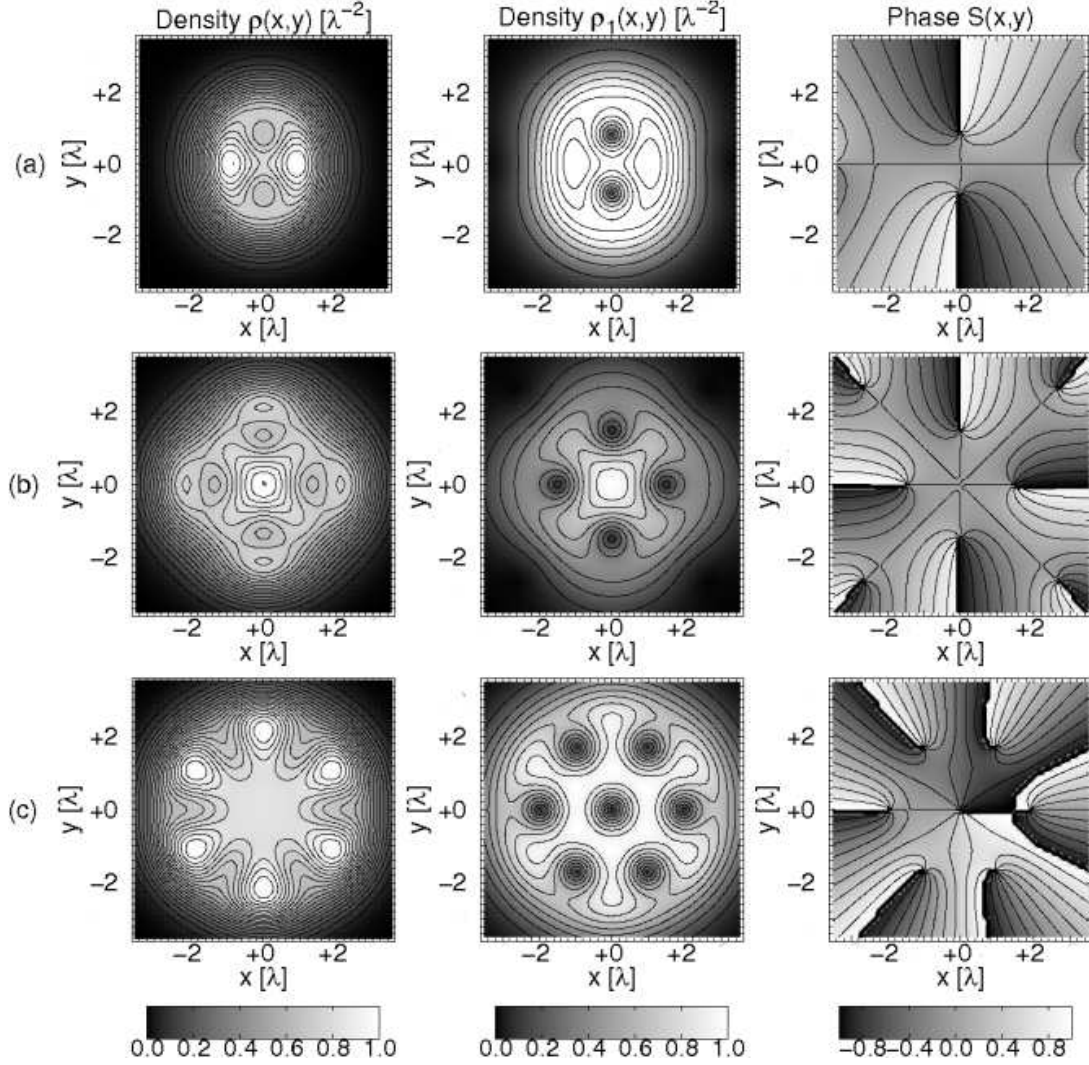


Figure 7.4: For  $N = 6$  the first two pictures on each row show the density contour plot of the ground state ( $\rho(x, y)$ ) and the  $\psi_1$  function ( $\rho_1(x, y)$ ) respectively. The third picture shows the map of the phase  $S(\vec{r})$  (see text). (a) shows a two vortex structure at  $\Omega = 0.941$  (where degeneracy between  $L = 10$  and  $12$  takes place). (b) shows a four vortex structure,  $\Omega = 0.979$  (degeneracy between  $L = 20, 22$  and  $24$ ). (c) shows a six-fold structure,  $\Omega = 0.983$  (degeneracy between  $L = 24, 26, 28$  and  $30$ ). In all cases  $\omega_{\perp} = g = 1$  in units of  $\ell$  and  $u = \hbar\omega_{\perp}$ .

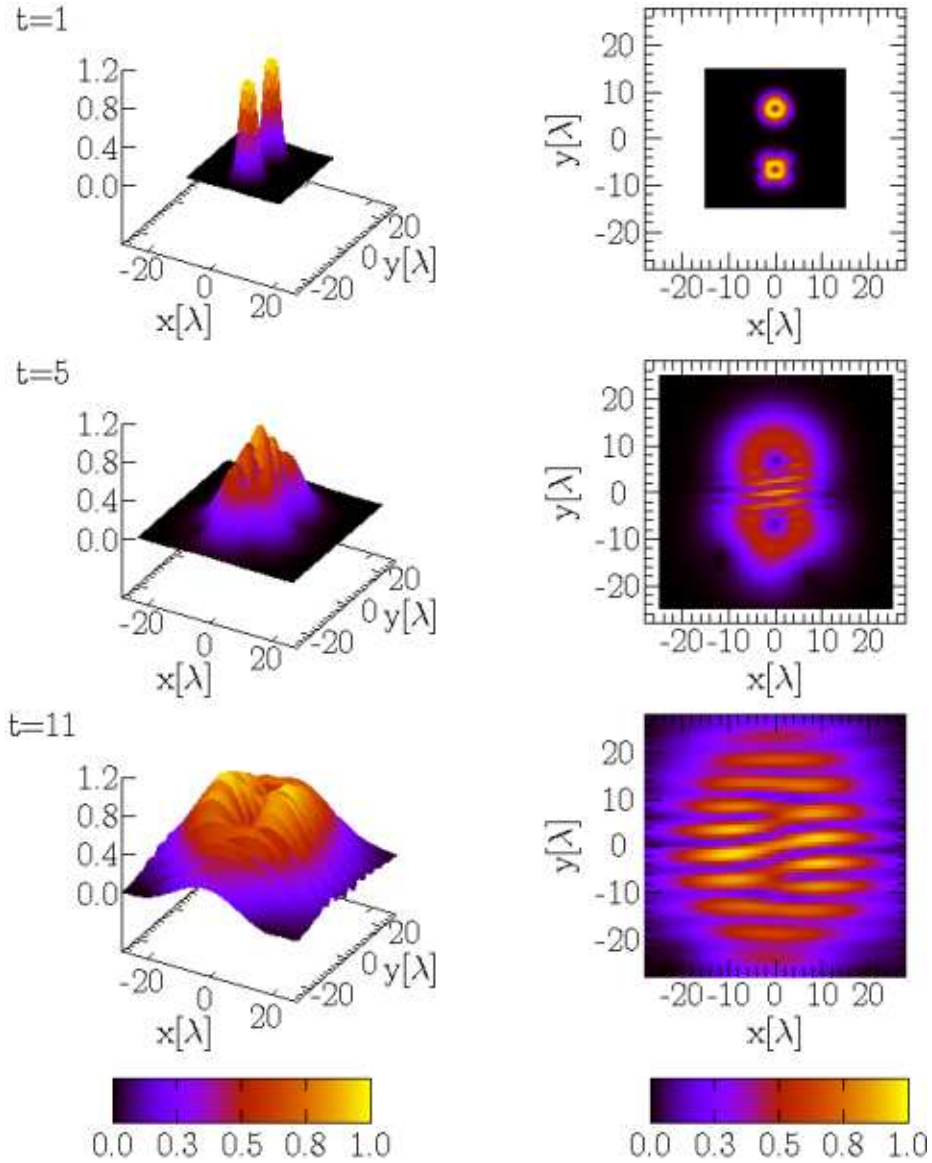


Figure 7.5: Time evolution of the interference pattern during the overlap of two released condensates initially separated by a distance  $d = 15\ell$ . Initially each condensate contains  $N = 6$  atoms and their ground states are characterized by  $L = 6$  at  $\Omega = 0.019$  and by a mixture of  $L = 6, 8$  and  $10$  at  $\Omega = 0.0847$  respectively (all quantities are in units of  $\ell$  and  $u$ ).

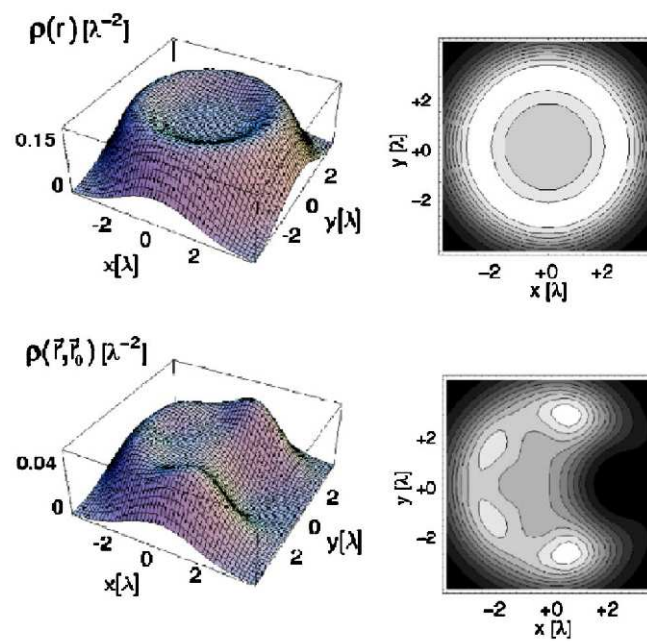


Figure 7.6: For  $N = 5$ , three-dimensional and contour plots of the density and pair correlation function of the Laughlin state ( $L = 20$ ).

---

# Quantum algorithm for the Laughlin state

---

One of the most important goals in the field of quantum computation is to achieve a faithful and efficient simulation of relevant quantum systems. Feynman first suggested [9, 145] the possibility of emulating a quantum system by means of other specially designed and controlled quantum systems. Nowadays, as it has been shown in the previous chapters, ultra-cold atoms in optical lattices are producing the first quantum simulators [15, 16] and many theoretical proposals have been already presented in order to approximately simulate strongly correlated systems [17, 266, 267, 268, 216, 232].

In the present chapter, a more ambitious approach to this issue is presented. It consists in finding the *exact quantum circuit* that underlies the physics of a given quantum system. Rather than searching for an analogical simulation, such an exact quantum circuit would fully reproduce the properties of the system under investigation without any approximation and for any experimental value of the parameters in the theory. It is particularly interesting to devise new quantum algorithms for strongly correlated quantum systems of few particles. These could become the first non-trivial uses of a small size quantum computer. It is worth recalling that strong correlations are tantamount to a large amount of entanglement in the quantum state and this, in

turn, implies that the system is hard to be simulated numerically [1, 143].

An exact quantum circuit would start from a simple product unentangled state and would create faithfully any desired state on demand. That is, such a quantum algorithm would diagonalize the dynamics of the target system. At present, very few cases are under control [269, 270, 149]. In Ref. [149], the underlying quantum circuit that reproduces the physics of the thoroughly studied XY Hamiltonian was obtained. The philosophy inspiring that circuit was to follow the steps of the analytical solution of that integrable model. It is not obvious how to design a quantum simulator for non-integrable systems. Here, we shall present a quantum circuit that allows the controlled construction of a particular case of the Laughlin wave function. Thus, the quantum algorithm we are putting forward will not produce the complete dynamics of a Hamiltonian but rather a specific state. That is, our quantum circuit will transform a trivial product state into a Laughlin state with filling fraction one by means of a finite amount of local two-body quantum gates.

Let us start by recalling the Laughlin [11] wave function for filling fraction  $\nu = 1/m$ , which corresponds to

$$\Psi_L^{(m)}(z_1, \dots, z_n) \sim \prod_{i < j} (z_i - z_j)^m e^{-\sum_{i=1}^n |z_i|^2/2}, \quad (8.1)$$

where  $z_j = x_j + iy_j$ ,  $j = 1, \dots, n$  stands for the position of the  $j$ -th particle. This state was postulated by Laughlin as the ground state of the fractional quantum Hall effect (FQHE) [10]. From the quantum information point of view, the Laughlin state exhibits a considerable von Neumann entropy between for any of its possible partitions [122]. It is, thus, classically hard to simulate such a wave function making it an ideal problem for a quantum computer.

## 8.1 Algorithm design

We shall construct the Laughlin state using a quantum system that consists of a chain of  $n$  qudits ( $d$ -dimensional Hilbert spaces). In our case, that is  $m = 1$ , the dimension of the qudits is needed to be  $d = n$ . Let us proceed to construct the quantum circuit by first considering the case of  $n = 2$  particles, then  $n = 3$  and, finally, the general case.

The Laughlin state can be written in terms of the single particle angular momentum eigenstates, also called Fock-Darwin states  $\varphi_l(z) = \langle z|l\rangle = z^l \exp(-|z|^2/2)/\sqrt{\pi l!}$ .

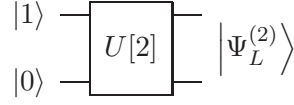


Figure 8.1: Scheme for the quantum circuit that generates the  $n = 2$  Laughlin state by acting on the product state  $|\Psi_0^{(2)}\rangle = |0, 1\rangle$ . Notice that the qubits of the input state are labeled from bottom to top.

Then, the  $n = 2$  Laughlin wave function reads

$$\Psi_L^{(2)}(z_1, z_2) = \frac{1}{\sqrt{2}} (\varphi_0(z_1)\varphi_1(z_2) - \varphi_1(z_1)\varphi_0(z_2)) . \quad (8.2)$$

Let us note that  $\Psi_L^{(2)}(z_1, z_2) = \langle z_1, z_2 | \Psi_L^{(2)} \rangle$  is simply the projection of the Laughlin state

$$|\Psi_L^{(2)}\rangle = \frac{1}{\sqrt{2}} (|0, 1\rangle - |1, 0\rangle) \quad (8.3)$$

in coordinates representation, where particle label is retained in the order of qubits and the angular momentum 0 or 1 is an element of the angular momentum basis. We switch the representation of the state from coordinates to angular momentum since we need a finite basis to simulate the state with a quantum circuit. Observables that depend on the position of the particles need to be written in the new basis in order to be measured at the circuit output.

### 8.1.1 Two particles

It is trivial to find a quantum circuit that transforms a product state into the above  $n = 2$  Laughlin state. Let us first prepare an initial state as  $|\Psi_0^{(2)}\rangle = |0, 1\rangle$  and perform on it the simple two-qubit gate  $U[2]$  as shown in Fig. 8.1. The exact form of the unitary operator  $U[2]$  in the angular momentum basis  $\{|0, 0\rangle, |0, 1\rangle, |1, 0\rangle, |1, 1\rangle\}$  is

$$U[2] = \begin{pmatrix} 1 & 0 & 0 & 0 \\ 0 & \frac{1}{\sqrt{2}} & \frac{1}{\sqrt{2}} & 0 \\ 0 & -\frac{1}{\sqrt{2}} & \frac{1}{\sqrt{2}} & 0 \\ 0 & 0 & 0 & 1 \end{pmatrix} . \quad (8.4)$$

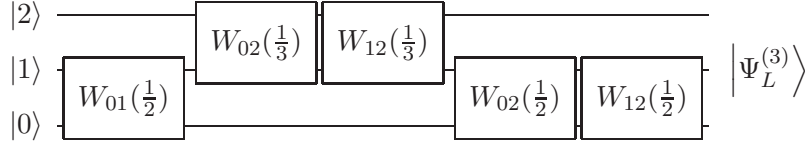


Figure 8.2: Quantum circuit that produces the  $n = 3$  Laughlin state acting on a product state  $|\Psi_0^{(3)}\rangle = |0, 1, 2\rangle$ .

### 8.1.2 Three particles

Let us now move to the more complicated case of the Laughlin state with three particles,  $n = 3$ . We now need to consider a system of three qutrits  $d = n = 3$ . Following similar steps as we did for  $n = 2$ , we take as initial state  $|\Psi_0^{(3)}\rangle = |0, 1, 2\rangle$ , that is, each qutrit is prepared in a different basis element, representing different angular momenta. The aim of the quantum circuit is to antisymmetrize this initial state, since the Laughlin wave function for  $m = 1$  is simply the Slater determinant of the single particle wave functions

$$\langle z_1, z_2, z_3 | \Psi_L^{(3)} \rangle = \frac{1}{\sqrt{6}} \begin{vmatrix} \varphi_0(z_1) & \varphi_0(z_2) & \varphi_0(z_3) \\ \varphi_1(z_1) & \varphi_1(z_2) & \varphi_1(z_3) \\ \varphi_2(z_1) & \varphi_2(z_2) & \varphi_2(z_3) \end{vmatrix}. \quad (8.5)$$

To do this, we define the two-qutrit unitary operators  $W_{ij}(p)$  as

$$\begin{aligned} W_{ij}(p)|ij\rangle &= \sqrt{p}|ij\rangle - \sqrt{1-p}|ji\rangle \\ W_{ij}(p)|ji\rangle &= \sqrt{p}|ji\rangle + \sqrt{1-p}|ij\rangle, \end{aligned} \quad (8.6)$$

for  $i < j$ ,  $0 \leq p \leq 1$ , and  $W_{ij}|kl\rangle = |kl\rangle$  if  $(k, l) \neq (i, j)$ . We realize that for the case of qubits and  $p = 1/2$  we recover the gate  $U[2]$  of Eq. (8.4). Let us note that the unitary operator  $W_{ij}$  is a linear combination of the identity ( $p = 1$ ) and the *simple transposition* ( $p = 0$ ) operators, where a simple transposition is defined as the transposition between two contiguous elements. The architecture of the quantum circuit that produces the  $n = 3$  Laughlin state in Eq. (8.5) by means of the local gates from Eq. (8.6) is presented in Fig. 8.2.

### 8.1.3 General case

So far, we have seen the quantum circuits that produce the Laughlin state for  $n = 2$  and 3. From these cases, a general scheme emerges that will produce the correct

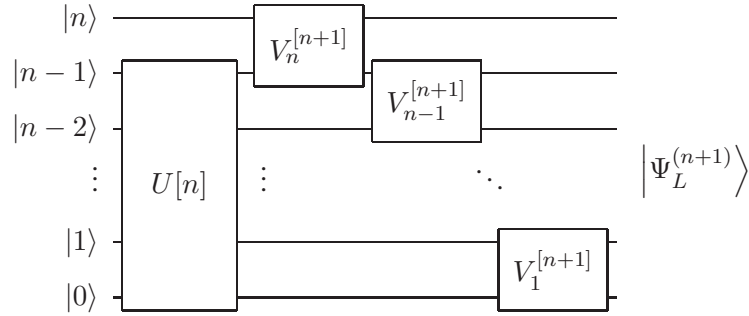


Figure 8.3: Quantum circuit that produces the Laughlin state for an arbitrary number of wires  $(n + 1)$  acting on a product state  $|\Psi_0^{(n)}\rangle = |0, 1, 2, \dots, n\rangle$ . Note its recursive structure,  $U[n + 1] = V_1^{[n+1]}V_2^{[n+1]} \dots V_n^{[n+1]}U[n]$ , where  $V$  gates are defined in Eq. (8.9).

quantum circuit for an arbitrary number of particles. Let us proceed by induction. We will assume that we already know the quantum circuit,  $U[n]$ , that produces the Laughlin state for  $n$  qudits when acting on  $|\Psi_0^{(n)}\rangle = |0, 1, 2, \dots, n - 1\rangle$ . We now need to complete the circuit to achieve the  $n + 1$  Laughlin state from the product state  $|\Psi_0^{(n+1)}\rangle = |0, 1, \dots, n - 1, n\rangle$ .

The Laughlin state for  $n$  qudits has the form

$$|\Psi_L^{(n)}\rangle = \frac{1}{\sqrt{n!}} \sum_{\mathcal{P}} \text{sign}(\mathcal{P}) |a_1, \dots, a_n\rangle, \quad (8.7)$$

where the sum runs over all the possible permutations of the set  $\{0, 1, \dots, n - 1\}$  and, given a permutation,  $a_k$  represents its  $k$ -th element. The relative sign between two permutations corresponds to the parity of the number of transpositions needed to transform one into the other. If we add another qudit, the system is in a product state  $|\Psi_L^{(n)}\rangle |n\rangle$ . According to Eq. (8.7), we want to generate a superposition of  $(n + 1)!$  permutations corresponding to the  $n + 1$  states of the Laughlin wave function, from the superposition of  $n!$  permutations that we already have in the  $n$ -qudit case.

Let us note that, if we have the set of  $n!$  permutations of  $n$  elements, we can generate the set of permutations of  $n + 1$  elements by performing successive simple transpositions between the new element and its preceding neighbour in the sequence  $(\{a_1, \dots, a_n, n\}, \{a_1, \dots, n, a_n\}, \dots, \{n, a_1, \dots, a_n\})$ . This idea suggests a circuit as the one shown in Fig. 8.3. In this scheme, the gate  $V_n^{[n+1]}$  should produce a superposition of all the permutations  $|a_1, \dots, a_n, n\rangle$  with  $|a_1, \dots, n, a_n\rangle$ . The gate  $V_{n-1}^{[n+1]}$  should do the same task in the next site, that is, should produce a superposition between

$|a_1, \dots, a_{n-1}, n, a_n\rangle$  and  $|a_1, \dots, n, a_{n-1}, a_n\rangle$ . This scheme works successively till  $V_1^{[n+1]}$ .

This general structure implies that  $V_n^{[n+1]}$  has to be decomposed in terms of the  $W$ -gates presented previously,

$$V_n^{[n+1]} = W_{0n}(p)W_{1n}(p)\dots W_{n-1n}(p), \quad (8.8)$$

where  $p$  is a common weight due to the fact that the  $0, \dots, n-1$  states in the Laughlin wave function are indistinguishable. Let us note that all the operators  $W_{in}$  in the previous expression commute among themselves and, therefore, the order in which they are applied is irrelevant.

In order to determine the weight  $p$  in the  $V_n^{[n+1]}$  gate, we realize that if all the transpositions only involve the state  $n$ , the states  $|a_1, \dots, a_n, n\rangle$  will not be affected by the rest of gates, and they should already have the correct normalization factor  $\frac{1}{\sqrt{(n+1)!}}$  after applying  $V_n^{[n+1]}$ . This implies  $p = \frac{1}{n+1}$ .

We proceed in a similar way to determine the rest of gates, and we obtain

$$V_k^{[n+1]} = \prod_{i=0}^{n-1} W_{in}, \quad (8.9)$$

where, given a  $k$ , all the  $W$  gates have the same weight  $1/(k+1)$  and  $k = 1 \dots n-1$ . Notice that the  $W_{ij}$  gates act on states with  $i < j$  along the whole circuit and, therefore, they always generate the negative combination  $\sqrt{p}|ij\rangle - \sqrt{1-p}|ji\rangle$ . This is the reason why each term of the final state has the appropriate sign, since a minus sign is carried in each transposition.

The above discussion produces our main result, that is, the circuit shown in Fig. 8.3 that uses the definition of its gates in Eq. (8.9). Such a quantum circuit will generate the  $m = 1$  Laughlin wave function for an arbitrary number of qudits. In particular, the quantum circuit corresponding to 5 qudits is presented in Fig. 8.4.

## 8.2 Circuit analysis

### 8.2.1 Scaling of the number of gates and the depth of the circuit respect to $n$

The recursive structure of the circuit (Fig. 8.3) makes easy to calculate how the number of gates  $N(n)$  and the depth  $D(n)$  of the circuit scale with the total number

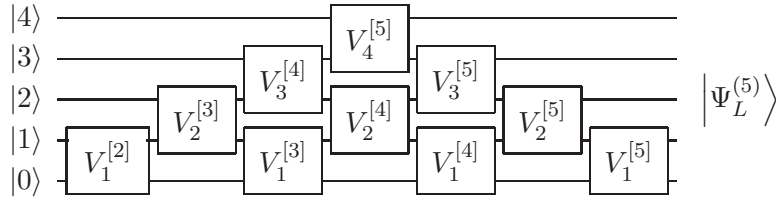


Figure 8.4: Quantum circuit that produces the Laughlin state of 5 particles acting on a product state  $|01234\rangle$ .

of particles  $n$ . An elementary counting gives the result

$$N(n) = (n-1) + N(n-1) = \frac{n(n-1)}{2}$$

$$D(n) = D(n-1) + 2 = 2n - 3, \quad (8.10)$$

with  $N(2) = 1$  and  $D(2) = 1$ . The quantum circuit that delivers the Laughlin state is, thus, efficient since the number of gates scales polynomially. This is a non-trivial result since, in general, an arbitrary unitary transformation acting on  $n$  qudits  $U(d^n)$  requires an exponential number of two-qudit gates  $O(d^{2n-3})$  to be performed [271].

### 8.2.2 Proof that the circuit is minimal

Let us now discuss the optimality of our quantum circuit. As we mentioned before, a simple transposition,  $s_i$ , is defined as the transposition between two contiguous elements,  $i$  and  $i+1$ . Any permutation can be decomposed in terms of a series of simple transpositions and its minimal decomposition is called the *canonical reduced decomposition* (CRD). There are two particular interesting permutations: (i) the minimum permutation  $(0, 1, 2, \dots, n-1)$  whose CRD is the identity, and (ii) the maximum permutation  $(n-1, n-2, \dots, 0)$  whose CRD reads  $s_1(s_2s_1)(s_3s_2s_1)\dots(s_{n-1}\dots s_1)$ , and it is the permutation with the largest number of simple transpositions in its CRD. Then, a circuit that produces the state corresponding to the maximum permutation needs as many gates as the number of simple transpositions of its CRD, that is  $n(n-1)/2$ . The Laughlin state contains this maximum permutation, therefore, its quantum circuit must have, at least,  $n(n-1)/2$  gates, that is precisely the number of gates in our proposal.

### 8.2.3 Entanglement

It is also possible to analyze the way entanglement grows along the circuit. In order to do this, we calculate how much entanglement each gate of the circuit generates, that is, we determine the increase of the von Neumann entropy between the two parts of the system separated by a given gate,

$$\Delta S(V_k^{[n]}) = \log_2 \left( \frac{n}{n-k} \right). \quad (8.11)$$

The von Neumann entropy between  $k$  particles and the rest of the system is simply the sum of the contributions of those gates that are in the row which separates the system in  $k$  and  $n-k$  wires. These gates are  $V_k^{[n']}$  for  $k+1 \leq n' \leq n$  and the entanglement entropy reads

$$S_{n,k} = \sum_{n'=k+1}^n \Delta S(V_k^{[n']}) = \log_2 \binom{n}{k}. \quad (8.12)$$

This expression recovers in a clean way the same result as the one found in Ref. [122], which was proven exact. Let us also remark that although each single particle is maximally entangled with the rest of the system, a subset of  $k \leq n/2$  particles does not saturate the entropy,

$$S_{n,k} \leq k \log_2 n. \quad (8.13)$$

## 8.3 Experimental realization

A experimental realization of our proposal will probably need to work on qubits rather than qudits. It is, then, necessary to find an efficient reduction of our algorithm to qubits. The easiest way to encode a qudit in terms of qubits is the binary basis. Then, an arbitrary single state  $|i\rangle$  can be decomposed as

$$|i\rangle = |i_r\rangle \dots |i_2\rangle |i_1\rangle, \quad (8.14)$$

where  $i = \sum_{k=1}^r 2^{k-1} i_k$ ,  $r \sim \log_2 n$  is the number of bits needed to represent  $n$ , and  $i_k = 0, 1 \forall k = 1, \dots, r$ .

Now, we want to find the gates that acting on these qubits implement the  $W$  gates.  $W_{ij}$  acts non trivially on the space spanned by the computational basis states  $|ij\rangle \equiv |i_r, \dots, i_1, j_r, \dots, j_1\rangle$  and  $|ji\rangle \equiv |j_r, \dots, j_1, i_r, \dots, i_1\rangle$ , and is the identity for the rest of states. Let us define  $\tilde{W}$  as the non trivial  $2 \times 2$  sub matrix of  $W$  that acts on

this subspace. According to Eq. (8.6),  $\tilde{W}$  takes the form

$$\tilde{W} \equiv \begin{pmatrix} \sqrt{p} & \sqrt{1-p} \\ -\sqrt{1-p} & \sqrt{p} \end{pmatrix}, \quad (8.15)$$

and it corresponds to the exponentiation  $\tilde{W} = \exp(i\theta\sigma_y)$  of the  $\sigma_y$  Pauli matrix for  $p = \cos^2(\theta/2)$ . In order to implement an arbitrary  $W_{ij}$  gate, we have to follow three steps: (i) first, we compare the binary expressions of  $i_r \dots i_1 j_r \dots j_1$  and  $j_r \dots j_1 i_r \dots i_1$ , and notice which bits are different. Then, we carry out a sequence of binary numbers, starting with  $ij$  and concluding with  $ji$ , such that adjacent members of the list differ in only one bit. These sequences are called *Gray codes* [145]. (ii) Next, we implement a quantum circuit performing a series of multi-qubit controlled gates that change the state  $ij$  according to the previous sequence. Each multi-qubit gate transforms the corresponding state of the sequence into the next one. These multi-qubits gates are carried out until it only remains a different bit between the last transformed state and  $ji$ . (iii) At this point, we perform a controlled- $\tilde{W}$  gate, or alternatively its complex conjugate  $\tilde{W}^\dagger$ , taking this different qubit as target. We will apply  $\tilde{W}$  or  $\tilde{W}^\dagger$  depending on the initial state in which the single gate is performed. Finally, the reversed previous sequence of multi-qubit controlled gates is performed.

This abstract construction can be illustrated with the example of the  $W_{35}$  gate that acts non-trivially on the states  $|011\ 101\rangle$  and  $|101\ 011\rangle$ . One possible sequence of Gray codes that connect  $011\ 101$  and  $101\ 011$  is

$$\begin{array}{cccc} 0 & 1 & 1 & 1 & 0 & 1 \\ 1 & 1 & 1 & 1 & 0 & 1 \\ 1 & 0 & 1 & 1 & 0 & 1 \\ 1 & 0 & 1 & 0 & 0 & 1 \\ 1 & 0 & 1 & 0 & 1 & 1. \end{array} \quad (8.16)$$

From this, we can read its corresponding circuit, shown in Fig. 8.5. Notice that the first three multi-qubit controlled gates transforms  $|011\ 101\rangle$  into  $|101\ 001\rangle$ . Next, the  $\tilde{W}$  gate is applied to the fifth qubit, affecting only the states  $|101\ 001\rangle$  and  $|101\ 011\rangle$  due to the conditions on rest of qubits. Finally, we reverse the application of the multi-qubit controlled gates, ensuring that  $|101\ 001\rangle$  gets swapped back with  $|011\ 101\rangle$ . It is important to point out that these multi-qubit controlled gates are not two-qubit gates, as, in principle, it would be suited. Nevertheless, it is known that these controlled operations can be performed by means of  $O(r)$  single qubit and CNOT gates [272,

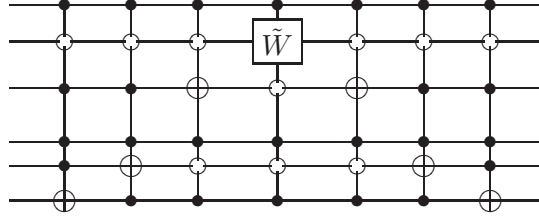


Figure 8.5: Implementation of the  $W_{35}$  gate in terms of multi-qubit control gates. Each of these controlled operations can be decomposed in single qubit and CNOT gates.

273] which can be implemented experimentally [274, 275]. Thus, if we consider that the number of  $W$ -gates that we have to perform to implement our proposal for  $n$  qudits is  $n(n-1)(2n-1)/6$ , the number of single qubit and CNOT gates required by our circuit scales as  $O(n^3(\log_2 n)^2)$ . In particular, for  $n=2$ , only 4 single and 2 CNOT gates are required to construct the Laughlin state. These gates can be performed experimentally in an ion trap by means of a sequence of 16 laser pulses. In the case of  $n=3$ , the circuit requires a total of 6 qubits and the action of 72 Toffoli gates, 18 CNOT gates and 20 single gates, which amounts to 1208 laser pulses using present technology. It seems likely that in a near future a quantum circuit for the  $n=3$  state might be experimentally feasible.

There is a second way of encoding a qudit in the state  $|i\rangle$ , that is, take  $n$  qubits, set the  $i$ -th one to  $|1\rangle$ , and then the rest to  $|0\rangle$ , *i. e.*  $|i\rangle = |0\dots 010\dots 0\rangle$ . Although this unary encoding requires  $n$  qubits, it has the advantage that allows us to implement the  $W$ -gates using  $O(n^3)$  gates. This unary encoding requires  $n$  qubits compared to the  $\log_2 n$  required before. Nevertheless, it has the advantage that allows us to implement the  $W$ -gates using  $O(n^3)$  gates.

Moreover, let us note that we can transform our antisymmetrization circuit into a symmetrization one by just changing the signs of the definition of the  $W$  gates in Eq. (8.6), *i.e.*  $\sqrt{p}|ij\rangle \mp \sqrt{1-p}|ji\rangle \rightarrow \sqrt{p}|ij\rangle \pm \sqrt{1-p}|ji\rangle$ . Another possibility of performing the same symmetrization would be to invert the order of the input state of the circuit ( $|n-1, \dots, 0\rangle$  instead of  $|0, \dots, n-1\rangle$ ) and to apply the gates  $W_{n-1-i, n-1-j}$ , instead of  $W_{ij}$ , along the circuit. In both cases,  $W$  gates always act in the positive combination and the final state obtained is fully symmetric in all permutations. This is the so-called “permanent” state and it is a universal state for quantum computation [276].

## 8.4 Conclusions

We have designed a quantum algorithm that creates the Laughlin state for an arbitrary number of particles  $n$  in the case of filling fraction one. Our proposal is efficient since it only uses  $n(n - 1)/2$  local qudit gates and its depth scales as  $2n - 3$ .

Moreover, the presented circuit can be used both to symmetrize and anti-symmetrize any product state. It has been also proven the optimality of the proposal using permutation theory arguments and studied how entanglement develops along the action of each gate. We have also shown its experimental feasibility decomposing the qudits and the gates in terms of qubits and two qubit-gates.

Finally, let us conclude with some comments on the generalization of our proposal to other values of  $m$ . The first observation is that, if  $m > 1$ , the number of states that appear in the superposition of the Laughlin wave function is much larger than the simple permutations of the input single states. The corresponding quantum circuit, therefore, cannot be only composed of  $W$ -gates. This will increase a lot the degrees of freedom of our elementary gates and, thus, its complexity. Though specific examples for low values of  $n$  and  $m$  can be found, a general scheme is still missing.



---

# Conclusions and outlook

---

In this thesis, we have addressed the simulation of Quantum Mechanics. We have used tools both from Quantum Information and from Condensed Matter Physics. In the first part, we have studied entanglement in many body quantum systems and analyzed which features of those systems can be simulated in a classical computer. It has been shown that any state that verifies the area-law for the entanglement entropy can be efficiently represented using tensor networks.

Nevertheless, an issue that it is not clear is which features a Hamiltonian must have so that its ground state fulfills area-law. On one hand, the situation is well understood for translationally invariant systems. If such a system has local interactions and is gapped, an area-law always emerges. If the system is at the critical point, and therefore gapless, entanglement entropy scales logarithmically. On the other hand, what happens with the non-translationally invariant systems is not clear yet. In fact, in Chapter 4, we have presented a simple XX spin chain with the appropriate fine tuning of the coupling constants that verifies a volume law for the entanglement entropy. A future direction of our work could be to study the necessary and sufficient conditions for having an area-law.

Another important conclusion of the first part of the thesis is that Quantum Information has provided a series of new tools to study Condensed Matter systems. Indeed, in Chapter 2, we see how the scaling of the entanglement entropy is com-

pletely connected with the criticality of the system and, therefore, with its correlation length. With this respect, we think that it would be interesting to study the connections between multi-partite entanglement and many body quantum systems. The main obstruction to do this is that a satisfactory definition of a multi-partite entanglement measure has not been found yet. With the aim of finding a measure of multi-partite entanglement, we have already started to study maximally entangled states in multipartite systems. Another interesting future work would be to study the scaling of entanglement and the simulation by tensor network techniques of strongly correlated systems like the Bose Hubbard model or a discretized version of the Fractional Quantum Hall Effect.

In the second part of the thesis, we have addressed the problem of simulating quantum many body systems using other well controlled quantum systems. We have seen that, due to the good experimental control, cold atoms are hot candidates to implement this kind of simulation. Hence, in Chapter 6, we have improved a proposal of generating a Mott state of Laughlin wave functions in an optical lattice. The current control on this kind of systems already allows the implementation of theoretical proposals. In this context, we think that the tensor networks mentioned before can be a very good tool in order to provide theoretical proposals of quantum simulators.

In Chapter 7, structures of vortex that appear in a rotating cloud of few atoms have been described by means of an order parameter. It is interesting to point out that by changing the rotation frequency of the trap, the structure of the ground state changes dramatically: from an order parameter (single particle wave function that describes perfectly the whole system) to the Laughlin state, *i. e.*, a strongly correlated state that cannot be described with less parameters. An interesting question that we would like to study in detail is how this transition takes place and, in particular, how entanglement evolves in this transition.

Finally, in the previous chapter, we have proposed a quantum circuit that produces the Laughlin state for filling fraction equal to one. We have shown that this may be one of the first applications of the quantum computer prototypes. Although, in this case, we have been able to find an efficient proposal, the number of single qubit gates and C-NOTs that must be performed in order to simulate a system of few particles is large. This will make the experimental realization of this kind of simulations difficult in a near future.

The interplay between Quantum Information and Condensed Matter physics will continue to be a fruitful field during the next years. On one hand, tensor networks will

be an excellent tool to develop theoretical proposals of strongly correlated systems of few particles. On the other hand, the current experimental control in ultra-cold atoms will allow us to see and to study some Condensed Matter phenomena that had been inaccessible until now.



# Contribution to the entanglement entropy and the single copy entanglement of large angular momenta modes

---

## A.1 Perturbation theory

We need to perform a perturbative computation for large momenta in order to determine the contribution to the total entropy and single copy entanglement of all angular momentum modes.

We organize our computation in three parts. In the first part, we carry out perturbation theory with matrices, following the same steps as explained in sec. (3.2.2) when considering the approximation  $l \gg N$ . This will produce an analytical expression for the  $\xi$ 's parameters. The second part of the computation consists in Taylor expanding the above results for  $\xi$  in a series in  $l^{-1}$ . Finally, we will get the entropy and single copy entanglement contributions, expanding the entropy and single copy modes in terms of  $l^{-1}$  powers, and summing over  $l$ . In this sum  $l$  take values from  $l_0$  until infinity, where  $l_0$  must be sufficiently large, such that all approximations done

previously are right.

### A.1.1 Computation of the $\xi$ parameter

Let us recall that, for  $l \gg N$ , the non diagonal elements of  $K$  in Eq. (3.20) are much smaller than the diagonal ones. That gives us the possibility of setting up a perturbative computation.

We split up the  $K$  matrix in a diagonal  $K_0$  and non diagonal  $\lambda\eta$ , matrices where  $\lambda$  is just introduced to account for the order in a perturbative expansion of the non-diagonal piece,

$$K = K_0 + \lambda\eta . \tag{A.1}$$

We will follow the steps described in Sec.3.2.2. We expand  $\Omega \equiv \sqrt{K}$  in its different contributions to order  $\lambda$ ,

$$\Omega = \Omega_0 + \lambda\epsilon + \lambda^2\tilde{\epsilon} + \lambda^3\hat{\epsilon} + O(\lambda^4) . \tag{A.2}$$

To get each term we impose the condition  $\Omega^2 = K$ ,

$$\begin{aligned} (\Omega_0)_{ij} &= \Omega_i \delta_{ij} \\ (\epsilon)_{ij} &= \epsilon_i \delta_{i+1,j} + \epsilon_j \delta_{j+1,i} \\ (\tilde{\epsilon})_{ij} &= \frac{\epsilon_i^2 + \epsilon_{i-1}^2}{\Omega_i + \Omega_j} \delta_{ij} + \frac{\epsilon_i \epsilon_{j-1}}{\Omega_i + \Omega_j} \delta_{i+2,j} \\ &\quad + \frac{\epsilon_j \epsilon_{i-1}}{\Omega_i + \Omega_j} \delta_{i,j+2} \\ (\hat{\epsilon})_{ij} &= \frac{(\epsilon\tilde{\epsilon} + \tilde{\epsilon}\epsilon)_{ij}}{\Omega_i + \Omega_j} . \end{aligned} \tag{A.3}$$

where  $\Omega_j$  and  $\epsilon_j$  are defined since

$$\begin{aligned} \Omega_j &\equiv \sqrt{\frac{l(l+D-2)}{j^2} + \omega_j} , \\ \omega_j &\equiv \left(1 + \frac{1}{2j}\right)^{D-1} + \left(1 - \frac{1}{2j}\right)^{D-1} + \mu^2 , \\ \epsilon_j &\equiv -\frac{j + \frac{1}{2}}{\sqrt{j(j+1)}} \frac{1}{\Omega_j + \Omega_{j+1}} . \end{aligned} \tag{A.4}$$

We structure  $\Omega$  in three matrices  $A$ ,  $B$  and  $C$ ,

$$\begin{aligned} A &\equiv \Omega(1 \div n, 1 \div n) = A_0 + \lambda A_1 + \lambda^2 A_2 + O(\lambda^3) \\ B &\equiv \Omega(1 \div n, n + 1 \div N) = \\ &= \lambda B_0 + \lambda^2 B_1 + \lambda^3 B_2 + O(\lambda^4) \\ C &\equiv \Omega(n + 1 \div N, n + 1 \div N) = \\ &= C_0 + \lambda C_1 + \lambda^2 C_2 + O(\lambda^3). \end{aligned} \quad (\text{A.5})$$

From these matrices, we define  $\beta$  and  $\gamma$  which we write in series of  $\lambda$

$$\begin{aligned} \beta &\equiv \frac{1}{2} B^T A^{-1} B = \lambda^2 \beta_0 + \lambda^3 \beta_1 + \lambda^4 \beta_2 + O(\lambda^4) \\ \gamma &\equiv C - \beta = \Omega_0 + \lambda \epsilon + O(\lambda^2), \end{aligned} \quad (\text{A.6})$$

where,

$$\begin{aligned} \beta_0 &= \frac{1}{2} B_0^T A_0^{-1} B_0 = \frac{\epsilon_n^2}{2\Omega_n} \delta_{i,1} \delta_{j,1} \\ \beta_1 &= \frac{1}{2} (B_1^T A_0^{-1} B_0 + B_0^T A_0^{-1} B_1 + B_0^T A_1^{-1} B_0) = -\frac{\epsilon_n^2}{2\Omega_n} \frac{\epsilon_{n+1}}{\Omega_n + \Omega_{n+2}} (\delta_{i,2} \delta_{j,1} + \delta_{i,1} \delta_{j,2}) \\ \beta_2 &= \frac{1}{2} (B_2^T A_0^{-1} B_0 + B_0^T A_0^{-1} B_2 + B_0^T A_2^{-1} B_0 + B_1^T A_0^{-1} B_1 + B_1^T A_1^{-1} B_0 + B_0^T A_1^{-1} B_1). \end{aligned} \quad (\text{A.7})$$

We shall see later, that at  $2n$  order perturbation in  $\lambda$ , only  $(\beta_2)_{11}$  and  $(\beta_2)_{22}$  of  $\beta_2$  are necessary. Then,

$$\begin{aligned} (\beta_2)_{11} &= \frac{\epsilon_n^2}{2\Omega_n} \left\{ \frac{\epsilon_{n-1}^2}{\Omega_n \Omega_{n-1}} + \frac{\epsilon_{n-1}^2 + \epsilon_n^2}{2\Omega_n^2} + \frac{\Omega_n}{\Omega_{n-1}} \frac{\epsilon_{n-1}^2}{(\Omega_{n+1} + \Omega_{n-1})^2} + \frac{2\epsilon_{n-1}^2}{\Omega_{n-1}(\Omega_{n+1} + \Omega_{n-1})} \right. \\ &\quad \left. + \frac{2}{\Omega_n(\Omega_n + \Omega_{n+1})} \left( \frac{\epsilon_{n+1}^2}{\Omega_n + \Omega_{n+2}} \frac{\epsilon_{n+1}^2 + \epsilon_n^2}{2\Omega_{n+1}} + \frac{\epsilon_n^2 + \epsilon_{n-1}^2}{2\Omega_n} + \frac{\epsilon_{n-1}^2}{\Omega_{n+1} + \Omega_{n-1}} \right) \right\} \\ (\beta_2)_{22} &= \frac{\epsilon_n^2}{2\Omega_n} \frac{\epsilon_{n+1}^2}{(\Omega_n + \Omega_{n+2})^2}. \end{aligned} \quad (\text{A.8})$$

Let us diagonalize  $\gamma$ ,

$$\gamma_D = V \gamma V^T, \quad (\text{A.9})$$

where  $V$  is an orthogonal matrix ( $VV^T = \mathbb{1}$ ). Therefore, the eigenvalues are

$$\begin{aligned} \det(\gamma - w\mathbb{1}) &= \prod_{i=1}^{N-n} (\Omega_{n+i} - w) + O(\lambda^2) = 0 \\ &\Rightarrow w_i = \Omega_{n+i} + O(\lambda^2), \end{aligned} \quad (\text{A.10})$$

and

$$(\gamma_D)_{ij} = (\Omega_{n+i} + O(\lambda^2))\delta_{ij}. \quad (\text{A.11})$$

If we impose (A.9) over  $V = V_0 + \lambda V_1 + \lambda^2 V_2 + O(\lambda^3)$ , we obtain,

$$\begin{aligned} V_0 &= \mathbb{1} \\ (V_1)_{ij} &= \frac{\epsilon_{n+i}}{\Omega_{n+i} - \Omega_{n+j}} \delta_{i+1,j} + \frac{\epsilon_{n+j}}{\Omega_{n+j} - \Omega_{n+i}} \delta_{i,j+1} \\ (V_2)_{11} &= \frac{1}{2} \left( \frac{\epsilon_{n+1}}{\Omega_{n+1} - \Omega_{n+2}} \right)^2. \end{aligned} \quad (\text{A.12})$$

Once we have  $V$  and  $\gamma_D$  we are able to compute  $\beta' = \lambda^2(\beta'_0 + \lambda\beta'_1 + \lambda^2\beta'_2 + O(\lambda^3))$ , which is defined by,

$$\beta' \equiv \gamma_D^{-\frac{1}{2}} V \beta V^T \gamma_D^{-\frac{1}{2}}. \quad (\text{A.13})$$

Thus,

$$\begin{aligned} \beta'_0 &= (\gamma_D^{-\frac{1}{2}})_0 \beta_0 (\gamma_D^{-\frac{1}{2}})_0 \\ \beta'_1 &= (\gamma_D^{-\frac{1}{2}})_0 \left[ \beta_1 + V_0 \beta_1 + \beta_1 V_0^T + V_1 \beta_0 + \beta_0 V_1^T \right] (\gamma_D^{-\frac{1}{2}})_0 \\ \beta'_2 &= (\gamma_D^{-\frac{1}{2}})_2 \beta_0 (\gamma_D^{-\frac{1}{2}})_0 + (\gamma_D^{-\frac{1}{2}})_0 \beta_0 (\gamma_D^{-\frac{1}{2}})_2 + (\gamma_D^{-\frac{1}{2}})_0 \left[ \beta_2 + V_1 \beta_1 + \beta_1 V_1^T + V_2 \beta_0 + \beta_0 V_2^T \right. \\ &\quad \left. + V_1 \beta_0 V_1^T \right] (\gamma_D^{-\frac{1}{2}})_0 \end{aligned} \quad (\text{A.14})$$

and therefore,

$$\begin{aligned} (\beta'_0)_{ij} &= \frac{\epsilon_n^2}{2\Omega_{n+1}\Omega_n} \delta_{i,1} \delta_{j,1} \\ (\beta'_1)_{ij} &= \frac{\epsilon_n^2}{2\Omega_{n+1}\Omega_n} \sqrt{\frac{\Omega_{n+1}}{\Omega_{n+2}}} \epsilon_{n+1} \left( \frac{1}{\Omega_{n+1} - \Omega_{n+2}} + \frac{1}{\Omega_n + \Omega_{n+2}} \right) (\delta_{i,1} \delta_{j,2} + \delta_{i,2} \delta_{j,1}) \\ (\beta'_2)_{11} &= \frac{(\beta_2)_{11}}{\Omega_{n+1}} - \frac{\epsilon_n^2}{2\Omega_n \Omega_{n+1}} \frac{\epsilon_{n+1}^2}{(\Omega_n - \Omega_{n-1})^2} \\ &\quad - \frac{\epsilon_n^2}{2\Omega_n \Omega_{n+1}} \left( \frac{2\epsilon_{n+1}^2}{(\Omega_{n+2} + \Omega_n)(\Omega_{n+1} - \Omega_{n+2})} - \frac{1}{2\Omega_{n+1}^2} \left( \epsilon_{n+1}^2 \frac{\Omega_{n+1} + \Omega_{n+2}}{\Omega_{n+1} - \Omega_{n+2}} - \epsilon_n^2 \frac{\Omega_n + \Omega_{n+1}}{\Omega_n} \right) \right) \\ (\beta'_2)_{22} &= \frac{\epsilon_n^2 \epsilon_{n+1}^2}{2\Omega_{n+2} \Omega_n} \left( \frac{1}{\Omega_{n+1} - \Omega_{n+2}} + \frac{1}{\Omega_n + \Omega_{n+2}} \right)^2. \end{aligned} \quad (\text{A.15})$$

It will be useful to write  $\beta'$  in its matrix form,

$$\beta' = \lambda^2 \begin{pmatrix} a_n + \lambda^2 c_n & \lambda d_n & 0 & \dots \\ \lambda d_n & \lambda^2 e_n & 0 & \dots \\ 0 & 0 & 0 & \dots \\ \vdots & \vdots & \vdots & \ddots \end{pmatrix} + O(\lambda^5), \quad (\text{A.16})$$

where,

$$\begin{aligned} a_n &\equiv \frac{\epsilon_n^2}{2\Omega_{n+1}\Omega_n} \\ d_n &\equiv a_n \sqrt{\frac{\Omega_{n+1}}{\Omega_{n+2}}} \epsilon_{n+1} \left( \frac{1}{\Omega_{n+1} - \Omega_{n+2}} + \frac{1}{\Omega_n + \Omega_{n+2}} \right) \end{aligned} \quad (\text{A.17})$$

and  $c_n$  and  $e_n$  are respectively  $(\beta'_2)_{11}$  and  $(\beta'_2)_{22}$ . We can observe now, that if we had not found the second order contribution of  $(\beta')_{11}$  and  $(\beta')_{22}$ , we would not have been able to compute the eigenvalues of  $\beta'$  to this order.

Diagonalizing  $\beta'$ , we find the eigenvalues  $v_1$  and  $v_2$ ,

$$\begin{aligned} v_1 &= \lambda^2 \left( a_n + \lambda^2 \left( c_n + \frac{d^2}{a_n} \right) + O(\lambda^3) \right) \\ v_2 &= \lambda^4 \left( e_n - \frac{d_n^2}{a_n} \right) + O(\lambda^5) = 0 + O(\lambda^5), \end{aligned} \quad (\text{A.18})$$

which allows us to compute the  $\xi_i$ 's parameters,

$$\xi_i = \frac{v_i}{1 + \sqrt{1 - v_i^2}}, \quad (\text{A.19})$$

and which read

$$\begin{aligned} \xi_1 &= \frac{\lambda^2}{2} \left( a_n + \lambda^2 \left( c_n + \frac{d^2}{a_n} \right) + O(\lambda^3) \right) \\ \xi_2 &= 0 + O(\lambda^5) \\ \xi_i &= O(\lambda^7) \quad \forall i > 2. \end{aligned} \quad (\text{A.20})$$

### A.1.2 Expansion of $\xi$ in terms of $l^{-1}$ powers

We rename  $\xi_1$  as  $\xi$ , and neglect the rest since at this order they are 0 and no contribute neither to the entropy nor to the single copy entanglement. We are interested in expanding  $\xi$  in powers of  $l^{-1}$ . To do this, we have to expand first  $\Omega_j$  and  $\epsilon_j$ ,

$$\Omega_n = l \sum_{i=0}^9 \frac{\Omega_n^{(i)}}{l^i} + O(l^{-9}), \quad (\text{A.21})$$

where,

$$\begin{aligned}
 \Omega_n^{(0)} &= \frac{1}{n} \\
 \Omega_n^{(1)} &= \frac{D-2}{2n} \\
 \Omega_n^{(2)} &= \frac{n\omega_n}{2} + \frac{(D-2)^2}{8n} \\
 \Omega_n^{(3)} &= \frac{(D-2)^3 - 4(D-2)n^2\omega_n}{16n} \\
 \Omega_n^{(4)} &= -\frac{5(D-2)^4 - 24(D-2)^2n^2\omega_n + 16n^4\omega_n^2}{128n} \\
 \Omega_n^{(5)} &= \frac{7(D-2)^5}{256n} + \frac{-40(D-2)^2n^2\omega_n + 48n^4\omega_n^2}{256n} \\
 &\vdots \quad .
 \end{aligned} \tag{A.22}$$

No more coefficients have been presented here since they have huge expressions and they don't shed any light on our arguments. Using  $\Omega_n$  we can obtain the expansion of  $\epsilon_n$ ,

$$\epsilon_n = \frac{1}{l} \sum_{i=0}^6 \frac{\epsilon_n^{(i)}}{l^i} + O(l^{-8}), \tag{A.23}$$

where,

$$\begin{aligned}
 \epsilon_n^{(0)} &= \frac{(\eta)_{n,n+1}}{\Omega_n^{(0)} + \Omega_{n+1}^{(0)}} \\
 \epsilon_n^{(1)} &= -\epsilon_n^{(0)} \frac{\Omega_n^{(1)} + \Omega_{n+1}^{(1)}}{\Omega_n^{(0)} + \Omega_{n+1}^{(0)}} \\
 \epsilon_n^{(2)} &= \epsilon_n^{(0)} \left( \left( \frac{\Omega_n^{(1)} + \Omega_{n+1}^{(1)}}{\Omega_n^{(0)} + \Omega_{n+1}^{(0)}} \right)^2 - \frac{\Omega_n^{(2)} + \Omega_{n+1}^{(2)}}{\Omega_n^{(0)} + \Omega_{n+1}^{(0)}} \right) \\
 &\vdots \quad .
 \end{aligned} \tag{A.24}$$

Once we have  $\Omega_n$  and  $\epsilon_n$  in series of  $l^{-1}$ , we can expand  $\xi$ ,

$$\xi = \frac{1}{l^4} \sum_{i=0}^6 \frac{\xi_i}{l^i} + O(l^{-10}), \tag{A.25}$$

with

$$\begin{aligned}\xi_0 &= \frac{(\epsilon_n^{(0)})^2}{4\Omega_n^{(0)} + \Omega_{n+1}^{(0)}} \\ \xi_1 &= \epsilon_n^{(0)} \frac{2\epsilon_n^{(1)}\Omega_n^{(0)}\Omega_{n+1}^{(0)} - \epsilon_n^{(0)}(\Omega_n^{(1)}\Omega_{n+1}^{(0)} + \Omega_n^{(0)}\Omega_{n+1}^{(1)})}{4((\Omega_n^{(0)})^2 + (\Omega_{n+1}^{(0)})^2)} \\ &\vdots\end{aligned}\tag{A.26}$$

Although  $\xi$  depends on the number of oscillators which we trace out, we have omitted the subindex  $n$  to simplify the notation.

### A.1.3 The entropy

The contribution to the entropy of a  $(l, \{m\})$ -mode becomes,

$$S_{l\{m\}} = -\log(1 - \xi_l) - \frac{\xi_l}{1 - \xi} \log \xi_l \simeq \sum_{k=1}^{\infty} \left( \frac{1}{k} - \log(\xi) \right) \xi^k.\tag{A.27}$$

If we substitute  $\xi$ ,

$$S_{l\{m\}} = \frac{1}{l^4} \sum_{k=0}^5 \frac{s_k + t_k \log l}{l^k} + O(l^{-10}),\tag{A.28}$$

where,

$$\begin{aligned}s_0 &= \xi_0 - \xi_0 \log \xi_0 \\ s_1 &= -\xi_1 \log \xi_0 \\ s_2 &= -\frac{\xi_1^2}{2\xi_0} - \xi_2 \log \xi_0 \\ s_3 &= \frac{\xi_1^3 - 6\xi_0\xi_1\xi_2}{6\xi_0^2} - \xi_3 \log \xi_0 \\ &\vdots\end{aligned},$$

and

$$\begin{aligned}t_i &= 4\xi_i \quad 0 < i \leq 3 \\ t_4 &= 4(\xi_0^2 + \xi_4) \\ t_5 &= 4(2\xi_0\xi_1 + \xi_5).\end{aligned}\tag{A.29}$$

To determine the contribution to the entropy of all modes with the same  $l$ , we use the expansion of the degeneration,

$$v(l, D) = \binom{l+D-1}{l} - \binom{l+D-3}{l-2} = l^{D-2} \sum_{k=0}^{\infty} \frac{v_k(D)}{l^k}, \quad (\text{A.30})$$

which allows us to sum over all the possible values of  $\{m\}$ ,

$$\sum_{\{m\}} S_{l\{m\}} = v(l, D) S_{l\{m\}} = \sum_{i=0}^5 \frac{\sigma_i \log l + \tau_i}{l^{6-D+i}} + O(l^{D-12}) \quad (\text{A.31})$$

where  $\tau_k \equiv \sum_{j=0}^k v_j t_{k-j}$  and  $\sigma_k \equiv \sum_{j=0}^k v_j s_{k-j}$ . Finally, we can compute the contribution to total entropy, for  $l$  from  $l_0$  to  $\infty$ , where  $l_0$  is big enough such that these approximations are justified.

$$\Delta S \simeq \sum_j^5 \sigma_j \left( \zeta(6-D+j) - \sum_{l=1}^{l_0} \frac{1}{l^{6-D+j}} \right) - \sum_j^5 \tau_j \left( \zeta'(6-D+j) + \sum_{l=1}^{l_0} \frac{\log l}{l^{6-D+j}} \right), \quad (\text{A.32})$$

being  $\zeta(k)$  the Riemann Zeta function, and  $\zeta'(k)$  its derivative.

#### A.1.4 The single-copy entanglement

We can do the same as for the entropy to find the contribution to the single-copy entanglement for large values of  $l$ . First, we expand the contribution to the total single-copy entanglement of the  $(l, \{m\})$  modes,

$$(E_1)_{l\{m\}} \simeq -\log(1 - \xi_l) = \sum_{i=0}^5 \frac{\kappa_i}{l^{4+i}} + O(l^{-10}), \quad (\text{A.33})$$

where,

$$\begin{aligned} \kappa_i &= \xi_i \quad 0 < i \leq 3 \\ \kappa_4 &= \left( \frac{\xi_0^2}{2} + \xi_4 \right) \\ \kappa_5 &= (\xi_0 \xi_1 + \xi_5). \end{aligned} \quad (\text{A.34})$$

Next, we sum for all possible values of  $\{m\}$ , using Eq.(A.30),

$$(E_1)_l = v(l, D) (E_1)_{l\{m\}} = \sum_{i=0}^5 \frac{\Lambda_i}{l^{D-6+i}}, \quad (\text{A.35})$$

where  $\Lambda_k \equiv \sum_{j=0}^k \nu_j \kappa_{k-j}$ . Proceeding as before, we finally get

$$E_1 \simeq \sum_{j=0}^5 \Lambda_j \left( \zeta(6-D+j) - \sum_{l=1}^{l_0} \frac{1}{l^{6-D+j}} \right). \quad (\text{A.36})$$



---

## Real space renormalization group in a XX model of 4 spins

---

We consider first a simple XX model with only 4 spins and couplings  $\{\lambda, 1, \lambda\}$ . We can rewrite the Hamiltonian of the system as a perturbation theory problem,

$$H = H_0 + \lambda V, \quad (\text{B.1})$$

where,

$$H_0 = \sigma_2^X \sigma_3^X + \sigma_2^Y \sigma_3^Y, \quad (\text{B.2})$$

and

$$V = \sigma_1^X \sigma_2^X + \sigma_1^Y \sigma_2^Y + \sigma_3^X \sigma_4^X + \sigma_3^Y \sigma_4^Y. \quad (\text{B.3})$$

The eigenstates of  $H_0$  are

$$\begin{aligned} |\psi_+\rangle &= \frac{1}{\sqrt{2}} (|01\rangle_{23} + |10\rangle_{23}) \\ |\psi_0\rangle &= |00\rangle_{23} \\ |\psi_1\rangle &= |11\rangle_{23} \\ |\psi_-\rangle &= \frac{1}{\sqrt{2}} (|01\rangle_{23} - |10\rangle_{23}) \end{aligned} \quad (\text{B.4})$$

with eigenvalues +2, 0, 0 and -2 respectively. We are interested in study what happens to the ground state (GS) of the Hamiltonian  $H$  when the perturbation  $\lambda V$  is

introduced. The ground state of  $H_0$  is degenerate and form a subspace of dimension 4. In particular, we choose the set of vectors  $\{|m\rangle\} = \{|0\rangle_1|\psi_-\rangle_{23}|0\rangle_4, |0\rangle_1|\psi_-\rangle_{23}|1\rangle_4, |1\rangle_1|\psi_-\rangle_{23}|0\rangle_4, |1\rangle_1|\psi_-\rangle_{23}|1\rangle_4\}$  as a basis.

We expect that the perturbation removes the degeneracy in the sense that there will be 4 perturbed eigenkets all with different energies. Let us call them  $\{|l\rangle\}$ . As  $\lambda$  goes to zero,  $|l\rangle$  tend to  $|l^{(0)}\rangle$  which are eigenstates of  $H_0$ , but which in general will not coincide with  $|m\rangle$ .

According to perturbation theory, let us expand the eigenstates and the eigenvalues of  $H$  in powers of  $\lambda$ ,

$$|l\rangle = |l^{(0)}\rangle + \lambda|l^{(1)}\rangle + \lambda^2|l^{(2)}\rangle + O(\lambda^3) \quad (\text{B.5})$$

and

$$E_l = E_{GS}^{(0)} + \lambda E_l^{(1)} + \lambda^2 E_l^{(2)} + O(\lambda^3). \quad (\text{B.6})$$

Notice that the zero order term in the energy expansion does not depend on  $l$ , since the ground state of the non-perturbed Hamiltonian is degenerate. Substituting the previous expansions into the Schrödinger equation,  $(H_0 + \lambda V)|l\rangle = E_l|l\rangle$ , and equating the coefficient of various powers of  $\lambda$ , we obtain a set of equations that will allow us to find the corrections to the perturbed eigenstates and eigenvalues.

At zero order in  $\lambda$  we recover the trivial non-perturbed Schrödinger equation. If we collect terms of order  $\lambda$ , we get

$$(E_D^0 - H_0)|l^{(1)}\rangle = (V - E_l^{(1)})|l^{(0)}\rangle. \quad (\text{B.7})$$

In order to calculate the first correction to the energy, we project the previous equation (B.7) to the degenerate ground state subspace

$$\sum_{m'=1}^4 V_{m,m'} \langle m'|l^{(0)}\rangle = E_l^{(1)} \langle m|l^{(0)}\rangle, \quad (\text{B.8})$$

where  $V_{m,m'} \equiv \langle m|V|m'\rangle$  is the projection of the interaction to this subspace. In our particular case, the matrix-elements  $V_{m,m'} = 0$  for all  $m$  and  $m'$ , hence,  $E_l^{(1)} = 0 \forall l$ . This means that the degeneration is not broken at first order in  $\lambda$  and forces us to consider the second order,

$$(E_D^0 - H_0)|l^{(2)}\rangle = (V - E_l^{(1)})|l^{(1)}\rangle - E_l^{(2)}|l^{(0)}\rangle. \quad (\text{B.9})$$

We proceed as previously and project this equation to the degenerate ground state subspace,

$$\langle m|V - E_l^{(1)}|l^{(1)}\rangle = E_l^{(2)} \langle m|l^{(0)}\rangle. \quad (\text{B.10})$$

From equation (B.7) we can compute the first order correction to the eigenstates  $|l\rangle$ ,

$$|l^{(1)}\rangle = \sum_{k \neq GS} \frac{\langle k^{(0)}|V|l^{(0)}\rangle}{E_{GS}^{(0)} - E_k^{(0)}} \quad (\text{B.11})$$

where  $|k^{(0)}\rangle$  are the  $H_0$  eigenstates that do not belong to GS. Now, we substitute this into (B.9) and get an equation for the 2nd order correction to the energies and the states  $|l^{(0)}\rangle$

$$\sum_{m',k} \frac{\langle m|V|k^{(0)}\rangle \langle k^{(0)}|V|m\rangle}{E_{GS}^{(0)} - E_k^{(0)}} \alpha_m^l = E_l^{(2)} \alpha_m^l \quad (\text{B.12})$$

where  $\alpha_m^l$  are the coefficients of  $|l^{(0)}\rangle \equiv \sum_m \alpha_m^l |m\rangle$  expressed in terms of the basis  $|m\rangle$ . Notice that eq. (B.12) is a diagonalization problem. For our particular Hamiltonian, it takes the form

$$2 \begin{pmatrix} 1 & 0 & 0 & 0 \\ 0 & 1 & 1 & 0 \\ 0 & 1 & 1 & 0 \\ 0 & 0 & 0 & 1 \end{pmatrix} \cdot \begin{pmatrix} \alpha_1 \\ \alpha_2 \\ \alpha_3 \\ \alpha_4 \end{pmatrix} = E_l^{(2)} \begin{pmatrix} \alpha_1 \\ \alpha_2 \\ \alpha_3 \\ \alpha_4 \end{pmatrix}. \quad (\text{B.13})$$

Now the degeneration is completely broken and the perturbed ground state becomes

$$|GS\rangle = |\psi_{-}\rangle_{14} |\psi_{-}\rangle_{23} - \lambda \frac{1}{\sqrt{2}} (|1001\rangle + |0110\rangle) + O(\lambda^2), \quad (\text{B.14})$$

with

$$E_{GS} = -2 + O(\lambda^3). \quad (\text{B.15})$$

We can obtain an effective Hamiltonian by projecting the original one into the subspace of lower energy formed by  $\{|l^{(0)}\rangle\}$ ,

$$H_{eff} = PHP^\dagger = -2 + \frac{\lambda^2}{2} (2 + \sigma_1^X \sigma_4^X + \sigma_1^Y \sigma_4^Y), \quad (\text{B.16})$$

where  $P = \sum_{l^{(0)}} |l^{(0)}\rangle \langle l^{(0)}|$  and  $|l^{(0)}\rangle \in \{|\psi_{-}\rangle_{14} |\psi_{-}\rangle_{23}, |\psi_0\rangle_{14} |\psi_{-}\rangle_{23}, |\psi_1\rangle_{14} |\psi_{-}\rangle_{23}, |\psi_{+}\rangle_{14} |\psi_{-}\rangle_{23}\}$ .



---

## BIBLIOGRAPHY

---

- [1] G. Vidal, “Efficient classical simulation of slightly entangled quantum computations,” *Phys. Rev. Lett.* **91** (2003) 147902.  
arXiv:quant-ph/0301063.
- [2] F. Verstraete, M. M. Wolf, D. Pérez-García, and J. I. Cirac, “Criticality, the area law, and the computational power of projected entangled pair states,” *Phys. Rev. Lett.* **96** (2006) 220601. arXiv:quant-ph/0601075.
- [3] M. Srednicki, “Entropy and area,” *Phys. Rev. Lett.* **71** (1993) 666–669,  
arXiv:hep-th/9303048.
- [4] G. Vidal, J. I. Latorre, E. Rico, and A. Kitaev, “Entanglement in quantum critical phenomena,” *Phys. Rev. Lett.* **90** (2003) 227902,  
arXiv:quant-ph/0211074.
- [5] J. I. Latorre, E. Rico, and G. Vidal, “Ground state entanglement in quantum spin chains,” *Quant. Inf. Comput.* **4** (2004) 48–92,  
arXiv:quant-ph/0304098.
- [6] J. Eisert, M. Cramer, and M. B. Plenio, “Area laws for the entanglement entropy - a review,”. arXiv:0808.3773.
- [7] D. S. Fisher, “Random antiferromagnetic quantum spin chains,” *Phys. Rev. B* **50** (1994) 3799–3821.

- 
- [8] C. Dasgupta and S.-K. Ma, “Low-temperature properties of the random Heisenberg antiferromagnetic chain,” *Phys. Rev. B* **22** (1980) 1305–1319.
- [9] R. P. Feynman, “Simulating physics with computers,” *Int. J. Theor. Physics* **21** (1982) 467–488.
- [10] D. C. Tsui, H. L. Stormer, and A. C. Gossard, “Two-dimensional magnetotransport in the extreme quantum limit,” *Phys. Rev. Lett.* **48** (1982) 1559–1562.
- [11] R. B. Laughlin, “Anomalous quantum hall effect: An incompressible quantum fluid with fractionally charged excitations,” *Phys. Rev. Lett.* **50** (1983) 1395–1398.
- [12] X. G. Wen, *Quantum Field Theory and Many-Body Systems*. Oxford University Press, Oxford, 2004.
- [13] B. Paredes, P. Fedichev, J. I. Cirac, and P. Zoller, “1/2-Anyons in Small Atomic Bose-Einstein Condensates,” *Phys. Rev. Lett.* **87** (2001) 010402. arXiv:cond-mat/0103251.
- [14] B. Paredes, P. Zoller, and J. I. Cirac, “Fermionizing a small gas of ultracold bosons,” *Phys. Rev. A* **66** (2002) 033609. arXiv:cond-mat/0203061.
- [15] M. Lewenstein, A. Sanpera, V. Ahufinger, B. Damski, A. S. De, and U. Sen, “Ultracold atomic gases in optical lattices: mimicking condensed matter physics and beyond,” *Adv. in Phys.* **56** (2007) 243. arXiv:cond-mat/0606771.
- [16] I. Bloch, J. Dalibard, and W. Zwerger, “Many-body physics with ultracold gases,” *Rev. Mod. Phys.* **80** (2008) 885–964. arXiv:0704.3011.
- [17] M. Popp, B. Paredes, and J. I. Cirac, “Adiabatic path to fractional quantum Hall states of a few bosonic atoms,” *Phys. Rev. A* **70** (2004) 053612. arXiv:cond-mat/0405195.
- [18] L. Pitaevskii and S. Stringari, *Bose-Einstein Condensation*. Oxford Sci. Pub., Oxford, 2003.
- [19] H. Häffner, C. Roos, and R. Blatt, “Quantum computing with trapped ions,” *Physics Reports* **469** (2008) 155 – 203. arXiv:0809.4368.

- 
- [20] A. Einstein, B. Podolsky, and N. Rosen, “Can quantum mechanical description of physical reality be considered complete?,” *Phys. Rev.* **47** (1935) 777–780.
- [21] J. S. Bell, “On the Einstein-Podolsky-Rosen paradox,” *Physics* **1** (1964) 195.
- [22] A. Aspect, P. Grangier, and G. Roger, “Experimental Tests of Realistic Local Theories via Bell’s Theorem,” *Phys. Rev. Lett.* **47** (1981) 460–463.
- [23] C. H. Bennett *et al.*, “Teleporting an unknown quantum state via dual classical and Einstein-Podolsky-Rosen channels,” *Phys. Rev. Lett.* **70** (1993) 1895–1899.
- [24] C. H. Bennett and S. J. Wiesner, “Communication via one- and two-particle operators on einstein-podolsky-rosen states,” *Phys. Rev. Lett.* **69** (1992) 2881–2884.
- [25] A. K. Ekert, “Quantum cryptography based on Bell’s theorem,” *Phys. Rev. Lett.* **67** (1991) 661–663.
- [26] M. B. Plenio and V. Vedral, “Entanglement in quantum information theory,” *Contemporary Physics* **39** (1998) 431. arXiv:quant-ph/9804075.
- [27] B. Schumacher and M. D. Westmoreland, “Relative entropy in quantum information theory,” *Contemporary Mathematics* **81** (2000) 68. arXiv:quant-ph/0004045.
- [28] M. B. Plenio and S. Virmani, “An introduction to entanglement measures,” *Quant. Inf. Comp.* **7** (2007) 1. arXiv:quant-ph/0504163.
- [29] R. Horodecki, P. Horodecki, M. Horodecki, and K. Horodecki, “Quantum entanglement,” *Rev. Mod. Phys.* **81** (2009) 865–942. arXiv:quant-ph/0702225.
- [30] L. Amico, R. Fazio, A. Osterloh, and V. Vedral, “Entanglement in many-body systems,” *Rev. Mod. Phys.* **80** (2008) 517–576. arXiv:quant-ph/0703044.
- [31] J. Eisert, “Entanglement in quantum information theory,” 2001. arXiv:quant-ph/0610253.
- [32] I. Bengtsson and K. Życzkowski, *Geometry of Quantum States - An Introduction to Quantum Entanglement*. Cambridge University Press, Cambridge, 2006.

- 
- [33] V. Vedral, “The role of relative entropy in quantum information theory,” *Rev. Mod. Phys.* **74** (2002) 197–234. arXiv:quant-ph/0102094.
- [34] D. Bruss, “Characterizing entanglement,” *J. Math. Phys.* **43** (2002) 4237. arXiv:quant-ph/0110078.
- [35] R. F. Werner, “Quantum states with Einstein-Podolsky-Rosen correlations admitting a hidden-variable model,” *Phys. Rev. A* **40** (1989) 4277–4281.
- [36] M. A. Nielsen, “Conditions for a class of entanglement transformations,” *Phys. Rev. Lett.* **83** (1999) 436–439. arXiv:quant-ph/9811053.
- [37] E. M. Rains, “Quantum codes of minimum distance two,”. arXiv:quant-ph/9704043.
- [38] K. Audenaert, M. B. Plenio, and J. Eisert, “Entanglement cost under positive-partial-transpose-preserving operations,” *Phys. Rev. Lett.* **90** (2003) 027901. arXiv:quant-ph/0207146.
- [39] C. H. Bennett, H. J. Bernstein, S. Popescu, and B. Schumacher, “Concentrating partial entanglement by local operations,” *Phys. Rev. A* **53** (1996) 2046–2052.
- [40] M. J. Donald, M. Horodecki, and O. Rudolph, “The Uniqueness Theorem for Entanglement Measures,” *J. Math. Phys.* **43** (2002) 4252. arXiv:quant-ph/0105017.
- [41] V. Vedral and M. B. Plenio, “Entanglement measures and purification procedures,” *Phys. Rev. A* **57** (1998) 1619–1633. arXiv:quant-ph/9707035.
- [42] P. Zanardi and N. Paunković, “Ground state overlap and quantum phase transitions,” *Phys. Rev. E* **74** (2006) 031123. arXiv:quant-ph/0512249.
- [43] P. Zanardi, M. Cozzini, and P. Giorda, “Ground state fidelity and quantum phase transitions in free Fermi systems,” *J. Stat. Mech.* (2006) L02002. arXiv:quant-ph/0606130.
- [44] H.-Q. Zhou, J.-H. Zhao, and B. Li, “Fidelity approach to quantum phase transitions: finite-size scaling for the quantum Ising model in a transverse field,” *J. Phys. A: Math. Theor.* **41** (2008) 492002.

- 
- [45] H.-Q. Zhou, R. Orús, and G. Vidal, “Ground state fidelity from tensor network representations,” *Phys. Rev. Lett.* **100** (2008) 080601. arXiv:0709.4596.
- [46] C. G. Callan, Jr. and F. Wilczek, “On geometric entropy,” *Phys. Lett.* **B333** (1994) 55–61, arXiv:hep-th/9401072.
- [47] T. M. Fiola, J. Preskill, A. Strominger, and S. P. Trivedi, “Black hole thermodynamics and information loss in two- dimensions,” *Phys. Rev.* **D50** (1994) 3987–4014, arXiv:hep-th/9403137.
- [48] J. Eisert and M. Cramer, “Single-copy entanglement in critical quantum spin chains,” *Phys. Rev. A* **72** (2005) 042112. arXiv:quant-ph/0506250.
- [49] I. Peschel and J. Zhao, “On single-copy entanglement,” *J. Stat. Mech.: Theory Exp.* (2005) 11002. arXiv:quant-ph/0509002.
- [50] R. Orús, J. I. Latorre, J. Eisert, and M. Cramer, “Half the entanglement in critical systems is distillable from a single specimen,” *Phys. Rev. A* **73** (2006) 060303. arXiv:quant-ph/0509023.
- [51] M. Keyl, T. Matsui, D. Schlingemann, and R. F. Werner, “Entanglement, Haag-duality and type properties of infinite quantum spin chains,” *Rev. Math. Phys.* **18** (2006) 935. arXiv:math-ph/0604071.
- [52] S. Sachdev, *Quantum Phase Transitions*. Cambridge University Press, Cambridge, 1999.
- [53] P. Christe and M. Henkel, *Introduction to Conformal Invariance and Its Applications to Critical Phenomena*, vol. vol m16. Springer, Berlin, 2001.
- [54] B. K. Chakrabarti, A. Dutta, and P. Sen, *Quantum Ising Phases and Transitions in Transverse Ising Models*, vol. vol m41. Springer, Berlin, 2001.
- [55] I. Peschel, M. Kaulke, and O. Legeza, “Density-matrix spectra for integrable models,” *Ann. Phys.* **8** (1999) 153. arXiv:cond-mat/9810174.
- [56] M.-C. Chung and I. Peschel, “Density-matrix spectra of solvable fermionic systems,” *Phys. Rev. B* **64** (2001) 064412. arXiv:cond-mat/0103301.
- [57] I. Peschel, “Calculation of reduced density matrices from correlation functions,” *Math. Gen.* **36** (2003) L205. arXiv:cond-mat/0212631.

- [58] I. Peschel and V. Eisler, “Reduced density matrices and entanglement entropy in free lattice models,” *J. Phys. A: Math. Theor.* **42** (2009) 504003. arXiv:0906.1663.
- [59] B. Q. Jin and V. E. Korepin, “Quantum Spin Chain, Toeplitz Determinants and Fisher-Hartwig Conjecture,” *J. Stat. Phys.* **116** (2004) 79. arXiv:quant-ph/0304108.
- [60] T. T. Wu, “Theory of Toeplitz Determinants and the Spin Correlations of the Two-Dimensional Ising Model. I,” *Phys. Rev.* **149** (1966) 380–401.
- [61] M. E. Fisher and R. E. Hartwig, “Toeplitz Determinants: Some Applications, Theorems, and Conjectures,” *Adv. Chem. Phys.* (2007) 333–353.
- [62] E. Basor, “A localization theorem for Toeplitz determinants,” *Indiana Math. J.* **28** (1979) 975.
- [63] E. L. Basor and C. A. Tracy, “The Fisher-Hartwig conjecture and generalizations,” *Physica A: Statistical Mechanics and its Applications* **177** (1991) 167 – 173.
- [64] A. Böttcher and B. Silbermann, *Analysis of Toeplitz Operators*. Springer, Berlin, 1990.
- [65] A. R. Its, B.-Q. Jin, and V. E. Korepin, “Entanglement in XY Spin Chain,” *Journal Phys. A: Math. Gen.* **38** 2975–2990. arXiv:quant-ph/0409027.
- [66] F. Franchini, A. R. Its, B.-Q. Jin, and V. E. Korepin, “Analysis of entropy of XY Spin Chain,” *Proceedings of the Third Feynman Workshop* (2006) .
- [67] F. Franchini, A. R. Its, B.-Q. Jin, and V. E. Korepin, “Ellipses of Constant Entropy in the XY Spin Chain,” *J. Phys. A: Math. Theor.* **40** (2007) 8467–8478. arXiv:quant-ph/0609098.
- [68] F. Franchini, A. R. Its, and V. E. Korepin, “Renyi Entropy of the XY Spin Chain,” *J. Phys. A: Math. Theor.* **41** (2008) 025302. arXiv:0707.2534.
- [69] A. M. Polyakov *Sov. Phys.-JETP Lett.* **12** (1970) 381.
- [70] P. H. Ginsparg, “Applied Conformal Field Theory,” arXiv:hep-th/9108028.

- [71] J. Cardy, “Conformal field theory and statistical mechanics,”  
arXiv:0807.3472.
- [72] C. Holzhey, F. Larsen, and F. Wilczek, “Geometric and renormalized entropy in conformal field theory,” *Nucl. Phys.* **B424** (1994) 443–467,  
arXiv:hep-th/9403108.
- [73] P. Calabrese and J. L. Cardy, “Entanglement entropy and quantum field theory,” *J. Stat. Mech.* **0406** (2004) P002, arXiv:hep-th/0405152.
- [74] P. Calabrese, J. Cardy, and E. Tonni, “Entanglement entropy of two disjoint intervals in conformal field theory,” *J. Stat. Mech.* **0911** (2009) P11001,  
arXiv:0905.2069 [hep-th].
- [75] H.-Q. Zhou, T. Barthel, J. O. Fjærestad, and U. Schollwöck, “Entanglement and boundary critical phenomena,” *Phys. Rev. A* **74** (2006) 050305.  
arXiv:cond-mat/0511732.
- [76] P. Calabrese and A. Lefevre, “Entanglement spectrum in one-dimensional systems,” *Phys. Rev. A* **78** (2008) 032329. arXiv:0806.3059.
- [77] L. Bombelli, R. K. Koul, J. Lee, and R. D. Sorkin, “Quantum source of entropy for black holes,” *Phys. Rev. D* **34** (1986) 373–383.
- [78] T. M. Fiola, J. Preskill, A. Strominger, and S. P. Trivedi, “Black hole thermodynamics and information loss in two dimensions,” *Phys. Rev. D* **50** (1994) 3987–4014.
- [79] D. N. Kabat and M. J. Strassler, “A Comment on entropy and area,” *Phys. Lett.* **B329** (1994) 46–52, arXiv:hep-th/9401125.
- [80] D. N. Kabat, “Black hole entropy and entropy of entanglement,” *Nucl. Phys.* **B453** (1995) 281–302, arXiv:hep-th/9503016.
- [81] H. Casini and M. Huerta, “Entanglement entropy in free quantum field theory,” *J. Phys. A: Math. Theor.* **A42** (2009) 504007, arXiv:0905.2562 [hep-th].
- [82] A. Riera and J. I. Latorre, “Area law and vacuum reordering in harmonic networks,” *Phys. Rev. A* **74** (2006) 052326. arXiv:quant-ph/0605112.

- 
- [83] M. Cramer, J. Eisert, M. B. Plenio, and J. Dreißig, “Entanglement-area law for general bosonic harmonic lattice systems,” *Phys. Rev. A* **73** (2006) 012309. arXiv:quant-ph/0505092.
- [84] T. Barthel, M.-C. Chung, and U. Schollwöck, “Entanglement scaling in critical two-dimensional fermionic and bosonic systems,” *Phys. Rev. A* **74** (2006) 022329. arXiv:cond-mat/0602077.
- [85] M. M. Wolf, “Violation of the Entropic Area Law for Fermions,” *Phys. Rev. Lett.* **96**. arXiv:quant-ph/0503219.
- [86] D. Gioev and I. Klich, “Entanglement Entropy of Fermions in Any Dimension and the Widom Conjecture,” *Phys. Rev. Lett.* **96**. arXiv:quant-ph/0504151.
- [87] E. Fradkin and J. E. Moore, “Entanglement Entropy of 2D Conformal Quantum Critical Points: Hearing the Shape of a Quantum Drum,” *Phys. Rev. Lett.* **97** (2006) 050404. arXiv:cond-mat/0605683.
- [88] S. Ryu and T. Takayanagi, “Aspects of holographic entanglement entropy,” *JHEP* **08** (2006) 045, arXiv:hep-th/0605073.
- [89] S. Ryu and T. Takayanagi, “Holographic Derivation of Entanglement Entropy from the anti de Sitter Space/Conformal Field Theory Correspondence,” *Phys. Rev. Lett.* **96** (2006) 181602. arXiv:hep-th/0603001.
- [90] T. Nishioka, S. Ryu, and T. Takayanagi, “Holographic entanglement entropy: An overview,” *J. Phys. A* **42** (2009) 504008. arXiv:0905.0932.
- [91] A. Kitaev and J. Preskill, “Topological entanglement entropy,” *Phys. Rev. Lett.* **96** (2006) 110404. arXiv:hep-th/0510092.
- [92] E. Fradkin, “Scaling of Entanglement Entropy at 2D quantum Lifshitz fixed points and topological fluids,” *J. Phys. A: Math. Theor.* **42** (2009) 504011. arXiv:0906.1569.
- [93] E. Lieb, T. Schultz, and D. Mattis, “Two soluble models of an antiferromagnetic chain,” *Ann. Phys.* **16** (1961) 407.
- [94] S. Katsura, “Statistical Mechanics of the Anisotropic Linear Heisenberg Model,” *Phys. Rev.* **127** (1962) 1508–1518.

- 
- [95] E. Barouch and B. M. McCoy, “Statistical Mechanics of the XY Model. II. Spin-Correlation Functions,” *Phys. Rev. A* **3** (1971) 786–804.
- [96] F. Igloi and R. Juhasz, “Exact relationship between the entanglement entropies of XY and quantum Ising chains,” *Europhys. Lett.* **81** (2008) 57003. arXiv:0709.3927.
- [97] J. L. Cardy, O. A. Castro-Alvaredo, and B. Doyon, “Form factors of branch-point twist fields in quantum integrable models and entanglement entropy,” *J. Stats. Phys.* **130** (2007) 129. arXiv:0706.3384.
- [98] O. A. Castro-Alvaredo and B. Doyon, “Bi-partite entanglement entropy in massive 1+1-dimensional quantum field theories,” *J. Phys. A: Math. Theor.* **42** (2009) 504006. arXiv:0906.2946.
- [99] H. Bethe, “Eigenwerte und eigenfunktionen der linearen atomkette,” *Z. Phys.* **71** (1931) 205.
- [100] N. Bogoliubov, A. Izergin, and V. Korepin, *Quantum Inverse Scattering Method and Correlation Functions*. Cambridge University Press, Cambridge, 1993.
- [101] M. Takahashi, *Thermodynamics of One-Dimensional Solvable Models*. Cambridge University Press, Cambridge, 1999.
- [102] E. Ercolessi, S. Evangelisti, and F. Ravanini, “Exact entanglement entropy of the XYZ model and its sine- Gordon limit,” arXiv:0905.4000 [hep-th].
- [103] J. Sato, M. Shiroishi, and M. Takahashi, “Exact evaluation of density matrix elements for the Heisenberg chain,” *J. Stat. Mech.* **0612** (2006) P017, arXiv:hep-th/0611057.
- [104] B. Nienhuis, M. Campostrini, and P. Calabrese, “Entanglement, combinatorics and finite-size effects in spin-chains,” *J. Stat. Mech.* (2009) P02063. arXiv:0808.2741.
- [105] G. Refael and J. E. Moore, “Entanglement entropy of random quantum critical points in one dimension,” *Phys. Rev. Lett.* **93** (2004) 260602. arXiv:cond-mat/0406737.
- [106] N. Laflorencie, “Scaling of entanglement entropy in the random singlet phase,” *Phys. Rev. B* **72** (2005) 140408. arXiv:cond-mat/0504446.

- 
- [107] G. De Chiara, S. Montangero, P. Calabrese, and R. Fazio, “Entanglement Entropy dynamics in Heisenberg chains,” *J. Stat. Mech.* **0603** (2006) P001, arXiv:cond-mat/0512586.
- [108] N. E. Bonesteel and K. Yang, “Infinite-randomness fixed points for chains of non-abelian quasiparticles,” *Phys. Rev. Lett.* **99** (2007) 140405. arXiv:cond-mat/0612503.
- [109] V. V. França and K. Capelle, “Entanglement in spatially inhomogeneous many-fermion systems,” *Phys. Rev. Lett.* **100** (2008) 070403. arXiv:0710.2095.
- [110] Y.-C. Lin, F. Iglói, and H. Rieger, “Entanglement entropy at infinite-randomness fixed points in higher dimensions,” *Phys. Rev. Lett.* **99** (2007) 147202. arXiv:0704.0418.
- [111] R. Yu, H. Saleur, and S. Haas, “Entanglement entropy in the two-dimensional random transverse field Ising model,” *Phys. Rev. B* **77** (2008) 140402. arXiv:0709.3840.
- [112] S. Garnerone, N. T. Jacobson, S. Haas, and P. Zanardi, “Fidelity Approach to the Disordered Quantum XY Model,” *Phys. Rev. Lett.* **102** (2009) 057205. arXiv:0808.4140.
- [113] N. T. Jacobson, S. Garnerone, S. Haas, and P. Zanardi, “Scaling of the fidelity susceptibility in a disordered quantum spin chain,” *Phys. Rev. B* **79** (2009) 184427. arXiv:0903.2069.
- [114] I. Affleck, N. Laflorencie, and E. S. Sorensen, “Entanglement entropy in quantum impurity systems and systems with boundaries,” *J. Phys. A: Math. Theor.* **42** (2009) 504009. arXiv:0906.1809.
- [115] H. J. Lipkin, N. Meshkov, and A. J. Glick, “Validity of many-body approximation methods for a solvable model : (I). Exact solutions and perturbation theory ,” *Nucl. Phys.* **62** (1965) 188.
- [116] N. Meshkov, A. J. Glick, and H. J. Lipkin, “Validity of many-body approximation methods for a solvable model : (II). Linearization procedures,” *Nucl. Phys.* **62** (1965) 199.

- 
- [117] A. J. Glick, H. J. Lipkin, and N. Meshkov, “Validity of many-body approximation methods for a solvable model : (III). Diagram summations,” *Nucl. Phys.* **62** (1965) 211.
- [118] J. I. Latorre, R. Orús, E. Rico, and J. Vidal, “Entanglement entropy in the Lipkin-Meshkov-Glick model,” *Phys. Rev. A* **71** (2005) 064101, arXiv:cond-mat/0409611.
- [119] T. Barthel, S. Dusuel, and J. Vidal, “Entanglement entropy beyond the free case,” *Phys. Rev. Lett.* **97** (2006) 220402. arXiv:cond-mat/0606436.
- [120] P. Ribeiro, J. Vidal, and R. Mosseri, “Exact spectrum of the Lipkin-Meshkov-Glick model in the thermodynamic limit and finite-size corrections,” *Phys. Rev. E* **78** (2008) 021106. arXiv:0805.4078.
- [121] J. Vidal, S. Dusuel, and T. Barthel, “Entanglement entropy in collective models,” *J. Stat. Mech.* **0701** (2007) P015. arXiv:cond-mat/0610833.
- [122] S. Iblisdir, J. I. Latorre, and R. Orús, “Entropy and Exact Matrix-Product Representation of the Laughlin Wave Function,” *Phys. Rev. Lett.* **98** (2007) 060402. arXiv:cond-mat/0609088.
- [123] M. Haque, O. Zozulya, and K. Schoutens, “Entanglement Entropy in Fermionic Laughlin States,” *Phys. Rev. Lett.* **98** (2007) 060401. arXiv:cond-mat/0609263.
- [124] O. S. Zozulya, M. Haque, and K. Schoutens, “Particle partitioning entanglement in itinerant many-particle systems,” *Phys. Rev. A* **78** (2008) 042326. arXiv:0804.0878.
- [125] M. Haque, O. S. Zozulya, and K. Schoutens, “Entanglement between particle partitions in itinerant many-particle states,” *J. Phys. A: Math. Theor.* **42** (2009) 504012. arXiv:0905.4024.
- [126] F. Verstraete, J. I. Cirac, J. I. Latorre, E. Rico, and M. M. Wolf, “Renormalization-Group Transformations on Quantum States,” *Phys. Rev. Lett.* **94** (2005) 140601. arXiv:quant-ph/0410227.
- [127] H. Casini and M. Huerta, “A finite entanglement entropy and the c-theorem,” *Phys. Lett. B* **600** (2004) 142–150, arXiv:hep-th/0405111.

- 
- [128] P. Calabrese and J. L. Cardy, “Evolution of Entanglement Entropy in One-Dimensional Systems,” *J. Stat. Mech.* **0504** (2005) P010, arXiv:cond-mat/0503393.
- [129] M. Fagotti and P. Calabrese, “Evolution of entanglement entropy following a quantum quench: Analytic results for the  $xy$  chain in a transverse magnetic field,” *Phys. Rev. A* **78** (2008) 010306. arXiv:0804.3559.
- [130] L. Cincio, J. Dziarmaga, M. M. Rams, and W. H. Zurek, “Entropy of entanglement and correlations induced by a quench: Dynamics of a quantum phase transition in the quantum Ising model,” *Phys. Rev. A* **75** (2007) 052321. arXiv:cond-mat/0701768.
- [131] N. Schuch, M. M. Wolf, K. G. H. Vollbrecht, and J. I. Cirac, “On entropy growth and the hardness of simulating time evolution,” *New J. Phys.* **10** (2008) 033032. arXiv:0801.2078.
- [132] A. Laeuchli and C. Kollath, “Spreading of correlations and entanglement after a quench in the one-dimensional Bose-Hubbard model,” *J. Stat. Mech.* (2008) P05018. arXiv:0803.2947.
- [133] P. Calabrese and J. Cardy, “Entanglement entropy and conformal field theory,” *J. Phys. A: Math. Theor.* **42** (2009) 504005. arXiv:0905.4013.
- [134] C. K. Burrell and T. J. Osborne, “Bounds on the speed of information propagation in disordered quantum spin chains,” *Phys. Rev. Lett.* **99** (2007) 167201. arXiv:quant-ph/0703209.
- [135] S. Bravyi, M. B. Hastings, and F. Verstraete, “Lieb-Robinson Bounds and the Generation of Correlations and Topological Quantum Order,” *Phys. Rev. Lett.* **97** (2006) 050401. arXiv:quant-ph/0603121.
- [136] J. Eisert and T. J. Osborne, “General entanglement scaling laws from time evolution,” *Phys. Rev. Lett.* **97** (2006) 150404. arXiv:quant-ph/0603114.
- [137] E. H. Lieb and D. W. Robinson, “The finite group velocity of quantum spin systems,” *Commun. Math. Phys.* **28** (1972) 251.
- [138] M. B. Hastings, “Locality in Quantum and Markov Dynamics on Lattices and Networks,” *Phys. Rev. Lett.* **93** (2004) 140402. arXiv:cond-mat/0405587.

- 
- [139] M. B. Hastings, “Lieb-schultz-mattis in higher dimensions,” *Phys. Rev. B* **69** (2004) 104431. arXiv:cond-mat/0305505.
- [140] M. B. Hastings and T. Koma, “Spectral gap and exponential decay of correlations,” *Commun. Math. Phys.* **265** (2006) 781. arXiv:math-ph/0507008.
- [141] W. Dür, L. Hartmann, M. Hein, M. Lewenstein, and H.-J. Briegel, “Entanglement in Spin Chains and Lattices with Long-Range Ising-Type Interactions,” *Phys. Rev. Lett.* **94** (2005) 097203. arXiv:quant-ph/0407075.
- [142] F. Verstraete and J. I. Cirac, “Renormalization algorithms for Quantum-Many Body Systems in two and higher dimensions,” arXiv:cond-mat/0407066.
- [143] G. Vidal, “Efficient simulation of one-dimensional quantum many-body systems,” *Phys. Rev. Lett.* **93** (2004) 040502. arXiv:quant-ph/0310089.
- [144] J. I. Latorre, “Entanglement entropy and the simulation of quantum mechanics,” *J. Phys. A: Math. Theor.* **40** (2007) 6689. arXiv:quant-ph/0611271.
- [145] M. A. Nielsen and I. L. Chuang, *Quantum Computation and Quantum Information*. Cambridge Univ. Press, Cambridge, 2000.
- [146] J. I. Latorre and M. A. Martín-Delgado, “Majorization arrow in quantum-algorithm design,” *Phys. Rev. A* **66** (2002) 022305. arXiv:quant-ph/0111146.
- [147] R. Orús, J. I. Latorre, and M. A. Martín-Delgado, “Natural majorization of the Quantum Fourier Transformation in phase-estimation algorithms,” *Quant. Inf. Proc.* **1** (2002) 283. arXiv:quant-ph/0206134.
- [148] R. Orús, J. I. Latorre, and M. A. Martín-Delgado, “Systematic analysis of majorization in quantum algorithms,” *Eur. Phys. J. D* **29** (2004) 119. arXiv:quant-ph/0212094.
- [149] F. Verstraete, J. I. Cirac, and J. I. Latorre, “Quantum circuits for strongly correlated quantum systems,” *Phys. Rev. A* **79** (2009) 032316. arXiv:0804.1888.

- 
- [150] J. I. Latorre, V. Pico, and A. Riera, “Quantum algorithm for the Laughlin wave function,” *arXiv:0902.4797*.
- [151] E. Farhi, J. Goldstone, S. Gutmann, J. Lapan, A. Lundgren, and D. Preda, “A Quantum Adiabatic Evolution Algorithm Applied to Random Instances of an NP-Complete Problem,” *Science* **292** (2001) 472.  
*arXiv:quant-ph/0104129*.
- [152] E. Farhi, J. Goldstone, S. Gutmann, and M. Sipser, “Quantum computation by adiabatic evolution,” *arXiv:quant-ph/0001106*.
- [153] S. A. Cook, “The complexity of theorem-proving procedures,” in *STOC ’71: Proceedings of the third annual ACM symposium on Theory of computing*, pp. 151–158. ACM, New York, NY, USA, 1971.
- [154] L. A. Levin, “Universal sorting problems,” *Prob. Inf. Trans.* **9** (1973) 265–266.
- [155] J. I. Latorre and R. Orús, “Adiabatic quantum computation and quantum phase transitions,” *Phys. Rev. A* **69** (2004) 062302.  
*arXiv:quant-ph/0308042*.
- [156] J. J. García-Ripoll and M. C. Bañuls, “Efficiency of structured adiabatic quantum computation,” *arXiv:0812.1760*.
- [157] R. Raussendorf and H. J. Briegel, “A one-way quantum computer,” *Phys. Rev. Lett.* **86** (2001) 5188–5191.
- [158] R. Raussendorf and H. J. Briegel, “Computational model for the one-way quantum computer: Concepts and summary,” *Quantum Inf. Comput.* **6** (2002) 433. *arXiv:quant-ph/0207183*.
- [159] P. Walther, K. J. Resch, T. Rudolph, E. Schenck, H. Weinfurter, V. Vedral, M. Aspelmeyer, and A. Zeilinger, “Experimental one-way quantum computing,” *Nature* **434** (2005) 169–176. *arXiv:quant-ph/0503126*.
- [160] D. Gross and J. Eisert, “Novel schemes for measurement-based quantum computation,” *Phys. Rev. Lett.* **98** (2007) 220503.  
*arXiv:quant-ph/0609149*.

- 
- [161] D. Gross, J. Eisert, N. Schuch, and D. Pérez-García, “Measurement-based quantum computation beyond the one-way model,” *Phys. Rev. A* **76** (2007) 052315. arXiv:0706.3401.
- [162] D. Gross and J. Eisert, “Quantum computational webs,”. arXiv:0810.2542.
- [163] M. V. den Nest, W. Dur, A. Miyake, and H. J. Briegel, “Fundamentals of universality in one-way quantum computation,” *New J. Phys.* **9** (2007) 204. arXiv:quant-ph/0702116.
- [164] G. K. Brennen and A. Miyake, “Measurement-Based Quantum Computer in the Gapped Ground State of a Two-Body Hamiltonian,” *Phys. Rev. Lett.* **101** (2008) 010502. arXiv:0803.1478.
- [165] D. Gross, S. T. Flammia, and J. Eisert, “Most quantum states are too entangled to be useful as computational resources,” *Phys. Rev. Lett.* **102** (2009) 190501. arXiv:0810.4331.
- [166] M. Fannes, B. Nachtergaele, and R. F. Werner, “Quantum spin chains with quantum group symmetry,” *Commun. Math. Phys.* **174** (1996) 477. arXiv:cond-mat/9504002.
- [167] D. Pérez-García, F. Verstraete, M. M. Wolf, and J. I. Cirac, “Matrix Product State Representations,” *Quant. Inf. Comp.* **7** (2007) 401. arXiv:quant-ph/0608197.
- [168] D. Pérez-García, F. Verstraete, J. I. Cirac, and M. M. Wolf, “PEPS as unique ground states of local Hamiltonians,” *Quant. Inf. Comp.* **8** (2008) 0650. arXiv:0707.2260.
- [169] L. Tagliacozzo, T. R. de Oliveira, S. Iblisdir, and J. I. Latorre, “Scaling of entanglement support for matrix product states,” *Phys. Rev. B* **78** (2008) 024410. arXiv:0712.1976.
- [170] F. Pollmann, S. Mukerjee, A. M. Turner, and J. E. Moore, “Theory of finite-entanglement scaling at one-dimensional quantum critical points,” *Phys. Rev. Lett.* **102** (2009) 255701. arXiv:0812.2903.
- [171] D. N. Page, “Expected entropy of a subsystem,” *Phys. Rev. Lett.* **71** (1993) 1291–1294, arXiv:gr-qc/9305007.

- 
- [172] W. Li, L. Ding, R. Yu, T. Roscilde, and S. Haas, “Scaling behavior of entanglement in two- and three-dimensional free-fermion systems,” *Phys. Rev. B* **74** (2006) 073103. arXiv:quant-ph/0602094.
- [173] D. V. Fursaev, “Entanglement entropy in critical phenomena and analogue models of quantum gravity,” *Phys. Rev. D* **73** (2006) 124025, arXiv:hep-th/0602134.
- [174] R. Emparan, “Black hole entropy as entanglement entropy: A holographic derivation,” *JHEP* **06** (2006) 012, arXiv:hep-th/0603081.
- [175] F. Verstraete, D. Porras, and J. I. Cirac, “Density matrix renormalization group and periodic boundary conditions: A quantum information perspective,” *Phys. Rev. Lett.* **93** (2004) 227205. arXiv:cond-mat/0404706.
- [176] M. B. Plenio, J. Eisert, J. Dreissig, and M. Cramer, “Entropy, entanglement, and area: analytical results for harmonic lattice systems,” *Phys. Rev. Lett.* **94** (2005) 060503, arXiv:quant-ph/0405142.
- [177] M. Cramer, J. Eisert, M. B. Plenio, and J. Dreissig, “An entanglement-area law for general bosonic harmonic lattice systems,” *Phys. Rev. A* **73** (2006) 012309, arXiv:quant-ph/0505092.
- [178] M. B. Hastings, “Solving gapped hamiltonians locally,” *Phys. Rev. B* **73** (2006) 085115. arXiv:cond-mat/0508554.
- [179] F. Verstraete, J. I. Cirac, J. I. Latorre, E. Rico, and M. M. Wolf, “Renormalization group transformations on quantum states,” *Phys. Rev. Lett.* **94** (2005) 140601, arXiv:quant-ph/0410227.
- [180] I. Peschel, “On the entanglement entropy for a XY spin chain,” *J. Stat. Mech.* (2004) P12005. arXiv:cond-mat/0410416.
- [181] M. Cramer and J. Eisert, “Correlations, spectral gap, and entanglement in harmonic quantum systems on generic lattices,” *New J. Phys.* **8** (2006) 71. arXiv:quant-ph/0509167.
- [182] A. Botero and B. Reznik, “Spatial structures and localization of vacuum entanglement in the linear harmonic chain,” *Phys. Rev. A* **70** (2004) 052329. arXiv:quant-ph/0403233.

- 
- [183] A. Hamma, R. Ionicioiu, and P. Zanardi, “Bipartite entanglement and entropic boundary law in lattice spin systems,” *Phys. Rev. A* **71** (2005) 022315. arXiv:quant-ph/0409073.
- [184] R. Orús and J. I. Latorre, “Universality of Entanglement and Quantum Computation Complexity,” *Phys. Rev. A* **69** (2004) 052308, arXiv:quant-ph/0311017.
- [185] M. C. Bañuls, R. Orús, J. I. Latorre, A. Pérez, and P. Ruiz-Femenía, “Simulation of many-qubit quantum computation with matrix product states,” *Phys. Rev. A* **73** (2006) 022344. arXiv:quant-ph/0503174.
- [186] F. Larsen and F. Wilczek, “Geometric entropy, wave functionals, and fermions,” *Ann. Phys.* **243** (1995) 280–298, arXiv:hep-th/9408089.
- [187] H. Casini, C. D. Fosco, and M. Huerta, “Entanglement and alpha entropies for a massive Dirac field in two dimensions,” *J. Stat. Mech.* **0507** (2005) P007, arXiv:cond-mat/0505563.
- [188] S. N. Solodukhin, “The Conical singularity and quantum corrections to entropy of black hole,” *Phys. Rev. D* **51** (1995) 609–617, arXiv:hep-th/9407001.
- [189] D. Aharonov, D. Gottesman, S. Irani, and J. Kempe, “The power of quantum systems on a line,” *Comm. Math. Phys.* **287** (2009) 41. arXiv:0705.4077.
- [190] G. Vidal, “Entanglement renormalization,” *Phys. Rev. Lett.* **99** (2007) 220405. arXiv:cond-mat/0512165.
- [191] J. I. Latorre, C. A. Lütken, E. Rico, and G. Vidal, “Fine-grained entanglement loss along renormalization-group flows,” *Phys. Rev. A* **71** (2005) 034301. arXiv:quant-ph/0404120.
- [192] R. Orús, “Entanglement and majorization in (1+1)-dimensional quantum systems,” *Phys. Rev.* **71** **71** (2005) 052327, arXiv:quant-ph/0501110.
- [193] A. B. Zamolodchikov, “Irreversibility of the Flux of the Renormalization Group in a 2D Field Theory,” *JETP Lett.* **43** (1986) 730–732.
- [194] A. Cappelli, D. Friedan, and J. I. Latorre, “C theorem and spectral representation,” *Nucl. Phys.* **B352** (1991) 616–670.

- 
- [195] S. Forte and J. I. Latorre, “A proof of the irreversibility of renormalization group flows in four dimensions,” *Nucl. Phys.* **B535** (1998) 709–728, arXiv:hep-th/9805015.
- [196] N. Schuch, M. M. Wolf, F. Verstraete, and J. I. Cirac, “Computational Complexity of Projected Entangled Pair States,” *Phys. Rev. Lett.* **98** (2007) 140506.
- [197] M. B. Hastings, “An area law for one-dimensional quantum systems,” *J. Stat. Mech.: Theor. Exp.* (2007) P08024. arXiv:0705.2024.
- [198] D. Jaksch, C. Bruder, J. I. Cirac, C. W. Gardiner, and P. Zoller, “Cold bosonic atoms in optical lattices,” *Phys. Rev. Lett.* **81** (1998) 3108–3111. arXiv:cond-mat/9805329.
- [199] M. Greiner, O. Mandel, T. Esslinger, T. W. Hänsch, and I. Bloch, “Quantum phase transition from a superfluid to a mott insulator in a gas of ultracold atoms,” *Nature* **415** (2002) 39–44.
- [200] I. Bloch, “Quantum gases in optical lattices,” *Physics World* **17** (2004) 25.
- [201] M. Popp, J. J. García-Ripoll, K. G. H. Vollbrecht, and J. I. Cirac, “Cooling toolbox for atoms in optical lattices,” *New J. Phys.* **8** (2006) 164. arXiv:cond-mat/0605198.
- [202] L. Della Pietra, S. Aigner, C. vom Hagen, S. Groth, I. Bar-Joseph, H. J. Lezec, and J. Schmiedmayer, “Designing potentials by sculpturing wires,” *Phys. Rev. A* **75** (2007) 063604. arXiv:cond-mat/0604619.
- [203] R. Grimm, M. Weidemüller, and Y. B. Ovchinnikov, “Optical dipole traps for neutral atoms,” *Adv. Mol. Opt. Phys.* **42** (2000) 95. arXiv:physics/9902072.
- [204] S. Hofferberth, I. Lesanovsky, B. Fischer, J. Verdu, and J. Schmiedmayer, “Radiofrequency-dressed-state potentials for neutral atoms,” *Nature Phys.* **2** (2006) 710. arXiv:quant-ph/0608228.
- [205] S. Inouye, M. R. Andrews, J. Stenger, H.-J. Miesner, S.-K. D. M., and W. Ketterle, “Observation of Feshbach resonances in a Bose-Einstein condensate,” *Nature* **392** (1998) 151.

- 
- [206] S. L. Cornish, N. R. Claussen, J. L. Roberts, E. A. Cornell, and C. E. Wieman, “Stable  $85\text{Rb}$  Bose-Einstein Condensates with Widely Tunable Interactions,” *Phys. Rev. Lett.* **85** (2000) 1795–1798. arXiv:cond-mat/0004290.
- [207] P. O. Fedichev, Y. Kagan, G. V. Shlyapnikov, and J. T. M. Walraven, “Influence of Nearly Resonant Light on the Scattering Length in Low-Temperature Atomic Gases,” *Phys. Rev. Lett.* **77** (1996) 2913–2916.
- [208] M. Theis, G. Thalhammer, K. Winkler, M. Hellwig, G. Ruff, R. Grimm, and J. H. Denschlag, “Tuning the Scattering Length with an Optically Induced Feshbach Resonance,” *Phys. Rev. Lett.* **93** (2004) 123001. arXiv:cond-mat/0404514.
- [209] G. Thalhammer, M. Theis, K. Winkler, R. Grimm, and J. H. Denschlag, “Inducing an optical feshbach resonance via stimulated raman coupling,” *Phys. Rev. A* **71** (2005) 033403. arXiv:cond-mat/0409552.
- [210] H. Feshbach, “Unified theory of nuclear reactions,” *Annals of Physics* **5** (1958) 357 – 390.
- [211] D. Jaksch and P. Zoller, “Creation of effective magnetic fields in optical lattices: The Hofstadter butterfly for cold neutral atoms,” *New J. Phys.* **5** (2003) 56. arXiv:quant-ph/0304038.
- [212] E. J. Mueller, “Artificial electromagnetism for neutral atoms: Escher staircase and Laughlin liquids,” *Phys. Rev. A* **70** (2004) 041603. arXiv:cond-mat/0404306.
- [213] K. Osterloh, M. Baig, L. Santos, P. Zoller, and M. Lewenstein, “Cold Atoms in Non-Abelian Gauge Potentials: From the Hofstadter "Moth" to Lattice Gauge Theory,” *Phys. Rev. Lett.* **95** (2005) 010403. arXiv:cond-mat/0502251.
- [214] R. N. Palmer and D. Jaksch, “High-Field Fractional Quantum Hall Effect in Optical Lattices,” *Phys. Rev. Lett.* **96** (2006) 180407. arXiv:cond-mat/0604600.
- [215] K. Góral, L. Santos, and M. Lewenstein, “Quantum phases of dipolar bosons in optical lattices,” *Phys. Rev. Lett.* **88** (2002) 170406. arXiv:cond-mat/0112363.

- [216] A. Micheli, G. K. Brennen, and P. Zoller, “A toolbox for lattice spin models with polar molecules,” *Nat. Phys.* **2** (2006) 341. arXiv:quant-ph/0512222.
- [217] R. Barnett, A. Turner, and E. Demler, “Classifying novel phases of spinor atoms,” *Phys. Rev. Lett.* **97** (2006) 180412. arXiv:cond-mat/0607253.
- [218] M. Baranov, Ł. Dobrek, K. Góral, L. Santos, and M. Lewenstein, “Ultracold dipolar gases - a challenge for experiments and theory,” *Phys. Scripta* **102** (2002) .
- [219] V. Ahufinger, L. Sanchez-Palencia, A. Kantian, A. Sanpera, and M. Lewenstein, “Disordered ultracold atomic gases in optical lattices: A case study of Fermi-Bose mixtures,” *Phys. Rev. A* **72** (2005) 063616.  
arXiv:cond-mat/0508042.
- [220] W. Ketterle, D. Durfee, and D. Stamper-Kurn, “Making, probing and understanding Bose-Einstein condensates,” in *In Bose-Einstein condensation in atomic gases: Proceedings of the International School of Physics "Enrico Fermi"*, pp. 67–176. IOS Press, Amsterdam, 1999.
- [221] E. Altman, E. Demler, and M. D. Lukin, “Probing many-body states of ultracold atoms via noise correlations,” *Phys. Rev. A* **70** (2004) 013603.  
arXiv:cond-mat/0306226.
- [222] A. Polkovnikov, E. Altman, and E. Demler, “Interference between independent fluctuating condensates,” *PNAS* **103** (2006) 6125.  
arXiv:cond-mat/0511675.
- [223] V. Gritsev, E. Altman, E. Demler, and A. Polkovnikov, “Full quantum distribution of contrast in interference experiments between interacting one dimensional Bose liquids,” *Nat. Phys.* **2** (2006) 705.  
arXiv:cond-mat/0602475.
- [224] L.-M. Duan, “Detecting Correlation Functions of Ultracold Atoms through Fourier Sampling of Time-of-Flight Images,” *Phys. Rev. Lett.* **96** (2006) 103201. arXiv:cond-mat/0511678.
- [225] M. Schellekens, R. Hoppeler, A. Perrin, J. V. Gomes, D. Boiron, A. Aspect, and C. I. Westbrook, “Hanbury Brown Twiss Effect for Ultracold Quantum Gases,” *Science* **310** (2005) 648–651. arXiv:cond-mat/0508466.

- [226] T. Jelte, J. M. McNamara, W. Hogervorst, W. Vassen, V. Krachmalnicoff, M. Schellekens, A. Perrin, H. Chang, D. Boiron, A. Aspect, and C. I. Westbrook, “Comparison of the Hanbury Brown-Twiss effect for bosons and fermions,” *Nature* **445** (2007) 402–405. arXiv:cond-mat/0612278.
- [227] D. A. Huse, M. P. A. Fisher, and D. S. Fisher, “Are superconductors really superconducting?,” *Nature* **358** (1992) 553 – 559.
- [228] J. I. Cirac and P. Zoller, “New frontiers in quantum information with atoms and ions,” *Physics Today* **57** (2004) 38–44.
- [229] D. Yoshioka, *The quantum Hall Effect*. Springer-Verlag, Berlin, 2002.
- [230] A. Kitaev, “Anyons in an exactly solved model and beyond,” *Annals of Physics* **321** (2006) 2 – 111. arXiv:cond-mat/0506438. January Special Issue.
- [231] B. Douçot, M. V. Feigel’man, L. B. Ioffe, and A. S. Ioselevich, “Protected qubits and Chern-Simons theories in Josephson junction arrays,” *Phys. Rev. B* **71** (2005) 024505. arXiv:cond-mat/0403712.
- [232] L.-M. Duan, E. Demler, and M. D. Lukin, “Controlling spin exchange interactions of ultracold atoms in optical lattices,” *Phys. Rev. Lett.* **91** (2003) 090402. arXiv:cond-mat/0210564.
- [233] L. Jacak, P. Hawrylak, and A. Wójs, *Quantum Dots*. Springer-Verlag, Berlin, 1998.
- [234] N. K. Wilkin and J. M. F. Gunn, “Condensation of “Composite Bosons” in a Rotating BEC,” *Phys. Rev. Lett.* **84** (2000) 6–9. arXiv:cond-mat/9906282.
- [235] N. R. Cooper, N. K. Wilkin, and J. M. F. Gunn, “Quantum Phases of Vortices in Rotating Bose-Einstein Condensates,” *Phys. Rev. Lett.* **87** (2001) 120405. arXiv:cond-mat/0107005.
- [236] N. Barberán, M. Lewenstein, K. Osterloh, and D. Dagnino, “Ordered structures in rotating ultracold Bose gases,” *Phys. Rev. A* **73** (2006) 063623. arXiv:cond-mat/0603200.
- [237] A. S. Sørensen, E. Demler, and M. D. Lukin, “Fractional Quantum Hall States of Atoms in Optical Lattices,” *Phys. Rev. Lett.* **94** (2005) 086803. arXiv:0706.0757.

- [238] C. Becker, P. Soltan-Panahi, J. Kronjäger, S. Dorscher, K. Bongs, and K. Sengstock, “Ultracold quantum gases in triangular optical lattices,” arXiv:0912.3646.
- [239] M. Born and V. A. Fock, “Beweis des adiabatenatzes,” *Zeitschrift für Physik a Hadrons and Nuclei* **51** (1928) 165–180.
- [240] N. Read and N. R. Cooper, “Free expansion of lowest-Landau-level states of trapped atoms: A wave-function microscope,” *Phys. Rev. A* **68** (2003) 035601. arXiv:cond-mat/0306378.
- [241] D. Jaksch, J. I. Cirac, P. Zoller, S. L. Rolston, R. Côté, and M. D. Lukin, “Fast quantum gates for neutral atoms,” *Phys. Rev. Lett.* **85** (2000) 2208–2211. arXiv:quant-ph/0004038.
- [242] O. Mandel, M. Greiner, A. Widera, T. Rom, T. W. Hänsch, and I. Bloch, “Coherent transport of neutral atoms in spin-dependent optical lattice potentials,” *Phys. Rev. Lett.* **91** (2003) 010407. arXiv:cond-mat/0301169.
- [243] J. Blaizot and G. Rypka, *Quantum Theory of Finite Systems*. The MIT Press, Cambridge, 1985.
- [244] N. Bogoliubov, “On the theory of superfluidity,” *J. Phys. USSR* **11** (1947) 23.
- [245] D. Butts and D. Rokhsar, “Predicted signatures of rotating Bose–Einstein condensates,” *Nature* **397** (1999) 327.
- [246] E. M. Wright, D. F. Walls, and J. C. Garrison, “Collapses and Revivals of Bose-Einstein Condensates Formed in Small Atomic Samples,” *Phys. Rev. Lett.* **77** (1996) 2158–2161.
- [247] M. Lewenstein and L. You, “Quantum Phase Diffusion of a Bose-Einstein Condensate,” *Phys. Rev. Lett.* **77** (1996) 3489–3493.
- [248] J. Javanainen and S. M. Yoo, “Quantum Phase of a Bose-Einstein Condensate with an Arbitrary Number of Atoms,” *Phys. Rev. Lett.* **76** (1996) 161–164.
- [249] Y. Castin and J. Dalibard, “Relative phase of two Bose-Einstein condensates,” *Phys. Rev. A* **55** (1997) 4330–4337.

- 
- [250] J. Javanainen, “Phonon approach to an array of traps containing Bose-Einstein condensates,” *Phys. Rev. A* **60** (1999) 4902–4909.
- [251] C. W. Gardiner, “Particle-number-conserving Bogoliubov method which demonstrates the validity of the time-dependent Gross-Pitaevskii equation for a highly condensed Bose gas,” *Phys. Rev. A* **56** (1997) 1414–1423.  
arXiv:quant-ph/9703005.
- [252] M. D. Girardeau, “Comment on “Particle-number-conserving Bogoliubov method which demonstrates the validity of the time-dependent Gross-Pitaevskii equation for a highly condensed Bose gas”,” *Phys. Rev. A* **58** (1998) 775–778.
- [253] Y. Castin and R. Dum, “Bose-Einstein Condensates in Time Dependent Traps,” *Phys. Rev. Lett.* **77** (1996) 5315–5319.
- [254] W. J. Mullin, R. Krotkov, and F. Laloe, “The origin of phase in the interference of Bose-Einstein condensates,” arXiv:cond-mat/0604371.
- [255] V. L. Ginzburg and L. D. Landau, “On the Theory of superconductivity,” *Zh. Eksp. Teor. Fiz.* **20** (1950) 1064–1082.
- [256] O. Penrose, “On the quantum mechanics of helium II,” *Phil. Mag.* **42** (1951) 1373–1377.
- [257] O. Penrose and L. Onsager, “Bose-Einstein Condensation and Liquid Helium,” *Phys. Rev.* **104** (1956) 576–584.
- [258] C. N. Yang, “Concept of Off-Diagonal Long-Range Order and the Quantum Phases of Liquid He and of Superconductors,” *Rev. Mod. Phys.* **34** (1962) 694–704.
- [259] F. Chevy, K. W. Madison, and J. Dalibard, “Measurement of the Angular Momentum of a Rotating Bose-Einstein Condensate,” *Phys. Rev. Lett.* **85** (2000) 2223–2227. arXiv:cond-mat/0005221.
- [260] M. Andrews, C. Townsend, H.-J. Miesner, D. Durfee, D. Kurn, and W. Ketterle, “Observation of Interference Between Two Bose Condensates,” *Science* **275** (1997) 637.

- [261] O. Vainio, C. J. Vale, M. J. Davis, N. R. Heckenberg, and H. Rubinsztein-Dunlop, “Fringe spacing and phase of interfering matter waves,” *Phys. Rev. A* **73** (2006) 063613. arXiv:cond-mat/0601690.
- [262] S. Ritter, A. Öttl, T. Donner, T. Bourdel, M. Köhl, and T. Esslinger, “Observing the Formation of Long-Range Order during Bose-Einstein Condensation,” *Phys. Rev. Lett.* **98** (2007) 090402. arXiv:cond-mat/0607102.
- [263] A. J. Daley, P. O. Fedichev, and P. Zoller, “Single-atom cooling by superfluid immersion: A nondestructive method for qubits,” *Phys. Rev. A* **69** (2004) 022306. arXiv:quant-ph/0308129.
- [264] A. Griessner, A. J. Daley, S. R. Clark, D. Jaksch, and P. Zoller, “Dark-state cooling of atoms by superfluid immersion,” *Phys. Rev. Lett.* **97** (2006) 220403. arXiv:cond-mat/0607254.
- [265] L. S. Cederbaum, A. I. Streltsov, Y. B. Band, and O. E. Alon, “Interferences in the Density of Two Bose-Einstein Condensates Consisting of Identical or Different Atoms,” *Phys. Rev. Lett.* **98** (2007) 110405. arXiv:cond-mat/0701277.
- [266] M. Hafezi, A. S. Sørensen, E. Demler, and M. D. Lukin, “Fractional quantum Hall effect in optical lattices,” *Phys. Rev. A* **76** (2007) 023613. arXiv:0706.0757.
- [267] H. P. Büchler, M. Hermele, S. D. Huber, M. P. A. Fisher, and P. Zoller, “Atomic quantum simulator for lattice gauge theories and ring exchange models,” *Phys. Rev. Lett.* **95** (2005) 040402. arXiv:cond-mat/0503254.
- [268] B. Paredes and I. Bloch, “Minimum instances of topological matter in an optical plaquette,” *Phys. Rev. A* **77** (2008) 023603. arXiv:0711.3796.
- [269] D. S. Abrams and S. Lloyd, “Simulation of Many-Body Fermi Systems on a Universal Quantum Computer,” *Phys. Rev. Lett.* **79** (1997) 2586–2589. arXiv:quant-ph/9703054.
- [270] G. Benenti and G. Strini, “Quantum simulation of the single-particle Schrodinger equation,” *Am. J. Phys.* **76** (2008) 657. arXiv:0709.1704.

- 
- [271] M. Reck, A. Zeilinger, H. J. Bernstein, and P. Bertani, “Experimental realization of any discrete unitary operator,” *Phys. Rev. Lett.* **73** (1994) 58–61.
- [272] C. Monroe, D. M. Meekhof, B. E. King, W. M. Itano, and D. J. Wineland, “Demonstration of a fundamental quantum logic gate,” *Phys. Rev. Lett.* **75** (1995) 4714–4717.
- [273] A. Barenco, C. H. Bennett, R. Cleve, D. P. DiVincenzo, N. Margolus, P. Shor, T. Sleator, J. A. Smolin, and H. Weinfurter, “Elementary gates for quantum computation,” *Phys. Rev. A* **52** (1995) 3457–3467.
- [274] J. I. Cirac and P. Zoller, “Quantum computations with cold trapped ions,” *Phys. Rev. Lett.* **74** (1995) 4091–4094.
- [275] G. Chen, D. Church, B. Englert, C. Henkel, B. Rohwedder, M. Scully, and M. Zubairy, *Quantum Computing Devices: Principles, Designs, and Analysis*. CRC Press, 2006.
- [276] S. Popescu, “Knill-Laflamme-Milburn Linear Optics Quantum Computation as a Measurement-Based Computation,” *Phys. Rev. Lett.* **99** (2007) 250501.